# A Statistical Model for the Dual Polarised MIMO Land Mobile Satellite Channel at S-band

Fióna Sinéad Dunwoody Ní Mhearáin

Submitted for the degree of Doctor of Philosophy

Heriot-Watt University

Institute of Sensors, Signals and Systems

School of Engineering & Physical Sciences

May 2018

# ABSTRACT

This thesis explores channel modelling approaches to the land mobile satellite (LMS) channel in S-band, focussing on the implementation of multiple input multiple output techniques through the use of dual polarisation. An Enhanced Statistical Model is presented and the output of this model is analysed and compared to the two current state-of-the-art models that simulate the dual polarised LMS channel, i.e. the statistical Liolis-CTTC model and the geometric ray-tracing QuaDRiGa model.

The enhanced model builds on the Liolis-CTTC model and presents solutions to a number of issues that arise in the statistical modelling process. The enhancements in the new model include imposing temporal correlation on the slow variations without unwanted high frequency components from low-pass filtering, introducing Doppler effects including Doppler shaping of the fast variations, implementing a smooth state transition process and also implementing an interpolation process to sample the channel at the required sub-symbol rate for transmission.

In addition to the analysis of the three models, real channel measurements of the dual polarised LMS channel from the MIMOSA campaign are analysed. A statistical comparison between the models and the real measurement data for simulated journeys in a number of user environments is conducted through analysis of the timeseries, the cumulative density function (CDF), average fading duration (AFD) and level-crossing rate (LCR). Capacity analysis and eigenvalue analysis is also conducted and allows for validation of the enhanced model. The comparisons with the measurement data show good agreement between the real measurement data and the enhanced model.

DEDICATION

*To Robin and Úna.*

# *Acknowledgements*

I would like to thank Prof Mathini Sellathurai of Heriot-Watt University for her supervision and for all her help and guidance throughout the PhD. Also, thanks to my second supervisor Prof Tharm Ratnarajah of the University of Edinburgh.

I would like to gratefully acknowledge Prof Fernando Pérez-Fontán of the University of Vigo and Dr Roberto Prieto-Cerdeira of ESTEC for the generous giving of their time & support and for kindly hosting me at their institutions. Thank you also to The Royal Society of Edinburgh who made those visits possible with the Lessell's Postgraduate Travel Award.

I would like to thank Heriot-Watt University for my scholarship, funding for travelling and support services and for giving me the opportunity to conduct this research.

A number of people have helped me with my work and the journey through the PhD, including Dr Christos Masouros and Dr Rongrong Qian, thank you.

A special thanks to Kevin for his unfaltering patience and encouragement. Also thanks to all my friends and family who have supported me on a personal level, you are too many to name but I appreciate all of you.

# Contents

**Abstract** i

**Dedication** ii

**Acknowledgements** iii

**List of Figures** v

**List of Tables** vi

**Abbreviations** vii

**Notations and Symbols** x

**1 Introduction** 1
- 1.1 Purpose of Thesis . . . 1
- 1.2 Purpose of Channel Modelling Research . . . 2
- 1.3 Research Context . . . 4
- 1.4 Methodology and Scope of Research . . . 6
- 1.5 Contributions . . . 7
- 1.6 Structure of Thesis . . . 8
- 1.7 Publications . . . 9
  - 1.7.1 Conference Proceedings . . . 9

**2 The Land Mobile Satellite Channel** 11
- 2.1 Introduction . . . 11
  - 2.1.1 The Role of Satellites in Communication Systems . . . 12
  - 2.1.2 Fixed and Mobile Satellite Channels . . . 14
- 2.2 Characteristics of The LMS Channel . . . 15
  - 2.2.1 Physics Affecting the Propagating Signal . . . 15
  - 2.2.2 How to Model the Physical Effect on the LMS channel . . . 17
  - 2.2.3 Time Dispersion . . . 17
  - 2.2.4 Rates of Signal Variation . . . 18
  - 2.2.5 States . . . 19

2.2.6 Statistical Distributions . . . 22
2.2.7 Joint distributions . . . 23
2.2.7.1 The Loo Model . . . 23
2.2.7.2 The Suzuki Model . . . 25
2.2.8 Doppler Spectrum . . . 26
2.2.8.1 Doppler shift in the direct signal . . . 26
2.2.8.2 Doppler spread in the multipath components . . . 27
2.3 Diversity in a Communication Systems . . . 28
2.3.1 Achieving Diversity in Satellite Systems . . . 29
2.3.2 Polarisation Diversity . . . 30
2.4 Summary . . . 32

**3 The Enhanced Dual Polarised LMS Model 34**
3.1 Introduction . . . 34
3.2 Liolis-CTTC as a Baseline Statistical Model . . . 35
3.3 Statistical Modelling of the Dual Polarised LMS channel . . . 36
3.3.1 Implementation of the Polarised Subchannels . . . 38
3.3.2 Implementation of Loo Distribution . . . 41
3.4 The Enhanced Statistical LMS Model . . . 43
3.5 Step-by-Step Guide to Channel Matrix Construction . . . 43
3.5.1 Generate the Direct Signal Component . . . 43
3.5.2 Generate the Multipath Signal Component . . . 45
3.5.3 Generate the Total Signal Component . . . 46
3.6 Spatial Correlation of the Subchannels . . . 48
3.6.1 The Weichselberger method . . . 49
3.7 Temporal Correlation of the Slow Variations . . . 50
3.7.1 Temporal Correlation through Autoregressive IIR Filtering . . . 52
3.7.2 Temporal Correlation through Low Pass FIR Filtering and Interpolating . . . 53
3.8 Smooth State Transition Process . . . 58
3.8.1 Step-by-Step Guide to Smooth State Transitioning . . . 62
3.9 Doppler Shaping of the Fast Variations . . . 63
3.9.1 Doppler Shaping through FIR filtering . . . 64
3.9.2 Doppler Shaping through IIR filtering . . . 67
3.9.3 Other Methods of Doppler Shaping . . . 68
3.9.4 Comparison of Doppler Shaping Methods . . . 69
3.9.5 Doppler Shift . . . 72
3.10 Variation of the XPC of the environment . . . 72
3.11 Interpolation to Symbol Rate Sampling . . . 72
3.11.1 Method . . . 73
3.11.2 Results of Multirate Filtering . . . 74
3.12 Capacity Analysis . . . 78
3.12.1 Capacity as a Function of Model Parameters . . . 79
3.12.2 MIMO over SISO Advantage . . . 85

3.12.3 MIMO vs SIMO . . . 88
3.12.4 Markov vs Semi-Markov . . . 92
3.13 Summary . . . 94

**4 Comparison of Enhanced Model with Liolis and QuaDRiGa models 96**
4.1 Introduction . . . 96
4.2 The Liolis-CTTC Model . . . 98
4.3 The QuaDRiGa Model . . . 101
4.3.1 Background . . . 101
4.3.2 Parameterisiation of the Model . . . 101
4.3.3 Polarisation and Antenna Modelling . . . 103
4.3.4 Setting Up and Running a QuaDRiGa Simulation . . . 104
4.4 Comparison of Results . . . 107
4.4.1 Initialisation of models . . . 107
4.4.2 Timeseries . . . 111
4.4.2.1 Magnitude of Received Signal During Good and Bad States . . . 111
4.4.2.2 Variation Between Same Polarisation Subchannels . . . 113
4.4.2.3 Variation in Signal Magnitude at State Transitions . . . 113
4.4.2.4 Number of State Transitions . . . 114
4.4.2.5 Variation in Signal Magnitude During States . . . 117
4.4.3 Timeseries at 20 dB XPD . . . 122
4.5 Doppler Shaping of Spectra . . . 124
4.6 Statistical Analysis . . . 127
4.6.1 Cumulative Distribution Function . . . 127
4.6.2 Average Fade Duration and Level Crossing Rate . . . 130
4.7 Eigenvalue Analysis . . . 133
4.8 Statistical Distribution of Received Signal . . . 136
4.9 Summary . . . 140

**5 Comparison of Enhanced Model with MIMOSA measurement data 142**
5.1 Introduction . . . 142
5.2 The MiLADY and MIMOSA Measurement Campaigns . . . 143
5.2.1 MIMOSA set-up . . . 143
5.2.2 MIMOSA Data Analysis . . . 145
5.2.3 MIMOSA Database . . . 145
5.3 Analysis of the Urban Environment . . . 147
5.3.1 Timeseries . . . 147
5.3.2 2nd order Statistics . . . 151
5.3.2.1 CDF . . . 151
5.3.3 Average Fade Duration . . . 154
5.3.4 Level Crossing Rate . . . 156
5.3.5 Eigenvalue Analysis . . . 158
5.4 Spectrum Analysis . . . 161

5.5 Analysis of the Suburban Environment . . . 163
5.5.1 Timeseries . . . 163
5.5.2 CDF . . . 165
5.5.3 AFD and LCR . . . 167
5.5.4 Spectrum . . . 170
5.6 Analysis of the Open Rural Environment . . . 172
5.6.1 Timeseries . . . 172
5.6.2 CDF . . . 174
5.6.3 ACF and LCR . . . 176
5.6.4 Spectrum . . . 179
5.7 Summary . . . 181

**6 Conclusions and Further Work** **182**
6.1 Review of Research Objectives . . . 182
6.2 Review of Methodology . . . 183
6.3 Achievements and Limitations . . . 184
6.4 Further Work . . . 186

**A Tables of Important Parameters** **189**

**B QuaDRiGa parameters** **193**

**Bibliography** **201**

# List of Figures


2.1 Diagram showing the variation arising in signal power as the mobile unit travels through the user environment and how a three state classification model compares to a two state classification model with 'good' and 'bad' states. . . . . 21
2.2 State diagram for a two-state Markov chain. . . . . 21
2.3 State diagram for a two-state semi-Markov chain. . . . . 21
2.4 Diagram showing the direction of the electric field vector for (i) left hand circular polarisation, (ii) right hand polarisation, (iii) vertical linear polarisation and (iv) horizontal linear polarisation. (Direction of travel of the wave is into the page) . . . . . 31
2.5 Diagram showing a 2x2 MIMO channel matrix with co-polar components RHCP/RHCP and LHCP/LHCP and also cross-polar components RHCP/LHCP and LHCP/RHCP. . . . . 31

3.1 Diagram of the 2x2 channel matrix achieved through the use of dual polarised antenna at the transmitter and the receiver. As right hand and left hand circularly polarised antenna are used, this creates 4 subchannels, RHCP/RHCP, RHCP/LHCP, LHCP/RHCP, LHCP/LHCP. The receiver may be a handheld device carried by a pedestrian or a portable device based in a moving car. . . . . 37
3.2 Schematic diagram of the simulation of the enhanced dual polarised MIMO LMS channel incorporating the Loo distribution and showing the inclusion of Doppler spreading in the multipath component (top rail) and rate conversion process for the direct signal component (bottom rail) which incorporates a two- step low-pass filtering and interpolation process. The multipath $\tilde{\mathbf{H}}$ and direct signal $\bar{\mathbf{H}}$ components are added together to obtain the total channel matrix $\mathbf{H}$. . . . . 47
3.3 A comparison of the signal magnitude (linear units) of the random sequence generated to create the direct signal component in the urban user environment using a low-pass filter (top) and an autoregressive filter (bottom). . . . . 55
3.4 A comparison of the signal magnitude (linear units) of the random sequence generated to create the direct signal component in the urban user environment using (top) a combination of low-pass filtering and interpolating and (bottom) low-pass filtering only. . . . . 56

3.5 A comparison of the temporal autocorrelation of the random sequence generated to create the direct signal component in the urban user environment using (top) a combination of low-pass filtering and interpolating and (bottom) low-pass filtering only. The $1/e$ autocorrelation distance of the urban environment is 128m for the co-polarisation subchannels and 129m for the cross-polarisation subchannels. . . . . 57
3.6 Schematic diagram of the implementation of the smooth state transitioning process through the generation of Loo parameters and the interpolation for these parameters to the correct state duration. A state transition is identified by different consecutive values in the interpolated Loo parameters series. Where a transition occurs in the series of the mean of the direct signal $M_A$, a mean slop of 5 dB/m is applied and the Loo parameters series are changed accordingly. . . . . 59
3.7 Timeseries for a mobile unit travelling within the urban user environment (top) with a close up between 85 m and 110 m to show the improved smooth state transitions of the enhanced model (bottom left) compared with instantaneous state transitions of the original baseline model (bottom right). The received signal level is normalised with respect to the LOS power level in dB. . . . . 61
3.8 Autocorrelation of the signal as a result of FIR filtering. . . . . 70
3.9 Frequency response of the signal as a result of FIR filtering. . . . . 70
3.10 Autocorrelation of the signal as a result of IIR filtering. . . . . 71
3.11 Frequency response of the signal as a result of IIR filtering. . . . . 71
3.12 Timeseries for a mobile unit travelling within the suburban user environment (top) with the interpolated timeseries using multirate filters to produce samples at the require symbol rate (bottom). The two timeseries show good agreement. . . . . 75
3.13 Magnitude response of the linear filter (top), the polyphase filter (middle) and the multirate filter (bottom). . . . . 76
3.14 A comparison of the original spectrum of the series samples at $\sim 815$ Hz, plotted in black and the interpolated series at $\sim 5.87$ kHz plotted in blue achieved by using a linear filter (top), a polyphase filter (middle) and a multirate filter (bottom). It can be seen that all filters result in a raising of the level of the spectrum in the main band between -100 and 100 Hz. . . . . 77
3.15 A plot of outage capacity against SNR for a range of antenna XPD values in the open rural user environment. . . . . 80
3.16 A plot of outage capacity against SNR for a range of antenna XPD values in the suburban user environment. . . . . 80
3.17 A plot of outage capacity against SNR for a range of antenna XPD values in the urban user environment for bad states only. . . . . 81
3.18 A plot of outage capacity against SNR for a range of satellite elevation angles in the open rural user environment. . . . . 81
3.19 A plot of outage capacity against SNR for a range of satellite elevation angles in the suburban user environment. . . . . 82

3.20 A plot of outage capacity against SNR for a range of satellite elevation angles in the urban user environment. . . . . 82
3.21 A plot of outage capacity against SNR for a range of small-scale polarisation correlation coefficient values, with $\rho_{tx}$=$\rho_{rx}$, for the open rural user environment. . . . . 83
3.22 A plot of outage capacity against SNR for a range of small-scale polarisation correlation coefficient values, with $\rho_{tx}$=$\rho_{rx}$, for the suburban user environment. . . . . 83
3.23 A plot of outage capacity against SNR for a range of small-scale polarisation correlation coefficient values, with $\rho_{tx}$=$\rho_{rx}$, for BAD states only in the urban user environment. . . . . 84
3.24 (i) The MIMO advantage obtained in open, suburban and urban environments at 15dB SNR plotted against (i) antenna XPD, (ii) satellite elevation angle, (iii) small-scale polarisation correlation coefficient. . . . 87
3.25 A comparison of suburban user environment timeseries with various antenna configurations, (i) SISO (ii) 2x1 SIMO (iii) 2x2 dual polarised MIMO, assuming a transmission from a GEO satellite at $40^o$ with mobile velocity of 50km/ hr and implementing semi-Markov state transition modelling. The received signal level is normalised with respect to the LOS power level in dB. . . . . 89
3.26 The BER and 1% outage capacity in open rural, suburban and urban environments for SISO, 2x1 SIMO and 4x1 SIMO architectures. . . . . 91
3.27 A comparison of open rural, suburban and urban user environments with (i) Markov state transition modelling and (ii) semi-Markov state transition modelling. . . . . 93

4.1 Flow chart of the generalised stages in modelling the dual polarised LMS channel using a statistical model such as the Liolis-CTTC model. 100
4.2 Flow chart of the setting up and running of a simulation to model the dual polarised LMS channel using the QuaDRiGa model. . . . . 105
4.3 The virtual 100,000 km track followed by the mobile receiver in the simulation of the received signal in the urban environment using the QuaDRiGa model. Along this track a series of LOS and NLOS states are experienced by the received signal. This graph was produced with code supplied within the QuaDRiGa software package. . . . . 108
4.4 Cumulative Distribution Function of the LOS states in QuaDRiGa timeseries simulated in an urban environment with satellite elevation angle 35°- 45°and mobile velocity of 50 km/h. Normalisation is set to coincide the probability of 50% of the co-polarised signal with a signal magnitude of 0 dB. . . . . 109
4.5 Cumulative Distribution Function of the NLOS states in QuaDRiGa timeseries simulated in an urban environment with satellite elevation angle 35°- 45°and mobile velocity of 50 km/h. Normalisation is set to coincide the probability of 50% of the cross-polarised signal with a signal magnitude of -19 dB. . . . . 110

4.6 Timeseries for a mobile travelling within the urban user environment at 50 km/h generated with the Liolis-CTTC model (top), the Enhanced Statistical Model with Jakes Spectrum Doppler shaping through Sum of Sinusoids method (middle) and the QuaDRiGa model (bottom). XPD is set to 15dB. The signal level is normalised with respect to the LOS power level in dB. . . . . 112
4.7 Timeseries for a mobile travelling within the urban user environment at 50 km/h generated with the QuaDRiGa model with the position of state transitions marked with a dashed line and the distance travelled. . 115
4.8 Timeseries for a mobile travelling within the urban user environment at 50 km/h generated with the QuaDRiGa model with the position of state transitions marked with a dashed line at the distance travelled, the same simulated track is used for both plots. Top: number of scatterer clusters in LOS and NLOS = 1. Bottom: number of scatterer clusters in LOS and NLOS = 10 . . . . . 119
4.9 Timeseries for a mobile travelling within the urban user environment at 50 km/h generated with the Enhanced Statistical model with only the direct signal component plotted (top) and the entire channel matrix plotted (bottom) . . . . . 121
4.10 Timeseries for a mobile travelling within the urban user environment at 50 km/h generated with the Liolis-CTTC model (top), the Enhanced Statistical Model with Jakes Spectrum Doppler shaping through Sum of Sinusoids method (middle) and the QuaDRiGa model (bottom). XPD = 20dB . . . . . 123
4.11 Four plots showing the frequency response of the Enhanced Statistical Model with Jakes Doppler spreading (top left), the Enhanced Statistical with Asymmetrical Jakes Doppler spreading with a minimum frequency of -100 Hz and a maximum frequency of 80 Hz (top right). Also included for comparison are the frequency response of the Liolis-CTTC model (bottom left) and the QuaDRiGa model (bottom right). The four MIMO subchannels are plotted, i.e the two co-polarisation subchannels RHCP/RHCP & LHCP/LHCP and the two cross-polarisation subchannels RHCP/LHCP & LHCP/RHCP. XPD = 20dB . . . . . 125
4.12 The normalised frequency response of the Enhanced Statistical Model with 1) Jakes, 2) Asymmetric Jakes (fmin = -80Hz, fmax = 100Hz), 3) Flat, 4) Gaussian, 5) Jakes through Sum of Sinusoids method ($\chi$ = 1, $K_o$=0.99), 5) QuaDRiGa XPD = 15 dB and normalised . . . . . 126
4.13 Comparison of the Cumulative Distribution Function for the Enhanced Statistical model with Jakes Doppler Shaping, the Liolis-CTTC model and the QuaDRiGa model. XPD = 15dB . . . . . 129
4.14 Comparison of the Average Fade Duration in wavelengths for the Enhanced Statistical model with Jakes Doppler Shaping, the Liolis-CTTC model and the QuaDRiGa model. XPD = 15dB . . . . . 131
4.15 Comparison of the Level Crossing Rate in crossings per wavelength for the Enhanced Statistical model with Jakes Doppler Shaping, the Liolis-CTTC model and the QuaDRiGa model. XPD = 15dB . . . . . 132

4.16 EigenAnalysis: comparison of the eigenvalues obtained during good states for QuaDRiGa model, Liolis model, enhanced statistical model with Jakes Doppler shaping, all based on received signal within an urban environment. . . . . 134
4.17 Eigenvalue analysis: comparison of the eigenvalues obtained during bad states for QuaDRiGa model, Liolis model, enhanced statistical model with Jakes Doppler shaping, all based on received signal within an urban environment. . . . . 135
4.18 Good states co-polarisation subchannel distributions with comparison to Theoretical Loo distribution with the same average Loo Parameters for the QuaDRiGa model, Liolis-CTTC model and Enhanced Statistical model with Jakes Doppler shaping . . . . . 139
4.19 Bad states co-polarisation subchannel distributions with comparison to Theoretical Loo distribution with the same average Loo Parameters for the QuaDRiGa model, Liolis-CTTC model and Enhanced Statistical model with Jakes Doppler shaping . . . . . 139

5.1 Timeseries for a mobile travelling within the urban user environment at 50 km/h generated with the Liolis-CTTC model (top), the Enhanced Statistical Model with Jakes Spectrum Doppler (middle) and the MIMOSA data(bottom). The XPD in the Enhanced Statistical model is set to 10dB. The signal level is normalised with respect to the LOS power level in dB. . . . . 146
5.2 Close up of the timeseries from Figure 5.1 for a mobile travelling within the urban user environment at 50 km/h with the Enhanced Statistical Model (top) and the MIMOSA data(bottom). These timeseries show the improvement in the state transition process in the Enhanced model and the closer resemblance to real state transitions in the MIMOSA data. 149
5.3 Comparison of the state transitions in (a) the Liolis-CTTC model, (b) the Enhanced Statistical Model and (c) MIMOSA measurement data all showing a state transition sequence from good to bad to good. . . . 150
5.4 Comparison of the Cumulative Distribution Function for the Enhanced Statistical model with Jakes Doppler Shaping, the Liolis-CTTC model and the MIMOSA data for the urban user environment. . . . . 153
5.5 Comparison of the Average Fade Duration in wavelengths for the Enhanced Statistical model with Jakes Doppler Shaping, the Liolis-CTTC model and the MIMOSA data for the urban user environment, all three timeseries sampled with a sampling frequency equivalent to that of the MIMOSA timeseries, i.e. 4232Hz. . . . . 155
5.6 Comparison of the Level Crossing Rate in crossings per wavelength for the Enhanced Statistical model with Jakes Doppler Shaping, the Liolis-CTTC model and the MIMOSA data for the urban user environment, all three timeseries sampled with a sampling frequency equivalent to that of the MIMOSA data, i.e. 4232Hz. . . . . 157

5.7 Eigenvalue analysis: comparison of the eigenvalues obtained during bad states for the Enhanced Statistical model with Jakes Doppler Shaping, the Liolis-CTTC model and the MIMOSA data for the urban user environment. . . . . 159
5.8 EigenAnalysis: comparison of the eigenvalues obtained during good states for the Enhanced Statistical model with Jakes Doppler Shaping, the Liolis-CTTC model and the MIMOSA data for the urban user environment. . . . . 160
5.9 Four plots showing the frequency response in the urban user environment of the Enhanced Statistical Model with Jakes Doppler spreading (top left), the Enhanced Statistical with Flat Doppler spreading (top right). Also included for comparison are the frequency response of the Liolis-CTTC model (bottom left) and the MIMOSA data (bottom right). The four MIMO subchannels are plotted, i.e the two co-polarisation subchannels RHCP/RHCP & LHCP/LHCP and the two cross-polarisation subchannels RHCP/LHCP & LHCP/RHCP. The Doppler frequency is plotted as a function of the sampling frequency ($f_s$) which has different inherent values for the channel model simulators and real-life measurement data. . . . . 162
5.10 Timeseries for a mobile travelling within the suburban user environment at 50 km/h generated with the the Enhanced Statistical Model with Jakes Spectrum Doppler (top) and the MIMOSA data (bottom). The XPD in the Enhanced Statistical model is set to 10dB. The signal level is normalised with respect to the LOS power level in dB. . . . . 164
5.11 Comparison of the Cumulative Distribution Function for the Enhanced Statistical model with Jakes Doppler Shaping and the MIMOSA data for the suburban user environment. . . . . 166
5.12 Comparison of the Average Fade Duration in wavelengths for the suburban user environment for a mobile travelling at 50 km/h for Enhanced Statistical model with Jakes Doppler Shaping sampled at a frequency of 815 Hz and the MIMOSA data sampled at a frequency of 4232 Hz. . 168
5.13 Comparison of the Level Crossing Rate per wavelength for the suburban user environment for a mobile travelling at 50 km/h for Enhanced Statistical model with Jakes Doppler Shaping sampled at a frequency of 815 Hz and the MIMOSA data sampled at a frequency of 4232 Hz. . 169
5.14 Comparison of the spectra obtained for the timeseries of the Enhanced Statistical model with Jakes Doppler shaping (top) and the MIMOSA measurement data (bottom) for the suburban user environment. . . . . 171
5.15 Timeseries for a mobile travelling within the open user environment at 50 km/h generated with the the Enhanced Statistical Model with Jakes Spectrum Doppler (top) and the MIMOSA data (bottom). The XPD in the Enhanced Statistical model is set to 10dB. The signal level is normalised with respect to the LOS power level in dB. . . . . 173
5.16 Comparison of the Cumulative Distribution Function for the open rural user environment for the Enhanced Statistical model with Jakes Doppler Shaping and the MIMOSA data. . . . . 175

5.17 Comparison of the Average Fade Duration in wavelengths for the open user environment for a mobile travelling at 50 km/h for Enhanced Statistical model with Jakes Doppler Shaping sampled at a frequency of 815 Hz and the MIMOSA data sampled at a frequency of 4232 Hz. . . . 177
5.18 Comparison of the Level Crossing Rate per wavelength for the open user environment for a mobile travelling at 50 km/h for Enhanced Statistical model with Jakes Doppler Shaping sampled at a frequency of 815 Hz and the MIMOSA data sampled at a frequency of 4232 Hz. . . . . 178
5.19 Comparison of the spectra obtained for the timeseries of the Enhanced Statistical model with Jakes Doppler shaping (top) and the MIMOSA measurement data (bottom) for the open user environment. . . . . 180

# List of Tables

3.1 The number of times per 500 m simulation good and bad states are experienced and the typical distance travelled in each state type for Markov and semi-Markov state transition modelling. . . . . 92

4.1 The number of times per 100 km simulation good and bad states are experienced by the received signal and the typical distance travelled in each state type for the Enhanced Statistical and QuaDRiGa model, both simulated in an urban environment. . . . . 116

4.2 Probability given by the Kolmogorov-Smirnov (K-S) test and the Cramér Von Mises (CVM) that the distribution of the output of each model is statistically identical to the theoretical distribution generated by Loo parameter triplet derived from the timeseries of each model. Significance level, $\alpha = 0.1$. 137

A.1 Parameters assumed for the simulation of the 2x2 dual polarised MIMO-LMS channel. [1] . . . . . 189

A.2 Parameters for the probability transition matrix for the Markov chain and the mean and standard deviation of state duration for the semi-Markov chain in Nepers [2]. Good states are denoted with a 1, bad states are denoted with a 2. . . . . 190

A.3 Statistical parameters for the generation of the Loo parameter triplet for three user environments. 1 represents a good state and 2 represents a bad state. [2] . . . . . 191

A.4 1/e autocorrelation distances obtained by [3] from experimental data . . . . 192

# Abbreviations

| | |
|---|---|
| (A)DSL | (Asymmetric) Digital Subscriber Line |
| AoA | Angle of Arrival |
| AoD | Angle of Departure |
| ARTES | Advanced Research in Telecommunication Systems project |
| AWGN | Additive White Gaussian Noise |
| BER | Bit error rate |
| BC | Broadcast Channel |
| BS | Base Station |
| BPR | Branch Power Ratio |
| CDF | Cumulative Distribution Function |
| CR | Cognitive Radio |
| CSI | Channel State Information |
| CSIR | Channel State Information at the Receiver |
| CSIT | Channel State Information at the Transmitter |
| dB | Decibel |
| DoF | Degree of Freedom |
| DP | Dual Polarised |
| DPC | Dual Polarised Circular |
| DSL | Digital Subscriber Line |
| DSP | Digital Signal Processor |
| DTT | Digital Terrestrial Television |
| DVB | Digital Video Broadcasting |
| ESA | European Space Agency |

| | |
|---|---|
| EM | Electromagnetic |
| (F)FT | (Fast) Fourier transform |
| GEO | Geostationary |
| GNSS | Global Navigation Satellite Systems |
| HAP | High-Altitude Platform |
| HTS | Heavy Tree Shadowed |
| i.i.d. | Independent and Identically Distributed |
| ISI | Inter-Symbol Interference |
| ITS | Intermediate Tree Shadowed |
| ITU-R | International Telecommunications Union-Recommendations |
| LHCP | Left-Hand Circularly Polarised |
| LTI | Linear Time Invariant |
| LTV | Linear time Variant |
| LOS | Line-of-Sight |
| LMS | Land Mobile Satellite |
| LTE | Long Term Evolution |
| MiLADY | Mobile satellite channeL with Angle DiversitY |
| MIMO | Multiple-Input Multiple-Output |
| MIMOSA | MIMO channel for mobile SAtellite systems |
| MISO | Multiple-Input Single-Output |
| MSB | Mobile Satellite Broadcasting |
| MSHS | Mobile Satellite and High-altitude platform System |
| MU | Mobile User |
| NLOS | Non-Line of Sight |
| PDF | Probability Density Function |
| OFDM | Orthogonal Frequency Division Multiplexing |
| QAM | Quadrature Amplitude Modulation |
| QoS | Quality of Service |
| QPSK | Quadrature Phase Shift Keying |
| QuaDRiGa | Quasi Deterministic Radio channel Generator |
| RHCP | Right-Hand Circularly Polarised |

| | |
|---|---|
| RF | Radio Frequency |
| RMS | Root Mean Square |
| SER | Symbol Error Rate |
| SIMO | Single-Input Multiple-Output |
| SINR | Signal-to-Interference-plus-Noise Ratio |
| SNR | Signal-to-Noise Ratio |
| SISO | Single-Input Single-Output |
| SPC | Single Polarised Circular |
| SVD | Singular Value Decomposition |
| UT | User Terminal |
| VP | Vertical Polarised |
| XPC | Cross-Polar Coupling |
| XPD | Cross-Polar Discrimination |
| WINNER | Wireless World Initiative for New Radio |
| WLAN | Wireless Local Area Network |

# Notations and Symbols

| | |
|---|---|
| $\odot$ | Element-wise multiplication |
| $\otimes$ | Tensor product |
| $(\cdot)^*$ | Conjugate operator |
| $(\cdot)^T$ | Transpose operator |
| $(\cdot)^H$ | Conjugate transpose operator |
| $(\cdot)^{-1}$ | Inversion operator |
| $(\cdot)^\dagger$ | Pseudoinverse operator |
| $diag(\cdot)$ | Form a diagonal matrix from a vector argument |
| $det(\cdot)$ | Determinant of a matrix |
| $\lvert \cdot \rvert$ | Amplitude of complex number |
| $\lVert \cdot \rVert$ | $l_2$-norm/Euclidean Norm |
| $i$ | Imaginary unit |
| $j$ | Imaginary unit |
| $\mathbf{E}\{\cdot\}$ | Expectation operator |
| $\mathbb{C}$ | The set of complex numbers |
| $\mathbb{R}$ | The set of real numbers |
| $Re\{\cdot\}$ | Real part of a complex number |
| $Im\{\cdot\}$ | Imaginary part of a complex number |
| $Tr\{\cdot\}$ | Trace of a matrix |
| $\mathbf{I}_n$ | Identity matrix of size $n$ |
| $\mathbf{0}_n$ | Zero matrix of size $n$ |

# Chapter 1

# Introduction

## 1.1 Purpose of Thesis

The purpose of this research was to enhance the current knowledge of and research into the land mobile satellite (LMS) channel with an aim to produce an accurate and easy-to-use channel model and simulation tool for investigating and analysing transmissions in the LMS channel using dual polarised antenna. The channel model should accurately reflect the physical processes that occur in wireless signal propagation, specifically considering transmissions from space to the Earth and should allow for analysis of transmission metrics in various scenarios and conditions.

We are accustomed to the notion of a satellite transmitting data to Earth, for example, many people will have used satellite television at home, used a Global Navigation Satellite Systems (GNSS) navigation system whilst driving or perhaps, although less likely, they may have used satellite radio in their car, a satellite phone to make a phone call from a remote area or used a phone or internet terminal on a ship at sea. These various examples of satellite transmissions introduce the idea that sometimes the receiver on Earth may be a fixed terminal, such as a home-based satellite TV receiver, or the receiver may be a mobile device, such as a satellite telephone. This research primarily focusses on transmissions from a satellite to a mobile terminal. In this scenario, we refer to the person on Earth receiving data from the satellite as the

user and we refer to the communications channel through which information is sent from the satellite to the user as the land mobile satellite channel. The LMS channel therefore describes a specific communications scenario in which a satellite in orbit around the Earth transmits data to a user with a mobile receiver on Earth.

In developing satellite systems we seek to create effective and efficient communications systems. The interaction between satellites, ground based segments or relays and the user must be thoroughly investigated through the process of channel modelling. Channel modelling also allows us to explore the application of new technologies in satellite systems and explore the potential of implementing new hardware or software components.

This research focusses on a specific channel in which a transmission occurs from a satellite directly to the user's mobile device. Although the specific application of the mobile device is not considered, we may assume that the device is receiving a broadcast signal from the satellite. As we are interested in a mobile scenario, we may consider the user is moving at a speed up to that typical of a moving car. In addition to this, the application of dual polarised antenna at the satellite and on the user's mobile receiver is explored. The application of dual polarised antenna is of interest as they allow the application of multiple-input multiple-output (MIMO) techniques in a satellite scenario. It is critical to explore if satellite systems can achieve similar gains to terrestrial systems that incorporate MIMO techniques and building a realistic, accurate and easy-to-use channel model will facilitate such research.

## 1.2 Purpose of Channel Modelling Research

Channel modelling is a crucial step in the design of communications systems. Different channels have unique challenges and accurate channel models allow designers and engineers to test and assess the impact of any aspect of a communication system including new hardware such as antenna, new protocols and various networking strategies. Considering the high cost of satellite deployment, simulations of the propagation environment are particularly important, as in-situ testing is too expensive.

The development of accurate models to simulate the land mobile satellite (LMS) channel is vital to provide tools for system design and performance analysis. There are a number of modelling approaches that may be used in the LMS context each offering a trade-off between accuracy and complexity/simulation time. Statistical models [1], [4] provide the benefits of low simulation time and are adequate in determining narrowband channels. Deterministic models[5] using ray-tracing algorithms or asymptotic methods provide more accurate wideband simulations for more complex scenarios such as Global Navigation Satellite Systems (GNSS), however they are time-consuming both in terms of creating the model and using the model for simulation. Hybrid physical-statistical approaches [6], [7] also exist which aim to offer low complexity and high accuracy.

At present two types of model are particularly popular in the simulation of the dual polarised LMS channel. The first is statistical models, these models have the benefit of low complexity and reduced simulation time. A 'versatile' two-state LMS model comprising of good and bad states with state transitions determined by either a Markov or semi-Markov chain is proposed in [2]. The model was adapted in [1] to include polarisation diversity techniques and produce the Liolis-CTTC model . The Liolis-CTTC model is further developed in this research to create the Enhanced Statistical Model [8], this model includes a number of extensions to the original statistical model including Doppler effects and smooth state transitions.

The second type of model is a geometric stochastic channel model that uses statistical ray-tracing and is developed from the analysis of data from the MIMO channel for mobile SAtellite systems (MIMOSA) measurement campaign. The Quasi Deterministic Radio channel Generator (QuaDRiGa) [7] is an evolution of the Wireless World Initiative for New Radio (WINNER) model for terrestrial radio [9]. A mobile receiver can be simulated to travel through the environment on a random path or a determined path. User environments are simulated that contain clusters of scatterers and the received signal is calculated from the addition of the reflected components from each scatterer cluster.

## 1.3 Research Context

Current state-of-the-art research follows parallel strands of advancements and improvements in channel modelling approaches and measurement campaigns which further inform channel model development. Research covers a wide range of areas and applications including but not limited to coverage for outdoor mobile devices for pedestrians using low frequency bands, coverage for indoor passengers on fast-moving trains using higher frequency bands, transmissions to aeronautical & nautical vessels and global satellite positioning services. Research not only involves producing accurate channel models and measurement campaign but also aims to develop transmission strategies, modulation schemes, signal processing techniques, networking strategies and to include advancements in hardware and technology.

Within the area of L-band or S-band research, channel models focus on a number of key modelling aspects, including state transitions, state duration and quantifying the impact of the environment on signal propagation. Narrowband models are typical as the LMS channel is considered not to be frequency selective and this assumption aids simplification of the modelling process without loss of accuracy. Narrowband models are presented in [1], [10], [11], [12].

In [13] a comprehensive list of measurement campaigns and channel models for multi-antenna satellite systems is presented. This provides an overview of diversity through dual polarisation MIMO, multi-satellite MIMO, and hybrid terrestrial-satellite systems and highlights the need for general, standardised measurements and validated models.

The characteristics of a three-state Markov and Loo distribution single-input single-output (SISO) LMS channel model are described in [14] which contains LOS, moderate shadowing and deep shadowing conditions. Also, channel measurements of an S-band LMS channel are presented to determine state probabilities and state transition probabilities for open, suburban, intermediate tree shadowed (ITS), heavy tree shadowed (HTS) and urban environments through a range of satellite elevation angles from 40°to 80°. Other parameters are derived from the data, including state duration, duration

of state transitions, parameters for determining the Loo distribution and intra-state correlation lengths.

In [4] a statistical model of the SISO LMS channel is presented which includes parameters to generate Loo distribution parameters and Markov chain parameters in L-band, S-band and Ka-bands and compare narrowband with wideband scenarios assuming the multipath component excess delays are exponentially distributed and including the analysis of instantaneous power delay profiles. The parameters are derived from a number of data sets including those obtained by the University of Bradford, DLR, IAS Gras and the University of Surrey.

A general shift towards channel models with two-states as opposed to three-states occurs within the SISO LMS context. In [2] a two-state SISO LMS model with Loo distribution and both semi-Markov and Markov chains is presented with versatile good and bad states that describe the variations in the received signal. Parameters are derived from data sets in S-band and L-band. This model shows better agreement with measurement data sets than previous three-state models.

Early dual polarised MIMO LMS channel models are based on the extension of SISO LMS models to include MIMO dimensions. A statistical two-state MIMO Markov model with Loo distribution is proposed in [1] and 1% outage capacity for a 2.2 GHz S-band LMS channel for open, suburban and urban environments are presented. This paper consolidates validated SISO LMS concepts and dual-polarisation concepts to produce a dual polarised MIMO LMS model with a simple to follow simulation method. It builds on the work of [14], [2] & [3]. A measurement of the dual polarised MIMO LMS channel is conducted in [3] and a subsequent narrowband channel model is presented with large-scale and small-scale correlation coefficients between MIMO channels derived from measurements of different environments.

The benefits of dual polarised MIMO in LMS channels are demonstrated in [15] by analysis of ergodic capacity of a dual polarised MIMO channel with Rician distribution, the authors find using dual polarised antennas provides 1.5 dB power gain

in high signal-to-noise ratio (SNR) scenarios compared with using non-polarised antennas. The authors of [16] also assess the capacity benefits of dual-polarisation per beam.

In [17] a two-state narrowband SISO LMS is proposed for a single-satellite configuration in S-band using parameters from the satellite diversity focussed Mobile satellite channeL with Angle DiversitY (MiLADY) measurement campaign. An improved approach to modelling the Loo distribution is proposed by analysis of the mean of the lognormal signal's relationship to state length. In addition a Doppler shift is applied through a Butterworth filter.

The MIMO channel for mobile SAtellite systems (MIMOSA) campaign provides the data for the Quasi Deterministic Radio channel Generator (QuaDRiGa) model [7], a geometric stochastic channel model that uses statistical ray-tracing for wideband and narrowband channels. The QuaDRiGa model is an evolution of the Wireless World Initiative for New Radio (WINNER) model for terrestrial radio and allows for varying speed of the mobile terminal, antenna parameters customisation and geometric polarisation modelling.

Wideband models are also presented in [18] and in [7] an evolution of the WINNER model is presented which encompasses narrowband and wideband models.

## 1.4 Methodology and Scope of Research

The objective of the research was to create a robust and realistic model of the LMS channel using dual polarised antenna that was suitable for use in a range of user environments. It was intended to produce a model to use as a simulation tool to generate a timeseries and allow analysis of the signal level with the ability to manipulate parameters to investigate a range of scenarios and user environments

It was observed after extensive review of the current literature of the research in this topic that a gap existed in which a full channel model for dual polarised LMS transmissions was needed. It was observed that research into this particular channel

was valid as use of dual polarised LMS transmission may be incorporated into existing satellite systems and may provide solutions to particularly remote or challenging circumstances in which people may need access to a communication system.

To achieve this goal a simple statistical model was used as a framework for development and enhancement into which various improvements were incorporated. Areas within the model were identified that were limited or could be improved upon to increase the model's reliability. Extensive research of models of various satellite channels and also of dual polarised transmissions in terrestrial setting yielded knowledge of area for improvement. The major contribution of the thesis is in applying Doppler shaping to the received signal in the channel model. Doppler effects are significant in the diffuse multipath component of the received signal and correct modelling of the Doppler effects is important in achieving an accurate model.

Validation of the new model was achieved through comparison with two widely accepted models of the dual polarised LMS channel, i.e. the statistical Liolis-CTTC model and the more complex geometric stochastic QuaDRiGa model. The agreement between the models was explored through statistical analysis of the timeseries output of each model. In addition to this the new model's output was also compared to real channel measurements taken from the European Space Agency's (ESA) MIMOSA measurement campaign. The enhancements to the model clearly improve the reliability of the model and further validate the model.

It is the aim of this research to provide a simulation tool useful for investigating applications of the dual polarised LMS channel through simulation of signal processing techniques and transmission schemes.

## 1.5 Contributions

This thesis aims to expand upon current channel models that exist in literature, for example, [1] & [19] and include some essential components to create a more realistic dual polarised LMS channel simulation tool.

The specific contributions to the process of channel modelling are:
(i) An enhanced statistical model is presented incorporating a number of important characteristics of the dual polarised LMS channel. These include:

- introducing Doppler effects including Doppler shaping of the fast variations for more realistic simulation of the channel and the spectrum of the received signal
- implementing a smooth semi-Markov state transition process for improved modelling of state transitions
- a temporal correlation process on the slow variations which does not create the unwanted high frequency components associated with low-pass filtering of the slow variations
- implementing an interpolation process to sample the channel at the required sub-symbol rate for transmission to allow simulation of different coding techniques

(ii) In addition to these contributions the thesis also includes a comparison with experimental measurement data enabling validation of the model and critical analysis of the enhancements within the model.

## 1.6 Structure of Thesis

The structure of this thesis is as follows:

*Chapter 2:* This chapter introduces the land mobile satellite channel with the application of dual polarised MIMO for the purpose of increased diversity and spectral efficiency. The characteristics of the dual polarised MIMO LMS channel are described along with the different modelling approaches used to simulate the LMS channel and generate a timeseries to facilitate analysis of the channel.

*Chapter 3:* The Enhanced Statistical LMS model is described with step-by-step instructions for modelling and simulation. The model includes a number of enhancements to the current baseline statistical model approaches in literature including

Doppler shaping of the fast variations, the implementation of a smooth state transition process and also the introduction of an interpolation process to sample the channel at the required sub-symbol rate for transmission.

*Chapter 4:* Two current state-of-the-art channel models are introduced, the statistical Liolis-CTTC model and the geometric QuaDRiGa model. An extensive analysis of the timeseries output of the Enhanced Statistical model is conducted and presented in addition to a comparison between the results and those of the Liolis-CTTC model and the QuaDRiGa model.

*Chapter 5:* Details of the MIMOSA measurement campaign are given from which real measurements of the dual polarised LMS channel were obtained and used for comparison and analysis of the models. Analysis of the timeseries output of the Enhanced Statistical model is conducted and the model is validated through comparison with measurement data from the MIMOSA campaign.

*Chapter 6:* The thesis concludes with an outline of the future work intended by the author and a summary and discussion of the implications of this body of research and the conclusions derived from it.

## 1.7 Publications

### 1.7.1 Conference Proceedings

Below is a list of publications that have been included in various conference proceedings and are available on the Institute of Electrical and Electronics Engineers (IEEE) Xplore Digital Library.

- "An Enhanced Statistical Model for the Dual Polarised MIMO Land Mobile Satellite Channel", F. Ní Mhearáin, M. Sellathurai and F. Pérez Fontán. Included in the proceedings of The 8$^{th}$ European Conference on Antennas and Propagation, 6-11$^{th}$ April 2014, The Hague, The Netherlands, pp. 1 - 5.

- "A Comparison of Precoding Techniques for the Dual Polarised Land Mobile Satellite Channel", F. Ní Mhearáin, M. Sellathurai and C. Mastouros.
  Included in the proceedings of The 7$^{th}$ Advanced Satellite Multimedia Systems Conference and the 13$^{th}$ Signal Processing for Space Communications Workshop, 8-10$^{th}$ September 2014, Livorno, Italy, pp. 32 - 36.

- "A Comparison of Statistical and Geometric Models for the Dual Polarised MIMO Land Mobile Satellite Channel", F. Ní Mhearáin, M. Sellathurai and F. Pérez Fontán
  Included in the proceedings of The 81$^{st}$ IEEE Vehicular Technology Conference, 11-14$^{th}$ May 2015, Glasgow, Scotland, pp. 3031 - 3035.

# Chapter 2

# The Land Mobile Satellite Channel

## 2.1 Introduction

This chapter describes general characteristics of the land mobile satellite (LMS) channel, i.e. the channel that comprises transmissions from a satellite to a mobile device on Earth. The key physics concepts that effect LMS transmissions are described and their inclusion in the channel modelling process is explored in addition to any assumptions that are typically made when modelling this particular communications channel.

One of the main characteristics of the LMS channel is the effect of shadowing and blockage on the signal travelling from the satellite to the user which leads to different categories of signal reception. Shadowing and blockage occur due to objects in the user environment causing the signal reception to change as the mobile receiver moves thus creating different signal level 'states'. A description of how to model different states is included by considering different rates of variation within the signal. Markov and semi-Markov chains are described and how they can be used to model the mechanism of changing from one state to another state within the model. In addition, aspects of the channel that lead to correlation in time and frequency are considered and common statistical distributions that describe the dynamic range of the received signal are outlined.

### 2.1.1 The Role of Satellites in Communication Systems

The role of satellites has become a major component of the European telecommunications industry. This is highlighted by the work of a number of organisations seeking to improve and develop European telecommunication infrastructure. For example, The European Space Agency (ESA) collaborate with third parties to support research and development within the telecommunications sector with a focus on satellite based services through the Advanced Research in Telecommunication Systems project (ARTES) [20]. Some of the projects within this initiative provide the bases of the research presented in this thesis and have promoted satellite research in academic contexts, for example the Characterisation of the MIMO Channel for Mobile Satellite Systems project (MIMOSA) [21] and the Mobile Satellite Channel with Angle Diversity project (MiLADY) [22], both projects will be discussed in more detail in Chapter 5.

Satellites were first used in telecommunications for remote telephone calls and transatlantic television broadcasts in the 1960's, since then their applications have diversified to provide a range of high speed, multimedia services for technologically advanced consumers, as well as providing global navigation system, earth observation systems and emergency response systems. A range of frequency bands exist which are specifically suited to different types of transmission and services.

Telecommunication transmissions involving satellites have an extremely high cost associated with them in comparison to Earth-based transmissions, due to the cost in the deployment of satellite technologies. However despite this obvious disadvantage in using satellite architectures for telecommunication systems, there are a number of scenarios that may make using a satellite system the best or only choice for telecommunications service providers. Some of the major advantages of using satellites in the deployment of telecommunication services include the ability of satellites to provide service coverage for extremely large areas and also being able to provide service in remote and otherwise isolated areas enabled by their very high vantage point in comparison to terrestrial transmitters.

According to [23], 28.7% of the population of Europe in rural areas does not have access to Internet services through digital subscriber loop (DSL) cables. Using satellite systems not only allows for isolated users to access a broadband internet connection when an alternative method might not exist but it also enables aeronautical and maritime users to access communication systems and furthermore enables fast and temporary connections for the likes of emergency services and off-site news reporting teams [24].

The main challenge facing satellite systems is whether they can guarantee the Quality of Service (QoS) customers expect based on their experiences of terrestrial services at an acceptable cost. However, as [24] explains, the poor perception of satellite systems in the past which arose due to delay and latency[1] has improved with advancements in technology and these issues are not significant except for highly interactive services such as video and voice.

The specific challenges facing a satellite system depend on a number of factors including location, the frequency band employed and whether a fixed or mobile receiver is used. Higher frequency bands such as Ku, K & Ka bands and above are susceptible to fading due to weather conditions and effects of the troposphere, this can be reduced by the use of lower frequency bands such as L and S bands although this has implications for the type of application the link can be used for. Also, systems can be designed to minimise the effects of fading using power margins and power control built into the link [24]. Satellite systems must also satisfy diverse receiving scenarios with a broad range of receiving devices employed, for example, having a large coverage area, providing good indoor and outdoor reception and the use of portable devices with adaptability to a range of user speeds from walking speed to high speed transport [23].

Satellites play a major role in a number of Digital Video Broadcasting (DVB) technical standards. Standardisation documents include DVB-Satellite Services to Handheld Devices (DVB-SH) [25], a standardisation of satellite transmissions of audio, video

[1] Latency for a satellite system is 240-280 ms

and data services to vehicles and handheld devices. This standard includes the DVB-Return Channel Satellite (DVB-RCS) to provide standardisation of two-way satellite broadband services with an extension for mobile devices (DVB-RCS+M). Also of importance within the terrestrial context is the standardisation for DVB - Next Generation Handheld (DVB-NGH) within which one of the major focuses is the suitability of multiple-input multiple-output (MIMO) architecture for handheld mobile devices. It is considered that MIMO may be implemented provided it provides a gain over the single-input multiple-output (SIMO) implementation currently used within DVB-SH and DVB-Terrestrial (DVB-T) standards and also if it can be successfully introduced using current receive and transmit infrastructure [26].

### 2.1.2 Fixed and Mobile Satellite Channels

Satellite transmissions can be categorised according the mobility of the receivers, i.e. transmissions from a satellite to a fixed terminal or transmissions from a satellite to a mobile terminal. Fixed mobile terminals have a number of advantages over mobile terminals, for example, they can be positioned at an ideal location where weather conditions are favourable and without nearby objects to reflect or interfere with the signal. Due to their static nature, fixed terminals can be large structures and also can be directed towards the transmitting satellite at all times. Highly directive antenna can be used allowing for the use of frequency reuse schemes to increase the spectral efficiency of the systems. Fixed services may also use frequency schemes in the region of 10-40 GHz. The use of Ku, K & Ka bands relieves some of the pressure on lower frequency bands such as L and S bands. The key issue in fixed terminal transmissions at these higher frequencies is the effect of the ionosphere and troposphere on the signal as it propagates through the atmosphere. Tropospheric effects such as rain and attenuation due to gasses are significant at higher frequencies but negligible at L-band and S-band [27]. The ionosphere causes an effect on electromagnetic waves travelling through it, the Faraday effect [28] , which acts to depolarise linear polarised waves. This is significant in systems employing linear polarisation as it can cause polarisation rotation of up to 48° in L-band transmissions [27] and polarisation-tracking equipment

must be employed to overcome the effects. Faraday rotation can be avoided by using circular polarisation, thus the phase of the wave is affected but not the polarisation.

The atmosphere also affects signals travelling to mobile terminals in the same way; however, the mobile user environment has a more significant detrimental effect and dominates the attenuation of signals to mobile terminals. In mobile systems, unlike fixed systems, a direct line-of-sight (LOS) link to the satellite is not guaranteed and therefore the received signal may often consist solely of reflections from objects near the receiver antenna, i.e. multipath components. Despite the difficulties involved in transmitting to mobile terminals, it is becoming an ever increasingly popular demand from consumers of digital services who are passengers and travellers on trains, ships and vehicles, in addition to consumers who are pedestrians with hand-held devices. In recent years, there has been a huge change in consumer expectations in relation to services relating to television and streaming on mobile devices. There has been a shift from television services on mobile devices being a novelty and perceived as a luxury to being a daily activity regarded as an essential feature of a mobile device. Satellites can provide a role in delivering this type of service in some circumstances where terrestrial based services can't deliver.

## 2.2 Characteristics of The LMS Channel

### 2.2.1 Physics Affecting the Propagating Signal

The dual polarised LMS channel under consideration in this project consists of S-band transmissions at $\sim 2.2\,\text{GHz}$ from a geostationary (GEO) satellite to a mobile user (MU) device on the Earth. The transmitted signal will propagate through space freely with the attenuation of the signal solely the result of free space path loss (FSPL) in which the attenuation is proportional to the squared distance between the transmitting and receiving antenna. This attenuation will be significant considering the vast distance between the antenna on the satellite and on the Earth.

When the transmitted signal reaches the Earth's atmosphere, it becomes subject to many physical phenomena. As described in the previous section, the set-up in most LMS channels aims to minimise the effects of the atmosphere through the low frequency of the carrier signal in S-band.

When the transmission reaches close to the surface of the Earth, the natural and artificial features that exist in the environment surrounding the user can have a major detrimental effect on the propagating signal. Large natural objects such as mountains and hills can cause the signal to be shadowed and thus attenuate the signal. Artificial objects such as high buildings can completely block the path of the propagating signal thus causing it is be reflected. If a signal is incident on the edge of a building, it may diffract around the edge of the building or between gaps between buildings. Smaller objects in the user environment such as trees, cars, telephone posts and people may also affect the signal, causing reflection, refraction and diffraction to occur many times before the signal is finally received by the user. These interactions may result in the signal being split into many components, each following a different propagation path to the user, these components are called multipath components. The received signal may be composed solely of diffuse multipath components if no direct link between the satellite and the user exists. The propagation paths of multipath components may have significantly different lengths thus resulting in a high amount of dispersion in the received signal as received symbols are spread out over time. Each time the signal interacts with an object in the user environment the signal may be altered and attenuated thus resulting in a particular level of signal reception which depends on the signal propagation path between the satellite and the user at that particular time, this may be a good reception with a high signal power and low multipath or may be a bad reception with low signal power and high multipath. In addition, the path of the signal is continuously changing as the user is mobile and moves throughout the environment, thus the reception changes between good and bad segments called states.

The received signal is categorised according the quality of the reception and user environments are categorised according to their geographical nature and the amount of

obstacles and scatterers they contain. This research focuses on open rural, suburban and urban user environments, although this list is not exhaustive and can be extended to include other user environments, for example, roadside trees or intermediate tree-shadowed (ITS). ITS is considered the worst propagation environment for satellite transmissions due to periods of deep shadowing and multipath from trees [29]. The majority of the focus in this thesis is on the urban environment as simulation parameters are more readily available in literature for this environment for the models investigated in this thesis. The urban environment is a very challenging environment for signal propagation which is particularly useful and interesting to investigate, it may have periods of complete signal obstruction and create high multipath components in the received signal.

### 2.2.2 How to Model the Physical Effect on the LMS channel

The following sections outline the generalised modelling techniques used and the assumptions made in order to create a statistical channel model that effectively recreates the physical effects on the propagating signal in the LMS channel. This includes the dispersion of the signal over time due to the multipath components in Section 2.2.3, the correlation in the signal due to the states which define the quality and power of the received signal in Section 2.2.4, how to mathematically model the changes in these states according to the movement of the user and the mobile receiver in Section 2.2.5. Statistical methods for modelling the magnitude and the dynamic range of the signal power in described in Section 2.2.6. The method of modelling the LMS channel through creating a direct signal component and a multipath component is discussed along with the modelling of the Doppler effects on each of these signal components in 2.2.8.

### 2.2.3 Time Dispersion

The time dispersion of a channel is an important factor in the modelling process and affects whether the channel is considered to be a narrowband or wideband channel.

If the channel has a large delay spread this means the multipath components arrive at the receiver over a large time delay and gives rise to a wideband signal. The modelling of a wideband channel involves creating individual multipath components and summing them using a tapped-delay line for each component. Wideband models have been proposed for the LMS channel [3] and some areas of research in which they are important are 21 and hybrid satellite and terrestrial systems that use High Altitude Platform (HAP) systems. In this scenario, because the HAP transmitter is located within the Earth's atmosphere, scatterers in the atmosphere cause reflections and create multipath components. A wideband channel will have a high level of diversity associated with it resolved using signal processing algorithms at the receiver.

Frequently in the modelling of the LMS channel, it is assumed that the channel is narrowband with a small time delay associated with the channel. This assumption has a number of advantages. Firstly, it reflects the fact that in a satellite system where the transmitter is outside of the Earth's atmosphere, the majority of the path along which the propagating signal travels from the satellite is in space and therefore free from scatterers. With an absence of scatterers, few multipath components are created. It is only when the signal reaches the user environment that multipath components are created through interactions between the signal and objects in the user's immediate vicinity. However, we also have to accept that there is a disadvantage when considering the lack of scatterers in the vicinity of the transmitter causes a reduction in the diversity within the channel that will lead to a limit on the gain we can achieve through MIMO techniques. Secondly, the assumption allows us to model a flat fading channel across all frequencies and we don't have to incorporate signal processing techniques at the receiver to resolve the signal.

### 2.2.4 Rates of Signal Variation

When the received signal is analysed the rate of change in the signal can be classified into three types of variation: fast, slow and very slow. The size of the variation in the signal amplitude depends on the size of the object that causes the fading

effect. For example, if we consider a signal received in an urban environment, there may be very slow variations in the signal amplitude that are caused by very large objects such as distant hills or very large buildings. There may also be slightly faster variations which have a smaller effect on the amplitude and are superimposed upon the very slow variations, these might be caused by large objects such as trees and houses. When the user moves past one of these objects the signal may be partially blocked for a period of time resulting in an attenuation of the signal. Finally, fast variations will also be experienced by the signal, these are small-scale effects and they are caused by multipath reflections and scattering caused by the objects which are close to the mobile such as people, cars, telephone boxes, etc. The received signal can be classified into one of three categories depending on the amount of shadowing it experiences [19]. Line-of-sight (LOS) propagation occurs when there is a direct transmission link between the transmitter and the receiver and there is no shadowing effect on the signal. When a direct LOS does not exist, the signal may be shadowed or blocked. Shadowed propagation occurs when the signal is partially obstructed. Blocked propagation occurs when the signal is completely obstructed.

### 2.2.5 States

As described in the previous sections, a transmitted signal can be considered as being unblocked, partially blocked or completely blocked. This description has allowed for the classification of the received signal into three types of states, see Figure 2.1.

Transitions between these states have previously been modelled using a three-state Markov chain [4]. However, a recent model proposed by Prieto-Cerdeira et al. [2] has reduced the number of available states by simplifying the three previous states of LOS, moderate shadowing and deep shadowing to two states, i.e. good and bad. These good and bad states do not necessarily match LOS and non-LOS (NLOS) conditions but may encompass a wide range of possible states between these two extreme conditions. A two-state first-order Markov chain model may be used to determine the transitions between good and bad states.

A first-order Markov chain is a stochastic process that can take on a number of discrete states where the probability of being in each state depends only on the previous state [2]. Thus a random walk can be generated through good and bad states; the transitions between states are determined by a state transition probability matrix **[P]** and a state probability matrix **[W]**. The probability of a transition occurring from state-$i$ to state-$j$ is given by probability matrix element P$ij$ [14]. The convergence property of the Markov chain is defined by :

$$[\mathbf{W}] = [\mathbf{W}][\mathbf{P}] \tag{2.1}$$

The length of time spent in a state is determined by state frame $L_{frame}$, which has been observed in experimental data of S-band measurements to be around 3-5 m [1]. Therefore, a new state will be entered every time the mobile user terminal (UT) travels a distance of around 5 m. The type of state entered depends on the probability matrix, the elements of which have been determined from experimental data.

The probability of entering a good or bad state is strongly influenced by the geographical environment of the user. For example, bad states are more probable in an urban environment as opposed to a suburban or an open rural environment. As the probability of entering and remaining in a bad state is highest in an urban area and the probability of entering and remaining in a good state is highest in an open rural area, the probability matrices used to determine the Markov chain random walk through the states are different for each user environment. In [2] the authors provide extensive measurement derived parameters to allow for the simulation of a Markov chain for different environment classifications at various satellite elevation angles.

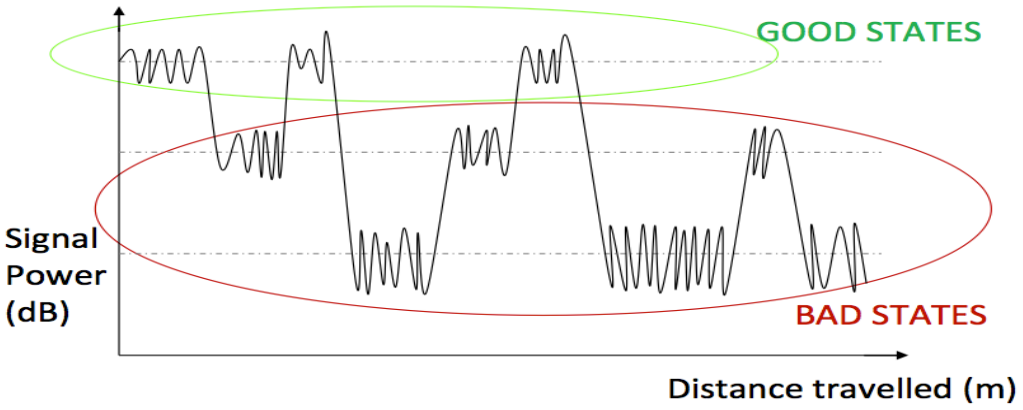


FIGURE 2.1: Diagram showing the variation arising in signal power as the mobile unit travels through the user environment and how a three state classification model compares to a two state classification model with 'good' and 'bad' states.

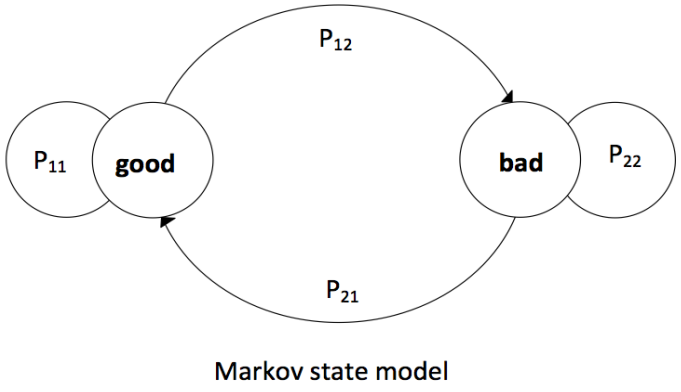


FIGURE 2.2: State diagram for a two-state Markov chain.

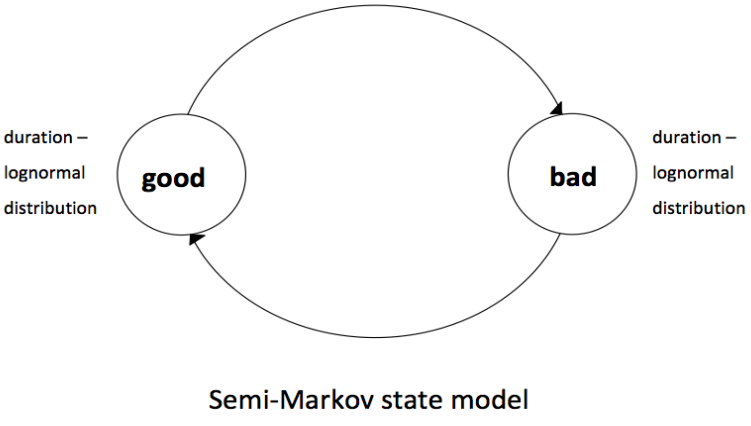


FIGURE 2.3: State diagram for a two-state semi-Markov chain.

In [2] a semi-Markov model is also proposed in which states are occupied for a particular time duration before making a transition to the next state type. The state durations are ruled by lognormal distribution parameters and it is suggested by the authors that this model may give more realistic state durations than the Markov chain model.

### 2.2.6 Statistical Distributions

The Rayleigh distribution model and the Rice distribution model are particularly popular fading models used to describe the probability of the received signal in a wireless channel. The key difference between these two distributions is whether or not a LOS component exists in the received signal.

The Rayleigh distribution is considered a worst-case scenario where the direct signal is completely blocked and the entire signal is comprised of multipath components [27]. The envelope of the of the signal will be given by Equation (2.2):

$$f(r) = \frac{r}{\sigma^2} \exp\left(-\frac{r^2}{2\sigma^2}\right) \text{ for } r \geq 0 \tag{2.2}$$

where $r$ is the received signal and $\sigma$ is the power of the multipath components.

The Rice distribution allows for the modelling of a signal subject to fading when the direct signal is partially blocked or not blocked [27]. It considers the amplitude of the direct signal $a$, which is allocated a value between 0 and 1. The value is 0 if the signal is completely blocked, or 1 of the signal is completely unblocked and unscattered. Therefore, the Rice distribution contains within it the Rayleigh distribution in the circumstance $a$=0. The envelope of the signal will have a PDF given by Equation (2.3):

$$f(r) = \frac{r}{\sigma^2} \exp\left(-\frac{r^2 + a^2}{2\sigma^2}\right) I_0\left(\frac{ar}{\sigma^2}\right) \text{ for } r \geq 0 \tag{2.3}$$

where $r$ is the received signal, $a$ is the direct signal power, $\sigma$ is the power of the multipath components and $I_0$ is modified Bessel function of the first kind and zero order.

The $k-factor$ [27] (also referred to as the Rice factor) is commonly used in the Rice distribution as a measure of the ratio of the power in the dominant LOS path to the power of the scattered multipath components given in Equation (2.4):

$$k = \frac{a^2}{2\sigma^2} \tag{2.4}$$

The Rice distribution can be interpreted in two ways [30]. The power of the direct signal component $a$ can be fixed while the total power varies due to the contribution of the multipath power $\sigma$. Alternatively, it can also be considered that the total power of the received signal is fixed and the powers of $a$ and $\sigma$ vary.

### 2.2.7 Joint distributions

Single distributions such as a Rayleigh or Rice distribution are not sufficient in the LMS context to adequately to describe the full dynamic range of the received signal. For the LMS channel a joint statistical distribution is required. The most popular of these distribution combinations is the Loo distribution [31], which incorporates Rice and lognormal distributions.

#### 2.2.7.1 The Loo Model

The Loo distribution models the amplitude of received signal as being Rician if we consider a very short time frame where the direct signal amplitude ($a$) is constant [27]. The Rician distribution is given by Equation (2.5):

$$f(r|a) = \frac{r}{\sigma^2} \exp\left(-\frac{r^2+a^2}{2\sigma^2}\right) I_0\left(\frac{ar}{\sigma^2}\right) \text{ for } r \geq 0 \tag{2.5}$$

For longer sections of received signal, the direct signal component ($a$) is lognormally distributed with two parameters controlling the distribution, the mean ($M$) and the standard deviation ($\Sigma$), which may be expressed in Nepers, Equation (2.6), or in Decibels, Equation (2.7). The factor 8.686 arises due to the conversion factor for Nepers (Np) to Decibels (dB).

$$f(a) = \frac{1}{\Sigma_{\mathrm{Np}} a\sqrt{2\pi}} \exp\left[-\frac{ln(a) - M_{Np}^2}{2\Sigma_{Np}^2}\right] \tag{2.6}$$

$$f(a) = \frac{8.686}{\Sigma_{\mathrm{dB}} a\sqrt{2\pi}} \exp\left[-\frac{20\log a - M_{dB}^2}{2\Sigma_{dB}^2}\right] \tag{2.7}$$

The probability distribution function of the received signal for a single state can be found using Equation (2.8) by combining Equations (2.5) and (2.6):

$$f(r) = \frac{8.686\, r}{\sigma^2 \Sigma_{\mathrm{dB}}\sqrt{2\pi}} \times \int_0^\infty \frac{1}{a} \exp\left[-\frac{(20\log a - M_{\mathrm{dB}})^2}{2\Sigma_{\mathrm{dB}}^2} - \frac{r^2 + a^2}{2\sigma^2}\right] I_0\left(\frac{ra}{\sigma^2}\right) da \tag{2.8}$$

It is often common to see this formula in literature [1] given with parameters in Nepers as in Equation (2.9), found by combining Equations (2.5) and (2.7):

$$f(r) = \frac{r}{b_0\sqrt{2\pi d_0}} \times \int_0^\infty \frac{1}{a} \exp\left[-\frac{(ln\, a - \mu)^2}{2d_0} - \frac{r^2 + a^2}{2b_0}\right] I_0\left(\frac{ra}{b_0}\right) da \tag{2.9}$$

These equations allow us to identify the Loo parameter triplet ($M_A$, $\Sigma_A$, MP), where $M$ is the mean and $\Sigma$ is the standard deviation with the subscript $A$ indicating these parameters both relate to the direct signal component $a$.

$$M_A = 20\log_{10}(\mu) \tag{2.10}$$

$$\Sigma_A = 20\log_{10}(\exp(\sqrt{d_0}) \tag{2.11}$$

$$\mathrm{MP} = 10\log_{10}(2b_0) \tag{2.12}$$

MP refers to the amount of diffuse multipath component. It is related to the parameters $\sigma$ in Equation (2.8) through Equation (2.13)

$$\sigma = \sqrt{\frac{10^{\mathrm{MP}/10}}{2}} \tag{2.13}$$

where MP is in dB.

A Rician distribution is favoured in the case of terrestrial mobile radio as a LOS path is likely, whereas in the case of LMS transmission, the Rayleigh case is considered more likely with no LOS component. However, the Rician distribution is adequate to describe the satellite case as it contains within in the Rayleigh case when the LOS component is zero. This is one of the major benefits of the Loo distribution in that it is highly versatile and adaptive to many scenarios that exist in the LMS channel including some extreme case scenarios.

#### 2.2.7.2 The Suzuki Model

The Suzuki model [32] is a joint distribution model that encompasses both the Rayleigh and lognormal distributions. It works on the assumption that the direct signal is obstructed and the received signal is comprised solely of multipath components. For short sections the signal can be described by the Rayleigh distribution in which the parameter $2\sigma^2$ is constant [30]. However, it also considers that for longer sections of received signal that $\sigma$ is lognormally distributed.

Therefore, the Suzuki distribution is given by,

$$f(r) = \frac{8.686\, r}{\sigma^2 \Sigma_{dB}\sqrt{2\pi}} \times \int_0^\infty \frac{1}{\sigma^3} \exp\left[-\frac{(20\log\sigma - M_{dB})^2}{2\Sigma_{dB}^2} - \frac{r^2}{2\sigma^2}\right] d\sigma \tag{2.14}$$

The Suzuki model may not be applicable for the duration of a transmission in the LMS channel but it may arise in highly dense urban scenarios where the direct signal may completely blocked and may describe the received signal for a bad state.

### 2.2.8 Doppler Spectrum

Transmitted signals have a particular carrier frequency $f_c$ however certain geometric phenomena can cause the carrier frequency to be affected and result in some changes to the characteristics in the frequency of the received signal. These changes in frequency are referred to as Doppler shifts. Doppler shifts are changes in frequency that arise due to movement of the receiver, the transmitter or scatterers in the user environment. Movement of any of the elements within the transmission structure can result in a change in the path length of the transmission. This causes a change in the dispersion of the signal in time and thus results in a frequency shift in the signal. A Doppler shift can occur in the direct signal due to a change in the relative position of the satellite and the user [27] and is particularly important in non-geostationary satellite systems if the satellite changes elevation in its orbit and the distance between the satellite and the user changes.

#### 2.2.8.1 Doppler shift in the direct signal

A Doppler shift may introduced to the direct signal component and will have a Doppler frequency up to the maximum frequency $f_{max}$ given by Equation (2.15) which is determined by the carrier frequency, the velocity of the user (assuming the satellite and the transmitter are stationary) and the angle of arrival of the signal [17]:

$$f_D = \frac{v_{mob}}{\lambda_c} \cos\alpha \cos\phi \tag{2.15}$$

where $v_{mob}$ is the mobile velocity with respect to the satellite, $\lambda_c$ is the carrier signal wavelength (defined by $c = f_c\lambda_c$; $c$ is the speed of light, $f_c$ is the frequency of the carrier signal) , $\alpha$ is the angle of arrival of the direct signal and $\phi$ is the satellite elevation angle.

#### 2.2.8.2 Doppler spread in the multipath components

In the case of a geostationary (GEO) satellite system, the Doppler shift of the direct signal may not be significant, however, the Doppler effects of the multipath signal can not be ignored and should be modelled correctly.

The multipath components each undergo an individual Doppler shift due to the different distances each component travels along its individual path and therefore has an individual Doppler frequency. The combination of each individual component results in a Doppler spread which is limited by the maximum Doppler frequency, Equation (2.16).

$$f_{max} = f_c \pm f_D \tag{2.16}$$

where $f_{max}$ is the maximum frequency, $f_c$ is the carrier frequency and $f_D$ is the Doppler frequency.

A multipath component may arrive at the receiver antenna from potentially any angle or direction; the direction will be determined by the objects which exist in the user environment and how they have influenced the particular propagation path for each multipath component. The angle of arrival of the multipath components is important factor in determining the shape of the Doppler spectrum and will depend on the position of scatterers in the user environment. If we assume a uniform angle of arrival in the multipath components then we can model the multipath components using the popular Jake's Spectrum that is commonly used in mobile radio and satellite transmission modelling. This spectrum modelling technique assumes that there is equal power received in all directions surrounding the receiver antenna. The total power can be found by summing the incident power over all angles and considering the antenna's isotropic gain [33]. In theory there will zero power received above or below the minimum/maximum Doppler frequency with the infinite received power at the frequencies at $f_{max}$ , however, in reality a received signal will have no infinite power and will be limited by a thermal noise floor [33].

The Doppler spectrum provides an insight into the geometry of the user environment and the relative positions of the scatterers around the mobile terminal. In addition, we may also gain an understanding of the autocorrelation of the channel. The auto correlation of the channel will depend on the angular spread of the Doppler components, if the Doppler spread is great then the autocorrelation of the channel decreases more rapidly and the channel is more time variant [33].

## 2.3 Diversity in a Communication Systems

The LMS channel is a particularly difficult channel to successfully transmit information through. Due to the inherent the low power constraints and huge transmission distances involved in satellite systems they incorporate adverse transmission conditions. Therefore, one area of research within the fields of satellite communications and satellite networks involves achieving gain through various methods of diversity within the system. Diversity is most effective and provides the most gain when there are independent samples of the transmitted signal [34], this can be achieved by creating independent paths for the transmitted samples.

Diversity can be introduced to a communications system in a number of ways:

- Time diversity - multiple transmissions a different times, e.g. Time Division Multiplexing.
- Frequency diversity - multiple transmissions at different frequencies, e.g. Frequency Division Multiplexing.
- Spatial diversity - multiple transmissions from different antenna, e.g. MIMO.
- Polarisation diversity - A form of spatial multiplexing with the added dimension of multiple polarisations, e.g. dual-polarised MIMO.
- Satellite diversity - A form of spatial multiplexing using multiple satellites to transmit data.

The key concept behind diversity is that multiple signals are transmitted through a channel, if one part of the transmitted signal is highly attenuated or corrupted then the additional information sent in the other transmitted signal will enable the receiver to determine the original signal information. It is assumed to be highly unlikely all signals will suffer the same attenuation and therefore information can be gained from each copy of the transmission or sub-channel. Sending multiple signals increases the overheads associated with the transmission and each method of achieving diversity has their own benefits and drawbacks. Satellite channels are slow fading channels, therefore the gain achievable from temporal diversity is limited. Frequency diversity schemes such as Orthogonal Frequency Division Multiplexing (OFDM) are most valuable for frequency selective channels which not all satellite channels are. Due to these reasons, spatial diversity dominates in satellite systems and can be implemented in the form of multiple satellite systems (satellite diversity) or multiple antennas (polarisation diversity) .

### 2.3.1 Achieving Diversity in Satellite Systems

As discussed in Section 2.1.1, existing satellite systems must strive to meet the ever-increasing demands of mobile subscribers. These systems must match the high quality of service (QoS) standards expected from terrestrial systems and also offer service coverage to extremely large areas, including remote and otherwise isolated areas. Mobile Satellite Broadcasting (MSB) systems offer a method of providing multimedia broadcast services to mobile user terminals (UTs) [35]. These systems can consist of a single beam or a number of beams in a multibeam system. In multibeam systems, polarisation may be incorporated to reduce interference between beams by creating adjacent beams of the same frequency that are orthogonally polarised.

The application of multiple-input multiple-output (MIMO) is of particular interest if we consider the benefits it achieves in terrestrial wireless systems, i.e. of the order of Gb/s [36]. Employing multiple antennas provides a significant gain over a single antenna as it takes advantage of multipath scattering. In a satellite system scatterers

are absent in the vicinity of the satellite, therefore multiple antennas do not necessarily provide the same gain in a satellite system as they do in a terrestrial system.

Recent research into the Land Mobile Satellite (LMS) channel has explored the application of MIMO techniques with the aim of achieving gains similar to those obtained in terrestrial settings [36]. As mentioned in Section 2.3 a number of possibilities exist for applying MIMO to the LMS channel, multiple satellite systems (satellite diversity) and multiple antennas on a single satellite (polarisation diversity) being the two most promising implementations. Of the two, polarisation diversity is currently the most appealing and has prompted a wealth of research into the statistical channel modelling of the dual polarised MIMO LMS channel [1] and the possible benefits of incorporating such a system into current MSB systems [37],[38]. It has been presented in [38] that incorporating a 2x2 dual polarised beams increases the detrimental effects of the carrier-to-interference ratio.

### 2.3.2 Polarisation Diversity

This thesis focuses on achieving diversity in the LMS channel through the application of polarisation diversity. Polarisation diversity, a form of spatial diversity, exploits oppositely polarised, multiple antennas at both sides of the transmission link and may provide a major improvement to the throughput associated with a satellite system.

Polarisation diversity may be achieved through transmissions involving right hand circularly polarised (RHCP) and left hand circularly polarised (LHCP) signals.

A simple dual polarised MIMO channel with four sub-channels creating a 2x2 MIMO channel matrix can be modeled, Fig.2.5. The system model can be described using two transmitters, each with orthogonally circularly polarised antenna, and two receivers, each with orthogonally circularly polarised antenna. Therefore the transmission link consists of two co-polar sub-channels and two cross-polar sub-channels.

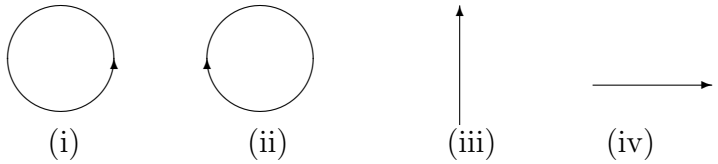


FIGURE 2.4: Diagram showing the direction of the electric field vector for (i) left hand circular polarisation, (ii) right hand polarisation, (iii) vertical linear polarisation and (iv) horizontal linear polarisation. (Direction of travel of the wave is into the page)

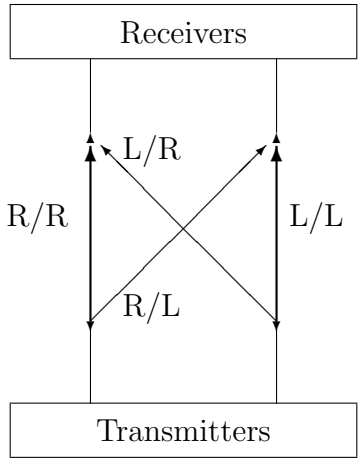


FIGURE 2.5: Diagram showing a 2x2 MIMO channel matrix with co-polar components RHCP/RHCP and LHCP/LHCP and also cross-polar components RHCP/LHCP and LHCP/RHCP.

In theory, the antenna should only detect the part of the signal that has the same polarisation, however in practice it is difficult to obtain a completely polarised antenna. The cross-polarisation discrimination of the antenna (XPD) is a measure of the ratio of the wanted co-polarised signal power and the unwanted cross-polarised signal power.

When the signal is propagating through the environment, interaction with scatterers in the environment may cause some of the signal energy to be transferred to the opposite polarisation. This effect is measured by the cross-polarisation coupling of the environment (XPC). Within a dual polarised system, this signal energy is not lost as it would be in a single polarisation system but is received by the other antenna.

Dual polarised systems can take advantage of this transfer of energy into the cross-polarisation subchannel and use schemes with appropriate signal processing techniques at the transmitter and the receiver that are able to monopolise upon this situation. Existing multibeam satellite systems already use single polarisation per beam, therefore the advancement to dual polarisation per beam is achievable with existing satellite architectures [37]. Therefore the application of polarisation to achieve a dual polarised MIMO LMS channel is an exciting research topic and provides the basis of the research on this thesis in achieving a consolidated channel model.

## 2.4 Summary

This chapter outlined the major aspects of general land mobile satellite channels before detailing the specific aspects of the dual polarised MIMO LMS channel in the next chapter. Modeling conventions have been justified. These include the assumption of a narrowband channel with a good and bad state sequence determined by a Markov or semi-Markov chain. The state durations of a semi-Markov chain are determined by a lognormal distribution. The overall distribution of the received signal is described by the Loo model with a Loo parameter triplet ($M_A, \Sigma_A$, MP) defining each state through the mean and standard deviation of the direct signal and the power of the diffuse multipath component. The relationship between user environment and Doppler

spreading of the multipath component is explained thus outlining the requirement for realistic Doppler shaping of the multipath component such as the Jake's spectrum.

# Chapter 3

# The Enhanced Dual Polarised LMS Model

## 3.1 Introduction

This chapter details the Enhanced Statistical land mobile satellite (LMS) channel model that incorporates multiple-input multiple-output (MIMO) through dual polarisation and gives a methodology for the simulation of the channel using the computing environment MATLAB. The channel model builds on the aspects of the LMS channel described in Chapter 2 and provides a timeseries generator for realistic simulation of the channel. The Enhanced Statistical LMS model is a stochastic model that uses the Liolis-CTTC model as a baseline and includes a number of enhancements to the model for a more accurate and detailed channel model of the dual polarised MIMO LMS channel. The enhancements in the new model include a method of imposing temporal correlation on the direct signal component without creating the unwanted high frequency effects associated with the traditional low-pass filtering approach to implementing temporal correlation on the direct signal. Doppler effects are included in the model, with a Doppler shift in the direct signal component and also Doppler shaping of the multipath component. A number of multipath Doppler shapes are

explored including the Jakes Doppler spectrum. The model implements a state sequence through a semi-Markov chain with a smooth state transition process avoiding sharp, sudden changes in signal magnitude. In addition to the considerations given to producing a realistic timeseries in the LMS channel model, a method is also included for producing channel samples at a rate sufficiently high to satisfy the required sub-symbol rate for transmission allowing for further aspects of the communication system to be simulated with the model output. A schematic diagram and a step-by-step guide to simulating the enhanced statistical dual polarised LMS channel are provided.

## 3.2 Liolis-CTTC as a Baseline Statistical Model

The Liolis-CTTC model, published in [1], included a descriptive step-by-step simulator for generating a timeseries for a dual polarised LMS channel. It combined known and accepted approaches to modelling the LMS channel with theory associated with dual polarised transmissions. It was a major advancement in the research of dual polarisation in a satellite context and has a number of advantages over other model types when it comes to generating a timeseries for the dual polarised LMS channel. The first advantage is the given the statistical approach used in the model, the model is relatively easy to produce in a language such as MATLAB. In addition to the ease of programming, parameters for the model are published and easily obtained. Finally, simulation time is short due to the low complexity of the model.

However, a number of areas were not addressed in the initial Liolis-CTTC model. For example, there is no modelling of Doppler effects including no shaping of the Doppler spread of the multipath components. The transitions between states are instantaneous which makes them unrealistically sharp with sudden changes in signal magnitude. Therefore, the Liolis-CTTC model makes an ideal starting point for the development of a more detailed dual polarised channel model, which addresses some of the limitations of the Liolis-CTTC model.

## 3.3 Statistical Modelling of the Dual Polarised LMS channel

A number of basic assumptions are common to both the Liolis-CTTC model and the Enhanced Statistical model in accordance with the Digital Video Broadcasting -Satellite Services to Handheld Devices (DVB-SH) baseline scenario [25]. A geostationary satellite at a $40^o$ elevation angle with a typical S-band operating frequency of 2.2 GHz is considered and the velocity of the mobile receiver is 50 km/h through a defined user environment with particular characteristics: open rural, suburban or urban (see Table A.1).

The channel is considered to contain a direct signal component, in which variations in the signal magnitude have a slow rate of change and are caused by large objects causing blockage or shadowing, and a multipath component, in which the variations in the signal magnitude have a fast rate and are caused by smaller scatterers in the vicinity of the receiver. To allow us to model these two signal components at different rates of change, the direct signal component $\bar{\mathbf{H}}$ and the multipath component $\tilde{\mathbf{H}}$ are generated separately and added together to give the total channel matrix $\mathbf{H}$, Equation (3.1):

$$\begin{aligned} \mathbf{H} &= \bar{\mathbf{H}} + \tilde{\mathbf{H}} \\ &= [\bar{h}_{ij}] + [\tilde{h}_{ij}], \quad (i,j = 1,2) \end{aligned} \tag{3.1}$$

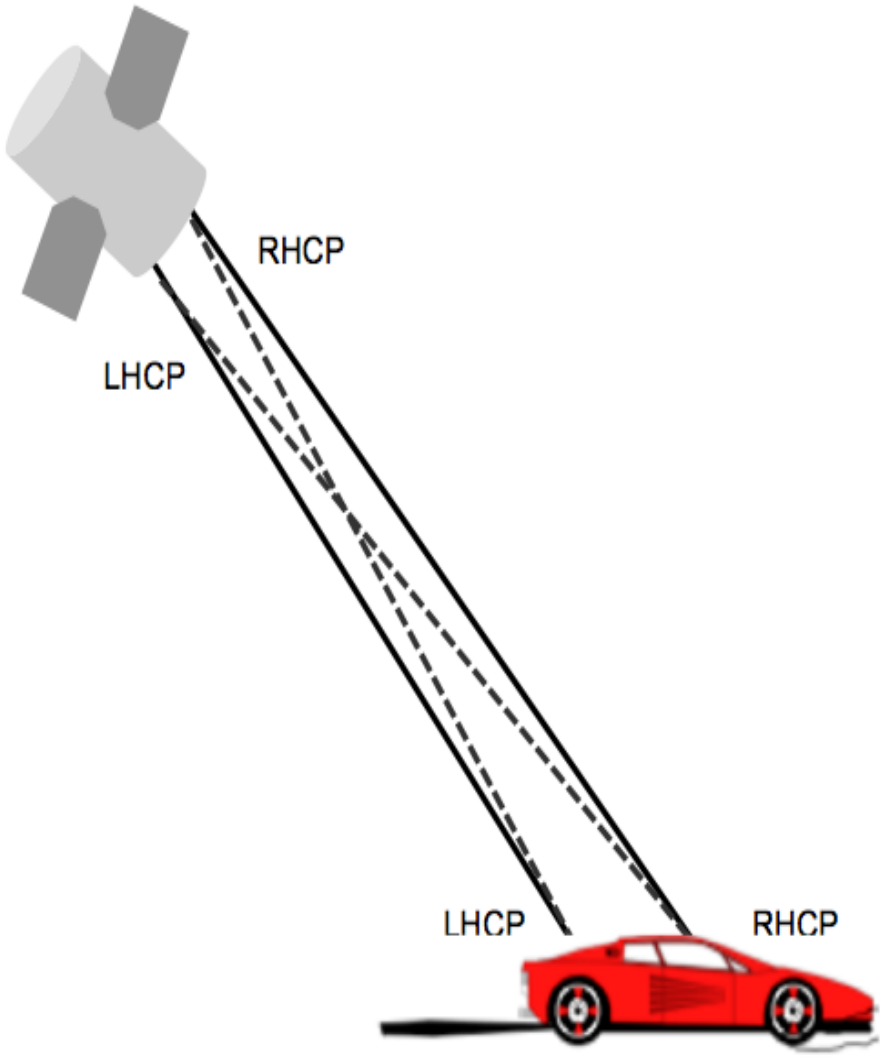


FIGURE 3.1: Diagram of the 2x2 channel matrix achieved through the use of dual polarised antenna at the transmitter and the receiver. As right hand and left hand circularly polarised antenna are used, this creates 4 subchannels, RHCP/RHCP, RHCP/LHCP, LHCP/RHCP, LHCP/LHCP. The receiver may be a handheld device carried by a pedestrian or a portable device based in a moving car.

### 3.3.1 Implementation of the Polarised Subchannels

To implement MIMO in the LMS channel, two orthogonally circularly polarised transmitters and two orthogonally circularly polarised receivers are used. The transmitter and receiver antenna pair each have right hand circularly polarised (RHCP) antenna and left hand circularly polarised (LHCP) antenna.

A 2x2 channel matrix arises due to this antenna configuration, with two co-polarised subchannels (RHCP/RHCP & LHCP/LHCP) and two cross-polarisation subchannels (RHCP/LHCP & LHCP/RHCP), as in Figure 3.1. To model the relative power of these four subchannels appropriately we need to measure the amount of cross-polarisation which occurs in the signal. There are a number of factors that contribute to the cross-polarisation effect, most significantly these are the cross-polarisation effects of the antenna and the cross-polarisation effects of the environment due to scatterers. These factors contributes to a depolarisation of the signal that results in the unwanted energy transfer from one polarisation to another.

The Branch Power Ratio (BPR) gives us the expected ratio between the co-polarised signal and the cross-polarised signal. We assume that the symmetry is conserved between the orthogonal polarisation subchannels and the BPR is 0 dB [39]. Thus mutual coupling does not degrade the performance of the dual polarised antenna set-up [33]. The BPR is given by Equation (3.2):

$$\mathrm{BPR} = 10 \log_{10} \left( \frac{E\left[ \mid h_{11} \mid^2 \right]}{E\left[ \mid h_{22} \mid^2 \right]} \right) \tag{3.2}$$

where $E[]$ denotes the expected power of the received signal, $i, j$ equal 1 or 2 and $\bar{h}$ is the

Firstly, if we consider the direct signal component, the cross-polarisation discrimination (XPD) affecting this part of the signal is due to cross-polarisation discrimination of the antenna ($\mathrm{XPD}_{\mathrm{ant}}$), i.e. its ability to discriminate between the two opposite polarisations, and also due to a small amount of depolarisation arising from shadowing of the direct signal.

We can express the XPD of the direct signal as the ratio of the received signal power in the co-polarisation subchannel ($\bar{h}_{ii}$) and the received signal power in the cross-polarisation subchannel ($\bar{h}_{ij}$), Equation (3.3).

$$\text{XPD} = 10\log_{10}\left(\frac{E\left[\mid \bar{h}_{ii} \mid^2\right]}{E\left[\mid \bar{h}_{ij} \mid^2\right]}\right) \tag{3.3}$$

Ideally a polarised antenna should only detect the signal transmitted from that of the same polarisation; however, antennas are susceptible to interference from signals of other polarisations. The antenna's ability to discriminate between the 'wanted' co-polarised signal and the 'unwanted' cross-polarised signal is defined by the cross-polarisation discrimination of the antenna and this is a major factor in determining the cross-polarisation effects in the direct signal.

In the simulation process we can implement an XPD value to determine the amount of signal power being transferred to the cross-polarisation subchannels in the direct signal components [1] by calculating the parameter $\beta$ as in Equation (3.4).

$$\text{XPD} = 10\log_{10}\left[\frac{(1-\beta)}{\beta}\right] \tag{3.4}$$

The parameter $\beta$ defines the amount of cross-polarisation that will occur in the direct signal during the simulation. It may be applied to correctly model the signal power in the direct signal co-polarisation subchannels, i.e. $\sqrt{1-\beta}$ and the signal power in the cross-polarisation subchannels, i.e. $\sqrt{\beta}$.

This leads us to the calculation of the expected power in the direct signal component ($E\left[\bar{\mathbf{H}}\bar{\mathbf{H}}\right]$) in which we also consider the Loo parameters which define the direct signal magnitude $M_A$ and standard deviation $\Sigma_A$, Equation (3.5) :

$$E\left[\bar{\mathbf{H}}\bar{\mathbf{H}}\right] = M_A^2 + \Sigma_A^2 \begin{bmatrix} 1-\beta & \beta \\ \beta & 1-\beta \end{bmatrix} \tag{3.5}$$

Another factor to be considered is the scattering of the propagating signal within the user environment. Depending on the object and the angle of scattering, the reflected signal may experience changes in polarisation. If the angle of reflection if greater than the Brewster angle then the wave experiences a change in polarisation [19]. The open, suburban and urban environments contain different scatterer densities and different types of scatterers thus each environment causes different amounts of cross-polarisation to occur. The amount of cross-polarisation that occurs in the signal due to interactions with scatterers and objects close to the user is defined as cross-polarisation coupling of the environment (XPC), Equation (3.6).

$$\mathrm{XPC} = 10 \log_{10} \left[ \frac{(1-\gamma)}{\gamma} \right] \tag{3.6}$$

The parameter $\gamma$ defines the amount of cross-polarisation that occurs due to the environment in the channel model.

The XPC affects the polarisation of the multipath signal components only. In addition to the effect of XPC, the multipath signal is also affected by the cross-polarisation effects of the antenna and the shadowing previously defined as the XPD. Therefore, to model the total cross-polarisation in the multipath signal components we need to consider the effects of the environment and the antenna. To model the signal power in the multipath component, a parameter $\delta$ is defined, Equation (3.7).

$$\delta = \beta\,(1-\gamma\,) + (1-\beta\,)\,\gamma \tag{3.7}$$

where $\beta$ and $\gamma$ are parameters whose values depend on the user environment and on the properties of the antenna as previously defined.

The parameter $\delta$ defines the amount of cross-polarisation that will occur in the multipath signal during the simulation. It may be applied to correctly model the signal power in the multipath signal co-polarisation subchannels, i.e. $\sqrt{1-\delta}$ and the signal power in the cross-polarisation subchannels, i.e. $\sqrt{\delta}$.

This leads us to the calculation of the expected power in the multipath signal component ($E\left[\tilde{\mathbf{H}}\tilde{\mathbf{H}}\right]$) in which we also consider multipath power (MP), Equation (3.8).

$$E\left[\tilde{\mathbf{H}}\tilde{\mathbf{H}}\right] = \mathrm{MP}\begin{bmatrix} 1-\delta & \delta \\ \delta & 1-\delta \end{bmatrix} \tag{3.8}$$

Appropriate values for the parameters $\beta$ and $\gamma$ to use in the model are determined from values obtained for XPD and XPC from experimental campaigns and can be found in [19], [40].

### 3.3.2 Implementation of Loo Distribution

The probability distribution of the received signal is described using the Loo model, Equation (2.9); it is a joint distribution based on the Rice model with variations in the direct signal modelled using a lognormal distribution [31].

A unique Loo parameter triplet ($\mathrm{M}_A, \Sigma_A$, MP) is generated for each state, each parameter is generated from a Gaussian distribution [2, 17]. Thus, the signal properties remain constant during a particular state and fading is implemented using the Loo parameter triplet.

Loo parameter triplet ($\mathrm{M}_A, \Sigma_A$, MP) is calculated according to the following distributions [2]:

$$\begin{aligned} f(M_A) &\sim \mathrm{Gaussian}(\mu_1, \sigma_1) \\ f(\Sigma_A \mid M_A) &\sim \mathrm{Gaussian}(\mu_2, \sigma_2) \\ f(\mathrm{MP}) &\sim \mathrm{Gaussian}(\mu_3, \sigma_3) \end{aligned} \tag{3.9}$$

where the values for the mean ($\mu_1$) and standard deviation ($\sigma_1$) for the mean of the direct signal $M_A$ and the mean ($\mu_3$) and standard deviation ($\sigma_3$) for the power of the

multipath signal MP are obtained directly from Table A.3, (p.191). The values for the mean ($\mu_2$) and standard deviation ($\sigma_2$) for the standard deviation of the direct signal $\Sigma_A$ have to be calculated as $\Sigma_A$ is a function of $M_A$, therefore the following relationships are used:

$$\begin{aligned} \mu_2 &= a_1 \times M_A^2 + a_2 \times M_A + a_3 \\ \sigma_2 &= b_1 \times M_A^2 + b_2 \times M_A + b_3 \end{aligned} \tag{3.10}$$

with values for $a_i$ and $b_i$ also obtained from Table A.3.

## 3.4 The Enhanced Statistical LMS Model

This section details the enhancements that are applied to the baseline statistical model. In depth descriptions of how each enhancement is performed are provided in sections 3.8 to 3.11, including the smooth state transitioning, spatial correlation of the subchannels, temporal correlation of the slow variations, Doppler effects and interpolation to symbol-rate sampling rate.

A step-by-step guide to the simulation process is provided below in which the major steps in the channel model are listed to give a general idea of how the channel model is constructed. Firstly in section 3.5, the steps in the generation of the direct signal component channel matrix $\bar{\mathbf{H}}$ are listed. This includes sample generation, temporal and spatial correlation, Loo parameters distribution, polarisation effects, exponentiation and phase consideration. Secondly in Section 3.5.2, the steps in the generation of the multipath signal component channel matrix $\tilde{\mathbf{H}}$ are listed. This includes sample generation, Doppler shaping, Loo parameters distribution and polarisation effects. Finally in section 3.5.3, the steps in combining the two channel matrix components to produce the total channel matrix $\mathbf{H}$ are listed.

A schematic is also provided in Figure 3.2 to further demonstrate how to implement the Enhanced Statistical dual polarised LMS model and how parameters are introduced and applied to the channel.

## 3.5 Step-by-Step Guide to Channel Matrix Construction

### 3.5.1 Generate the Direct Signal Component

The instructions below outline the methodology of the dual polarised MIMO LMS channel simulator and the processes that must be implemented in turn to obtain the direct signal component.

**Generate the Direct Signal Component $\bar{\mathbf{H}}$**

- *Step 1: Sample Generation*

  Four real subchannels are created by generating random sequences with zero mean and unit variance using a Gaussian random number generators G(0,1). One sample is generated per metre of simulation distance.

- *Step 2: Spatial Correlation*

  The 4x4 positive semi-definite Hermitian covariance matrix $\bar{\mathbf{C}}$ is produced by the Weichselberger method of considering the spatial correlation matrices $\bar{\mathbf{R}}_{tx}$ and $\bar{\mathbf{R}}_{rx}$ which determine the transmit and receive signal spatial correlation. The four subchannels are spatially correlated by finding the product of the four subchannels with the Choelsky decomposition of the matrix $\bar{\mathbf{C}}$.

- *Step 3: Temporal Correlation*

  The samples are temporally correlated using a single coefficient infinite impulse response (IIR) low-pass filter and the sample rate is increased to match a sampling rate of $\lambda/8$ using a cubic spline interpolation technique.

- *Step 4 : Loo Parameters*

  A Loo Parameter triplet for each sample is generated using Gaussian random number generators with mean and standard deviations specified by the particular environment and conditions. The mean $M_A$ and standard deviation $\Sigma_A$ of the signal is determined by applying the appropriate Loo parameters to each sample in the subchannels.

- *Step 5: Polarisation Effects*

  The mean of the subchannels are adjusted to reflect the polarisation effects related to the XPD of the antenna. The magnitude of the signal in the two co-polarisation subchannels is reduced by the parameter $\beta$, the magnitude of the signal in the two cross-polarisation subchannels is given by $\beta$.

- *Step 6: Exponentiation*
  The subchannels are converted from dB to linear resulting in four lognormal subchannels.
- *Step 7: Addition of Phase*
  The phase component given by $e(j\theta)$ is added to each sub-channel.
- **Result**: 2 x 2 x $n$ channel matrix $\bar{\mathbf{H}}$ in $n$ x 4 vector form, where $n$ is the number of samples.

### 3.5.2 Generate the Multipath Signal Component

The instructions below outline the methodology of the dual polarised MIMO LMS channel simulator and the processes that must be implemented in turn to obtain the diffuse multipath signal component.

**Generate the Multipath Signal Component $\tilde{\mathbf{H}}$**

- *Step 1: Sample Generation*
  Four complex subchannels are created by generating random sequences with zero mean and unit variance using two sets of Gaussian random number generators G(0,1) per subchannel.
- *Step 2: Spatial Correlation*
  The 4x4 positive semi-definite Hermitian covariance matrix $\tilde{\mathbf{C}}$ is produced by the Weichselberger method using the transmit spatial covariance matrix $\tilde{\mathbf{R}}_{tx}$ and the received spatial covariance matrix $\tilde{\mathbf{R}}_{rx}$. The four subchannels are spatially correlated by finding the product of the four subchannels with the Choelsky decomposition of the matrix $\tilde{\mathbf{C}}$.

- *Step 3: Doppler Shaping*

  The Doppler effects are modelled using a method of IIR filtering with coefficients determined from the theoretical autocorrelation function of the desired Doppler spectrum.

- *Step 4: Loo Parameters*

  The multipath power of each subchannel is determined by applying $\sigma$ determined from the Loo Parameter MP.

- *Step 5: Polarisation Effects*

  The effects of the cross-polarisation of the antenna and the cross-coupling effects of the environment are modelled using the parameter $\delta$. The power of the signal in the co- polarisation subchannels are reduced by $\sqrt{\delta}$ and the power cross-polarisation subchannels is given by $\sqrt{\delta}$.

- **Result**: 2 x 2 x $n$ channel matrix $\tilde{\mathbf{H}}$ in $n$ x 4 vector form, where $n$ is the number of samples.

### 3.5.3 Generate the Total Signal Component

When the two separate signal components are obtained, i.e. the direct signal component and the multipath signal component, the total channel matrix may be obtained as per the instructions below.

**Generation of Total Channel Matrix H**

- *Step 1:* Addition of matrices $\bar{\mathbf{H}}$ and $\tilde{\mathbf{H}}$.

- *Step 2:* Reshaping of matrix from $n$x4 to 2x2x$n$ .

- **Result**: 2 x 2 x $n$ channel matrix $\mathbf{H}$, where $n$ is the number of samples.

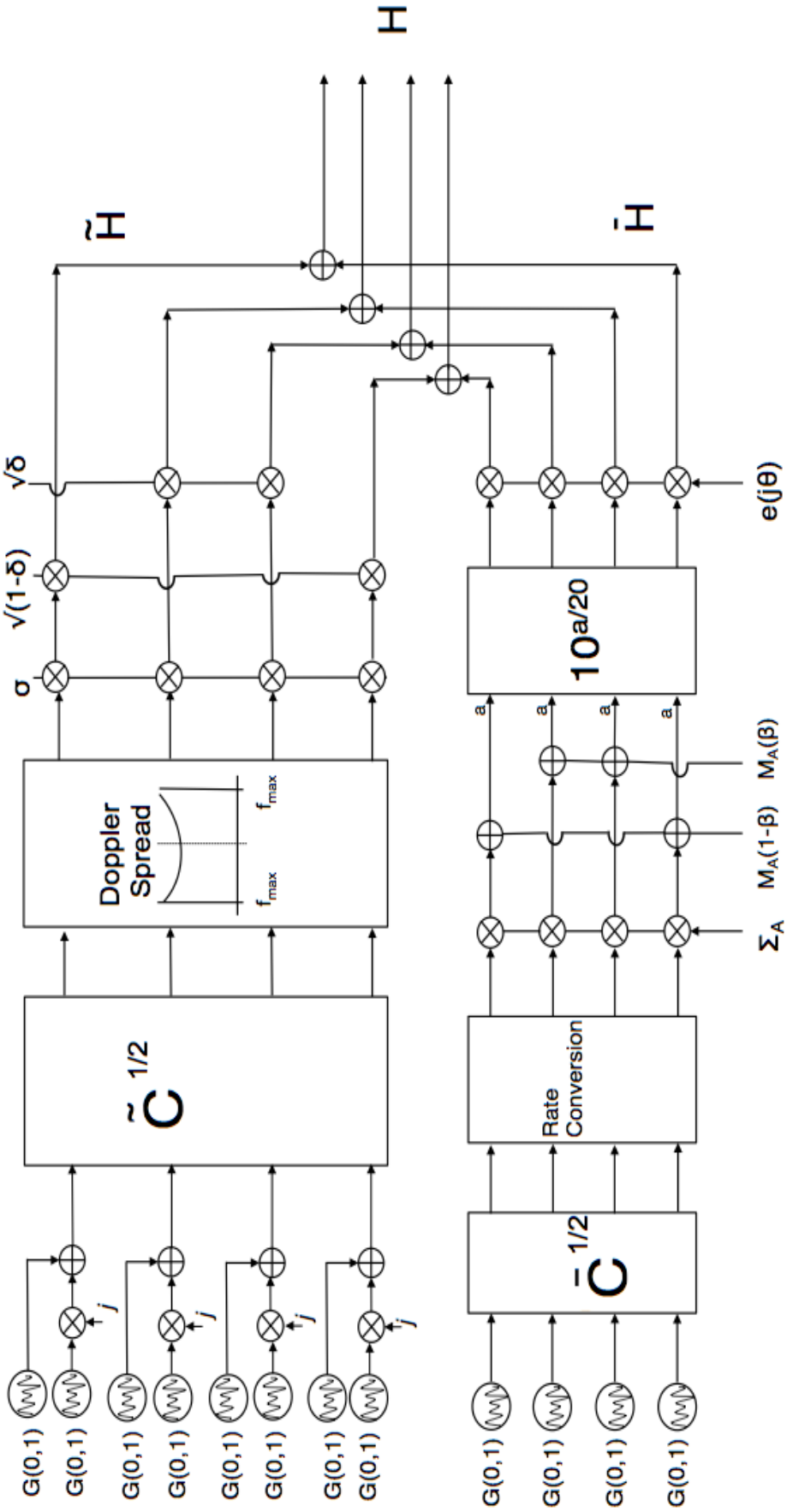


FIGURE 3.2: Schematic diagram of the simulation of the enhanced dual polarised MIMO LMS channel incorporating the Loo distribution and showing the inclusion of Doppler spreading in the multipath component (top rail) and rate conversion process for the direct signal component (bottom rail) which incorporates a two- step low-pass filtering and interpolation process. The multipath $\tilde{\mathbf{H}}$ and direct signal $\bar{\mathbf{H}}$ components are added together to obtain the total channel matrix $\mathbf{H}$.

## 3.6 Spatial Correlation of the Subchannels

The four subchannels that make up the 2x2 MIMO channel matrix undergo both spatial and temporal correlation. In the direct signal component the high spatial correlation that exists is due to the huge transmission distance the signal travels and the small distance between the receive antenna. Typically the receive antenna will be arranged so that they are a few wavelengths apart. This antenna arrangement causes a high level of similarity between the propagation paths and leads to high correlation in the direct signal component.

The ratio between the small separation distance between the receiver antenna and the relatively large angular spread of the multipath component causes correlation between the four subchannels. We can introduce spatial correlation of the four subchannels through multiplying the series by a positive semi-definite Hermitian covariance matrix $\mathbf{C}$, Equation (3.11):

$$\mathrm{vec}\left(\mathbf{H}_{corr}\right) = \mathbf{C}^{1/2} \cdot \mathrm{vec}\left(\mathbf{H}_{uncorr}\right) \tag{3.11}$$

where $\mathbf{C}^{1/2}$ is the square matrix root of the covariance matrix $\mathbf{C}$, $\mathbf{H}_{uncorr}$ is an independent and identically distributed (i.i.d.) channel matrix and $\mathbf{H}_{corr}$ is a correlated series [41].

The direct signal component and the multipath component each have different covariance matrices. The covariance matrix $\bar{\mathbf{C}}$ for the direct signal component is obtained experimentally for each user environment is given in [3]. The values in [3] have been used in multiple studies of the dual polarised LMS channel [1], [2], [42] [43].

For the multipath component we determine the covariance matrix $\tilde{\mathbf{C}}$ using the Weichselberger model [44] and use it to produce a correlated data stream $\tilde{\mathbf{H}}_{corr}$ through Equation (3.11)

The Weichselberger method [44] is used as an alternative to the Kronecker method [45] employed in the spatial correlation process in [1]. The Kronecker model determines

$\mathbf{C}$ through the Kronecker product of the covariance matrices of the receiver $\tilde{\mathbf{R}}_{rx}$ and transmitter $\tilde{\mathbf{R}}_{tx}$, which take into account the correlation from the geometry of the transmitter and receiver and are obtained from the polarisation coefficients of the transmitter $\tilde{\rho}_{tx}$ and of the receiver $\tilde{\rho}_{rx}$, Equations (3.12) & (3.13):

$$\tilde{\mathbf{R}}_{tx} = \begin{bmatrix} 1 & \tilde{\rho}_{tx} \\ \tilde{\rho}_{tx} & 1 \end{bmatrix} \tag{3.12}$$

$$\tilde{\mathbf{R}}_{rx} = \begin{bmatrix} 1 & \tilde{\rho}_{rx} \\ \tilde{\rho}_{rx} & 1 \end{bmatrix} \tag{3.13}$$

The Kronecker method assumes that the channel is separable. This implies that the channel at the transmitter and the receiver are uncorrelated and therefore separable. This assumption is acceptable in some cases in the LMS channel, for example in non-line-of-sight (NLOS) conditions. However, it is shown in [3] that this assumption of separability can not be maintained in line-of-sight (LOS) conditions and the therefore and alternative method should be employed in these conditions which models the joint correlation of the transmit and receive ends of the transmission link.

### 3.6.1 The Weichselberger method

The Weichselberger method involves the eigen-decomposition of the covariance matrices of the receiver $\tilde{\mathbf{R}}_{rx}$ and transmitter $\tilde{\mathbf{R}}_{tx}$. These matrices are eigen-decomposed to obtain the singular value matrices $\sqrt{\mathbf{\Lambda}}_{tx}$ & $\sqrt{\mathbf{\Lambda}}_{rx}$ and the corresponding orthonormal eigenvectors $\mathbf{U}_{tx}$ & $\mathbf{U}_{rx}$ according to Equation (3.14) & Equation (3.15) [33]:

$$\mathbf{R}_{tx} = \mathbf{U}_{tx}\, \mathbf{\Lambda}_{tx}\, \mathbf{U}_{tx}^{H} \tag{3.14}$$

$$\mathbf{R}_{rx} = \mathbf{U}_{rx}\, \mathbf{\Lambda}_{rx}\, \mathbf{U}_{rx}^{H} \tag{3.15}$$

This allows us to define a power coupling matrix $\mathbf{\Omega}_{\text{weich}}$ given by 3.16

$$\mathbf{\Omega_{weich}} = \sqrt{\mathbf{\Lambda}}_{rx}^{T} \cdot \sqrt{\mathbf{\Lambda}}_{tx} \tag{3.16}$$

where

$$\sqrt{\mathbf{\Lambda}}_{tx} = diag(\lambda_{tx,1}, ....., \lambda_{tx,n}) \tag{3.17}$$

$$\sqrt{\mathbf{\Lambda}}_{rx} = diag(\lambda_{rx,1}, ....., \lambda_{rx,n}) \tag{3.18}$$

and allows us to determine the correlated channel $\mathbf{H}_{corr}$

$$\mathbf{H}_{corr} = \mathbf{U}_{rx} \left( \mathbf{\Omega_{weich}} \cdot \mathbf{H}_{uncorr} \right) \mathbf{U}_{tx}^{H} \tag{3.19}$$

## 3.7 Temporal Correlation of the Slow Variations

As discussed previously in Section 2.2.4, the direct and multipath signals vary at different rates due to the interactions they encounter with different sized objects. To simulate this within the model, the samples needed for each signal component are generated at different rates. The different rates of generation pose a challenge when combining these two channel components.

Based on the assumption of S-band transmission with a carrier frequency of 2.2 GHz and a mobile user (MU) velocity of 50 km/h, the carrier signal has a wavelength ($\lambda_c$) of ∼13.6 cm. To adequately sample the multipath component that has a much smaller wavelength than the carrier signal, a sampling distance equivalent to an eighth of the carrier signal wavelength ($\lambda_c/8$) is implemented [2], this corresponds to a sampling frequency of approximately 815 Hz.

The slow-varying direct signal samples must be generated at a rate equivalent to that of the multipath signal, however, with a slower rate of change described by an exponentially decaying temporal autocorrelation function (ACF) based on the specific correlation distance $l_{corr}$ relating to the user environment. In [3] experimental measurement of the *1/e* autocorrelation distances for both co-polarised and cross-polarised subchannels are presented, Table A.4.

One method to achieve a slower rate of change in the direct signal as adopted in [1] is to use the parameters $l_{corr}$, the mobile velocity $v$ and the sampling period $T_s$ to determine $A$, the coefficient of a low-pass IIR filter, Equations (3.20) - (3.21). $A$ is a single value coefficient with a value less than 1.

$$y_n = x_n + A \cdot y_{n-1} \tag{3.20}$$

$$A = \exp\left(\frac{vT_s}{l_{corr}}\right) \tag{3.21}$$

After filtering the direct signal components, the series is scaled by a factor $b$ to account for the filter gain and restore the statistics of the original series. The filter output ($y_{filt}$), therefore, has the desired exponential ACF.

$$y_{filt} = b(y_n) \tag{3.22}$$

$$b = \sqrt{1 - A^2} \tag{3.23}$$

One drawback of using this short filtering method is that due to the high sampling rate used it produces unwanted high frequency components in the associated timeseries of the direct signal. These unwanted high frequency components can be seen in Figure 3.4. It was considered that this effect caused an unrealistic direct signal component and it was though that generating a smooth direct signal would provide a more realistic

timeseries. Therefore, it was investigated if these high frequency components could be eliminated with a different filtering approach.

### 3.7.1 Temporal Correlation through Autoregressive IIR Filtering

The first filter type to be investigated was an autoregressive IIR filter. An autoregressive IIR filter introduces memory into the series through time-domain recursion, where the output is based on the input and also the weighted sum of the previous outputs, as defined in Equation (3.24).

$$y[n] = -\sum_{k=1}^{p} a_k y[n-k] + x[n] \tag{3.24}$$

A method of determining the filter coefficients in an autoregressive model is set out in [46] where it is argued that autoregressive models are able to approximate discrete-time random processes. This method allows us to create a correlated series by considering the desired autocorrelation sequence of the series. The autocorrelation of the direct signal series we aim to simulate is defined by a parameter $A$ given in Equation (3.21) and is related to the velocity of the mobile device, the sampling period and the correlation distance.

The autocorrelation function is sampled and used to create a positive semi-definite autocorrelation matrix $\mathbf{R}_{xx}$. This matrix is a Toeplitz matrix with 1's along the diagonal, defined by Equation (3.25) [46]:

$$\mathbf{R}_{xx}\mathbf{a} = -\mathbf{v} \tag{3.25}$$

where

$$\mathbf{R}_{xx} = \begin{bmatrix} R_{xx}[0] & R_{xx}[1] & \dots & R_{xx}[-p+1] \\ R_{xx}[1] & R_{xx}[0] & \dots & R_{xx}[-p+2] \\ \vdots & \vdots & \ddots & \vdots \\ R_{xx}[p-1] & R_{xx}[p-2] & \dots & R_{xx}[0] \end{bmatrix} \tag{3.26}$$

$$\mathbf{a} = \begin{bmatrix} a_1 & a_2 & \dots & a_p \end{bmatrix}^T \tag{3.27}$$

$$\mathbf{v} = \begin{bmatrix} R_{xx}[1] & R_{xx}[2] & \dots & R_{xx}[p] \end{bmatrix}^T \tag{3.28}$$

and thus solving a set of Yule-Walker equations allows us to determine the filter coefficients $\mathbf{a}$. The implementation of this method requires a small error value $\epsilon \sim 10^{-9}$ to the diagonal of $\mathbf{R}_{xx}$

Once implemented, it was found that this filter did not achieve the conditions we had hoped for. In this instance, the autoregressive filter reduces to a very short filter with only four coefficients. This results in the filtered signal having the desired ACF but it also retains the unwanted high frequency components we had hoped to eliminate as the filter is not long enough, see Figure 3.3.

### 3.7.2 Temporal Correlation through Low Pass FIR Filtering and Interpolating

An alternative approach was therefore investigated to achieve the desired results of a smoother signal and appropriate autocorrelation function. It was decided to use a two-step method. The first step involved generating the samples of the direct signal

at a much rate slower than that of the multipath. A sample rate of 1 sample per metre was chosen, a reduction from approximately 60 samples per metre. The series is then filtered using the low pass IIR filter defined in Equation (3.20). The sampling period $T_S$ used in determining the filter coefficient is equivalent to 0.02 s, a much higher value than the original value $T_S = 0.0012$ s. The co-polarisation subchannels and the cross-polarisation subchannels were filtered with coefficients determined by Equation (3.21) using the values of $l_{corr}$ from Table A.4

The second step involves cubic spline interpolation of the series to increase the sample number to the required number to match that of the multipath samples. Interpolation of the signal alone is very effective in smoothing the signal and removing the high frequency components. It was a concern that the interpolation process may affect the correlation previously implemented with the filtering process, however, the ACF was investigated and it was found that this method offers effective smoothing of the direct signal and adequate preserving of the exponential ACF, Figure 3.4. This method was then incorporated into the channel model to generate the correlated random sequence used for the direct signal.

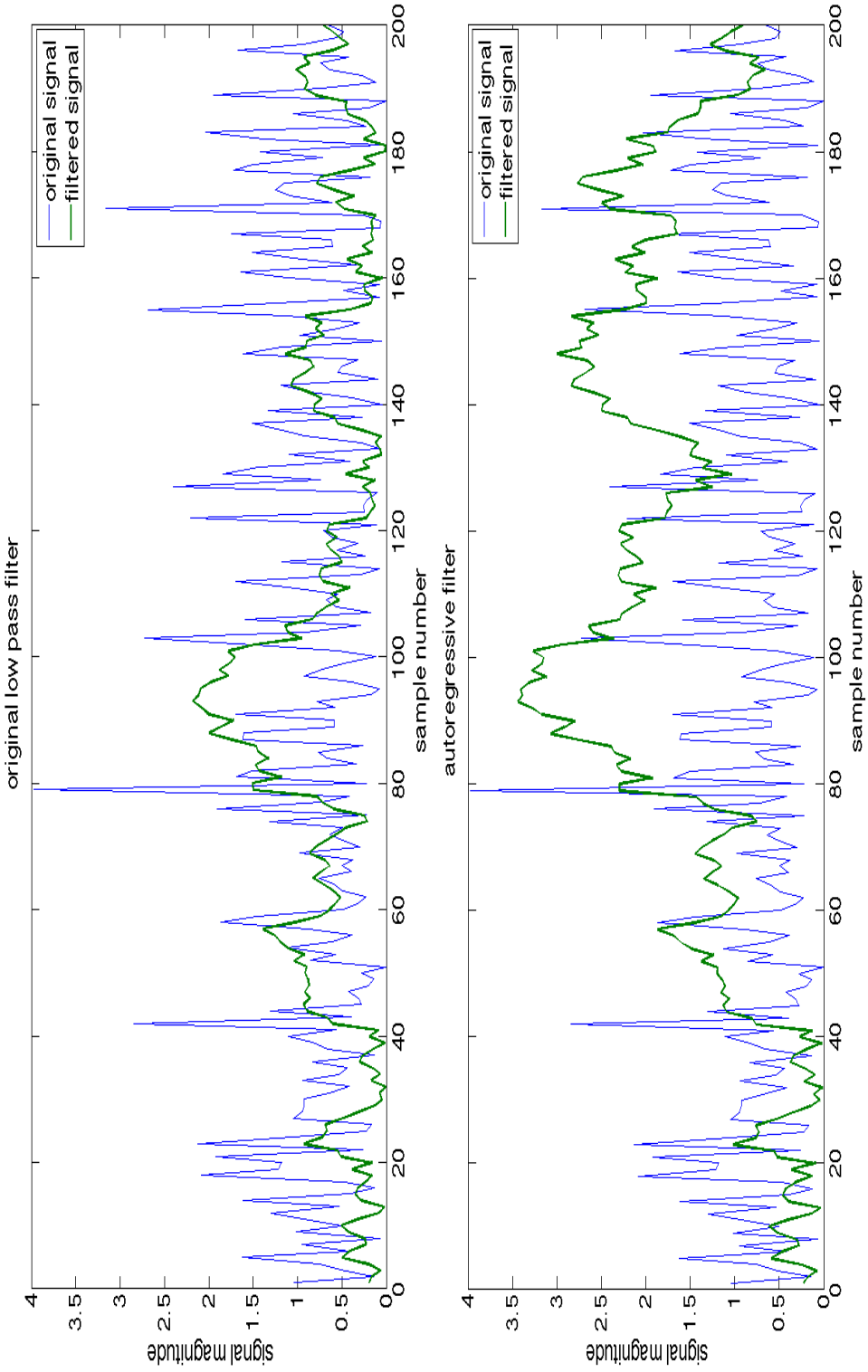


FIGURE 3.3: A comparison of the signal magnitude (linear units) of the random sequence generated to create the direct signal component in the urban user environment using a low-pass filter (top) and an autoregressive filter (bottom).

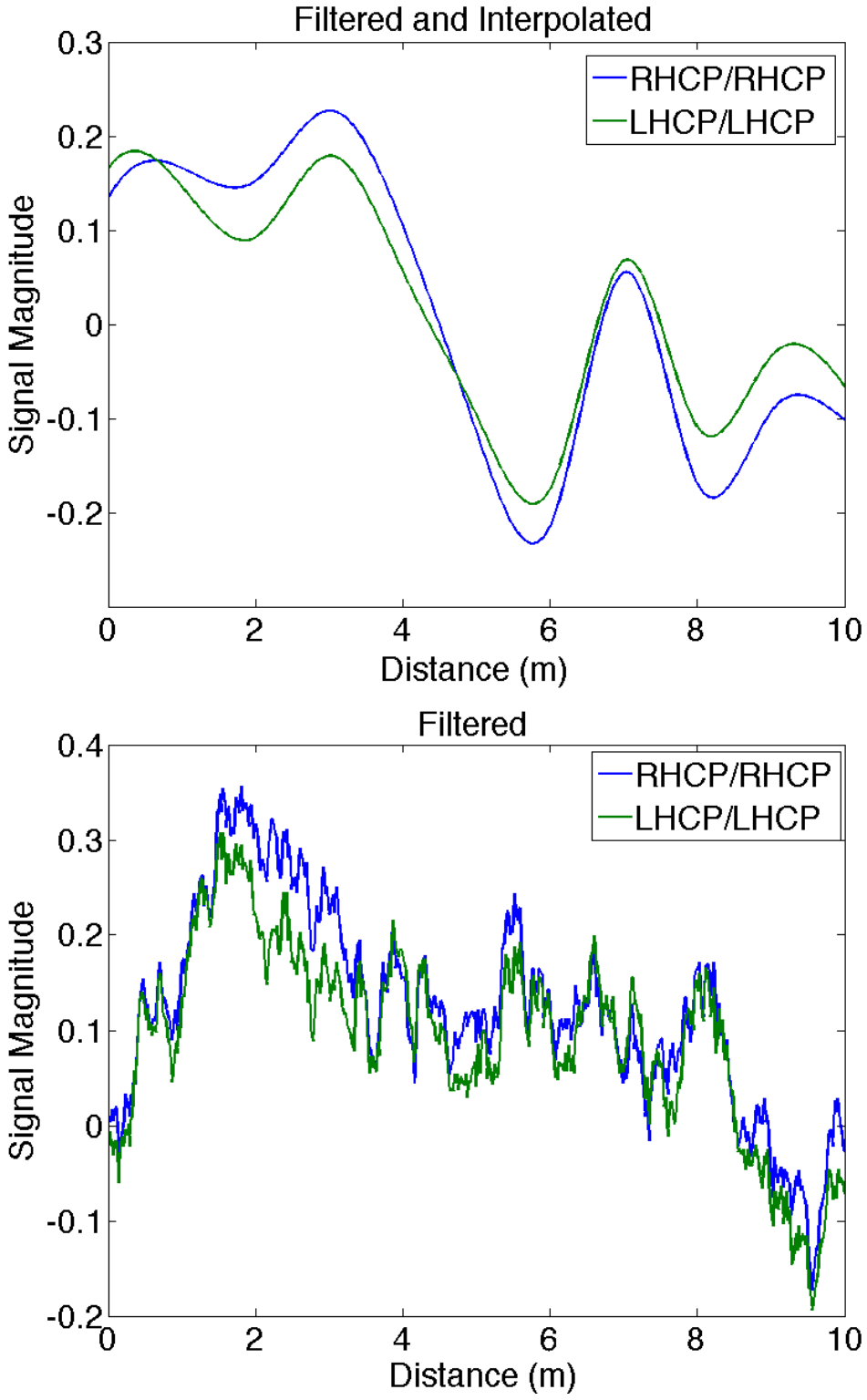


FIGURE 3.4: A comparison of the signal magnitude (linear units) of the random sequence generated to create the direct signal component in the urban user environment using (top) a combination of low-pass filtering and interpolating and (bottom) low-pass filtering only.

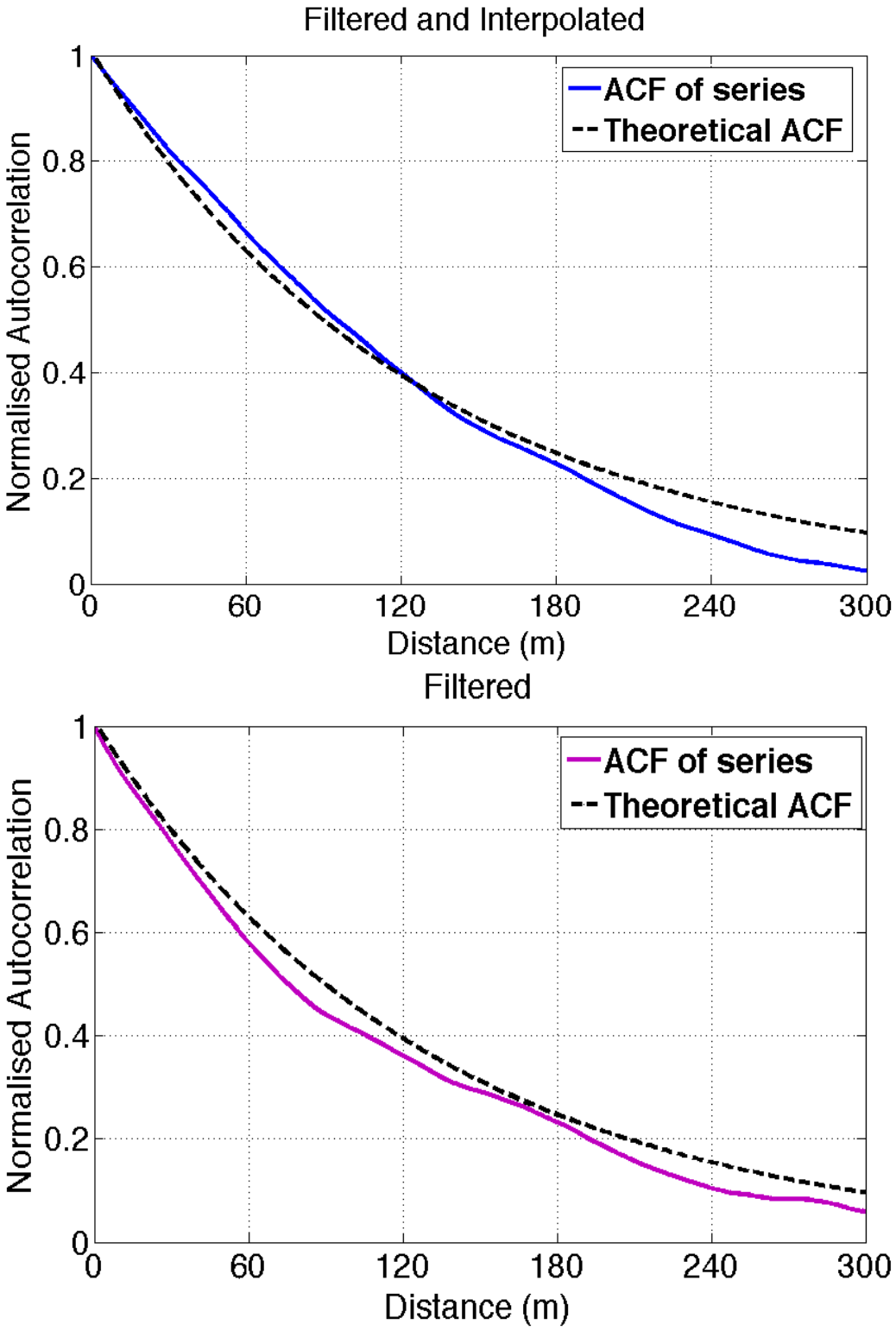


FIGURE 3.5: A comparison of the temporal autocorrelation of the random sequence generated to create the direct signal component in the urban user environment using (top) a combination of low-pass filtering and interpolating and (bottom) low-pass filtering only. The $1/e$ autocorrelation distance of the urban environment is 128m for the co-polarisation subchannels and 129m for the cross-polarisation subchannels.

## 3.8 Smooth State Transition Process

In addition to the small-scale temporal correlation explored in Section 3.7 , the received signal is also temporally correlated on a large scale as very slow variations due to very large obstacles cause the signal to experience states, i.e. there are relatively long periods of time during which the channel conditions are considered to remain constant. Models which describe the state type and the state duration in the LMS channel have evolved from three state models [4] to two state models [2] under the premise that two state models can describe the range of fading conditions adequately and give a better fit to experimental data. The good states comprise of instances involving line-of-sight (LOS) and also light shadowing conditions, whereas the bad states correspond to moderate to heavy shadowing and NLOS conditions. The state types can overlap, thus some bad states potentially have a higher signal magnitude that a poor good state. It's also worth noting that the good states do not necessarily contain a LOS component.

In the two-state approach employed in this thesis, the mobile terminal moves through its environment and the received signal experiences a series of *good* and *bad* states. The transitions between successive good and bad states are modelled using a semi-Markov chain and the duration of the state is determined from a lognormal distribution, the mean and standard deviation of which are given in [2].

To avoid unrealistic sharp changes in the signal magnitude during a state change, a method for incorporating smooth state transitions was developed. A mean slope of 5 dB per metre was imposed onto the magnitude of the direct signal component by manipulating the Loo parameter triplets. This method is not completely ideal as it does not take into account the fact that transitions will be steeper the closer the MU is to the object. A slope of 5 dB/m was chosen as it is in line with the values implemented in [17], [2].

Figure 3.6 shows how the slope between states is implemented. A Loo parameter triplet is initially generated for each state and then interpolated using the state duration in metres to determine the number of samples per state. We then have a Loo

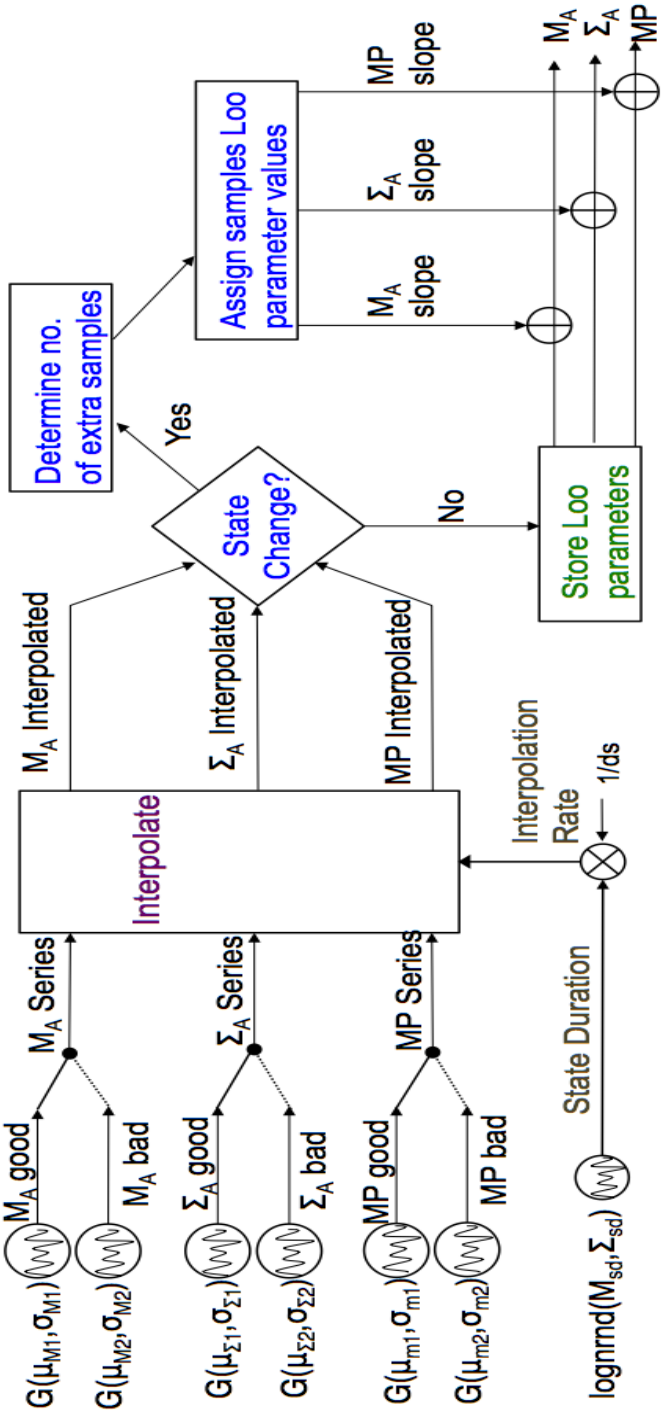


FIGURE 3.6: Schematic diagram of the implementation of the smooth state transitioning process through the generation of Loo parameters and the interpolation for these parameters to the correct state duration. A state transition is identified by different consecutive values in the interpolated Loo parameters series. Where a transition occurs in the series of the mean of the direct signal $M_A$, a mean slop of 5 dB/m is applied and the Loo parameters series are changed accordingly.

parameter triplet corresponding to each individual sample. The parameter triplet gives us the information needed to generate the direct signal magnitude ($M_A$) and standard deviation ($\Sigma_A$) along with the power of the multipath component (MP) taking into account whether the sample belongs to a good or bad state. To create a smooth transition between changing Loo triplet values and thus allow for smooth state transitions, we focussed primarily on the mean of the direct signal, i.e. $M_A$ is adjusted to allow for the determined slope by calculating the number of samples required to create such a transition. These additional samples with successive increasing or decreasing values of $M_A$ are inserted into the series of $M_A$ values to create a gradually increasing or decreasing slope in the values of $M_A$. Subsequently, $\Sigma_A$ and MP are also adjusted by the same method with the same slope as determined for $M_A$ creating gradually increasing or decreasing slopes in the values of $\Sigma_A$ and MP.

Figure 5.3 shows the results of the implementation of the smooth transition process by comparing a state transition sequences in a timeseries without the process and with the process.

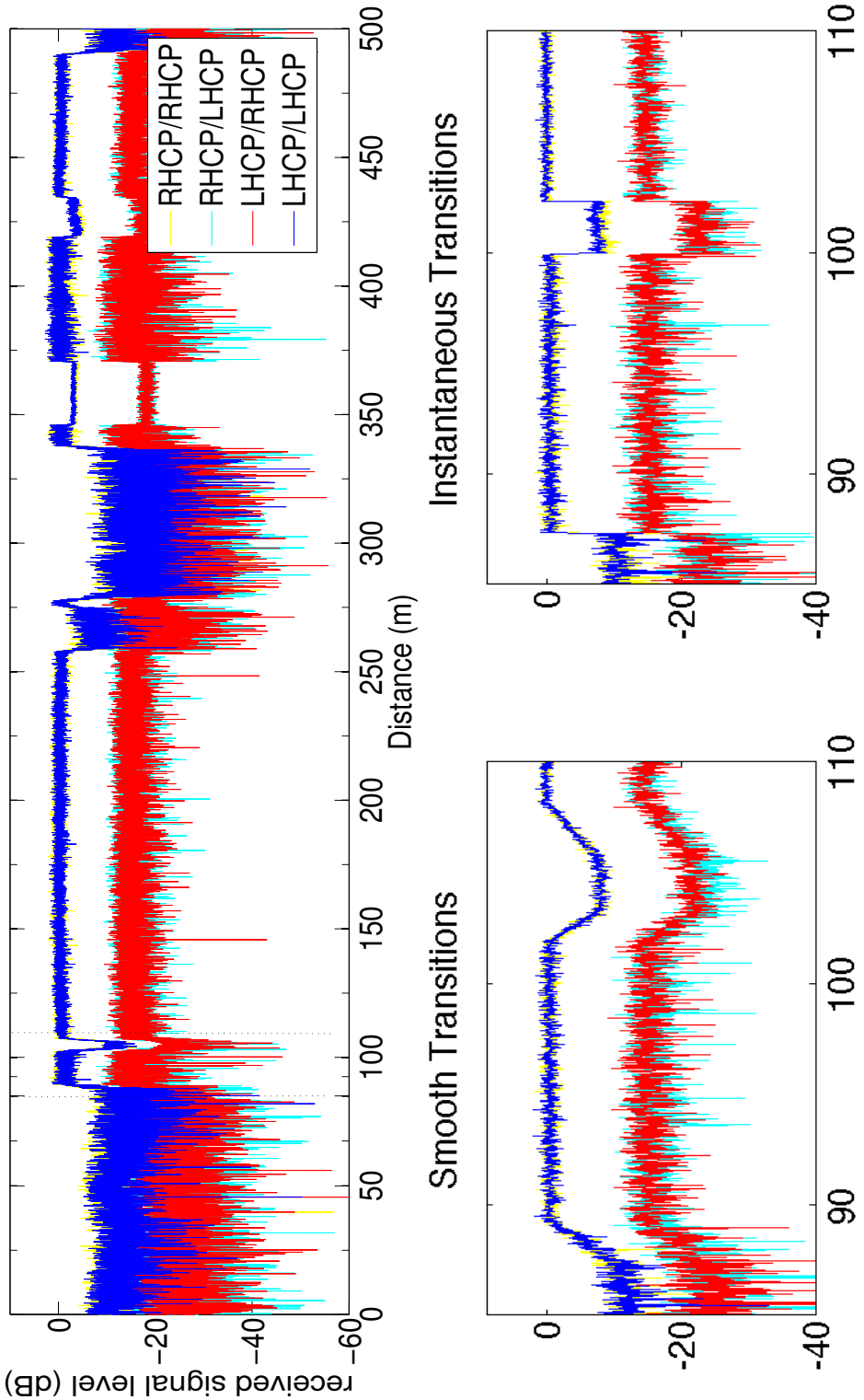


FIGURE 3.7: Timeseries for a mobile unit travelling within the urban user environment (top) with a close up between 85 m and 110 m to show the improved smooth state transitions of the enhanced model (bottom left) compared with instantaneous state transitions of the original baseline model (bottom right). The received signal level is normalised with respect to the LOS power level in dB.

### 3.8.1 Step-by-Step Guide to Smooth State Transitioning

The instructions below outline the methodology for implementing the smooth state transitions when generating the Loo Parameter sequence.

**Generation of Loo Parameter Series with Smooth State Transitioning**

- *Step 1: Loo Triplet Generation*
  Each Loo Parameter ($M_A, \Sigma_A$, MP) is generated using a Gaussian random number generator $\mathrm{G}(\mu, \sigma)$ with mean and standard deviation dependent on the user environment, the specific conditions of simulation and the state type under consideration. A series of alternating good and bad Loo Triplets are generated and interlaced together forming a sequence.

- *Step 2: Generation of State Durations*
  The duration of each state is determined using a lognormal random number generator, i.e. lognrand($M, \Sigma$) which produces the mean and standard deviation of the state duration.

- *Step 3: Interpolation of Loo Triplet Series*
  The state duration is used to interpolate the Loo Parameter triplet to create a triplet for each sample in the state.

- *Step 4: Identification of State Transition*
  State transitions are easily identified as this is where two consecutive values of $M_A, \Sigma_A$ and MP will not be identical.

- *Step 5: Identification of State Transition*
  A slope with a mean of 5 dB/m for the signal magnitude is determined for each individual state transition and thus the number of samples required to produce each slope is determined considering the values of the mean of the direct signal magnitude on either side of the transition.

- *Step 6: State Transition Loo Parameter*
  New Loo Parameter values are determined which gradually change in successive values according to the slope and then are inserted into the Loo Parameter Series.

- **Result**: Loo Parameter Matrix
  A matrix containing a series of Loo parameter triplets of
  form [$M_A$, $\Sigma_A$, MP] x $n$, where $n$ is the number of samples.

## 3.9 Doppler Shaping of the Fast Variations

As the mobile moves through the user environment, the diffuse multipath components each undergo a Doppler shift which results in a Doppler spread. To model this effect on the multipath components, a Doppler spectrum can be implemented depending on the assumed distribution of the angle of arrival of the multipath components.

In the LMS channel the classic U-shaped Jakes Doppler spectrum is commonly assumed for the Doppler spread where the angles of arrival of the multipath components are uniformly distributed at the receiver. However, it is not considered that this spectrum can completely describe the Doppler spreading for the entire journey. An interesting alternative to the Jakes Doppler spectrum, the Asymmetric Jakes Doppler spectrum is commonly assumed in aeronautical or mobile satellite channel [47], which has parameters for adjusting the maximum and minimum frequencies contained within the spectrum. The Jakes and Asymmetric Jakes Doppler spectra were both implemented in addition to a flat Doppler spectrum and a Gaussian spectrum through both finite impulse response (FIR) [47] and infinite impulse response (IIR) [46] filtering methods described below.

In [47], the author describes some of the conditions that apply to particular Doppler spectra. The Jakes spectrum is used when a number of criteria can be met, i.e. the received signal waves propagate horizontally, the arrival of the wave is uniform at the receiver over [-$\pi$, $\pi$] and the antenna at receiver is omnidirectional. The Flat Doppler spectrum is suitable for a 3D isotropic scattering environment. The angle of arrival is assumed uniform in the elevation plane and the azimuth plane. A Gaussian Doppler spectrum is associated with conditions that involve long delays in the multipath components such high frequency terrestrial communications.

In [7] the authors explain that the Doppler spectrum must be known when designed appropriate receive algorithms and when testing synchronisation and channel estimation.

### 3.9.1 Doppler Shaping through FIR filtering

A series with the appropriate Doppler spectrum can be generated by filtering a random, complex, zero-mean & unit variance Gaussian sequence with a FIR Doppler filter derived from the method outlined in [47].

This filtering method occurs in the time domain with the frequency response properties being transferred into an impulse response. The first step of this method uses a theoretical expression for the power spectral density (PSD) of the spectrum in question, $S(f)$. From the PSD, the amplitude of the frequency response $H(f)$ is obtained from the square root of $S(f)$. The impulse response $h(t)$ is then obtained by the inverse Fourier Transform (IFFT) of the frequency response. Depending on the spectrum in question, i.e. whether the impulse response naturally decays to zero or not, the impulse response sequence may need to be windowed and sampled to provide the discrete-time impulse response $h[n]$. In this instance, if required, a Blackman window is implemented, thus providing the coefficients for the filter, where $a = h[n]$.

The theoretical expressions for the power spectral density of various Doppler spectra are given in [47]. The PSD for the Jakes spectrum is given by:

$$S_{Jakes}(f) = \frac{1}{\pi f_d \sqrt{1 - (\frac{f}{f_d})^2}}, \qquad |f| \leq f_d \tag{3.29}$$

The magnitude of the amplitude of the frequency response is given by:

$$|H_{Jakes}(f)| = \sqrt{(S_{Jakes}(f))} \tag{3.30}$$

The impulse response is given by:

$$h_{Jakes}(t) = \Gamma(3/4) \left( \frac{f_d}{\pi |t|} \right)^{(1/4)} I_{1/4}(2\pi f_d |t|) \tag{3.31}$$

where $\Gamma(.)$ is the gamma function and $I_{1/4}$ is the Bessell function of order 1/4.

The discrete-time impulse response, sampled and truncated to $M$ points and causal (delayed by $M/2$ points) is given by:

$$\begin{aligned} h_{Jakes}[m] &= h_{Jakes}(t = (m - M/2)t_s) \\ &= \Gamma(3/4) \left( \frac{f_d}{\pi |(m - M/2)t_s|} \right)^{(1/4)} \mathrm{x}\, I_{1/4}(2\pi f_d |(m - M/2)t_s|) \end{aligned} \tag{3.32}$$

for $m$= 0,1,.... $M$-1.

The baseband normalised Flat Doppler spectrum is given by:

$$S_{Flat}(f) = \frac{1}{2f_d}, \qquad |f| \leq f_d \tag{3.33}$$

The impulse response is given by:

$$h_{Flat}(t) = \sqrt{2f_d}\mathrm{sinc}(2f_d t) \tag{3.34}$$

The discrete-time impulse response is given by:

$$h_{Flat}[m] = \sqrt{2f_d}\text{sinc}(2f_d(m - M/2)ts) \tag{3.35}$$

for $m$= 0,1,.... $M$-1.

The baseband normalised Gaussian Doppler spectrum is given by:

$$S_{Gauss}(f) = \frac{1}{\sqrt{2\pi\sigma^2_{Gauss}}} \exp\left(-\frac{f^2}{2\sigma^2_{Gauss}}\right), \quad |f| \leq f_d \tag{3.36}$$

The impulse response is given by:

$$h_{Gauss}(t) = (2\pi)^{1/4}\sqrt{\sigma_{Gauss}}\exp(-4\pi^2\sigma^2_{Gauss}t^2) \tag{3.37}$$

The discrete-time impulse response is given by:

$$h_{Gauss}[m] = (2\pi)^{1/4}\sqrt{\sigma_{Gauss}}\exp(-4\pi^2\sigma^2_{Gauss}((m - M/2)ts)^2) \tag{3.38}$$

for $m$= 0,1,.... $M$-1.

The baseband normalised Asymmetric Jakes Doppler spectrum is given by:

$$S_{ASJakes}(f) = \frac{A_{ASJakes}}{\pi f_d\sqrt{1 - (f/f_d)^2}}, \; -f_d \leq f_{d,min} \leq f \leq f_{d,max} \leq f_d \tag{3.39}$$

with $A_{ASJakes}$ given by equation 3.42.

The discrete-time impulse response is found by performing an inverse Fast Fourier Transform (FFT) on the frequency-sampled version of the amplitude of the frequency response.

### 3.9.2 Doppler Shaping through IIR filtering

As discussed previously in Section 3.7.1 an autoregressive IIR filter [46] may be used to implement correlation if the desired autocorrelation is known. This method may be used to implement a Doppler spectrum and it is the approach used in the Enhanced Statistical model.

Theoretical expressions are given in [47] for the autocorrelation functions of important Doppler shapes and are reproduced below. From these theoretical ACF expressions, the autoregressive IIR filter coefficients may be obtained by creating an autocorrelation matrix and solving the Yule-Walker equations as described by Equations (3.26), (3.27), (3.28).

The autocorrelation function of the Jakes spectrum is given by Equation (3.40):

$$R_{Jakes}(\tau) = I_0(2\pi f_d \tau) \tag{3.40}$$

where $I_0$ is a Bessel function of the first kind of order 0.

The autocorrelation function of an Asymmetric Jakes spectrum is given by Equation (3.41):

$$R_{ASJ}(\tau) = \frac{A_{ASJakes}}{\pi}\left[\int_a^b \cos(2\pi f_d \tau \sin\phi)d\phi - j\int_c^d \sin(2\pi f_d \tau \cos\phi)d\phi\right] \tag{3.41}$$

where $a = \sin^{-1}(\frac{f_{d,min}}{f_d})$, $b = \sin^{-1}(\frac{f_{d,max}}{f_d})$, $c = \cos^{-1}(\frac{f_{d,min}}{f_d})$, $d = \cos^{-1}(\frac{f_{d,max}}{f_d})$ and $f_{d,max}$ is the maximum Doppler shift, $f_{d,min}$ is the minimum Doppler shift where the spectrum is non-zero and $A_{ASJakes}$ is the amplitude of the spectrum given by Equation (3.42):

$$A_{ASJakes} = \frac{\pi}{\sin^{-1}(\frac{f_{d,max}}{f_d}) - \sin^{-1}(\frac{f_{d,min}}{f_d})} \tag{3.42}$$

The autocorrelation function of a Flat Doppler spectrum is given by Equation (3.43):

$$R_{Flat}(\tau) = \text{sinc}(2f_d\tau) \tag{3.43}$$

The autocorrelation function of a Gaussian spectrum is given by Equation (3.44):

$$R_{Gauss}(\tau) = \exp(-2\pi^2\sigma^2\tau^2) \tag{3.44}$$

where $\sigma$ is defined the 3 dB cut-off frequency ($f_c$); $f_c = \sigma\sqrt{2\ln(2)}$.

Given the autocorrelation functions of each spectrum, the filter coefficients can be determined for an IIR filter by forming an autocorrelation matrix from the sample autocorrelation function and determining the vector **a** as in Equation (3.25). The filter coefficients A and B are: $A$ = [1 a], and B =1. Filtering the multipath component with the IIR filter gives a series with the desired spectrum.

### 3.9.3 Other Methods of Doppler Shaping

The resultant Doppler spreads were also compared with Jakes Doppler implementation using the popular Sum of Sinusoids (SoS) method [42], which contains the parameters $K_o$ and $\chi$ to shape the spectrum, Figure 4.11. The results are discussed further in section 4.5. This method is of interest as it allows for the channel model to have varying mobile unit speeds.

The authors in [2] use a Butterworth filter to implement Doppler shaping with a transfer function given by Equation (3.45)

$$\mid H_{butt}(f) \mid^2 = \frac{B}{1 + (f/f_c)^{2k}} \tag{3.45}$$

where $f_c$ is the cut-off frequency, $B$ is a constant to normalise energy of the filtered series to 1 and $k$ is the order of the filter.

This achieves a relatively flat spectrum up to the cut-off frequency and gives a reasonable approximation for the spectrum of the multipath components.

### 3.9.4 Comparison of Doppler Shaping Methods

After analysis of the autocorrelation and spectra of the product of the FIR filtering process and the IIR filtering process it was decided to implement the IIR filtering method based on the autocorrelation technique from [47].

The IIR method gives better match to the theoretical autocorrelation shape, a better U-shaped Doppler spectrum and also does not require discarding of an initial amount of filtered samples until the filter stabilises as in the FIR filter case.

The autocorrelation and the spectrum of both the FIR and IIR filtering methods are plotted below using the Jakes Doppler spectrum as an example.

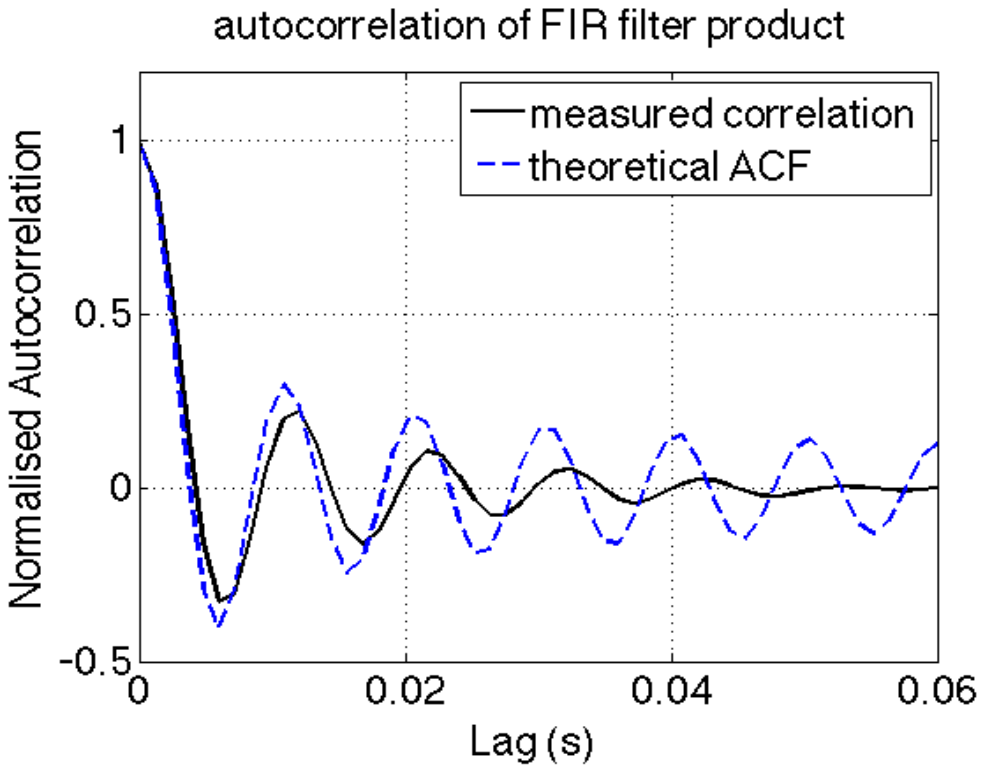


FIGURE 3.8: Autocorrelation of the signal as a result of FIR filtering.

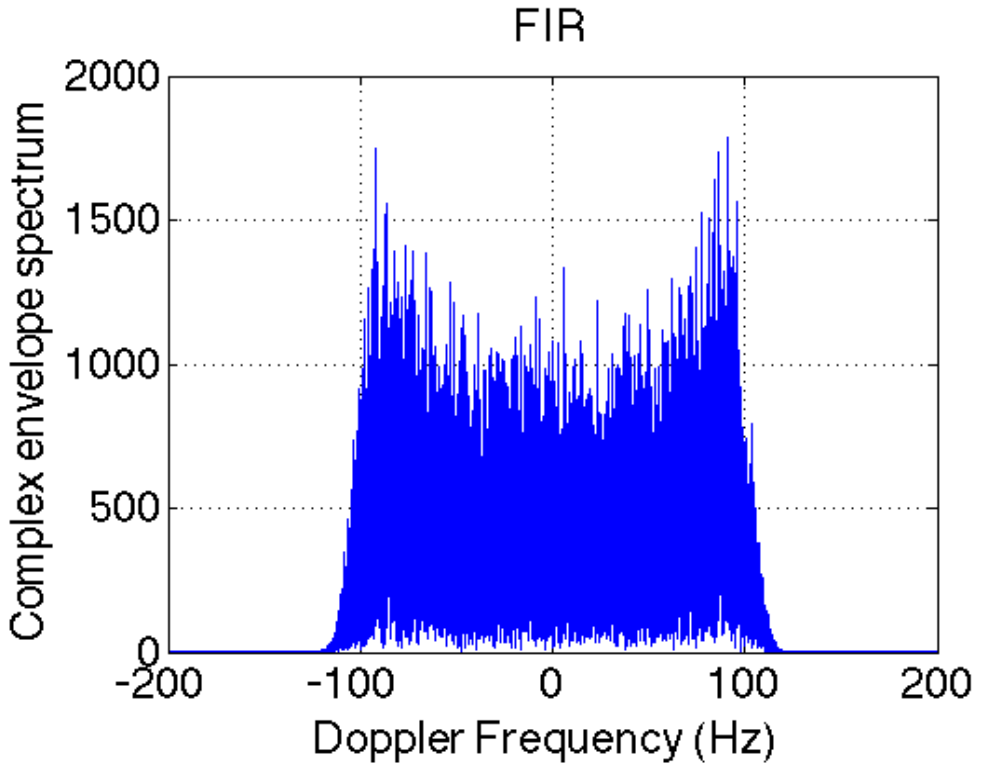


FIGURE 3.9: Frequency response of the signal as a result of FIR filtering.

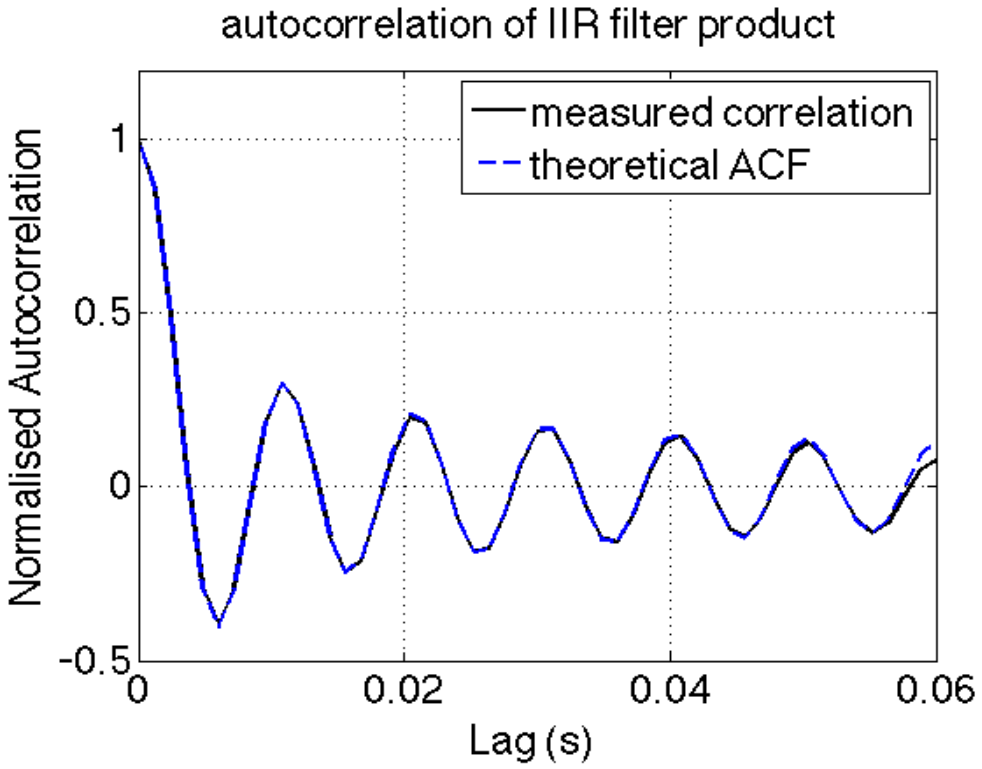


FIGURE 3.10: Autocorrelation of the signal as a result of IIR filtering.

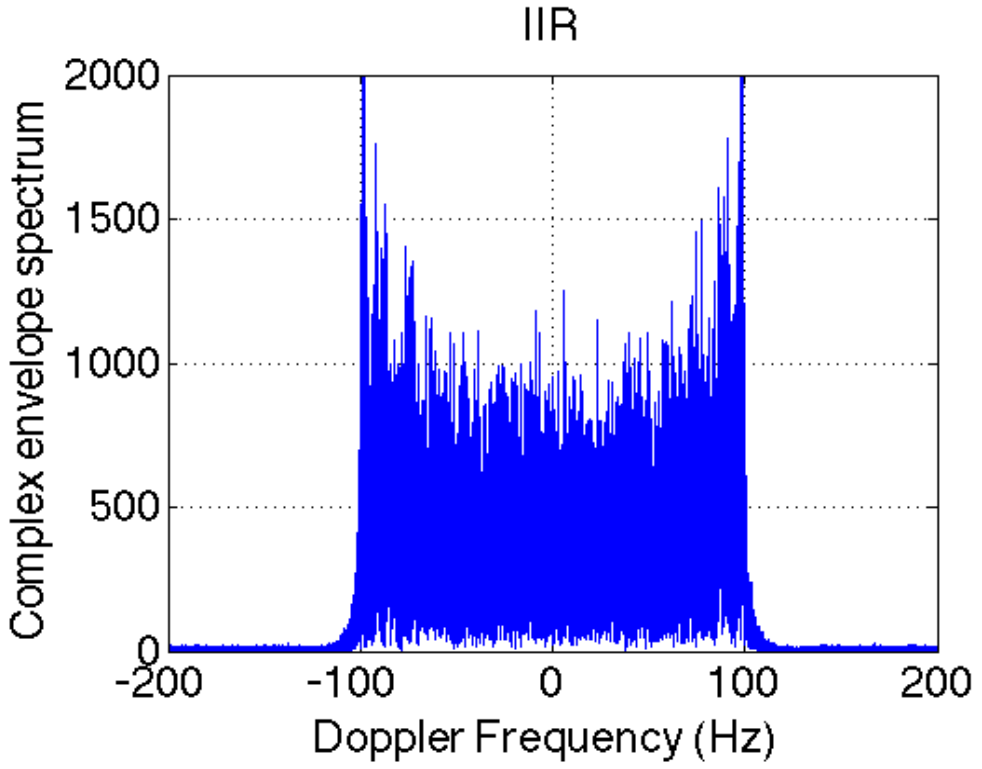


FIGURE 3.11: Frequency response of the signal as a result of IIR filtering.

### 3.9.5 Doppler Shift

The direct signal also has Doppler effects applied to it through the additional of an initial random phase $\theta$ that has a Doppler shift applied with the maximum Doppler frequency $f_{max}$ as given by Equation (2.15) and through the method outlined in section 2.2.8.1.

## 3.10 Variation of the XPC of the environment

As opposed to keeping the cross-polarisation coupling (XPC) of the environment constant throughout the entire simulated journey using parameters from [1], the XPC was allowed to vary throughout the journey according to the distributions given for various user environments in [40]. This allows different XPC values to exist for good and bad states.

## 3.11 Interpolation to Symbol Rate Sampling

The channel samples are generated at a rate equivalent to a sampling frequency of ∼815 Hz. This is the minimum sampling frequency that satisfies the requirement for the multipath component to be sampled eight times per wavelength of the carrier frequency in order to obtain enough detail of the multipath which varies at a faster rate than the direct signal [2]. Sampling at a lower frequency would not give us adequate insight into the detailed fluctuations of the multipath component. Although sampling at a higher frequency may seem like an attractive prospect, it rises questions around the benefit of further detailed knowledge gained versus the increased computation load of the simulation resulting in increased data production and increased simulation time. Therefore, it is important to strike the correct balance between computational complexity and more detailed simulation characteristics.

However, if we wish to further assess the performance of transmission schemes or particular coding schemes in the dual polarised LMS channel, we may wish to simulate the application of signal processing algorithms to transmissions through the channel. In order to apply signal processing algorithms to the channel, we must sample the channel at a rate that matches the symbol rate of the transmitted data through the channel in real life scenarios. This requires sampling the channel at a much higher frequency than that used thus far in the simulation of the dual polarised LMS timeseries.

In order to avoid simulating the timeseries at a sampling frequency that would cause the simulator to be too slow, the application of an interpolation technique was considered that would increase the sampling frequency to match the transmission rate $R_s$ whilst preserving the channel characteristics.

A multirate filtering technique comprised of polyphase and linear interpolation is recommended in [47] as an optimal trade off between speed & accuracy. The combination of the polyphase and linear interpolation provides an improved preservation of the second order statistics, such as the average fade duration and the level crossing rate of the timeseries, than linear interpolation alone.

### 3.11.1 Method

For the transmissions for voice and data applications in satellite based L-band and S-band systems, typical bit rates of $\sim$9.6 - 64 kbits$^{-1}$ are used [24]. To simulate transmission at the two extreme values of this range, interpolation factors of 11.8 and 78.5 would be required.

For simplicity, an integer expansion rate was assumed and the interpolation rate $L$ set to a value of 72; therefore the polyphase interpolation factor $L_p$ was set to 12 and the linear interpolation factor $L_l$ was set to 6.

$$L = R_s/f_s = L_p L_l \tag{3.46}$$

where $R_s$ is the desired channel sampling rate.

In [47], the author describes how linear interpolation is achieved by increasing the sampling rate through zero-padding and then using a low-pass interpolation filter to remove undesired spectral images in the frequency domain. In polyphase filtering, the interpolation filter is reordered into a bank of $L_p$ polyphase filters thus reducing the computational load by a factor of $1/L_p$ as the coefficients corresponding to zero input samples are not included in the filters, and each output sample is filtered by only one polyphase filter. Inbuilt MATLAB functions exist to implement polyphase and linear filters and combine them to form a multirate filter.

### 3.11.2 Results of Multirate Filtering

The multirate filter was used to filter the timeseries thus interpolating the channel samples to a frequency of 5.87 kHz. The magnitude response of the linear filter, the polyphase filter and the multirate combination filter are compared in Figure 3.13. Analysis of the filtered timeseries shows a good agreement with the original timeseries, Figure 3.12. Figure 3.14 shows how the Doppler spectrum is retained by the three filters for a mobile unit journey simulated in the suburban user environment with an angle of arrival of the direct signal at 180°. There is a good agreement although the filtering process raises the power of the spectrum in the main frequency band between -100 and 100 Hz.

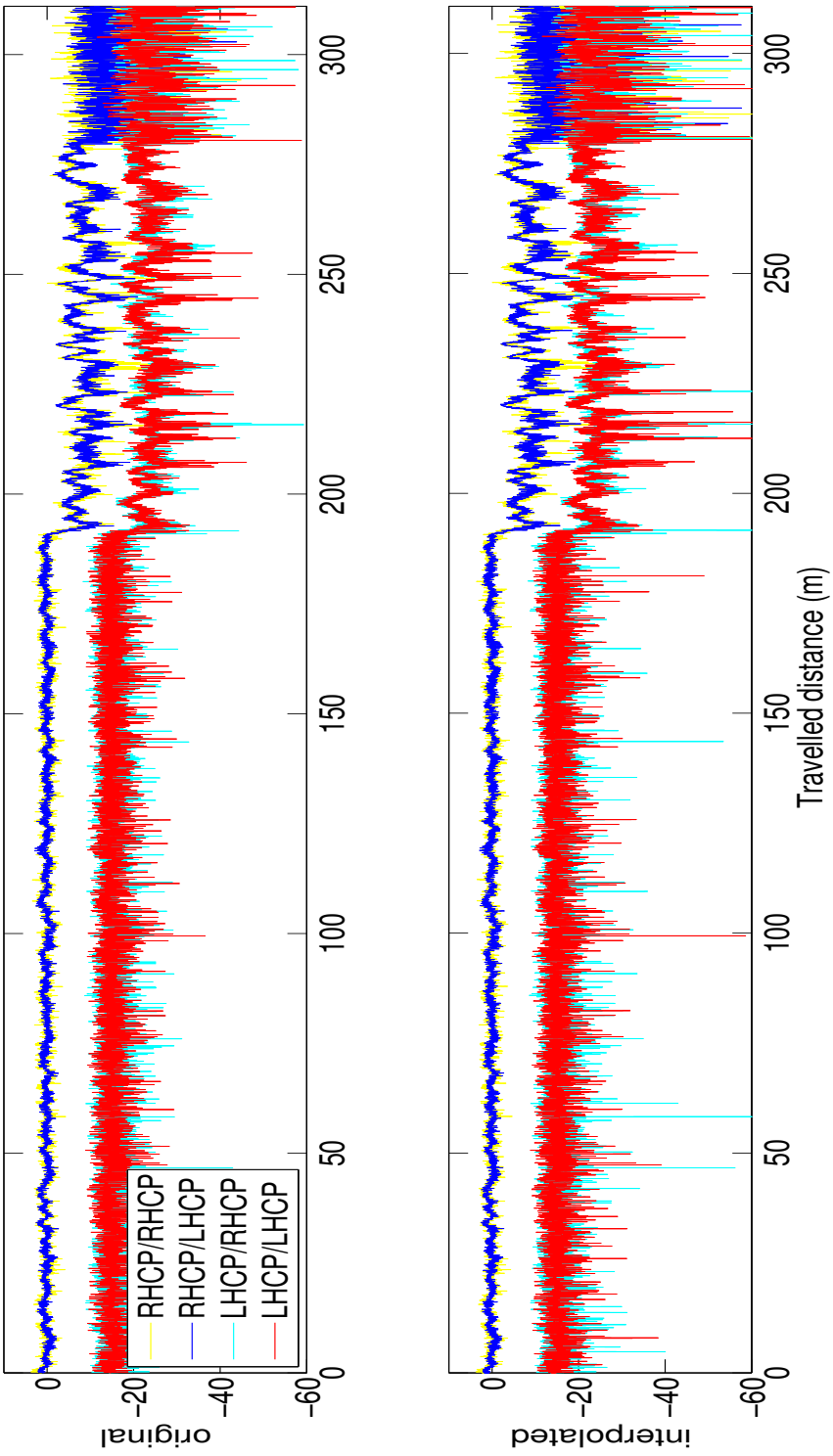


FIGURE 3.12: Timeseries for a mobile unit travelling within the suburban user environment (top) with the interpolated timeseries using multirate filters to produce samples at the require symbol rate (bottom). The two timeseries show good agreement.

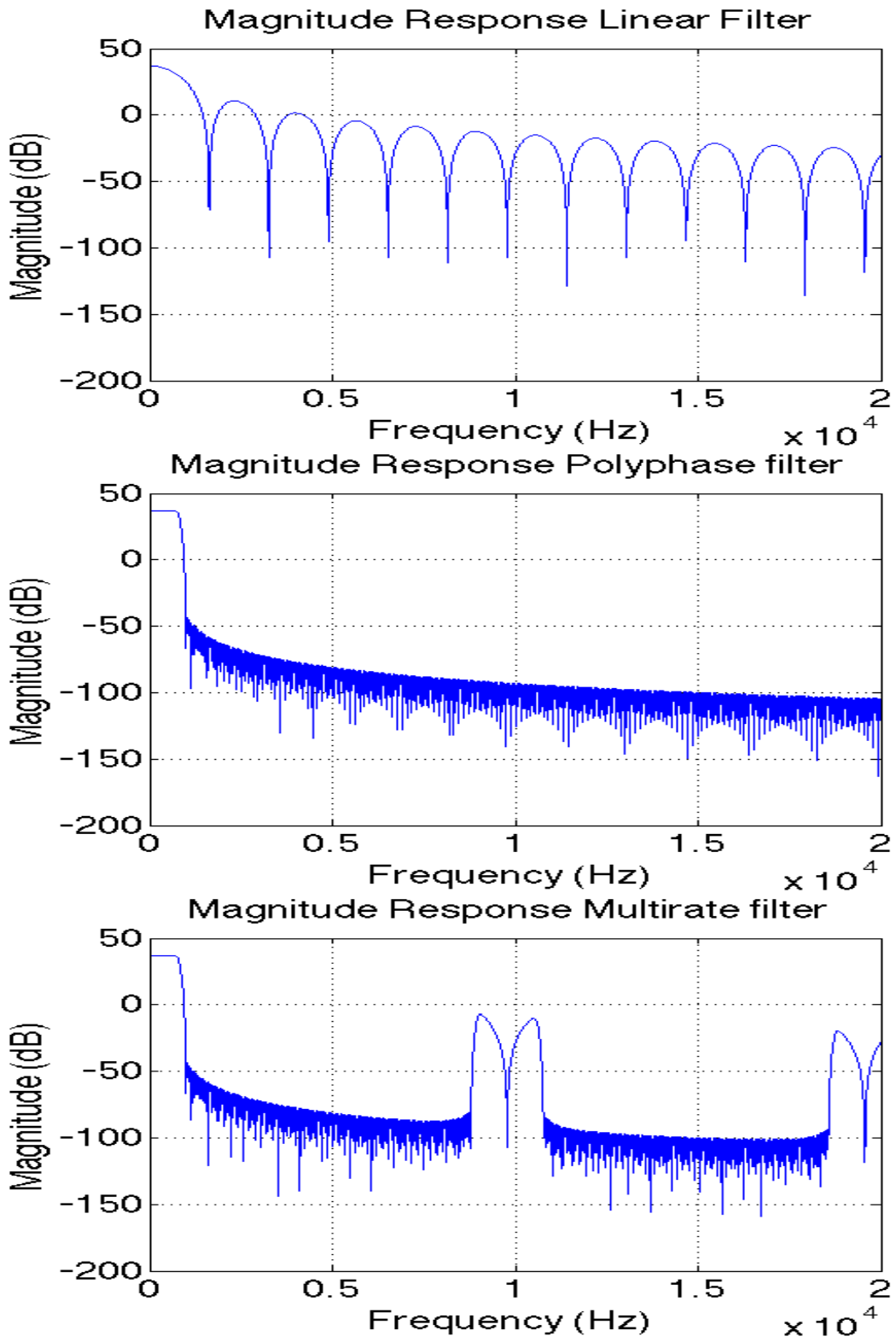


FIGURE 3.13: Magnitude response of the linear filter (top), the polyphase filter (middle) and the multirate filter (bottom).

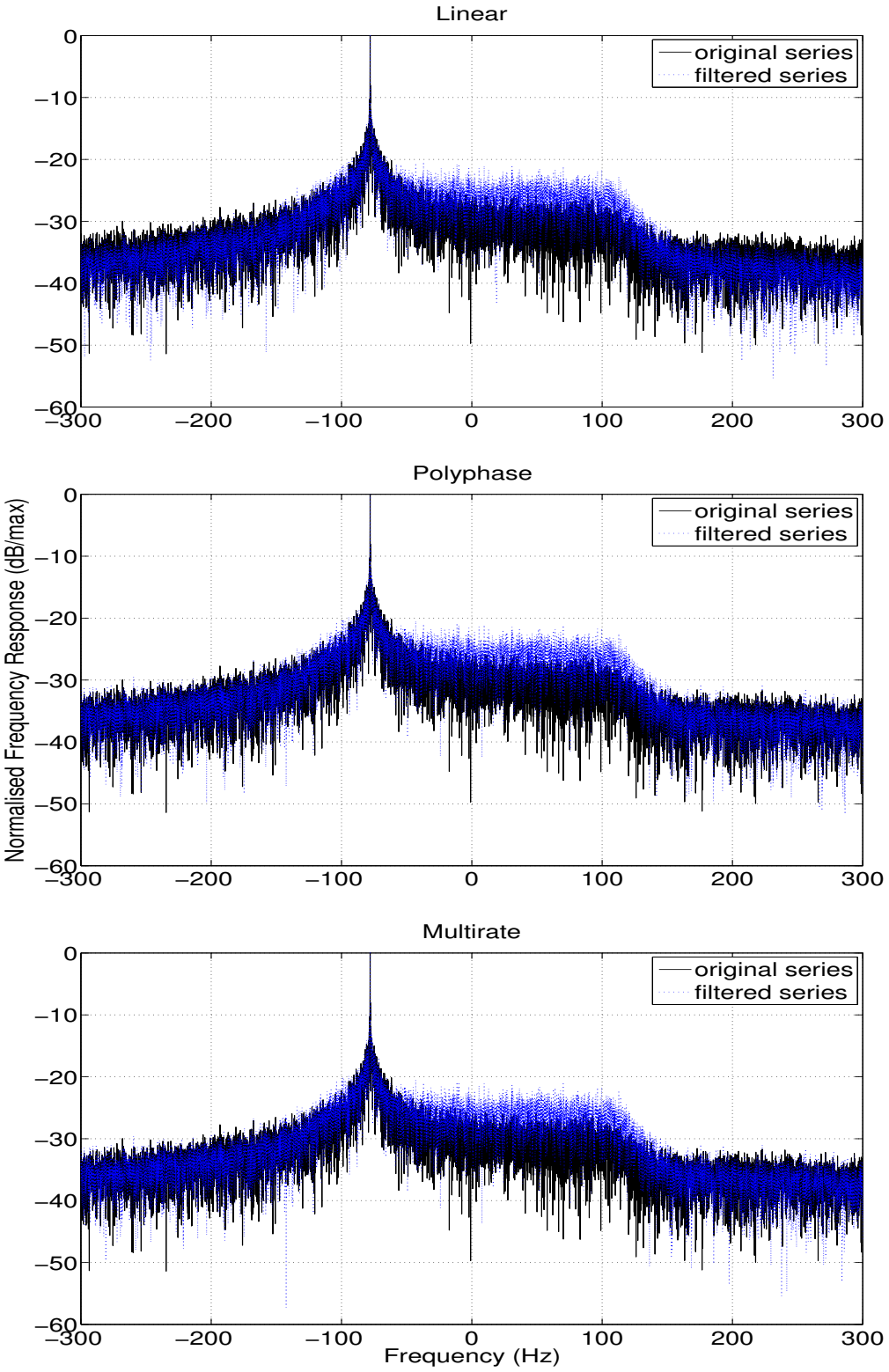


FIGURE 3.14: A comparison of the original spectrum of the series samples at $\sim$ 815 Hz, plotted in black and the interpolated series at $\sim$ 5.87 kHz plotted in blue achieved by using a linear filter (top), a polyphase filter (middle) and a multirate filter (bottom). It can be seen that all filters result in a raising of the level of the spectrum in the main band between -100 and 100 Hz.

## 3.12 Capacity Analysis

To analyse the performance of the LMS channel under certain conditions, the outage capacity was determined. The capacity of a channel is related to the measure of the information that can be transmitted for a specific of signal-to-noise ratio [36]. We can determine the mutual information ($I$) transmitted through the channel, assuming there is no channel state information at the transmitter, $I$ is given by Equation 3.47:

$$I = \log_2 \det \left( \mathbf{I}_{M_R} + \frac{E_s}{M_T N_0} \mathbf{H}\mathbf{H}^{\mathbf{H}} \right) \tag{3.47}$$

where $E_s$ is the energy per sympol, $N_o$ is the noise power, $M_R$ and $M_T$ are the number of receiver and transmitter antenna, $\mathbf{H}$ is the channel matrix and $\mathbf{H}^{\mathrm{H}}$ is the Hermitian, complex conjugate of the channel matrix. The unit of measurement for information is b/s/Hz.

The outage capacity ($C_{out,q}$) is the information rate that is guaranteed for (100- $q$)% of the channel realisations. If $I$ is lower than this rate, the channel is said to be in outage, Equation 3.48:

$$P(I \leq C_{out,q}) = q\% \tag{3.48}$$

For example, if we set $q = 1$, we may investigate the 1% outage capacity of a channel, we find the information rate guaranteed in 99% of the channel realisations, with only 1% of the channels being in outage.

Another performance indicator is the bit error rate (BER), which can be determined for an uncoded quadrature phase-shift keying (QPSK) single-input multiple-output (SIMO) LMS system using maximal ratio combining (MRC) [48], given by Equation 3.49:

$$BER(h) = \frac{1}{2}\text{erfc}\sqrt{\frac{E_b}{N_o}\sum_{i=1}^{N} \mid h_i \mid^2} \tag{3.49}$$

where erfc is the complementary error function, $E_b$ is the energy per bit.

### 3.12.1 Capacity as a Function of Model Parameters

The effect of the model parameters of the dual polarised MIMO channel on the outage capacity and also the gain associated with a MIMO channel in comparison the single-input single-output (SISO) channel were explored.

The cross-polarisation of the antenna is a measure of the antennas ability to distinguish between orthogonally polarised signals. As the XPD of the antenna increases, we expected the outage capacity of the channel to increase as the unwanted cross-polarised signals cause less interference and the channel becomes more diagonal [1]. This is seen in Figure 3.15, as XPD increases, the 1% outage capacity for the open rural environment also increases. This pattern is also seen in the suburban and urban environments, Figures 3.16 and 3.17.

As satellite elevation angle increases, the amount of obstructions from environmental objects such as buildings decreases and this increases the probability of establishing a clear line of sight between satellite and mobile receiver. Figures 3.18 - 3.20 shows the expected increase in outage capacity with satellite elevation angle as simulated for the open rural, suburban and urban user environments.

The small-scale polarisation coefficient ($\rho$) determines the amount of polarisation correlation that occurs between subchannels within the MIMO channel matrix. As correlation has a detrimental effect on capacity, we expect that as $\rho$ increases from 0.1 (least correlation) to 0.9 (greatest correlation), outage capacity will decrease. Figures 3.21 and 3.22 show this expected pattern for the open rural and suburban environments and Figure 3.23 shows this expected pattern for the urban environment with only bad states included in the calculation of the outage capacity.

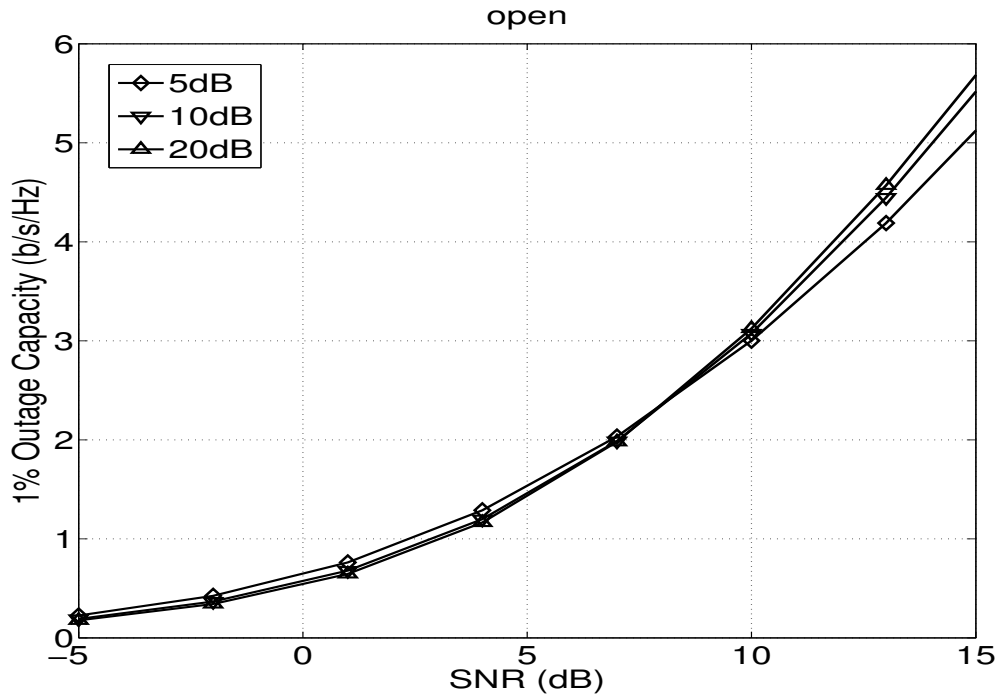


FIGURE 3.15: A plot of outage capacity against SNR for a range of antenna XPD values in the open rural user environment.

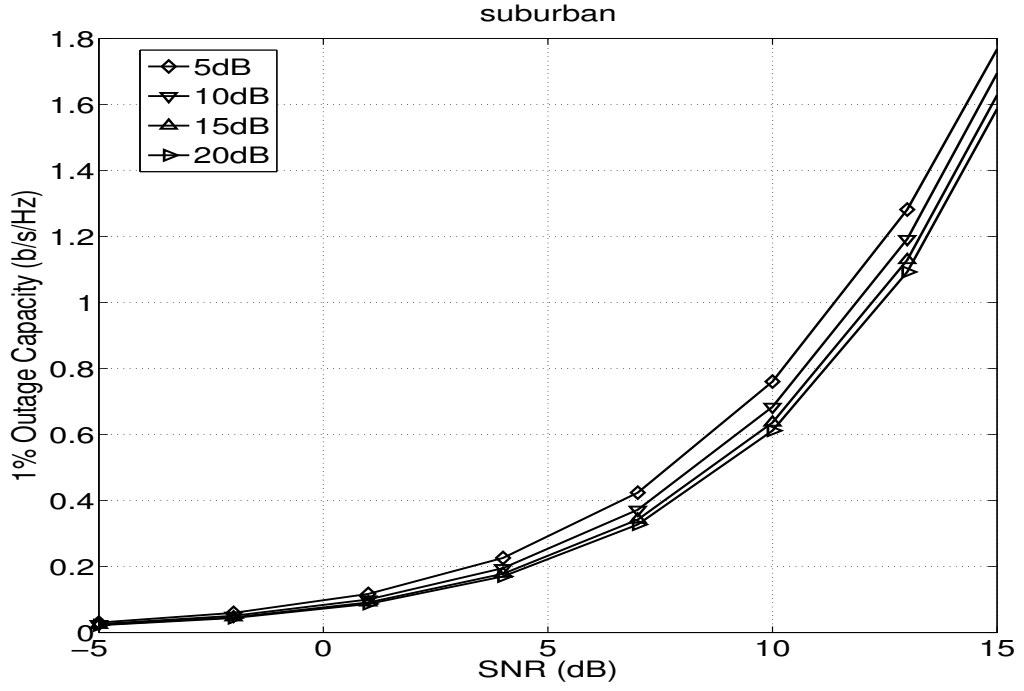


FIGURE 3.16: A plot of outage capacity against SNR for a range of antenna XPD values in the suburban user environment.

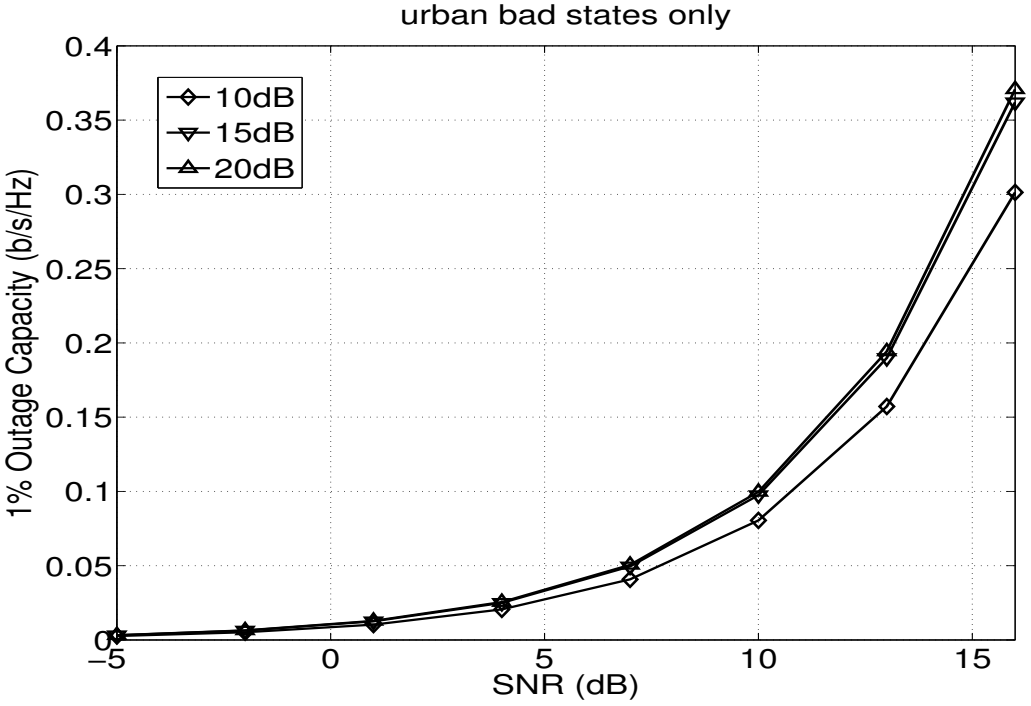


FIGURE 3.17: A plot of outage capacity against SNR for a range of antenna XPD values in the urban user environment for bad states only.

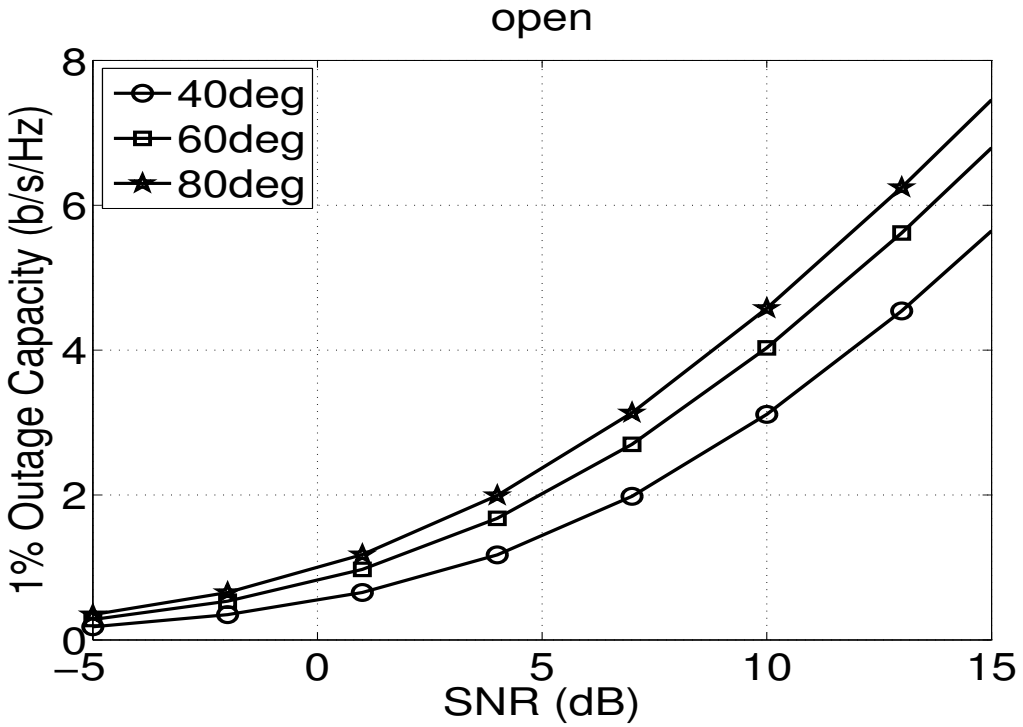


FIGURE 3.18: A plot of outage capacity against SNR for a range of satellite elevation angles in the open rural user environment.

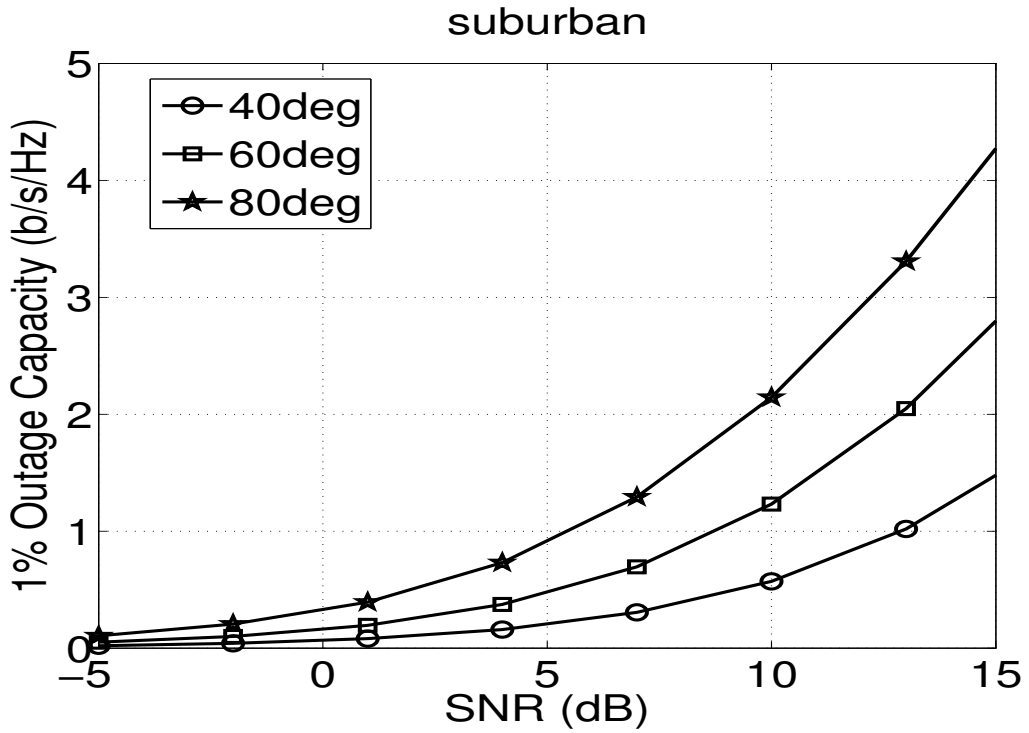


FIGURE 3.19: A plot of outage capacity against SNR for a range of satellite elevation angles in the suburban user environment.

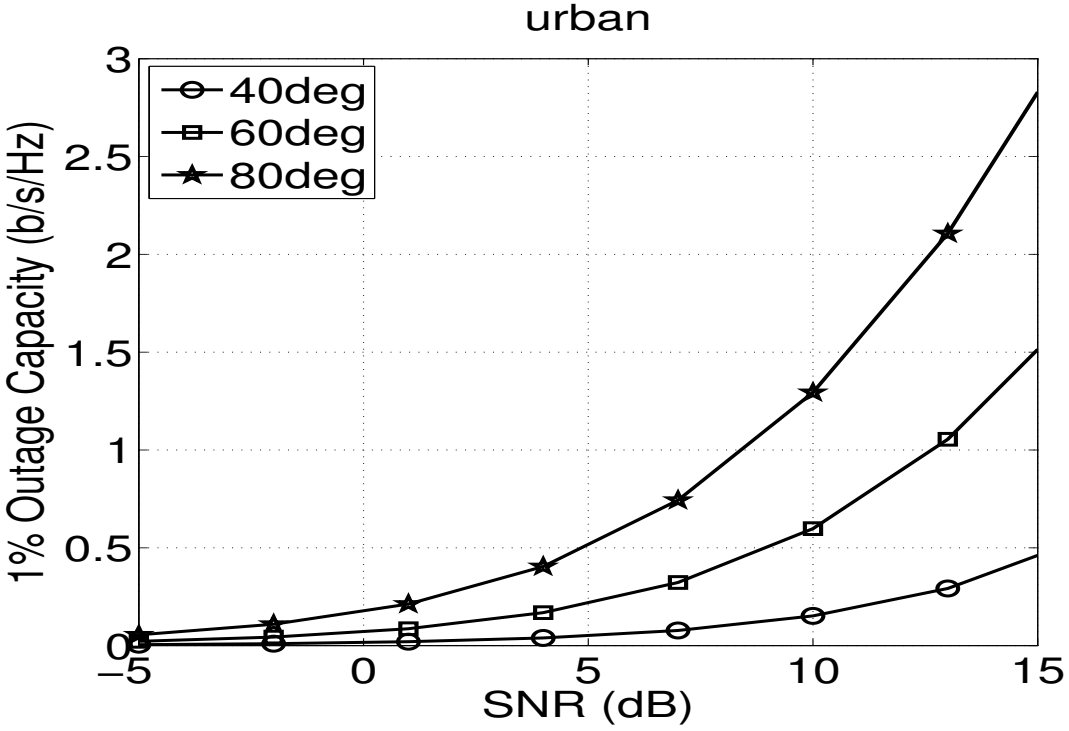


FIGURE 3.20: A plot of outage capacity against SNR for a range of satellite elevation angles in the urban user environment.

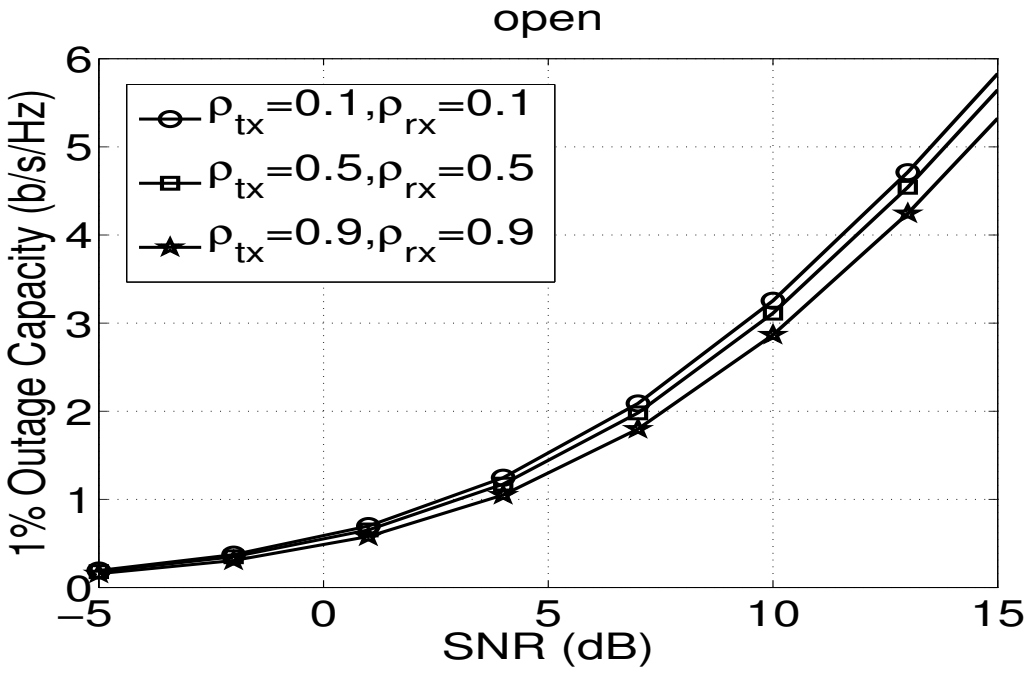


FIGURE 3.21: A plot of outage capacity against SNR for a range of small-scale polarisation correlation coefficient values, with $\rho_{tx}$=$\rho_{rx}$, for the open rural user environment.

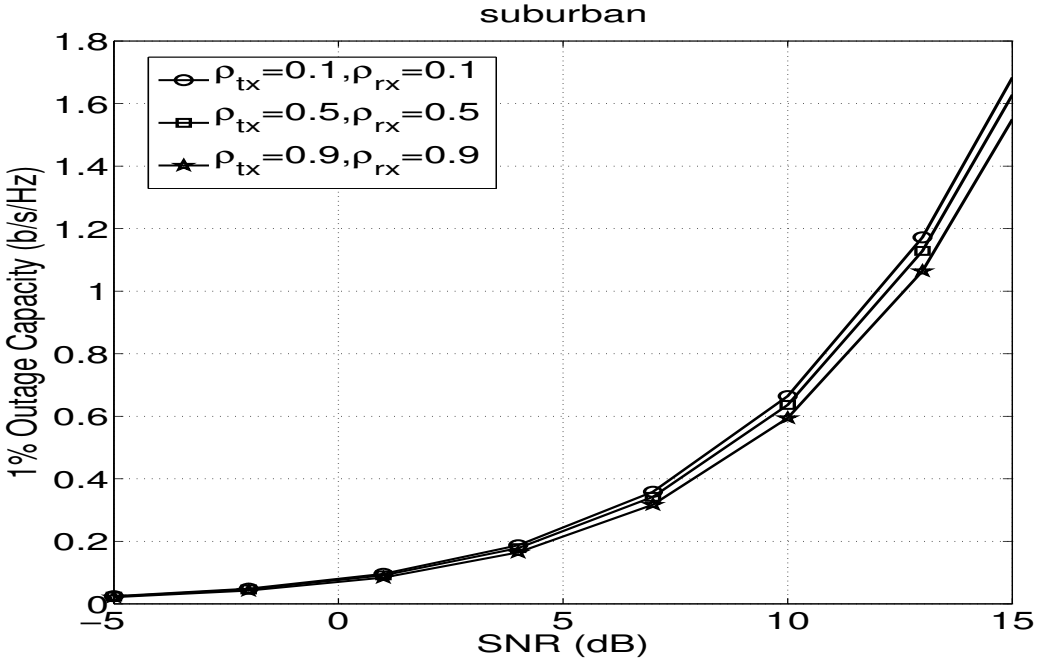


FIGURE 3.22: A plot of outage capacity against SNR for a range of small-scale polarisation correlation coefficient values, with $\rho_{tx}$=$\rho_{rx}$, for the suburban user environment.

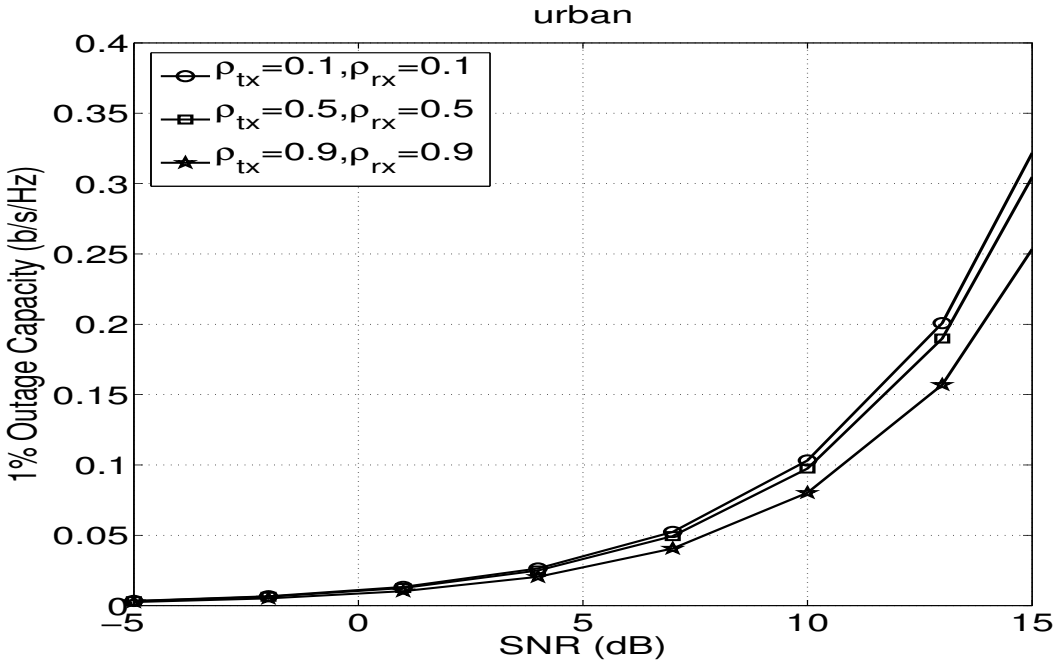


FIGURE 3.23: A plot of outage capacity against SNR for a range of small-scale polarisation correlation coefficient values, with $\rho_{tx}$=$\rho_{rx}$, for BAD states only in the urban user environment.

### 3.12.2 MIMO over SISO Advantage

A useful comparison can be made between the outage capacity of a 2x2 MIMO matrix and the outage capacity of two orthogonally polarised SISO channels as these two systems will have equal transmit power and bandwidth. As polarisation is already used in as an extra colour in frequency reuse schemes, [38] describes the importance of investigating the gain to be found in moving from this existing arrangement of two orthogonally polarised SISO channels to a dual polarised MIMO channel and finding the optimal conditions for dual polarised MIMO implementation.

The MIMO advantage (MA) is a dimensionless ratio of the outage capacity of the 2x2 dual polarised MIMO channel to the outage capacity of 2 orthogonal SISO subchannels. The main difference between these two arrangements is that with the SISO case the two cross-polarisation channels act as interference to the co-polarisation channels, whereas with the dual polarised MIMO case, the joint signal processing utilities these cross-polarisation channels to its advantage. If the MIMO advantage is greater than 1 then the capacity of the MIMO arrangement exceed that of the 2*SISO arrangement. As can be seen on Figure 3.24, the MIMO advantage exceeds 1 in all simulations.

Figure 3.24 shows the plots of the MIMO advantage when three parameters are investigated for the three user environments simulated at 15 dB SNR and using the baseline parameters in Table A.1. In the three plots, the MIMO advantage is greater in the urban user environment and decreases when moving to the suburban area and then decreases again in the open rural environment. This is due to the ability of the MIMO arrangement to take advantage of the rich scattering in urban areas and the high level of environmental cross-polarisation coupling the signal undergoes in this environment. This effect decreases as we change from urban, suburban to open, thus open rural environments benefit least from the implementation of dual polarised MIMO architecture.

A number of other patterns emerge from Figure 3.24; the MA decreases with increasing antenna XPD, increasing small-scale polarisation correlation coefficient and increasing

satellite elevation angle. As the cross-polarisation of the antenna increases, the interference of the two SISO channels from the cross-polarised signals will decrease, thus reducing the gain from implementing MIMO. As the satellite elevation angle increases, the chance of obtaining a line-of sight signal (or partially shadowed signal) improves, thus reducing the reliance on multipath scattering and cross-polarised signal components for received signal. The change in satellite elevation angle has little effect on the MIMO advantage in the open rural user environment due to the high probability of LOS states. The improvement in MIMO capacity relies on receiving independent signals, thus it is greatly affected by increased correlation between the subchannels and the MA is reduced by increasing the polarisation correlation coefficient.

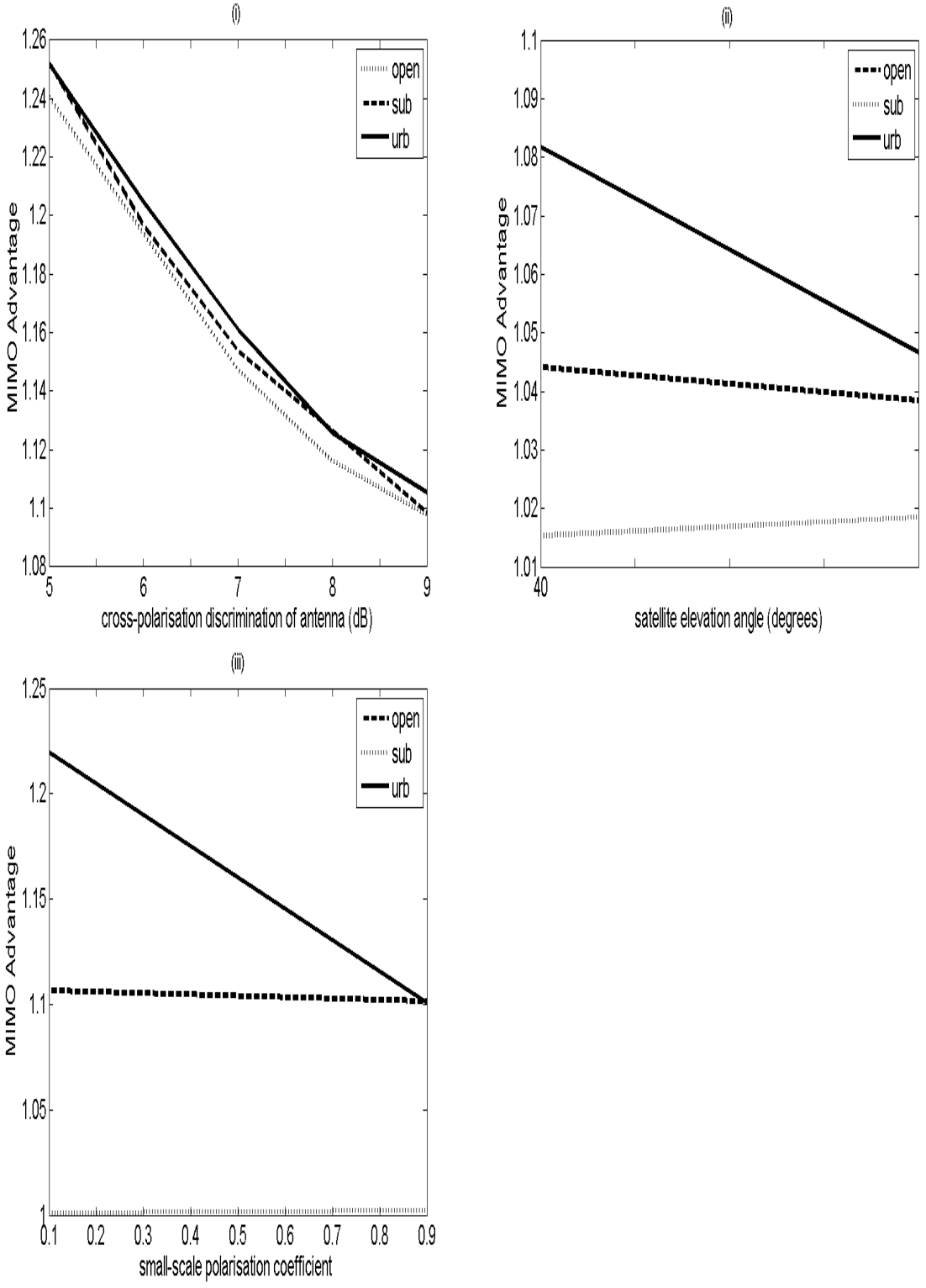


FIGURE 3.24: (i) The MIMO advantage obtained in open, suburban and urban environments at 15dB SNR plotted against (i) antenna XPD, (ii) satellite elevation angle, (iii) small-scale polarisation correlation coefficient.

### 3.12.3 MIMO vs SIMO

Figure 3.25 shows three timeseries simulated for the suburban user environment using SISO, SIMO and MIMO architectures. These simulations use a semi-Markov chain to model the transitions between good and bad states. The SISO timeseries shows a series of good and bad states, although the state types are not completely obvious as they are somewhat obscured by the large variations in the received signal level. In the timeseries of the SIMO and MIMO arrangements, the additional antenna and the associated diversity advantage result in a decrease of the fading margins, and therefore the good and bad states are much more pronounced in the these simulations. In the SIMO timeseries, the received signal at the two receivers is very similar and one almost completely overlaps the other. In the MIMO timeseries, the same is true of the two co-polarisation components ($h_{11}$ and $h_{22}$) and also of the two cross-polarisation components ($h_{12}$ and $h_{21}$), although the two types of components are easily identifiable, with the cross-polarisation having a much lower signal power than the co-polarisation components.

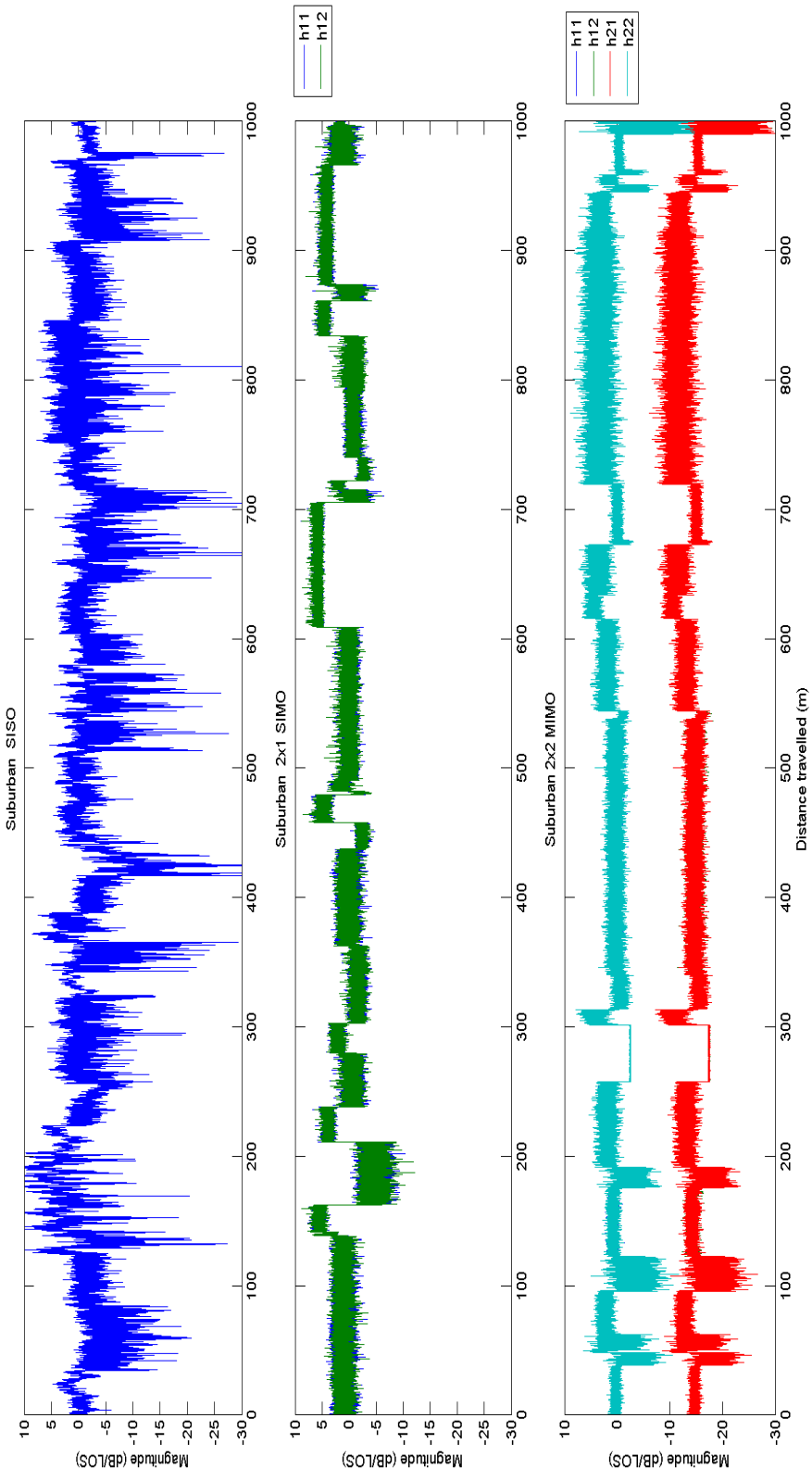


FIGURE 3.25: A comparison of suburban user environment timeseries with various antenna configurations, (i) SISO (ii) 2x1 SIMO (iii) 2x2 dual polarised MIMO, assuming a transmission from a GEO satellite at $40^o$ with mobile velocity of 50km/ hr and implementing semi-Markov state transition modelling. The received signal level is normalised with respect to the LOS power level in dB.

Figure 3.26 shows how BER and outage capacity are affected by increasing the number of receive antenna in a SIMO system. Three architectures are considered per user environment: a 1x1 SISO channel, a 2x1 SIMO channel and a 4x1 SIMO channel. Maximal ratio combining (MRC) is used to combine the multiple subchannels and as expected, the outage capacity and BER both improve as the number of receiver antenna increase.

The open rural environment provides the best outage capacity and BER of the three environments investigated, at 15dB SNR the 1x1 SISO, 2x1 SIMO and 4x1 SIMO arrangements have outage capacities of approximately 4 b/s/Hz, 5 b/s/Hz and 6 b/s/Hz, respectively. In the suburban environment at 15 dB SNR the outage capacities for the three antenna arrangements (in the same order) are approx. 1.5 b/s/Hz, 2.5 b/s/Hz and 3 b/s/Hz. These values decrease further in the urban environment to approx. 0.6 b/s/Hz, 1.0 b/s/Hz, 1.4 b/s/Hz. The urban environment stands to gain the most from the multiple antenna configuration in the SIMO scenario in comparison to the open and suburban environments due to the scattering richness of the urban environment. The increased scattering in the urban environment will lead a decrease in the correlation of the output signals and thus increase the performance of the channel and the outage capacity. This can be seen in Figure 3.26 as the gain in outage capacity for the urban environment when the SIMO antenna configuration is increased from two antenna to four antenna is significant and relatively greater than achieved in the open and suburban environments.

In the open rural environment a BER of $10^{-5}$ is achieved at 13.5 dB, 11 dB, 8.5 dB for the SISO, 2x1 SIMO and 4x1 SIMO arrangements respectively. In the suburban environment a greater SNR is required to reach the same BER, this increases to 30 dB, 25 dB and 22.5 dB for the three antenna arrangements. In the urban environment none of the antenna arrangements reach a BER of $10^{-5}$ below 30 dB SNR.

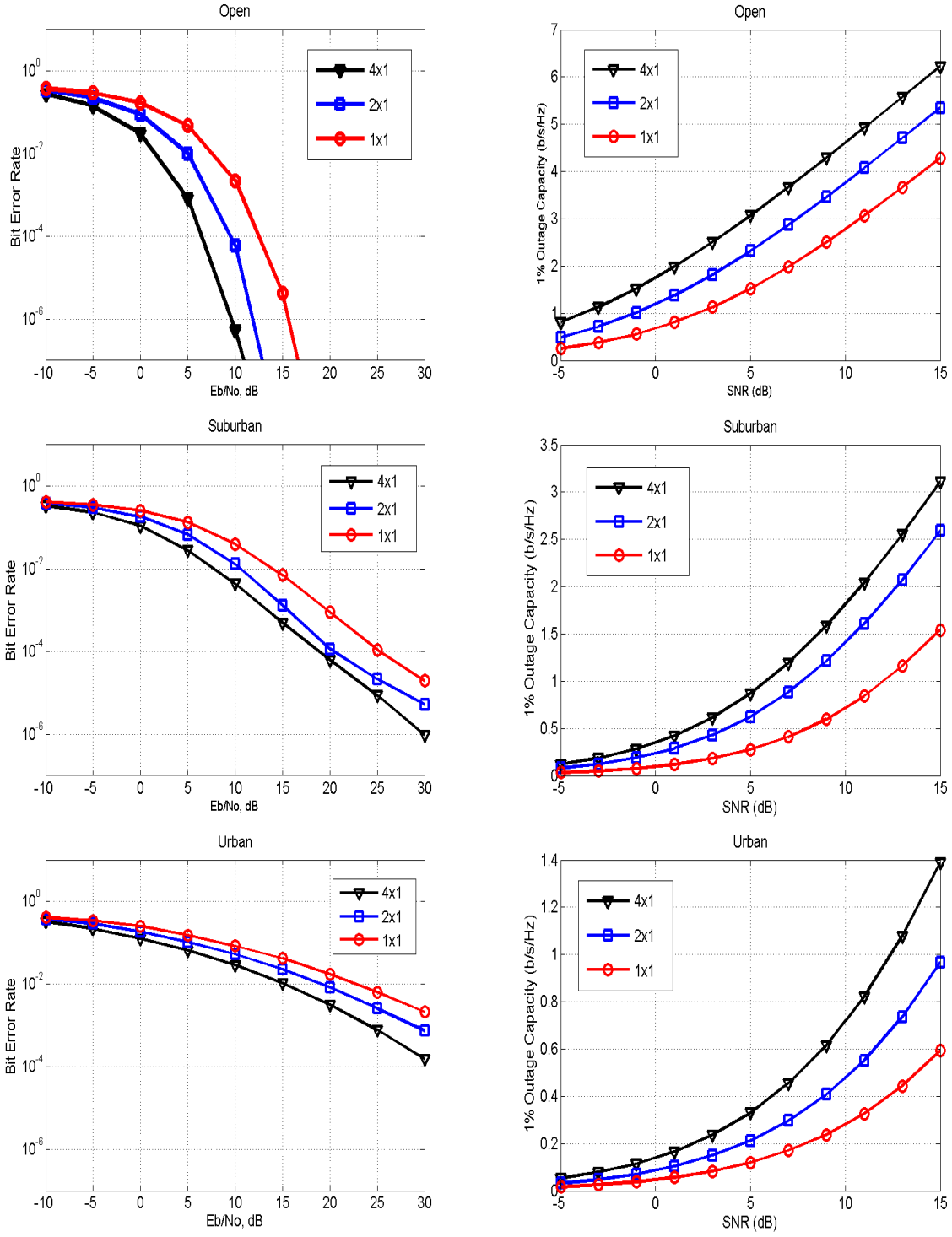


FIGURE 3.26: The BER and 1% outage capacity in open rural, suburban and urban environments for SISO, 2x1 SIMO and 4x1 SIMO architectures.

So far polarisation effects have not been introduced to the SIMO simulations. A fairer comparison between the MIMO and SIMO architectures would be possible after introducing polarisation effects to the SIMO model as most satellite transmissions incorporate polarisation. The performance indicated in the results above may be affected by the omission of polarisation effects.

### 3.12.4 Markov vs Semi-Markov

Table 3.1 shows the number of good and bad states and the typical duration spent in each state type for a travelled distance of 500 m for each user environment. A surprising observation from this table is that the number of good and bad states in each user environment is approximately equivalent; therefore it is not the case that good states or bad states dominate any particular environment. The large difference in outage capacity for each environment is due to the fact that the good and bad states are not equivalent as we move from environment to environment, with a bad state in an urban environment producing a much lower capacity than a bad state in an open rural environment. In the open rural environment the bad states last longer than the good states, this is due to the large-scale of the objects that are interfering with the signal to cause a bad state, i.e. very large objects causing partial shadowing of the direct signal.

TABLE 3.1: The number of times per 500 m simulation good and bad states are experienced and the typical distance travelled in each state type for Markov and semi-Markov state transition modelling.

| Semi-Markov modelling | Open Rural | Suburban | Urban |
|---|---|---|---|
| No. good states | 3 | 7 | 5 |
| No. of bad states | 3 | 7 | 5 |
| Distance in good states (m) | 160 | 299 | 225 |
| Distance in bad states (m) | 340 | 201 | 275 |
| **Markov modelling** | **Open Rural** | **Suburban** | **Urban** |
| No. good states | 3 | 6 | 5 |
| No. of bad states | 3 | 6 | 5 |
| Distance in good states (m) | 150 | 306 | 261 |
| Distance in bad states (m) | 350 | 194 | 239 |

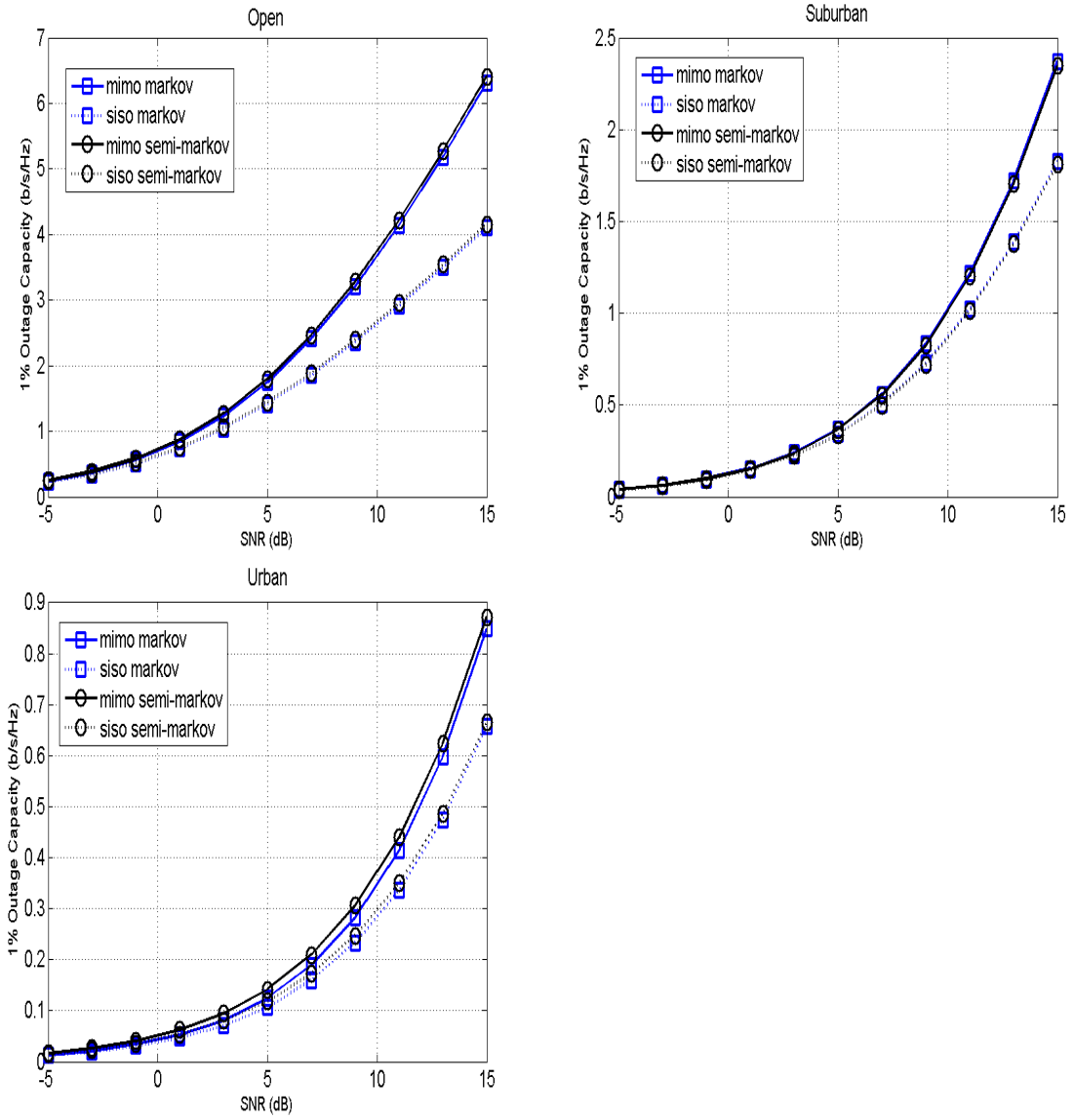


FIGURE 3.27: A comparison of open rural, suburban and urban user environments with (i) Markov state transition modelling and (ii) semi-Markov state transition modelling.

## 3.13 Summary

This chapter details the Enhanced Statistical LMS channel model that incorporates MIMO through dual polarisation and gives a step-by-step methodology for the simulation of the channel using MATLAB. The Enhanced Statistical LMS model is a stochastic model that uses the Liolis-CTTC model as a baseline and includes a number of enhancements to the model for a more accurate timeseries generator better resembling transmissions obtained in real-life scenarios.

A method of producing the temporal correlation in the direct signal component is implemented which achieves an exponential autocorrelation function of the signal and does not produce unwanted high-frequency components produced as a result of low-pass filtering. The direct signal component was generated at a slower rate of 1 sample per metre, filtered with a single coefficient IIR filter and interpolated to match the sample rate of the multipath component.

The spatial correlation in both the direct signal component and the multipath signal component where implemented through the Weichselberger method of creating a covariance matrix based on the eigen-decomposition of the covariance matrices of the receiver and the transmitter.

The modelling of the state series was modified to incorporate an improved semi-Markov chain model with state duration calculated from lognormal distributions. The state transition process was enhanced to include a state transition slope in which the signal magnitude is gradually changed from the mean signal magnitude of one state to the mean signal magnitude of the next state.

A Doppler shift was applied to the direct signal component based on the velocity of the mobile and the angle of arrival of the signal and the satellite elevation angle. A Doppler shift was also applied to the multipath component, resulting in a complex spectrum in the multipath component achieved through IIR filtering. A number of methods of applying the Doppler spectra to the series and a range of Doppler shapes

where investigated including the Jakes Doppler spectrum, a Flat spectrum, a Gaussian spectrum and an Asymmetric Jakes Doppler spectrum.

The model output shows the capacity of the dual polarised MIMO LMS channel provides a gain over SISO capacity by analysis of the MIMO advantage. The relationship between 1% outage capacity of the channel and a number of model parameters were investigated and it was found that outage capacity increased with increasing satellite elevation angle, increasing cross-polarisation of the antenna and decreasing values for the cross-polarisation coefficient used for determining the correlation in the multipath signal component. This relationship is observed in all user environments, i.e. open, suburban and urban.

# Chapter 4

# Comparison of Enhanced Model with Liolis and QuaDRiGa models

## 4.1 Introduction

In this chapter we compare the stochastic and deterministic channel models in the dual polarised satellite communications context. The dual polarised multiple-input multiple-output (MIMO) land mobile satellite (LMS) channel may be modelled using a variety of approaches, these are classed as either stochastic or deterministic, hybrid approaches incorporating both methods are also possible.

Stochastic models are based on statistical methods and generalised parameters to model the received signal that may be produced in a particular channel. This type of model has certain advantages; the model is attractive due to the low complexity involved and thus high speed of simulation. Stochastic models may be used to simulate the channel conditions in a wide range of situations and environments simply by changing a small number of key simulation parameters. The drawbacks of this modelling approach include a lack of ability to simulate specific environments or specific details in the simulated journey. Statistical models comprise of a few different approaches: geometric models, parametric models and correlation based models [33].

Geometric stochastic models build hypothetic propagation environments and model interactions between the wave and reflectors & scatterers in the environment and groups of reflectors & scatterers in the environment. To build knowledge of typical environmental geometry in specific environments, fisheye images may be taken in various environments and types of location [49], thus realistic environments can be modelled that have the correct number of objects in them with the correct distribution with correct relative sizing, for example, number of cars, number of lamp posts, building size and density, street width.

Parametric models involve detailed modelling of interactions between the wave of the signal and the objects in the environment. This type of model allows insight into the angle of arrival of the multipath signal at the receiver and frequency selective properties of the channel and thus wideband models can be developed. A wideband model may be necessary for further analysis of the channel performance for such applications as Global Navigation Satellite Systems (GNSS) [50]. However the benefits of more accurate modelling are counterbalanced by high computational complexity.

Correlation based models use methods like the Kronecker and Weichselberger to determine the correlation that exists between dependant realisations of the channel. The Liolis-CTTC model is an example of a stochastic model that includes channel correlation applied through the Kronecker method and other stochastic methods are simulated using filtering to simulate a complex dual polarised MIMO channel.

Deterministic models simulate the precise receive environment and may involve ray-tracing algorithms which determine the exact physical interactions that occur between the wave of the signal and the environment. Detailed knowledge of the environment is required and the results of the simulation will be the same each time unless the environment geometry is changed. The Quasi Deterministic Radio channel Generator (QuaDRiGa) model is an example of a semi-deterministic channel model that also incorporates geometric-stochastic methods.

## 4.2 The Liolis-CTTC Model

The Enhanced Statistical LMS model is an evolution of the Liolis-CTTC model therefore many of the modelling procedures are the same or similar.

The main benefits of the Liolis-CTTC model are that it brings together standard and accepted modelling techniques for both MIMO channels and polarisation diversity and applies them to the LMS model for the first time. It was a significant contribution to the modelling of LMS communication systems and is widely accepted and highly regarded within the channel modelling community. The key differences between the modelling techniques in the Liolis-CTTC and those in the Enhanced statistical model as previously described are summarised below.

- The state transitions occur instantaneously and the probability of transitioning from one state type (i.e. good or bad) to another state type is modelled using a Markov Chain. The parameters for generating the random walk of the Markov Chain are in Table A.2.
- The temporal correlation of the direct signal component is obtained by using a single coefficient low-pass filter. The direct signal samples are generated at a rate that equals that of the multipath sample generation (i.e. eight samples per wavelength of the carrier signal) and the rate of variation in the direct signal is then is decreased using the filtering process.
- The spatial correlation of the direct signal component is obtained using the covariance matrix $\bar{\mathbf{C}}$ from the experimentally derived values in Table A.1.
- The spatial correlation of the multipath components is obtained by deriving the covariance matrix $\tilde{\mathbf{C}}$ through the Kronecker product of the two covariance matrices $\tilde{\mathbf{R}}_{\mathbf{rx}}$ and $\tilde{\mathbf{R}}_{\mathbf{tx}}$ [1]:

$$\tilde{\mathbf{R}}_{tx} = \mathrm{MP} \cdot \begin{bmatrix} 1 & 2\sqrt{(1-\gamma)\,\gamma}\tilde{\rho}_{tx} \\ 2\sqrt{(1-\gamma)\,\gamma}\tilde{\rho}_{tx} & 1 \end{bmatrix} \tag{4.1}$$

$$\tilde{\mathbf{R}}_{rx} = \mathrm{MP} \cdot \begin{bmatrix} 1 & 2\sqrt{(1-\gamma)\,\gamma}\tilde{\rho}_{rx} \\ 2\sqrt{(1-\gamma)\,\gamma}\tilde{\rho}_{rx} & 1 \end{bmatrix} \tag{4.2}$$

$$\tilde{\mathbf{C}} = \tilde{\mathbf{R}}_{tx}^{T} \otimes \tilde{\mathbf{R}}_{rx} \tag{4.3}$$

- The cross-polarisation coupling (XPC) of the environment remains constant throughout the entire simulated journey in a particular environment with values taken from [19, 40].
- There are no Doppler effects modelled, i.e. there is no Doppler spectrum applied to the multipath components thus they are without memory. Also, no Doppler shift is applied to the direct signal component.
- $\mathrm{T}_s$ changes according to environment because it depends on the coherence time of the channel, thus urban $\mathrm{T}_s$= 0.0008 s, suburban $\mathrm{T}_s$ = 0.0012 s, open $\mathrm{T}_s$ = 0.0011 s

The Liolis-CTTC model has low complexity, easy to change parameters and low simulation time. It is used to help validate the Enhanced Statistical model as it can be observed from analysis if enhancements made within the model results in more accurate time series production.

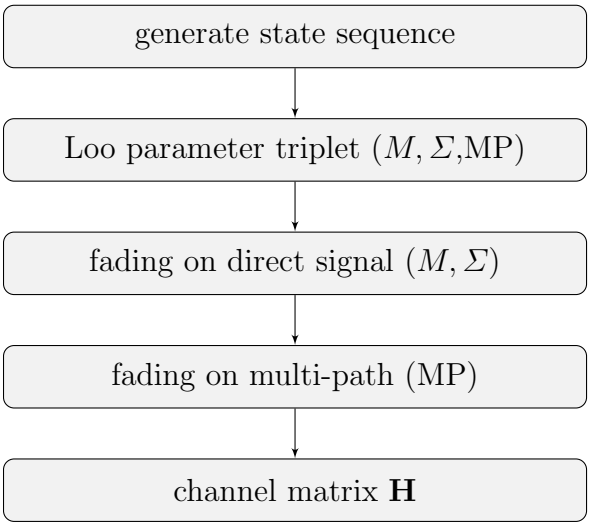


FIGURE 4.1: Flow chart of the generalised stages in modelling the dual polarised LMS channel using a statistical model such as the Liolis-CTTC model.

## 4.3 The QuaDRiGa Model

### 4.3.1 Background

The QuaDRiGa [51] is the second model used for comparison in this thesis. QuaDRiGa is a geometric-stochastic channel model that uses statistical ray-tracing to model the effects of the environment on the propagating wave of the signal. QuaDRiGa's statistical element arises from the fact that exact geometric representations of the environments are not created as in typical ray-tracing models, instead, simulation environments are created that contain randomly positioned scatterer clusters. The received signal is calculated from the addition of the reflected components from each scatterer cluster using ray-tracing as the receiver moves through the environment. There is an added level of complexity in this model over a purely statistical model as the physical effects of each scatterer cluster on the propagating signal are modelled thus increasing the computational workload of the simulation. Thus, each individual multipath component is determined, along with parameters associated with the multipath component including the total path length of multipath component, the angle of departure from scatterer cluster,and the angle of arrival at receiver [51].

### 4.3.2 Parameterisiation of the Model

QuaDRiGa is a complex and detailed generic model that uses different parameter sets to model different propagating environments and scenarios. The QuaDRiGa model and its parameter sets were developed after analysis of two major measurement campaigns that were conducted as part of the European Space Agency's (ESA) ARTES programme. The Mobile Satellite Channel with Angle Diversity project (MiLADY) concluded in 2009 [22] and the Characterisation of the MIMO Channel for Mobile Satellite Systems project (MIMOSA) concluded in 2013 [21]. QuaDRiGa builds on the Wireless World Initiative for New Radio (WINNER) model for terrestrial cellular radio [9]. It includes some of the parameters from the WINNER model and other parameters from the MIMOSA measurement campaign, therefore it is highly adaptive

and and can be used to simulate transmissions in a vast range of scenarios including land mobile satellite transmissions and outdoor to indoor cellular transmissions. Each QuaDRiGa scenario is described by a configuration file that contains over 50 parameters, these are used to determine a large-scale correlation parameter map used for determining the channel coefficients, an example configuration file is included in Appendix B

The parameter lists contains information about the seven main Large Scale Parameters (LSPs), which are: the root mean square (RMS) Delay Spread (DS), K-Factor (KF), Shadow Fading (SF), the Azimuth spread of Departure (AsD) at the scatterer cluster, the Azimuth spread of Arrival (AsA) at the receiver, the Elevation spread of Departure (EsD) at the scatterer cluster and the Elevation spread of Arrival (EsA) at the receiver. The parameter list is not confined to these seven parameters and other information is contained in each environment file such as the path loss needed for normalisation. For the purposes of land mobile satellite transmissions, a series of MIMOSA configuration files exists containing the required parameters for simulation. A satellite elevation range may be chosen from 10°- 45°, 16°- 25°, 25°- 35°or 35°- 45°.

QuaDRiGa encompasses two modelling approaches, a narrowband model and a wideband model. The narrowband models offers much of the analysis capabilities of a typical statistical model, for example it incorporates a two state semi-Markov model with Doppler shaping filters and the delay spread is considered to be zero. The wideband extension allows for additional analysis including consideration of the frequency selective properties of the channel, detailed multipath modelling, the distribution of the Angle of Arrival of the multipath components. In addition, the time evolution within the model allows for the continuous reassessment of channel conditions due to a moving receiver in terms of drifting within the channel and scatterer cluster evolution [51]. The wideband model is used for the purposes of this thesis and a narrowband timeseries is extracted ignoring the addition specular components and delay spread information generated within the model.

Although QuaDRiGa allows us to simulate very detailed and complex scenarios, the increased complexity leads not only to increased simulation time but also increased

difficulty in the initialisation and running of simulations as many parameters must be considered and designed. The following sections describe the main aspects involved in designed and controlling a QuaDRiGa simulation.

### 4.3.3 Polarisation and Antenna Modelling

QuaDRiGa builds on the WINNER model however; some aspects of its implementation are further advanced than the WINNER model, such as the newly developed three-dimensional propagation modelling approach which includes antenna modelling and polarisation modelling [51]. QuaDRiGa contains extensive antenna modelling and allows for the application of a wide variety of antenna types and antenna parameters may be controlled by the user. The antenna patterns are described with spherical co-ordinates using matrices and are modelled with matrix transformations. Antenna types include an omnidirectional antenna, a dipole, a right-hand circularly polarised (RHCP) dipole, a left-hand circularly (LHCP) dipole and a LHCP/RHCP-dipole. Customisable properties of the antenna include the direction of antenna orientation, the angle of the dipole opening, and the coupling between dipoles. The rotation of the antenna polarisation affects the received power in the co- and cross-polarised subchannels.

Although the antenna modelling is customisable, the default settings were used or the simulations conducted for the baseline simulations used in this thesis. The settings in the satellite tutorial within QuaDRiGa were used as a template, i.e. the transmitter and receiver arrays were constructed out of two customisable diodes with 90° openings, which are coupled using a coupling matrix to produce two orthogonally circularly polarised signals. The coupling matrix is customisable and may be used to create independent antenna elements by setting the coupling matrix equal to an identity matrix. For the dual polarised simulations, the circularly polarised signals are created by feeding the antenna a single signal that is split between the two antenna elements and shifted out of phase with one another by 90 degrees [51]. Equation (4.4) describes the coupling matrix (CM) used.

$$\mathrm{CM} = \frac{1}{\sqrt{2}} \begin{bmatrix} 1 & 1 \\ \mathrm{j} & \text{-j} \end{bmatrix} \tag{4.4}$$

The antenna properties within QuaDRiGa are separated from the polarisation effects of the channel. QuaDRiga uses a new polarisation model that is developed to model complex polarisation effects using the Jones model developed for polarisation effects in optical fibres [52]. In line-of-sight (LOS) conditions, the polarisation is calculated through simple linear matrix transformations, taking into account the orientations of the transmitter and receiver. For non line-of-sight (NLOS) conditions, as the polarisation of the wave may change during interactions with objects within the propagation environment for example reflections may result in a change of polarisation, therefor the cross-polarisation ratio (XPR) of the environment also affects the polarisation of the signal.

### 4.3.4 Setting Up and Running a QuaDRiGa Simulation

The QuaDRiGa model is implementable in MATLAB, set up and simulation of the model requires a number of stages and offers control and adaptability over a number of parameters that are not available in the Liolis-CTTC model. The QuaDiGa model is divided into separate sections; the state sequence generator (SSG), the propagation parameter generator (PPG) and the small-scale fast-fading model (SSFM). The SSFM model in QuaDRiGa may be narrowband or wideband.

The following method is based on the satellite tutorial that is included in the open-source QuaDRiGa software package. Initially the frequency of the simulation is set to an S-band value of 2.2 GHz and where possible simulations parameters are changed to match those used in the statistical models, for example, the velocity of the mobile receiver, the mean and standard deviation of the lognormal parameters for state duration generation.

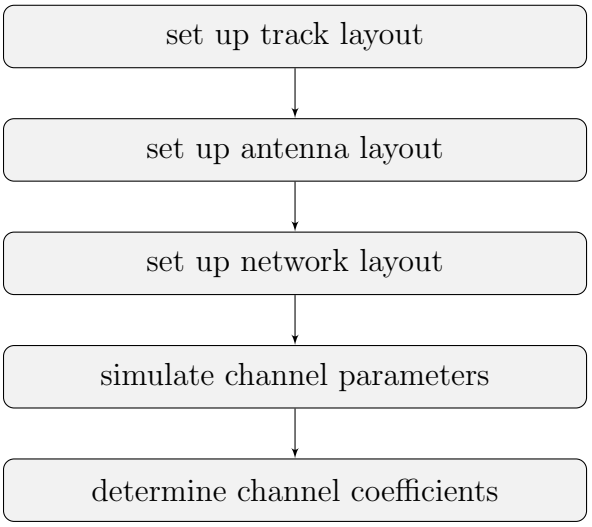


FIGURE 4.2: Flow chart of the setting up and running of a simulation to model the dual polarised LMS channel using the QuaDRiGa model.

- ***Set Up Track Layout***

  A virtual track for the mobile receiver to move along is created. The track is the path the receiver will follow during the simulation and consists of virtual streets of various lengths and may include turns at junctions with parameters to control likelihood of turning. A series of good and bad states are generated, this algorithm was adapted to mirror the semi-Markov model with lognormally distributed state lengths as used in the statistical models. Snapshots are obtained for each state and interpolated to obtain a reasonable sample density allowing for enough detail but without creating onerous processing requirements.

- ***Set Up Antenna Layout***

  The antenna type is defined along with the opening size of the patch. A transmitter array is created from the desired antenna elements with circularly polarised antenna elements created through copying the antenna, phase shifting and coupling the signal passed to each antenna. The antenna polarisation and angle may be rotated to a chosen value around any axis. The receiver array is then created by duplicating the first array and both antenna arrays are rotated to face towards each other.

- ***Set Up Network Layout***

  The track and antenna arrays are combined to create the complete simulation network, with parameters being defined such as: satellite elevation angle, satellite azimuth angle, satellite orbital distance and receiver latitude.

- ***Generate Correlated Large Scale Parameters***

  Tables of parameters exist for each environment at a specific satellite elevation range and state type (i.e. LOS and NLOS). The list of parameters includes the mean and variance for the parameter in that particular scenario and from these parameters Large Scale Parameter correlation maps are produced.

- ***Calculate Channel Coefficients***

  The channel coefficients are generated for each segment based on the generated LSP maps. The channel coefficients of each segment are then combined into a continuous channel with a certain amount of overlap between each segment.

The channel is then interpolated again to produce a higher sample density which considers the speed of the receiver.

## 4.4 Comparison of Results

The following section compares results from each of the three models beginning with a comparison of the different set-up and initalisation requirements of the models followed by an in-depth analysis of the timeseries output from each of the models and analysis of the 2nd order statistics.

### 4.4.1 Initialisation of models

The QuaDRiGa timeseries is simulated with parameters for urban environments with satellite elevation of 35°- 45°, with the transmitter and receiver arrays comprised of coupled patch antenna to produce a RHCP and LHCP signal at a carrier frequency of 2.2 GHz. The vehicle-mounted mobile velocity was constant throughout simulation at 50 km/h. The turning probability when reaching the end of a 100 m street was 0.4, Figure 4.3 shows the simulated track layout for the 100,000 km simulation. A list of the parameters used is contained within Appendix B.

The LOS and NLOS signals are each separately normalised by manually setting the path loss. The LOS states were normalised so that the cumulative Distribution Function (CDF) of the co-polarised signal at 50% coincides with a signal magnitude of 0 dB. The NLOS states were normalised so that the CDF of cross-polarised signal at 50% coincides with a signal magnitude of -19 dB. Figures 4.4 and 4.5 show the normalise CDF of the LOS states and the NLOS states from a QuaDRiGa simulation of a mobile receiver travelling in an urban environment.

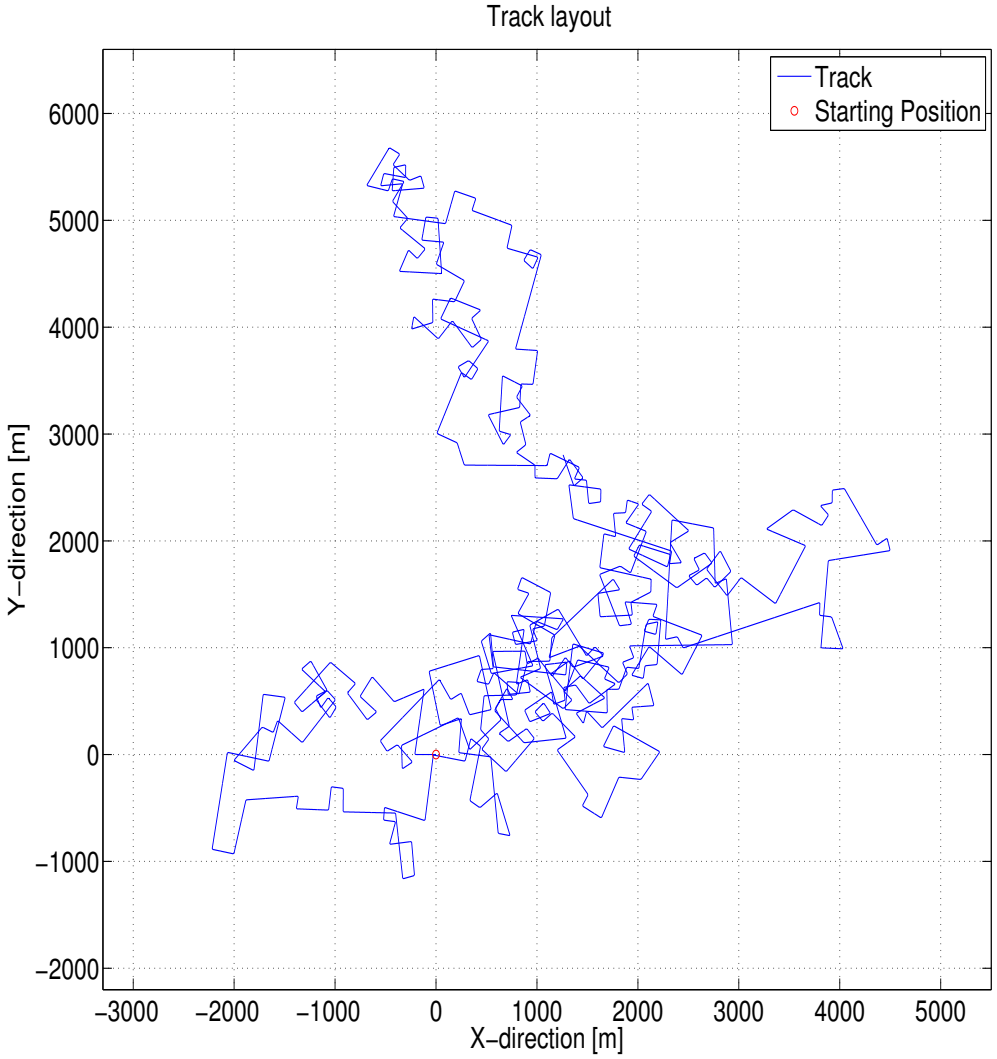


FIGURE 4.3: The virtual 100,000 km track followed by the mobile receiver in the simulation of the received signal in the urban environment using the QuaDRiGa model. Along this track a series of LOS and NLOS states are experienced by the received signal. This graph was produced with code supplied within the QuaDRiGa software package.

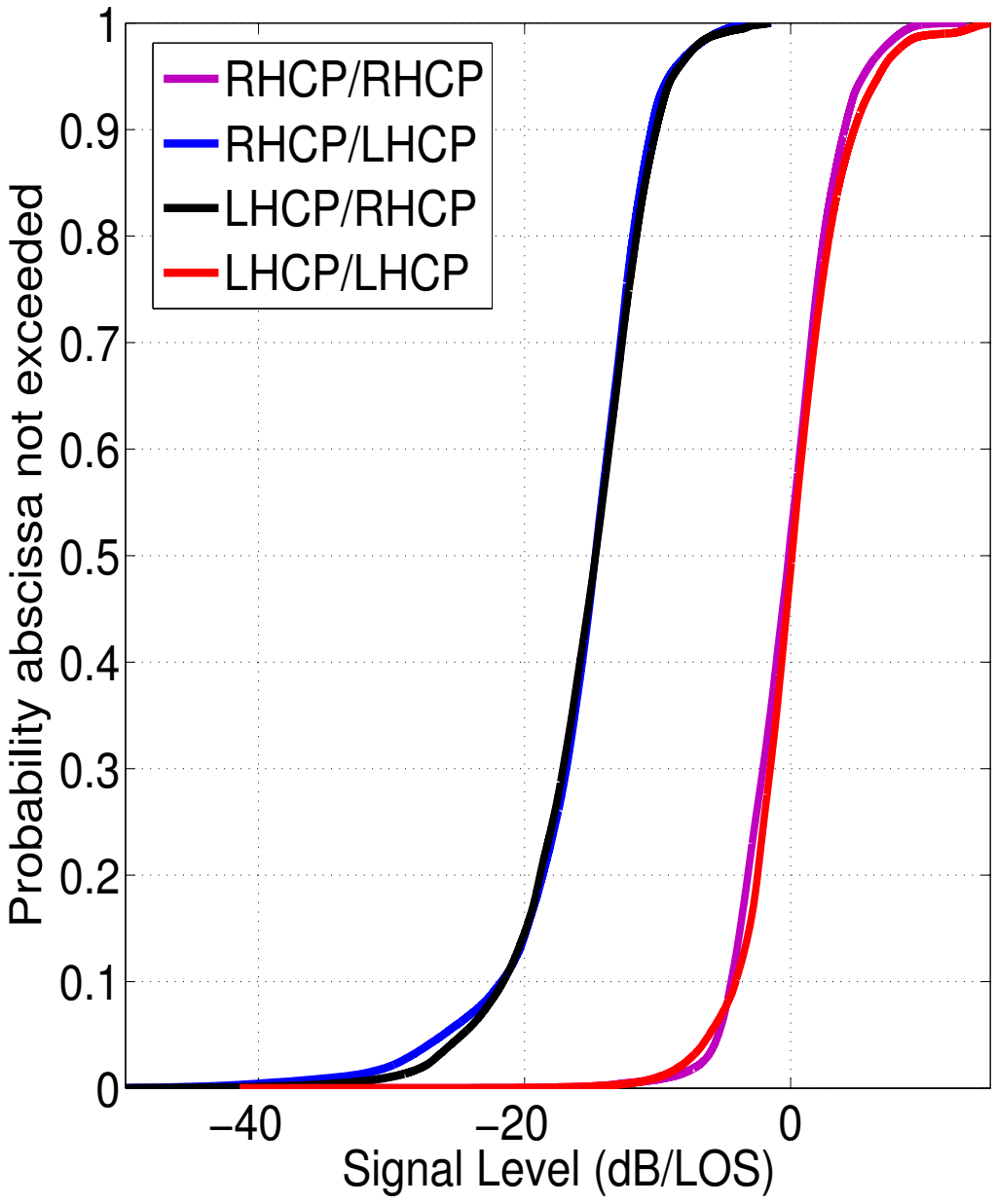


FIGURE 4.4: Cumulative Distribution Function of the LOS states in QuaDRiGa timeseries simulated in an urban environment with satellite elevation angle 35°-45°and mobile velocity of 50 km/h. Normalisation is set to coincide the probability of 50% of the co-polarised signal with a signal magnitude of 0 dB.

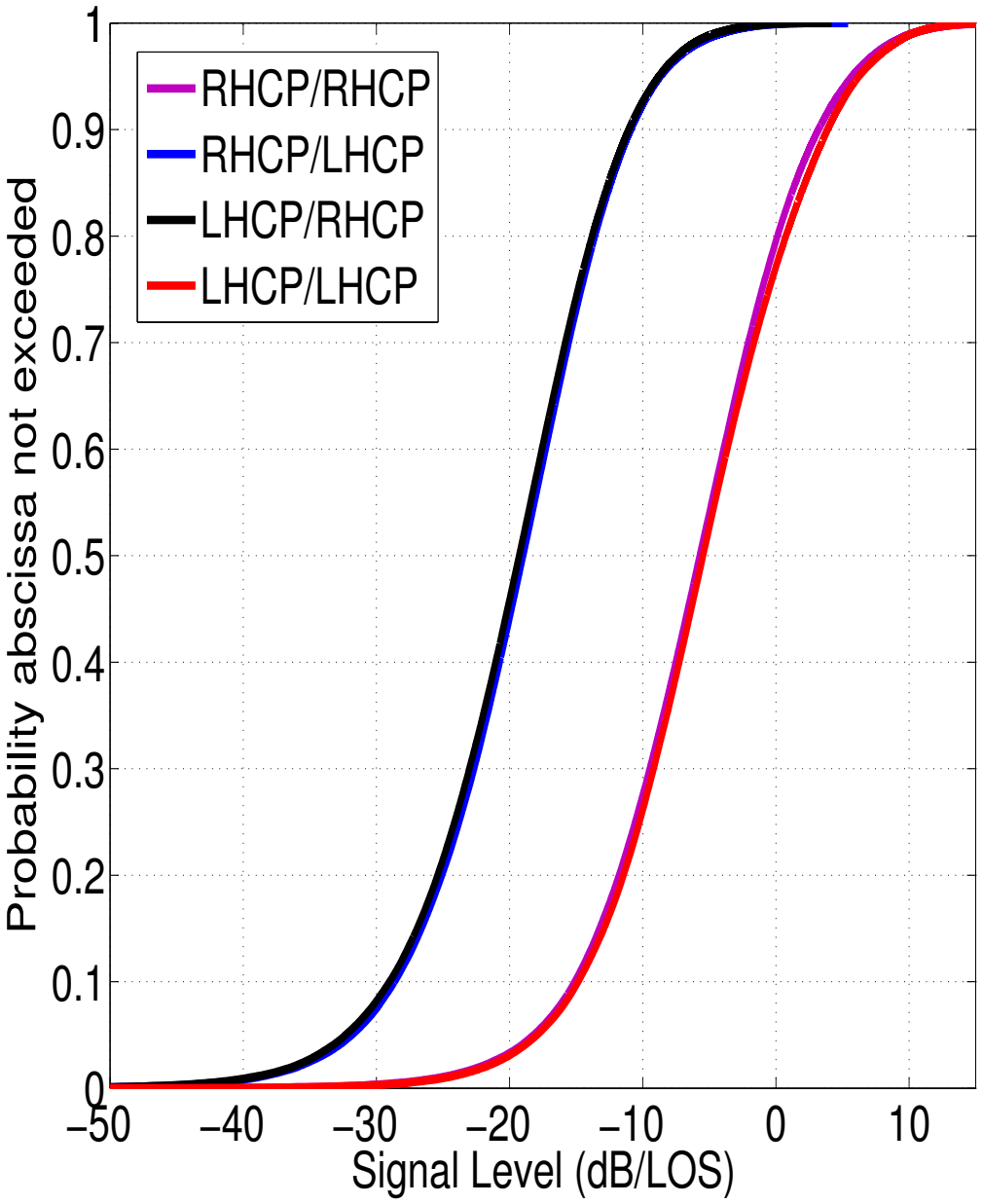


FIGURE 4.5: Cumulative Distribution Function of the NLOS states in QuaDRiGa timeseries simulated in an urban environment with satellite elevation angle 35°-45°and mobile velocity of 50 km/h. Normalisation is set to coincide the probability of 50% of the cross-polarised signal with a signal magnitude of -19 dB.

### 4.4.2 Timeseries

The timeseries for the Enhanced Statistical model, the Liolis-CTTC model and the QuaDRiGa model are plotted in Figure 4.10 for mobile travelling at 50 km/h in an urban environment. Although they are not an exact match, the three models give good agreement in terms of the magnitude of the received signal showing similar separation of the co-polarisation and cross-polarisation subchannels. It would be expected that the Enhanced Statistical model and the Liolis-CTTC model share common features in their timeseries as they are both statistical models that share common simulation processes. There are a number of key differences in the parameterisation of the statistical and geometric-statistical models and in the simulation processes that should be considered when comparing the timeseries output from the three models.

The unit used for the signal level in the timeseries plots throughout this chapter is dB/LOS. This unit is used to indicate that the simulated received signal power level is obtained by nomalising the MIMO channel with respect to the LOS power level in dB. This arises due to the fact that the Loo statistical parameters obtained from the data in [2] are normalised thus producing a normalised timeseries.

#### 4.4.2.1 Magnitude of Received Signal During Good and Bad States

The first obvious, observable difference in the plotted timeseries is that the QuaDRiGa simulated signal reaches higher received signal magnitudes than the Enhanced Statistical simulated timeseries or the Liolis-CTTC simulated timeseries, Figure 4.10. This is due to the fact that QuaDRiGa model always assumes LOS and NLOS conditions as opposed to the more versatile good and bad states of the statistical models. This means in an LOS state QuaDRiGa always has a LOS component in the received signal and therefore may reach higher signal magnitudes than a good state as defined in the statistical models.

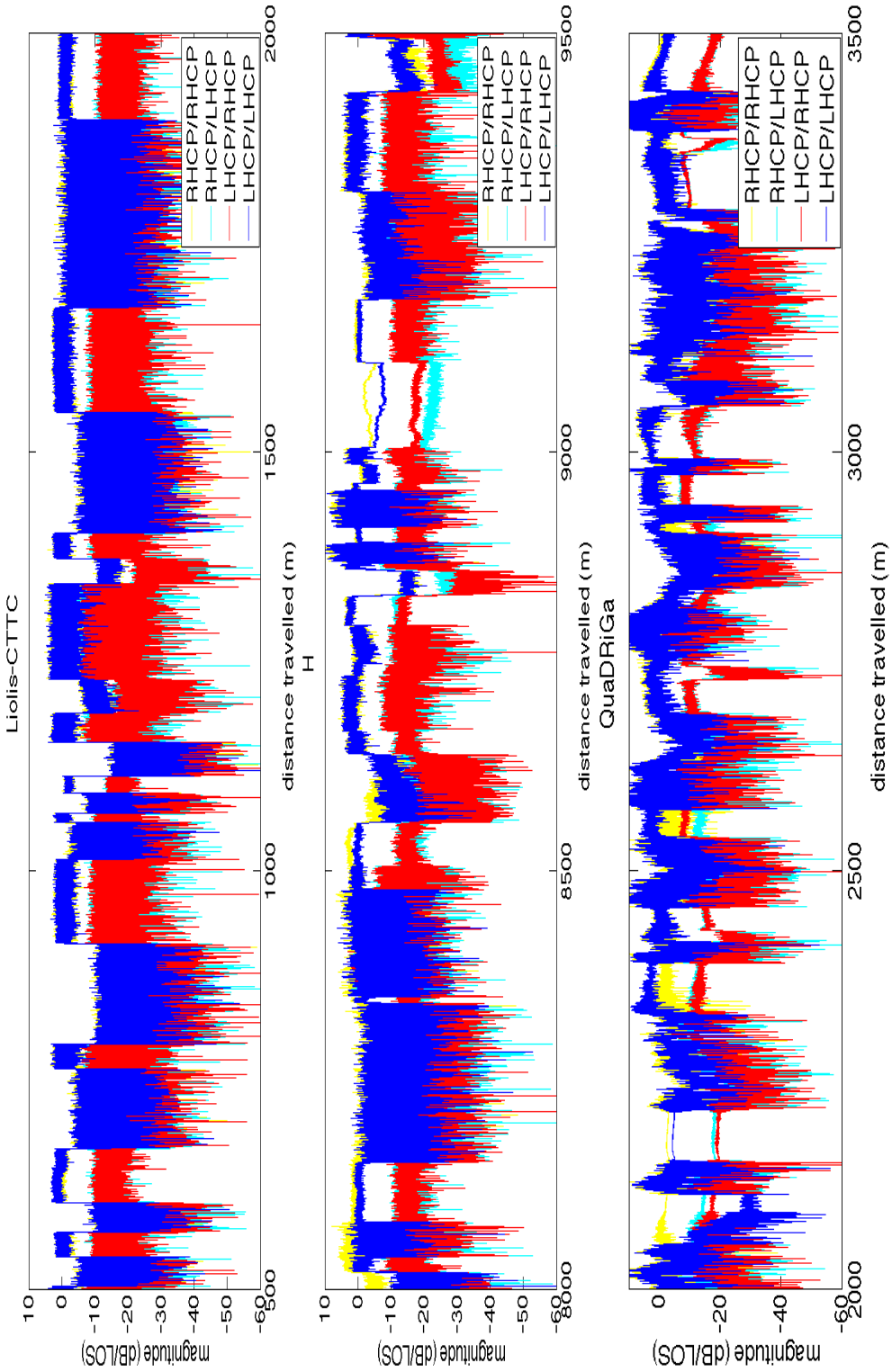


FIGURE 4.6: Timeseries for a mobile travelling within the urban user environment at 50 km/h generated with the Liolis-CTTC model (top), the Enhanced Statistical Model with Jakes Spectrum Doppler shaping through Sum of Sinusoids method (middle) and the QuaDRiGa model (bottom). XPD is set to 15dB. The signal level is normalised with respect to the LOS power level in dB.

#### 4.4.2.2 Variation Between Same Polarisation Subchannels

The second observable difference between the QuaDRiGa simulated received signal and the statistical model simulated timeseries is the scale of the variations in the signal magnitude within each state, Figure 4.7. In plotted timeseries of the Liolis-CTTC model, there appears to be little variation in the signal magnitude within each state, i.e. each state is quite boxlike in its shape. In addition to this characteristic, the magnitude of the received signal by each antenna is almost identical, with very little difference between the two co-polarised received signals and the two cross-polarised received signals. These features are to be expected when we consider that the RHCP and LHCP transmitted signals are modelled in the same way and there is very little within the model to create a difference in the received signal magnitude, only some randomly generated effects. In addition, the cross-polarised discrimination (XPD) of the antenna and the cross-polarised coupling (XPC) of the environment, the parameters that may cause different effects within states and between different subchannels, are constant throughout the entire simulation. This fact, in combination with the fact that the Loo parameter triplet which controls the state conditions also remains constant for an entire state, leads to the unchanging, boxlike states with high similarity between the two co-polarisation subchannels and also between the two cross-polarisation subchannels in the Liolis-CTTC model.

#### 4.4.2.3 Variation in Signal Magnitude at State Transitions

In comparison to the timeseries output from the statistical models, the QuaDRiGa model, exhibits a high degree of variation in the signal magnitude. It is much more difficult to ascertain if a state has changed or remained the same within a given travelled distance of the simulated journey due to the high level of variation in the signal in a single state. In Figure 4.7, we consider the timeseries from the QuaDRiGa model for the distance travelled between 2053 - 2538 m, the distance at which the state transitions actually occur are marked on the plot with dashed lines. It is interesting to consider the signal variations within the states and also to note the trend in the

signal at the position of the state change. In particular, the first state from 2053 - 2114 m may seem to be comprised of two different states, one with greater standard deviation of the signal magnitude and one with a lesser amount of standard deviation. The magnitude of the signal in all the subchannels also decreases slightly, however, the magnitude of the LHCP/LHCP subchannel appears to decrease significantly from approx. -20 dB to approx. -30 dB. With the state positions marked it is easy to identify the series of good and bad states, however, it would be more difficult to judge by eye where exactly the state transitions occur using the only changes in the received signal as a guide. For the good to bad state change that occurs at 2213 m, the signal magnitude decreases after the marked state change position. In comparison, at the next bad to good state change that occurs at 2329 m, it appears that the signal magnitude is beginning to increase slightly before the state change position is marked. This effect may due to the method in which QuaDRiGa adds together segments of the simulated journey by allowing for a certain degree of overlapping to exist between segments, in the case of this simulation an overlapping of 10% was allowed. However, it may simply be caused by the high level of signal variation within the state causing a change in signal magnitude that is unrelated to the state change.

#### 4.4.2.4 Number of State Transitions

It would appear from the timeseries that the QuaDRiGa received signal undergoes more state transitions than the statistical models on the simulated journey of 1500 m as plotted in Figure 4.6. However, all models use the same parameters for the semi-Markov model used to determine state durations. The number of states the Enhanced Statistical model and the QuaDRiGa model were analysed to find if there was a difference.

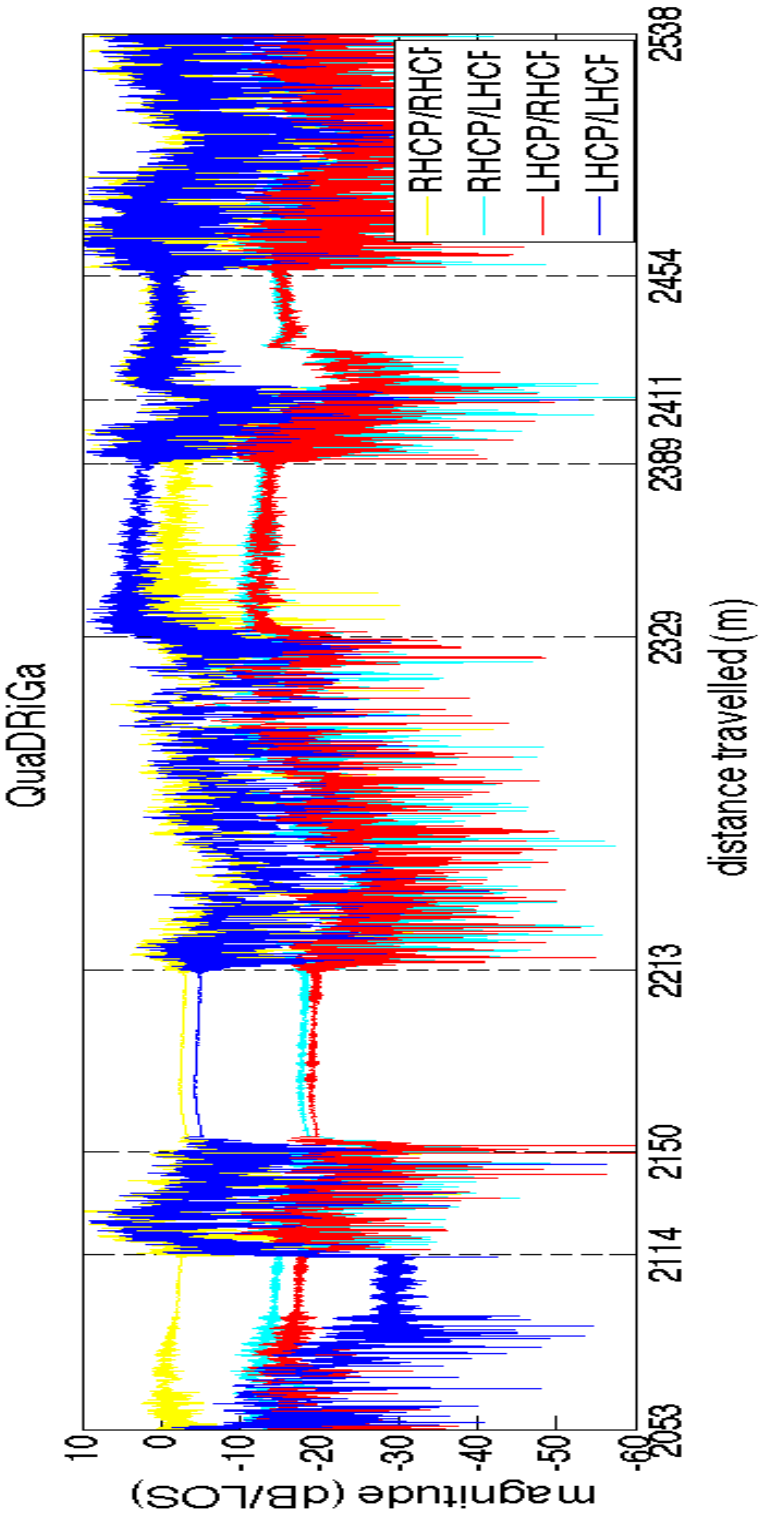


FIGURE 4.7: Timeseries for a mobile travelling within the urban user environment at 50 km/h generated with the QuaDRiGa model with the position of state transitions marked with a dashed line and the distance travelled.

TABLE 4.1: The number of times per 100 km simulation good and bad states are experienced by the received signal and the typical distance travelled in each state type for the Enhanced Statistical and QuaDRiGa model, both simulated in an urban environment.

| Model | Enhanced Statistical | QuaDRiGa |
|---|---|---|
| No. good states | 909 | 965 |
| No. of bad states | 910 | 964 |
| Total state transitions | 1819 | 1929 |
| Distance in good states (m) | 44,887 | 45,706 |
| Distance in bad states (m) | 55,823 | 59,949 |
| Total distance travelled (m) / 104,652 | 105,655 | |

Table 4.1 shows the number of state transitions per model for a minimum 100 km simulation. It is appears that the QuaDRiGa model changes states more often than the Enhanced Statistical model, i.e. 1929 times in 105.7 km in comparison with 1819 times in 104.7 km for the QuaDRiGa and Enhanced Statistical models respectively. The main reason for this difference is due to the method used for the state transition process in the Enhanced Statistical model. As this process adds extra samples to each state in order to create a smooth transition process. This implementation serves to slightly elongate each state therefore changing state less often in a given simulated travelled distance. Without the added extra samples from the smooth state transition process, the simulated journey would have been 100,710 m. If the Enhanced Statistical model is used to simulate a journey of 105.7 km without the implementation of the smooth state transition process, the total number of states is 1906, which is a much closer match to the 1929 total number of states in the QUaDRiGa simulated journey.

It may be appropriate to modify the algorithm for the state transition mechanism to allow for the slope changing between one state to the next to be contained within the first state, or even to be spread across the two states without adding extra samples. This would not be an onerous update to make to the model; comparison with real measurement data would be useful in deciding if this modification would be worthwhile.

#### 4.4.2.5 Variation in Signal Magnitude During States

During a single state the QuaDRiGa timeseries displays a lot of variation in the signal magnitude. If we consider the state that occurs between 2454 m and 2538 m in Figure 4.7, the signal magnitude of the co-polarised RHCP-RHCP and LHCP-LHCP subchannels are initially around 0 dB. The signal magnitudes then increase slightly by a few dB and then dips to approximately -10 dB before rising back to just below 0 dB again. A similar level of variation is not observable in the Liolis-CTTC model. The effect arises from the constantly evolving nature of the QuaDRiGa model with the channel being comprised of states that overlay a track layout of streets with varying orientations. Therefore factors that affect the channel may change within a

state, for example when the vehicle changes direction. The track may change direction three times during a state determined by a defined probability and therefore within the state the characteristics of the received signal may change slightly. Scatterer clusters are randomly placed within the environment and affect the multipath signal causing greater or lesser variance in the received signal. As the mobile receiver moves through the environment, a specific cluster may stop or start having an influence on the received signal.

In Figure 4.8 we can see the changes that occur in the received signal for 5 successive states when the number of clusters within both LOS and NLOS states are both set to the minimum value possible, i.e. 1 (NB: 0 not being permissible as no multipath signal would then exist) and then the effect of the scatter clusters on the signal when the number of clusters within both LOS and NLOS states are both set to 10. By minimising the scatterer clusters in the environment within QuaDRiGa, we can observe that variations occur due to the increased number of scatterer clusters. However, this plot also allows us to observe the variations in the magnitude of the direct signal whilst the multipath signal is minimised. This is the best analysis of the direct signal we can obtain in QuaDRiGa because, it is unlike the statistical models in which the direct and multipath components are generated separately and therefore easily analysed.

Figure 4.8 shows that good states have little variation on the received signal magnitude. For example the state that runs from 580 m to 763 m shows a smooth state with very little deviation from a signal magnitude of 0 dB in the LHCP/LHCP subchannel, except when the state transition is approaching. By contrast the bad states show variation in the magnitude of the direct signal within the state. For example, the state that runs from 559 m to 580 m shows a number of bumps in the signal magnitude between 0 dB and -5 dB.

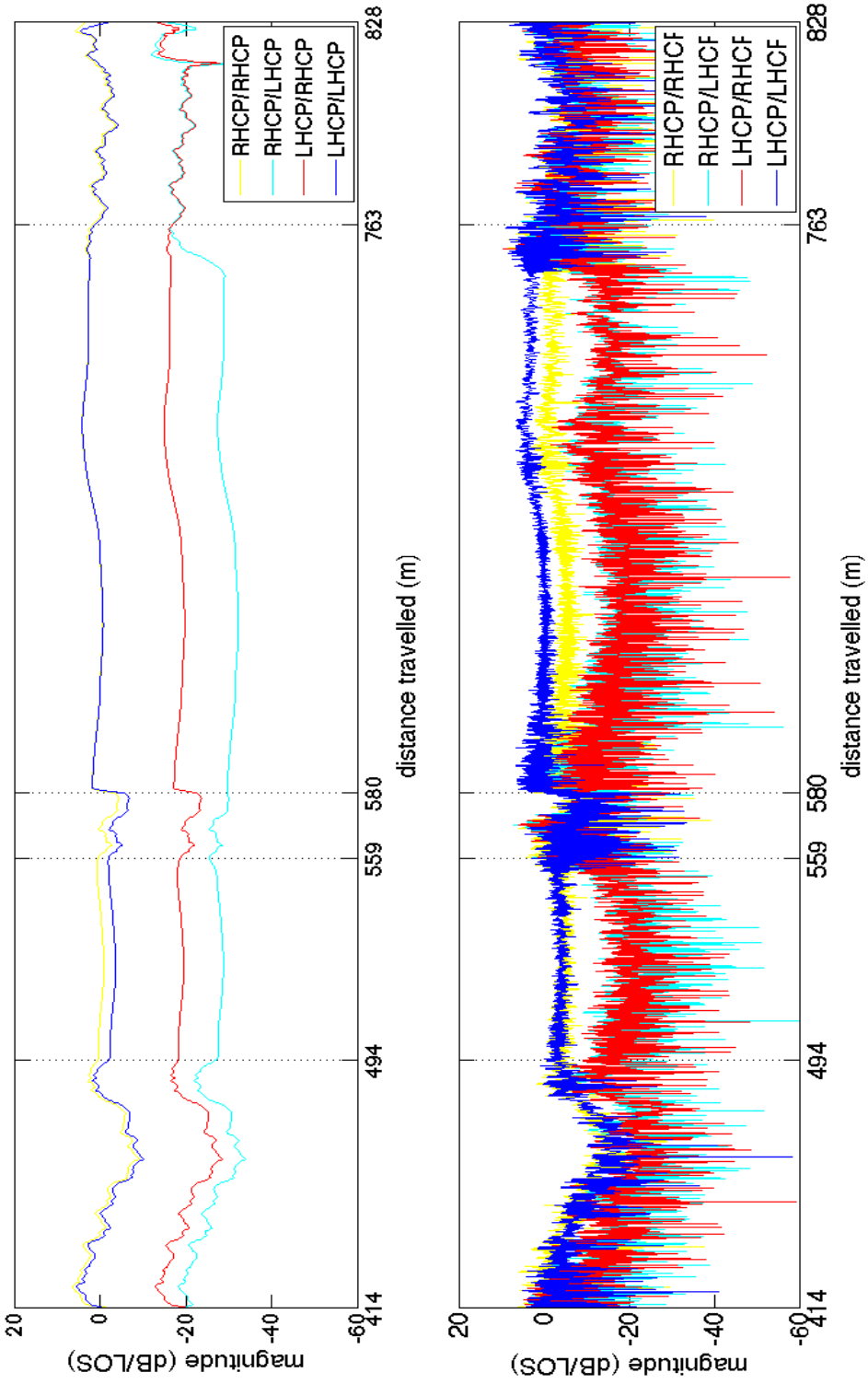


FIGURE 4.8: Timeseries for a mobile travelling within the urban user environment at 50 km/h generated with the QuaDRiGa model with the position of state transitions marked with a dashed line at the distance travelled, the same simulated track is used for both plots. Top: number of scatterer clusters in LOS and NLOS = 1. Bottom: number of scatterer clusters in LOS and NLOS = 10

Figure 4.9 shows a number of consecutive states simulated using the Enhanced Statistical Model. The Enhanced Statistical model shows a greater degree of variation within each particular state than the Liolis-CTTC model. This is achieved by allowing some of the parameters to vary throughout the simulation. For example, the XPC of the environment varies throughout the simulated journey with each state having it's own particular value. The first state plotted from 5734 m to 5929 m shows a variation in the received signal magnitude of the co-polarised subchannels that begins with a mean value of approximately -10 dB which risings to approximately 0 dB and decreases below -10 dB again towards the end of the state. This mirrors effects observed in the QuaDRiGa model in Figure 4.7.

In addition to the varying signal magnitude, the Enhanced Statistical model also shows some level of separation between polarisation subchannels of the same type. For example, a clear separation is seen between the RHCP/RHCP subchannel and the LHCP/LHCP subchannel in the state between 6001 m to 6905 m.

The variations in signal magnitude must arise due to greater variations in the direct signal compared to the Liolis-CTTC model timeseries. The method of producing the direct signal by filtering and then interpolation may enhance differences in the random samples used to generate the signal component.

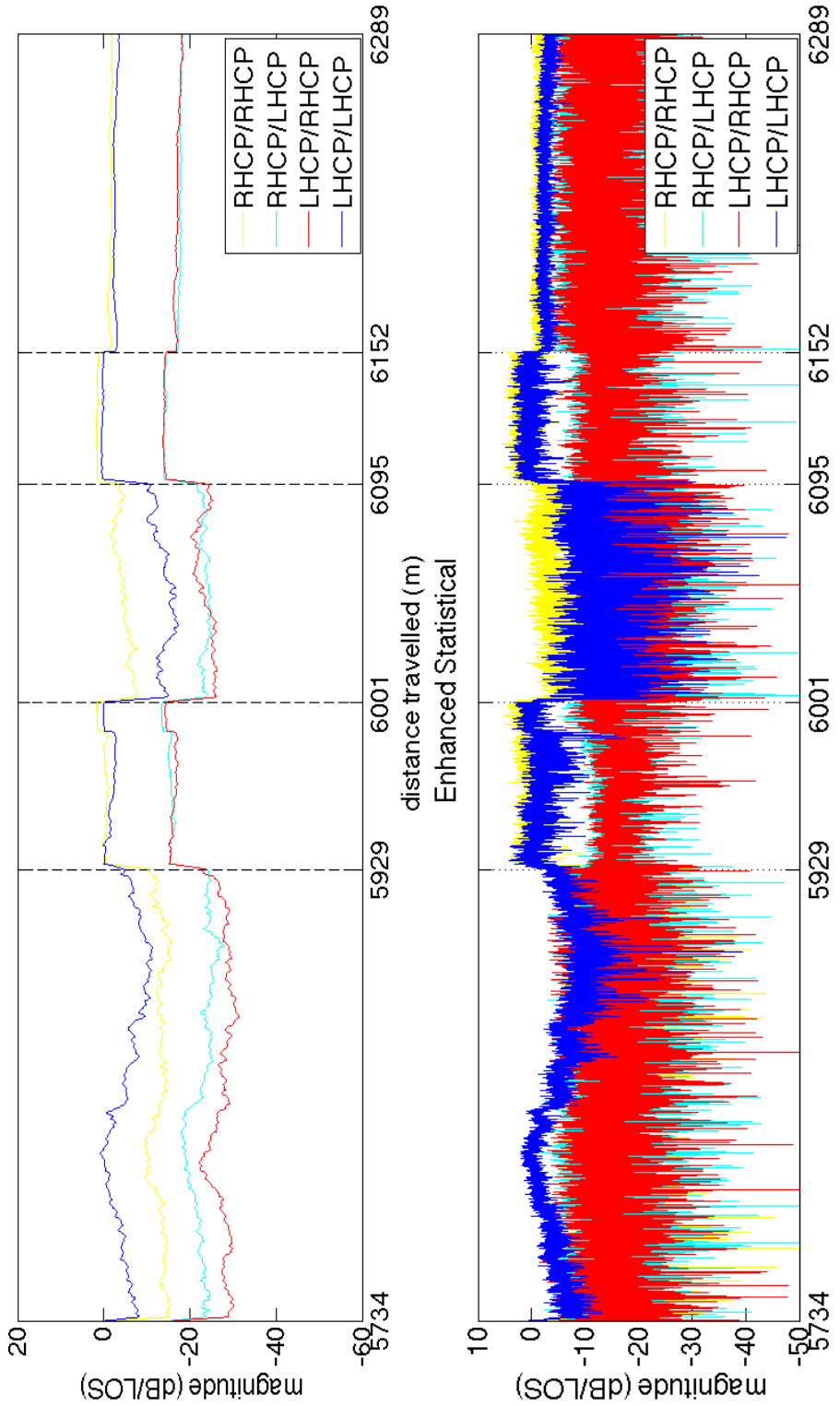


FIGURE 4.9: Timeseries for a mobile travelling within the urban user environment at 50 km/h generated with the Enhanced Statistical model with only the direct signal component plotted (top) and the entire channel matrix plotted (bottom)

### 4.4.3 Timeseries at 20 dB XPD

The Enhanced Statistical model shows greater similarity to the QuaDRiGa model if we simulate with an antenna XPD of 20 dB, Figure 4.10. The Enhanced model displays less variation in the good states, for example the good state centred on 9800 m is very narrow and mirrors some of the narrow states observable in the QuaDRiGa timeseries, such as that centred on 4000 m. Greater variation in the cross-polarisation subchannels is also observable. This is due to the greater sensitivity of the antenna in being able to determine between the co-polarisation and cross-polarisation subchannels. Antenna of this high a XPD value are not common in LMS scenarios, therefore this plot is only included for comparison.

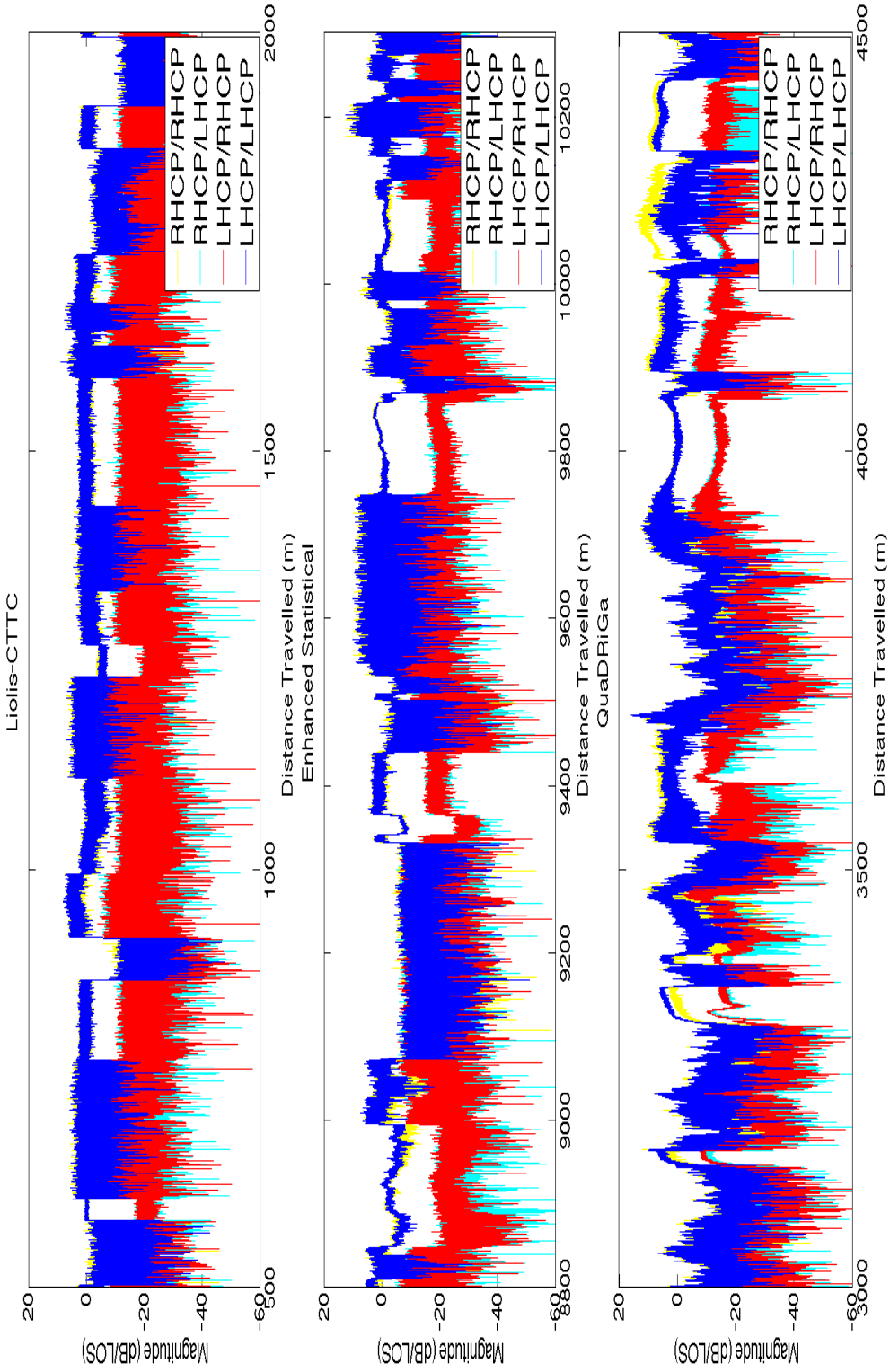


FIGURE 4.10: Timeseries for a mobile travelling within the urban user environment at 50 km/h generated with the Liolis-CTTC model (top), the Enhanced Statistical Model with Jakes Spectrum Doppler shaping through Sum of Sinusoids method (middle) and the QuaDRiGa model (bottom). XPD = 20dB

## 4.5 Doppler Shaping of Spectra

Figure 4.11 shows the frequency response of the Enhanced Statistical model using both the Jakes Spectrum and Asymmetrical Jakes Spectrum. It is clear when we compare the frequency response of the Enhanced Statistical model to the frequency response of the Liolis-CTTC model, which applies no Doppler shaping to the multipath component, the inclusion of Doppler effects on the multipath components offers a more realistic simulation of the spectral properties of the channel.

If we consider the frequency response of the QuaDRiGa model, there are a number of interesting features. In the frequency range 50 to 100 Hz the frequency response appears to have a Jakes shape, however at the other end of the spectrum between -50 to -100 Hz, the spectrum appears to have a shape which more resembles a flat Doppler spectrum. Also, there is a separation between the co- and cross-polarisation subchannels towards the middle of the spectrum around 0 Hz.

The Enhanced Statistical LMS model with the Jakes Spectrum implemented gives a good approximation of the QuaDRiGa spectrum as the general shapes are similar and there is a slight separation of the co- and cross-polarisation subchannels towards the centre of the spectrum, although this is not as pronounced as in the QuaDRiGa spectrum. The Enhanced Statistical LMS model with the Asymmetric Jakes spectrum implemented with a minimum frequency of -100 Hz and a maximum frequency of 80 Hz appears to be closest to the QuaDRiGa model as it achieves an unsymmetrical spectrum and also consists of regions with a separation between the co- and cross-polarisation subchannels, especially from approximately -100 Hz to -80 Hz.

Figure 4.12 shows the five different Doppler spectra that were applied to the Enhanced Statistical model to investigate effects of each spectrum on the statistical output of the series. It may be possible to further increase the similarity between the frequency response of the Enhanced Statistical Model and the QuaDRiGa model by creating and applying a more complex Doppler shape after careful analysis of the frequency response during particular states in the QuaDRiGa model and also real data from the MIMOSA campaign.

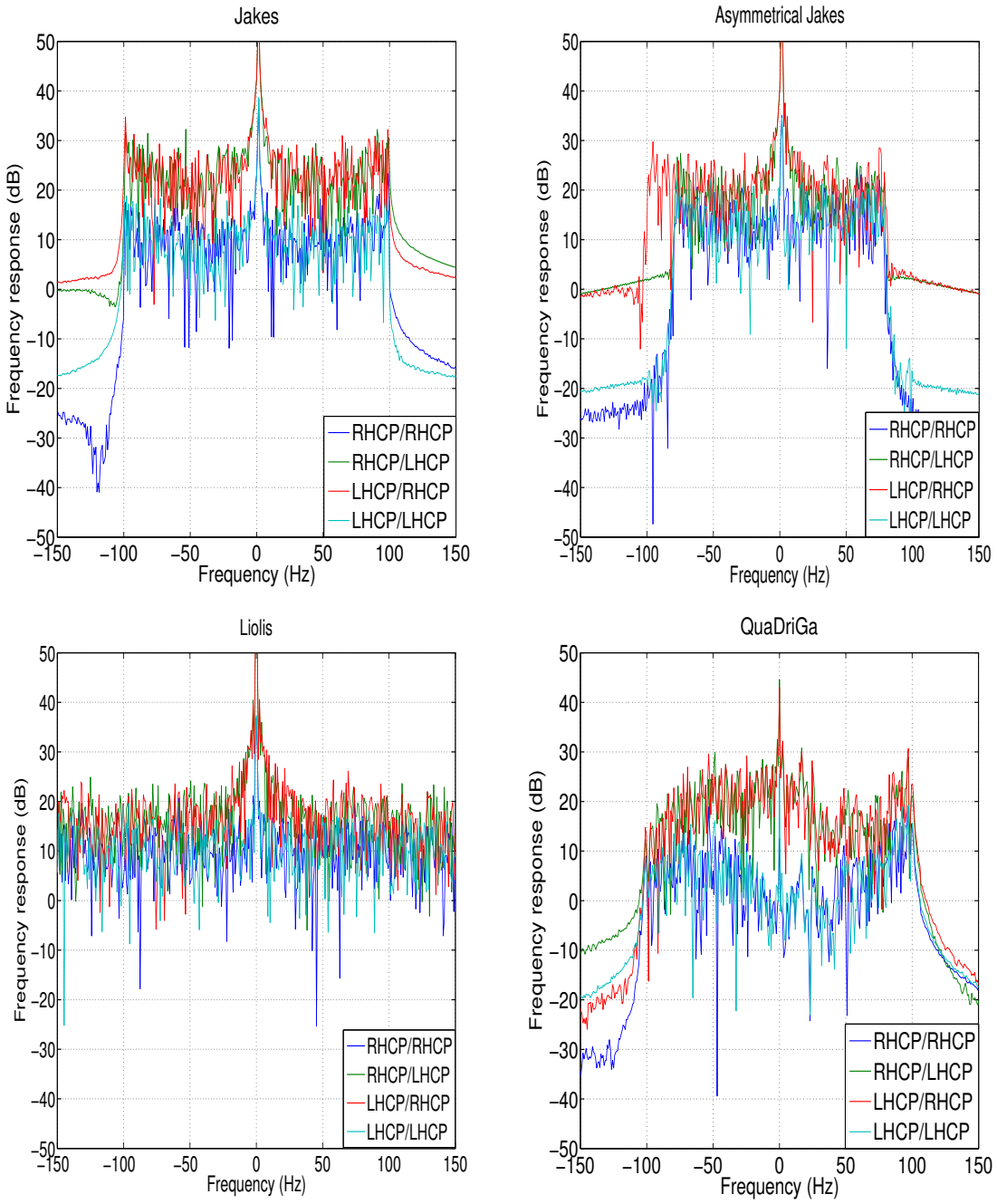


FIGURE 4.11: Four plots showing the frequency response of the Enhanced Statistical Model with Jakes Doppler spreading (top left), the Enhanced Statistical with Asymmetrical Jakes Doppler spreading with a minimum frequency of -100 Hz and a maximum frequency of 80 Hz (top right). Also included for comparison are the frequency response of the Liolis-CTTC model (bottom left) and the QuaDRiGa model (bottom right). The four MIMO subchannels are plotted, i.e the two co-polarisation subchannels RHCP/RHCP & LHCP/LHCP and the two cross-polarisation subchannels RHCP/LHCP & LHCP/RHCP. XPD = 20dB

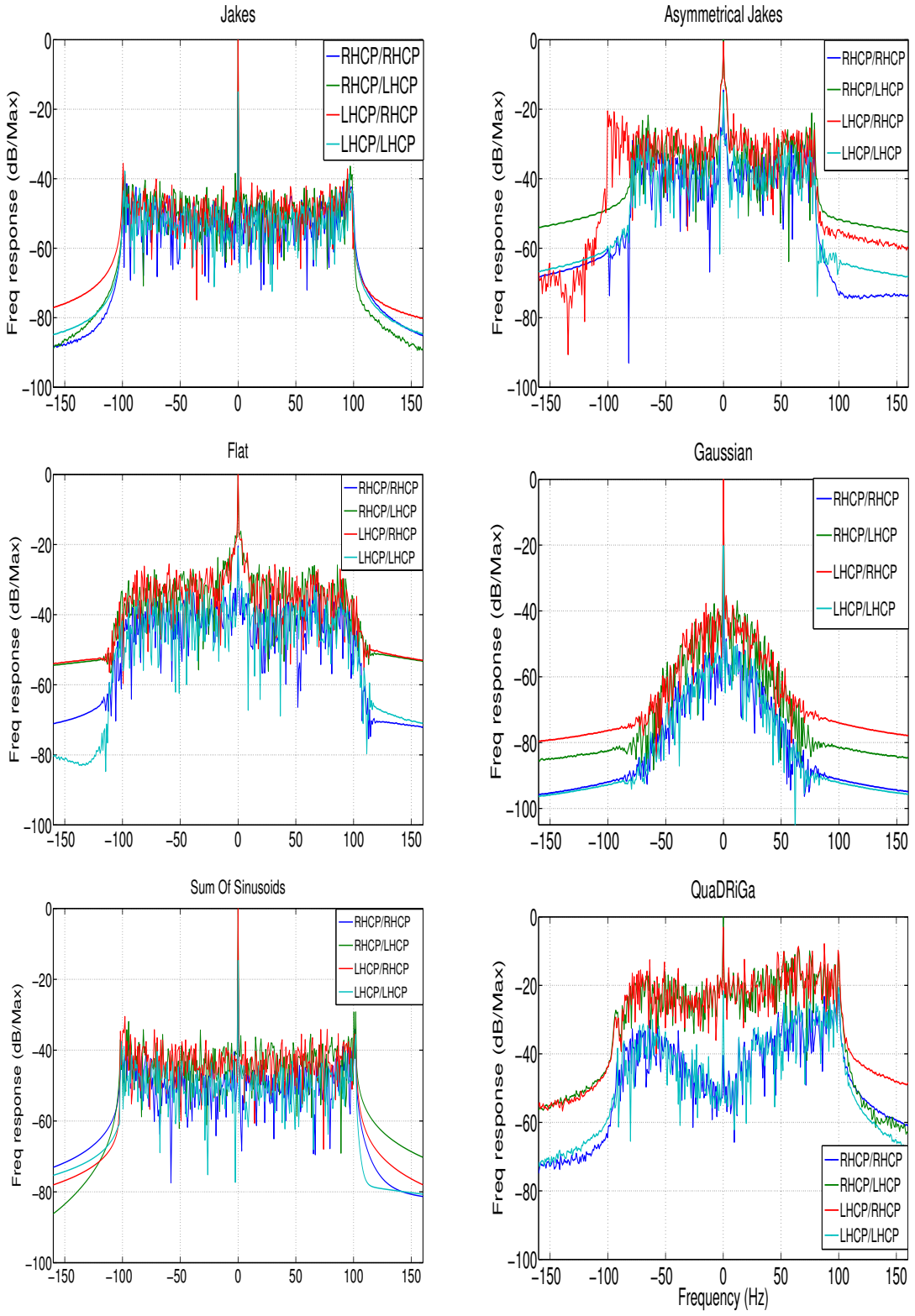


FIGURE 4.12: The normalised frequency response of the Enhanced Statistical Model with 1) Jakes, 2) Asymmetric Jakes (fmin = -80Hz, fmax = 100Hz), 3) Flat, 4) Gaussian, 5) Jakes through Sum of Sinusoids method ($\chi = 1$, $K_o$=0.99), 5) QuaDRiGa XPD = 15 dB and normalised

## 4.6 Statistical Analysis

Statistical analysis of the timeseries from the channel model includes the cumulative distribution function (CDF) and second order statistics, the average fade duration (AFD) and the level crossing rate (LCR). The second order statistics depend on the mobile speed and are also influenced by the frequency used for sampling the timeseries.

The CDF is the useful in determining the outage probability of a system as it provides information regarding the probability that a specific signal level is not exceeded. This signal level may be the system's operation threshold, the outage probability may be determined and fade margins for the system may be calculated [27].

The AFD and LCR are useful in determining suitable error protection coding schemes and interleaving algorithms for the channel [27]. To calculate the AFD, a reference signal is chosen and the number of occasions the signal falls below this reference is counted along with the time the signal spends at levels below the reference, the ratio between the two parameters gives the average fade duration. In this thesis the AFD was calculated for reference signals at 1 dB intervals between the maximum signal magnitude and the minimum signal magnitude for each subchannel independently. Information about the time duration a signal may be below the operating threshold helps determine how many bits could potentially be lost during a fade. To calculate the LCR, the number of occasions the signal crosses a reference signal is a specified time period is counted. In this case, as with the AFD reference signals in 1 dB intervals between each subchannel's maximum and minimum signal level was determined and the sampling frequency of the model was used as the specific time interval.

### 4.6.1 Cumulative Distribution Function

Figure 4.13 shows the cumulative distribution function (CDF) of the normalised received signal for the urban user environment for the Liolis-CTTC model, the Enhanced Statistical LMS model with Jakes Doppler Spectrum and the QuaDRiGa model travelling at 50 km/h for a simulated journey of 100 km. To make the plot easier to analyse,

only one of each of the two co-polarisation and cross-polarisation subchannels are plotted as there is a high similarity between the two co-polarisation subchannels and the two cross-polarisation subchannels.

The three models show excellent agreement with each other in terms of their distribution plots especially at low and very low signal levels. At higher signal levels, for example over $\sim$-10 dB the Enhanced Statistical model and the Liolis-CTTC model show a joint distribution as the signal level moves from the region in which it is dominated by 'good' states with less probability of heavy shadowing on the signal. Although LOS conditions are not highly likely in an urban environment, the received signal at higher signal levels will have a stronger direct signal component that will be modelled by lognormal distribution and the multipath component will be modelled by a Rician distribution.

Low and very low signal levels in the CDF plot will represent the received signal in bad states and will be dominated by multipath components. It is clear in Figure 4.13 that all the models follow a similar Rayleigh distribution for the multipath components of the signal as the signal power decreases by 10 dB over a decade of probability.

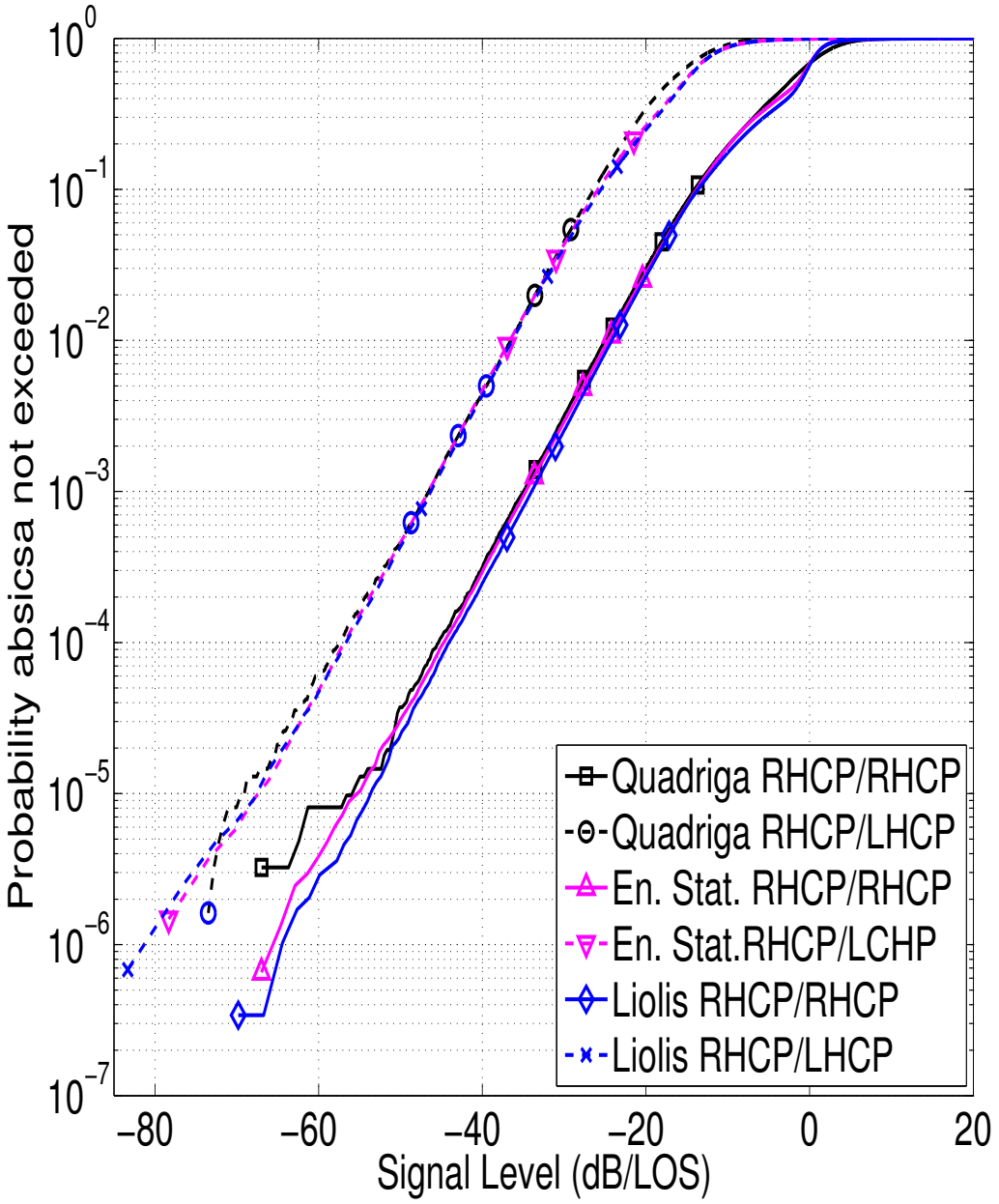


FIGURE 4.13: Comparison of the Cumulative Distribution Function for the Enhanced Statistical model with Jakes Doppler Shaping, the Liolis-CTTC model and the QuaDRiGa model. XPD = 15dB

### 4.6.2 Average Fade Duration and Level Crossing Rate

Figure 4.14 shows the average fade duration (AFD) and Figure 4.15 shows the level crossing rate (LCR) of the normalised received signal for urban user environment for the Enhanced Statistical dual polarised LMS model, the original Liolis-CTTC model and the QuaDRiGa model.

The AFD plot shows good agreement between the Enhanced Statistical Model and the QuaDRiGa model in both the co-polarisation subchannel and the cross-polarisation subchannels, also the QuaDRiGa model does not show the bump that both the Enhanced Statistical model and the Liolis-CTTC model show in the co-polarisation subchannel plot at signal magnitudes of 0 dB. The difference in the minimum fade durations at low signal magnitudes arises from the different sampling frequencies used within each model.

The LCR plot show prominent bumps in the curve of the co-polarisation subchannel at signal magnitudes of 0 dB for the Enhanced Statistical model and the Liolis-CTTC model. These bumps show the meeting of the two different scenarios for the good states and the bad states for each model with good states dominating above signal magnitudes of 0 dB and bad states dominating at signal magnitudes lower than 0 dB. In comparison the QuaDRiGa co-polarisation subchannel is much smoother - the good and bad states seem to merge more seamlessly with a much smaller bump in the curve at approximately 10 dB. The cross-polarisation subchannels in all three models plotted in Figure 4.15 show smoother curves with maximums at signal magnitudes of around -10 dB. The Enhanced Statistical model and the QuaDRiGa model show greater similarity especially in the cross-polarisation subchannel.

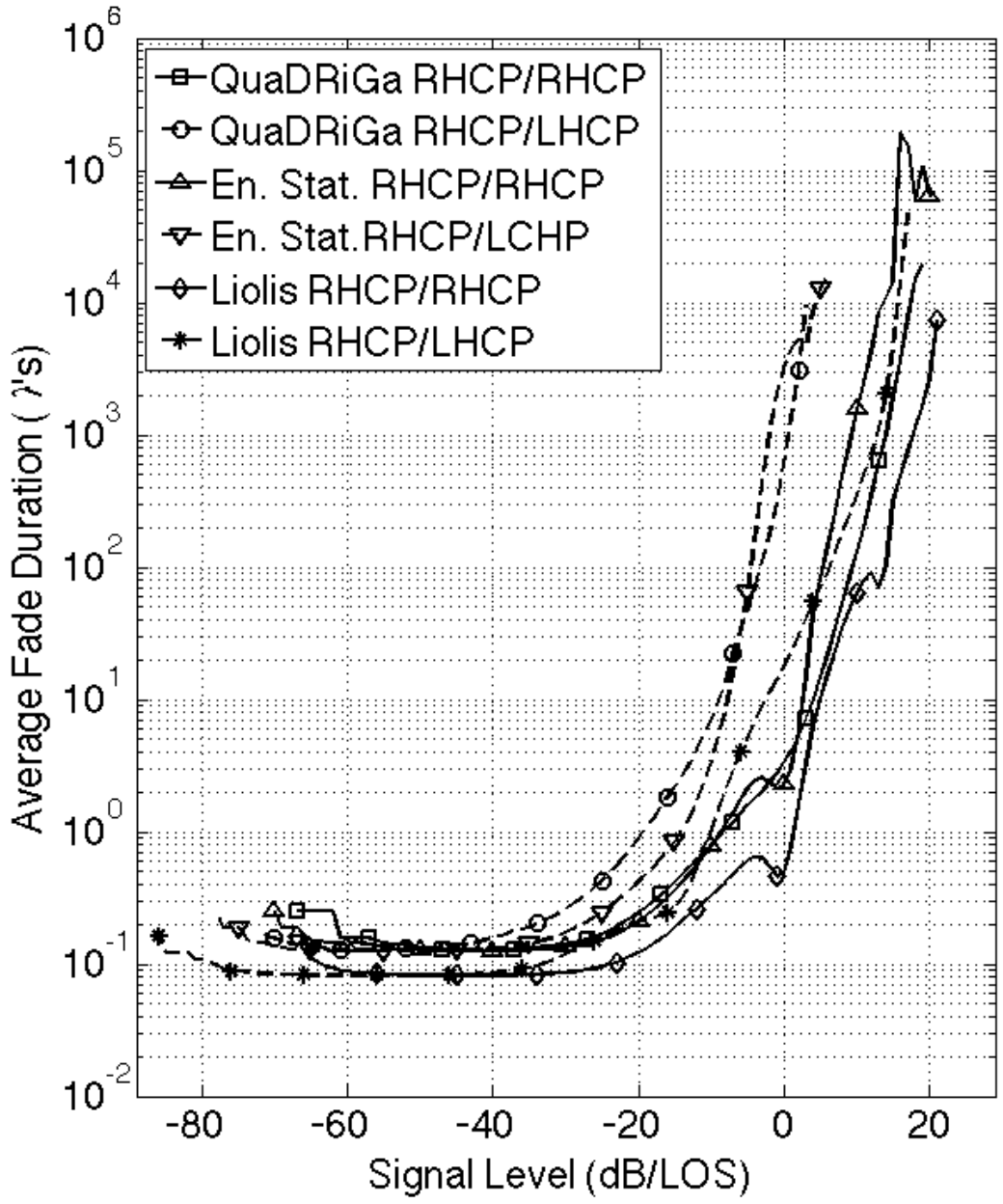


FIGURE 4.14: Comparison of the Average Fade Duration in wavelengths for the Enhanced Statistical model with Jakes Doppler Shaping, the Liolis-CTTC model and the QuaDRiGa model. XPD = 15dB

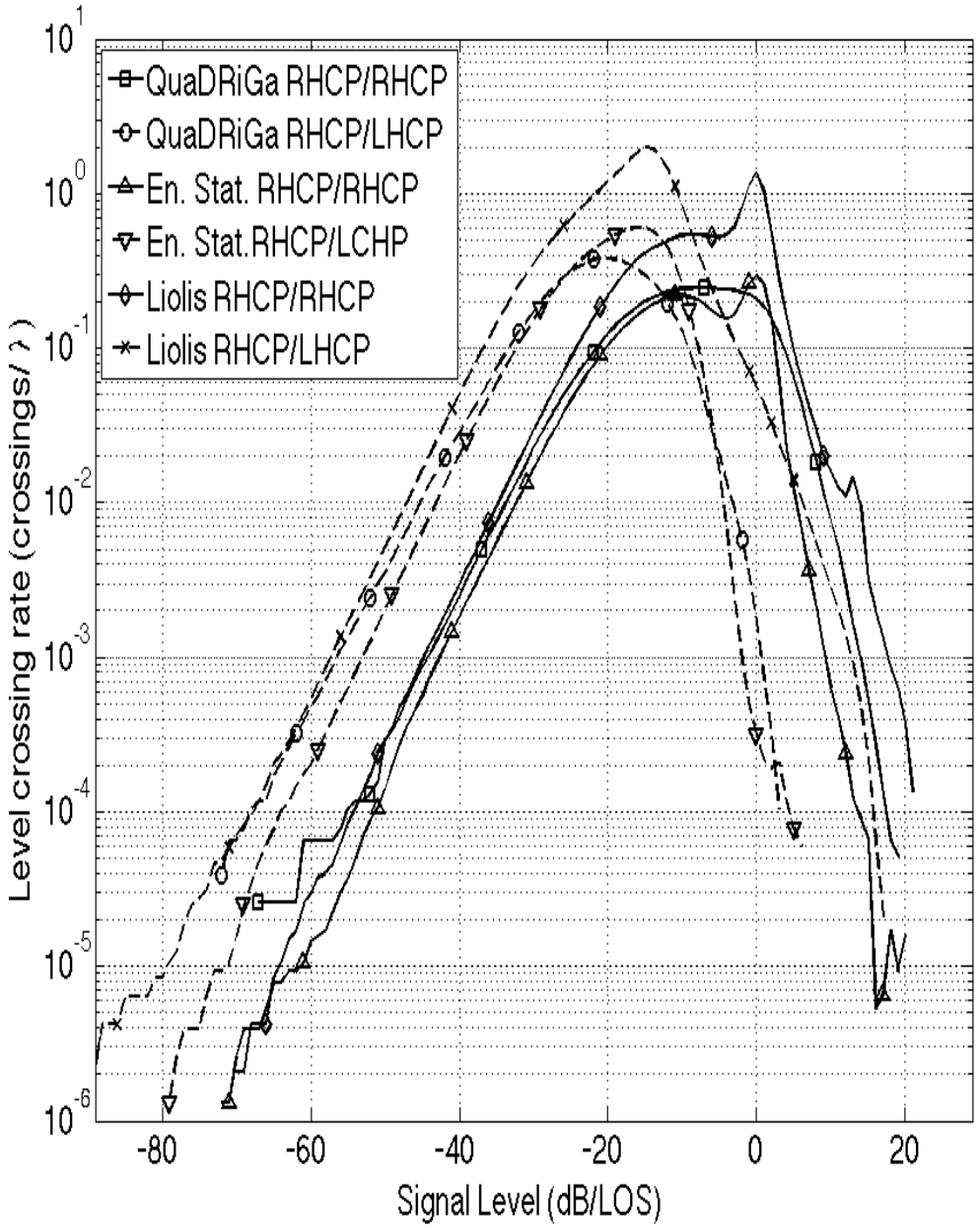


FIGURE 4.15: Comparison of the Level Crossing Rate in crossings per wavelength for the Enhanced Statistical model with Jakes Doppler Shaping, the Liolis-CTTC model and the QuaDRiGa model. XPD = 15dB

## 4.7 Eigenvalue Analysis

Performing analysis of the eigenvalues inherent to the channel can give insight into the channel's properties, specifically providing an understanding of the channel's capability to fulfil gains through either polarisation multiplexing or diversity. This is useful information when considering which transmission and signal processing strategies to implement in real satellite systems employing MIMO through dual polarisation.

Eigenvectors and eigenvalues can be obtained through eigendecomposition of **HH'**, where **H** is the 2x2 channel matrix. By looking at the separation of the eigenvalues $\lambda_n$, where $n$ is 1 or 2 for a 2x2 dual polarised MIMO system, we can assess the polarisation multiplexing gain or diversity.

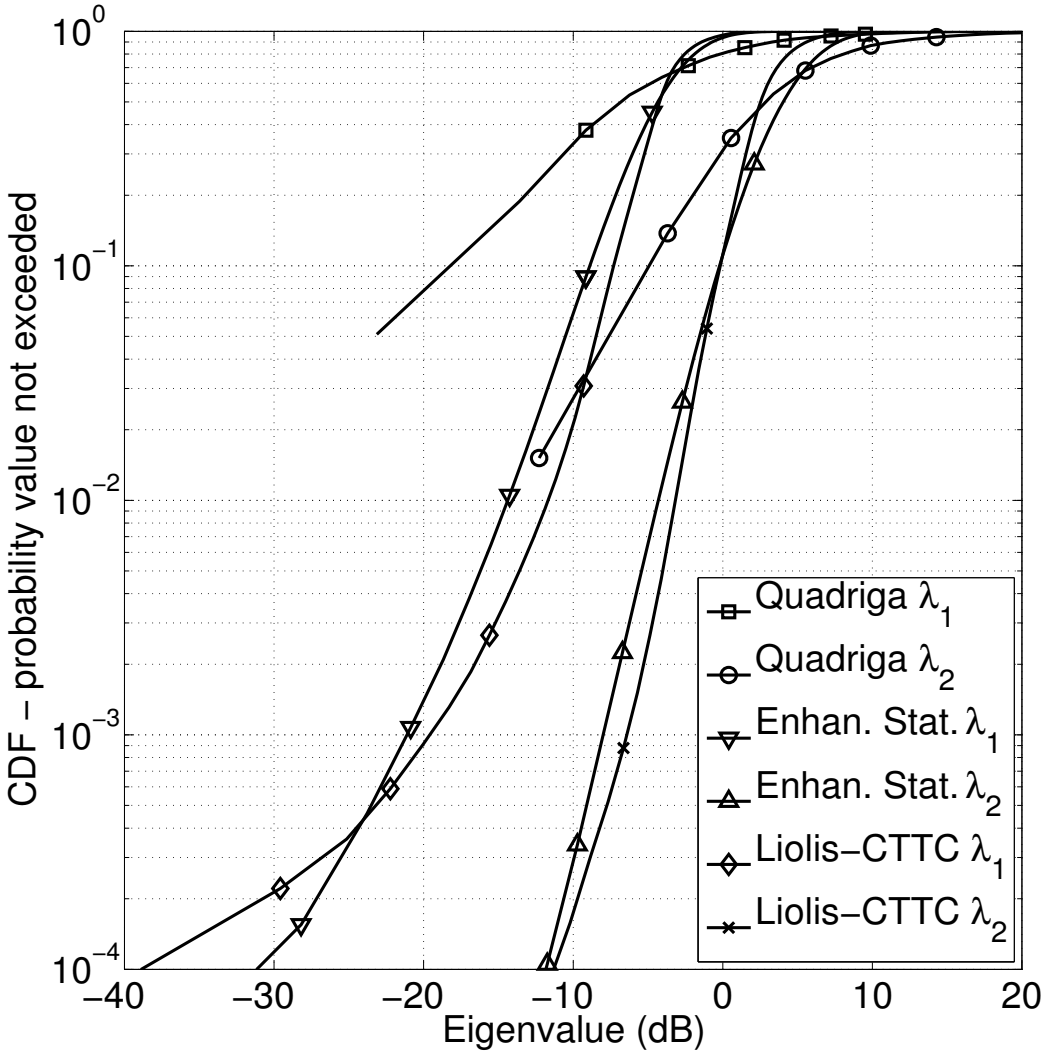


FIGURE 4.16: EigenAnalysis: comparison of the eigenvalues obtained during good states for QuaDRiGa model, Liolis model, enhanced statistical model with Jakes Doppler shaping, all based on received signal within an urban environment.

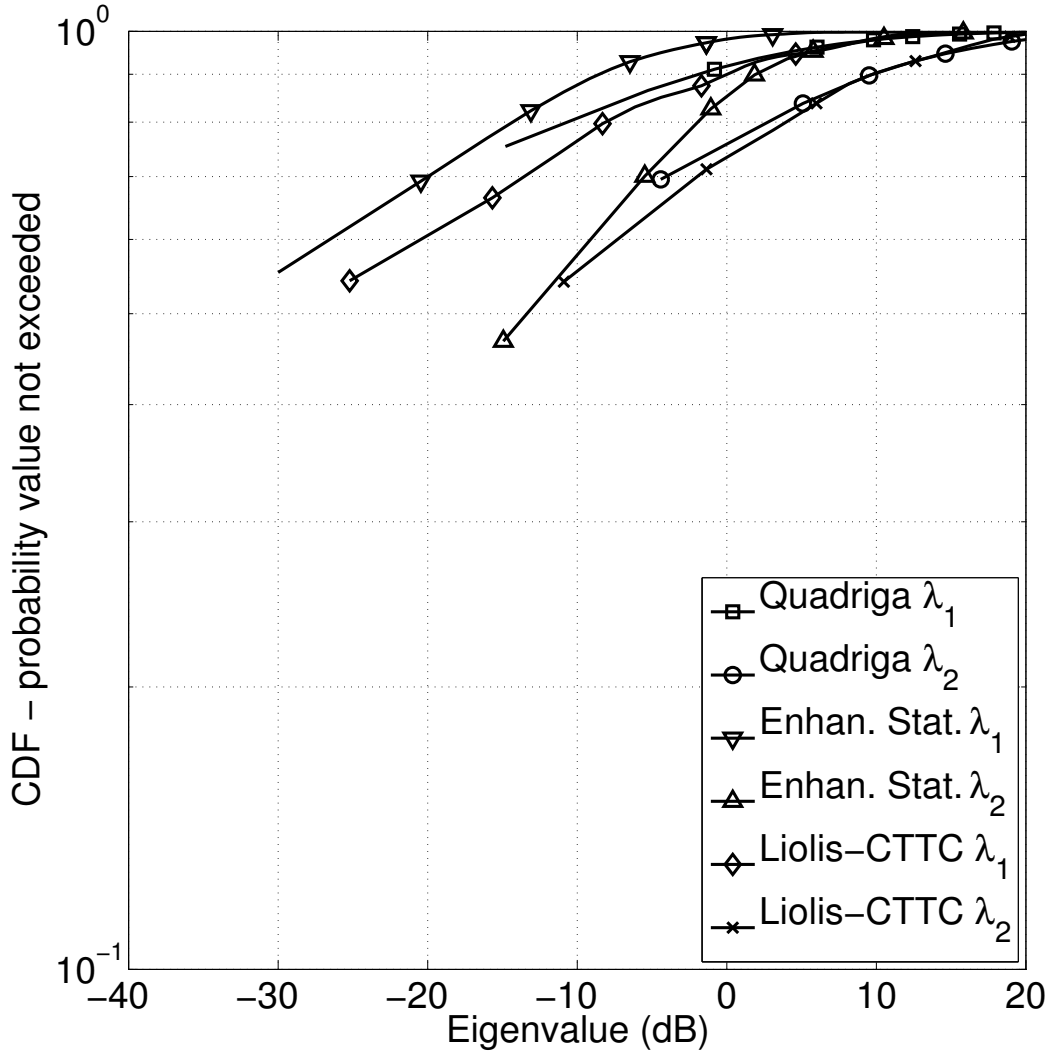


FIGURE 4.17: Eigenvalue analysis: comparison of the eigenvalues obtained during bad states for QuaDRiGa model, Liolis model, enhanced statistical model with Jakes Doppler shaping, all based on received signal within an urban environment.

Figure 4.16 plots the CDFs of eigenvalues obtained from a series of good states from the channels generated using the three aforementioned models. It is clear that all models show rich polarisation multiplexing within the good states as the eigenvalues $\lambda_1$ and $\lambda_2$ lie close together [10]. There is a very close agreement between the eigenvalues distributions of the two statistical models with the QuaDRiGa model displaying eigenvalues of greater magnitude greater separation of the two eigenvalues.

Figure 4.17 plots the eigenvalue distributions obtained from a series of bad states from the channels generated using the three models. The eigenvalue distributions from the bad states contain much lower eigenvalues than those from the good states and also as their is a greater separation in eigenvalue distributions, the achievable gains through polarisation multiplexing are reduced in these states. An increased separation between eigenvalue distributions $\lambda_1$ and $\lambda_2$ indicates an increase in scatterers in the environment surrounding the user's receiver [10] indicating the channel is rich in diversity rather than multiplexing gain.

## 4.8 Statistical Distribution of Received Signal

In the Liolis-CTTC and Enhanced Statistical models the probability distribution of the received signal is described using the Loo model, Equation (2.9). This joint distribution is applied during the simulation process through the generation of unique Loo parameter triplets ($M_A, \Sigma_A$, MP) for each state. $M_A, \Sigma_A$ relate to the lognormal fading of the direct signal component and MP relates to the Rician fading of the multipath signal component.

Another distribution that is of interest and commonly used in the mobile radio context is the Suzuki distribution, Equation (2.14) . This is considered a 'worst case' scenario where there is no direct signal component and all the received signal is comprised of the diffuse multipath [30].

Analysis of the statistical distributions of the simulated received signals in each of the models was performed and the distributions were compared to theoretical distributions

defined by parameters derived from the simulated data. The agreement between the observed and theoretical distributions were measured through comparison of the probability distributions (PDF), comparison of the cumulative distribution functions (CDF) and through statistical testing of these distribution using the Kolmogorov-Smirnov (K-S) test and the Cramér Von Mises (CVM) test. Table 4.2 gives the probability that the CDF of the output of each model matches the CDF produced by a theoretical Loo distribution with the given Loo parameter triplet with a significance level of $\alpha = 0.1$ for each statistical test.

TABLE 4.2: Probability given by the Kolmogorov-Smirnov (K-S) test and the Cramér Von Mises (CVM) that the distribution of the output of each model is statistically identical to the theoretical distribution generated by Loo parameter triplet derived from the timeseries of each model. Significance level, $\alpha = 0.1$.

| Model | $(M_A, \Sigma_A, MP)$ dB | K-S | CVM |
|---|---|---|---|
| Liolis - Good states | (0.122, 0.726, -11.82) | 0.9482 | 0.9947 |
| Enhan. Stat. - Good states | (0.246, 0.771, -14.497) | 0.7567 | 0.9922 |
| QuaDRiGa - Good states | (2.116,3.198,-11.22) | 0.3669 | 0.7483 |
| Liolis - Bad states | (-9.974,7.889,-9.42) | 0.194 | 0.992 |
| Enhan. Stat. - Bad states | (-9.952,7.151,-10.766) | 0.345 | 0.984 |
| QuaDRiGa - Bad states | (-9.229,8.107,-15.22) | 0.9998 | 0.9972 |

Five theoretical distributions were generated for the statistical testing purposes; these were Rayleigh, Rice, Lognormal, Loo and Suzuki. The parameters for the generation of the theoretical distributions were derived from the simulated data. For the data from the two statistical models, i.e. the Liolis-CTTC model and the Enhanced Statistical model, accessing the necessary parameters to generate a theoretical distribution was a straightforward process as the parameters were inherent to the simulation process, i.e. the Loo parameter triplet. However, for the simulated data from the QuaDRiGa model that doesn't use Loo parameters in the simulation process, these parameters had to be obtained through a filtering process to obtain separate direct signal and multipath components from which the Loo parameters could be derived. Thus, having obtained mean and standard deviation of the direct signal component and the multipath power, tests to assess the 'goodness of fit' were designed for the following comparisons: the multipath component distribution with either Rayleigh or Rician distributions, the direct signal component distribution with the Lognormal distribution and also the total received signal with the Loo and Suzuki distributions.

Figures 4.18 & 4.19 shows the CDFs of the three models output during good states and bad states, compared with the theoretical distributions of the derived Loo parameters. It is clear that there is excellent agreement between the distributions of all models during the bad states and the LOS component in the QuaDRiGa model causes a difference in distributions between it and the statistical models.

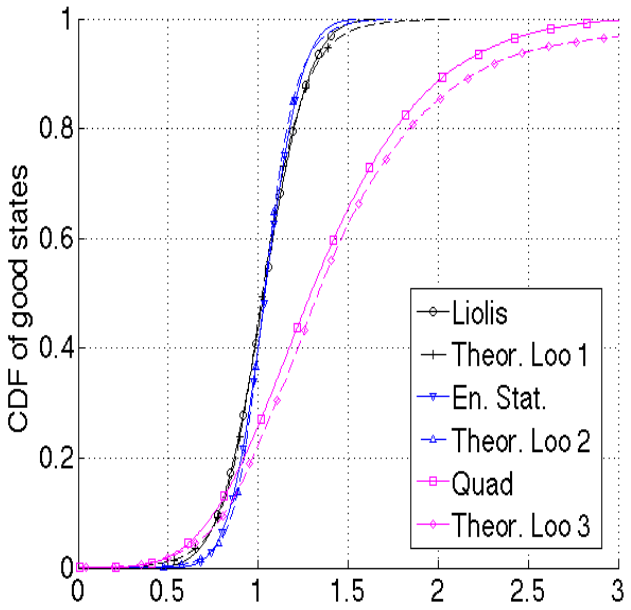


FIGURE 4.18: Good states co-polarisation subchannel distributions with comparison to Theoretical Loo distribution with the same average Loo Parameters for the QuaDRiGa model, Liolis-CTTC model and Enhanced Statistical model with Jakes Doppler shaping

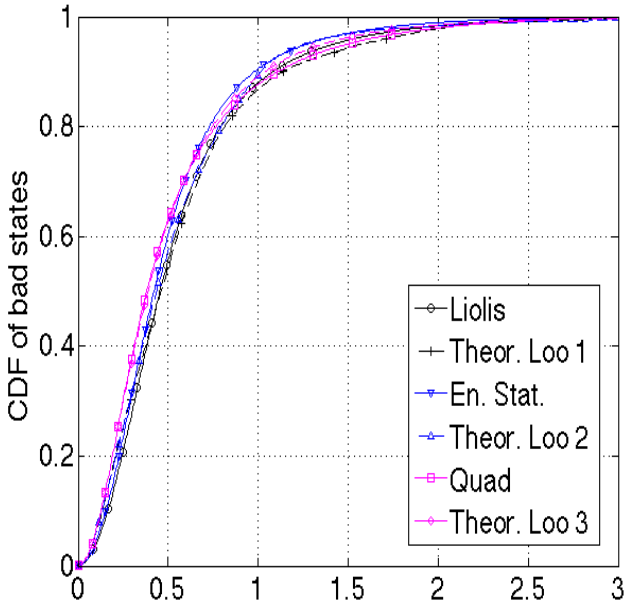


FIGURE 4.19: Bad states co-polarisation subchannel distributions with comparison to Theoretical Loo distribution with the same average Loo Parameters for the QuaDRiGa model, Liolis-CTTC model and Enhanced Statistical model with Jakes Doppler shaping

## 4.9 Summary

In this chapter we compare the Enhanced Statistical LMS model with state-of-the-art stochastic and deterministic channel models in the dual polarised satellite communications context, the statistical Liolis-CTTC model, and the semi-deterministic geometric-stochastic QuaDRiGa model. The enhanced channel model output shows a number of similarities to the statistical Liolis-CTTC model because many parameters used in the simulation process are the same and the statistical models are both constructed in the same way. The enhanced channel model also provides a greater similarity to the QuaDRiGa model in a number of aspects thus providing a more accurate timeseries, whilst the model retains the two major benefits of a statistical model of low complexity and low simulation time.

The Enhanced Statistical LMS model timeseries shows a higher level of variation within states, both in terms of signal magnitude and multipath variation. This is an improvement over the Liolis-CTTC model in which the signal magnitude and the amount of signal variation around the mean signal value seem quite fixed. The Enhanced Statistical LMS model timeseries shows variation between the two co-polarisation subchannels RHCP/RHCP and LHCP/LCHP and the two cross-polarisation subchannels RHCP/LHCP and LHCP/RHCP. These effects were achieved by varying the cross-polarisation coupling of the environment throughout the simulated journey. The Enhanced Statistical LMS model timeseries shows smooth transitions between that which are also observable in the QuaDRiGa model timeseries

The cumulative distribution function plot of the Enhanced Statistical LMS model gives good agreement with the QuaDRiGa model, although the QuaDRiGa model has higher simulated received signal levels. The average fade duration analysis of shows longer fades than the Liolis-CTTC model and closer in duration to the fades of the QuaDRiGa model. The level crossing rate analysis shows a lower number of level crossings per wavelength than the Liolis-CTTC model and closer in duration to the fades of the QuaDRiGa model.

The spectrum of the enhanced channel model and the QuaDRiGa model both show an improvement over the Liolis-CTTC model as they both provide Doppler shaping of the small-scale variations resulting in a complex Doppler spectrum of the received signal. It does not seem that the QuaDRiGa model's spectrum can be described by one single shape, with elements resembling Jakes spectrum, a flat spectrum and an asymmetric Jake's spectrum. All of these spectra can be implemented within the enhanced channel model.

It is worth noting that although the Liolis-CTTC model is used as the baseline model in this thesis, the enhancements applied through the Enhanced Statistical model may be applied to other statistical models that incorporate a Rician distribution for the modelling of the multipath signal components, for example, the King model [3].

# Chapter 5

# Comparison of Enhanced Model with MIMOSA measurement data

## 5.1 Introduction

This chapter uses data from the European Space Agency's (ESA) and the Fraunhofer Institute's measurement campaign of the dual polarised land mobile satellite (LMS) channel, MIMO Channel for Mobile Satellite Systems (MIMOSA), to compare with the Enhanced Statistical LMS model and validate the model. The details of the campaign are described and comparisons are made between the recorded data in urban, suburban and open rural environments and the simulated timeseries from the Enhanced Statistical LMS model under similar environmental conditions. The results show that the Enhanced model offers a good agreement to the data in terms of timeseries, 2nd order statistics and eigenvalue decomposition. The Enhanced Statistical model also shows a better match to the MIMOSA measurement data than the Liolis-CTTC model for the urban user environment especially in terms of having more realistic shape and distribution of good and bad states in the timeseries, increased levels of signal variation within states, smother state transitions, a closer agreement in the cumulative distribution function, the average fade duration, the level crossing rate and the eigenvalue distribution and a more realistic spectrum with Jakes spectrum

shaping and Flat spectrum shaping appearing to be good matches to the MIMOSA data.

## 5.2 The MiLADY and MIMOSA Measurement Campaigns

The ESA commissioned the Characterisation of the MIMOSA project [21] through the ARTES programme [20] and it was implemented by the Fraunhofer Institute. MIMOSA followed on from the Mobile Satellite Channel with Angle Diversity project (MiLADY) [22], also funded by the ESA and conducted by the Fraunhofer Institute. The MiLADY campaign focused on measurements of the LMS channel using spatial diversity implemented with transmissions from multiple satellites. The aim of the project was to obtain information regarding the azimuth-elevation angle separation of the combinations of multiple satellites. This was achieved through the analysis of the effect of angle diversity on the statistics of the received signal from multiple satellite. The resulting measurement data contained vast information on single-input single-output (SISO) and multiple-input single-output (MISO) LMS channels and an informed channel model, the MiLADY model, based on the measurements was created which provided parameter databases for various satellite elevation and azimuth angles for single satellite reception [17] and for dual satellite reception [53]. The MIMOSA project was designed to fill the gap that existed in multiple-input multiple-output (MIMO) satellite measurements and validated LMS channel models using dual polarised antenna. It aimed to quantify the capacity increase for mobile reception and evaluate the potential benefits of using in a satellite system what had proven to be a highly advantageous antenna configuration in terrestrial systems

### 5.2.1 MIMOSA set-up

The MIMOSA measurement campaign was an extensive campaign comprising of measurements of S-band transmissions to a mobile receiver based on the roof of a moving

car and is described in [21],[7],[51]. The campaign consisted of two separate experiments; firstly the Channel Measurement Equipment (CME) obtained narrowband data from real W2A satellite transmissions in multiple receiver environments taken in three locations: Berlin, Lake Constance and Erlangen, and secondly a RUSK satellite emulator in an urban environment provided a more detailed analysis of the multipath angle of arrival (AoA) measurements for implementation of a wideband semi-deterministic model.

Transmissions consisted of a satellite signal at an S-band frequency of 2.187 GHz, with left-hand circularly polarised (LHCP) and right-hand circularly polarised (RHCP) signals transmitted in parallel. A multitone signal was used containing several carrier wave signals, described in the MIMOSA literature as an orthogonal frequency division multiplexing (OFDM) waveform reduced to continuous pilots by stripped of additional payload data.

The mobile receiver consisted of various antennas mounted on the roof of the moving car, multiple antennas allowing for comparison between a different antenna architectures, including single-input multiple-output (SIMO), MISO and MIMO. Five antennas were used: one RHCP Single Polarisation Circular (SPC) antenna, one LHCP SPC antenna, two Dual Polarisation Circular (DPC) antenna each with RHCP and LHCP outputs, and a Vertical Polarised (VP) antenna. This provided 7 output ports that allowed for 6 different antenna architectures to be recorded. A SIMO scenario was measured using the two LHCP ports from DPC1 and DPC2. Three MIMO scenarios were measured, one co-located with LHCP and RHCP from DPC1, one with a 31 cm separation with LHCP from DPC1 and RHCP from DPC2 and another with a 40.5 cm separation with LHCP from SPC1 and RHCP from SPC2. Finally a MISO scenario was measured using the output from the VP antenna.

The DPC and SPC antenna used had properties consistent with commercial polarised antennas currently available for mobile devices of 5 dB and 10 dB respectively.

### 5.2.2 MIMOSA Data Analysis

The recorded data is initially classified according to the correct environment., e.g. urban, suburban, etc. Then the channel matrix data was created by normalising and reformatting the data to create 12 signal bins per antenna per polarisation at a constant speed of 50.78 km/h. The frequency off-set is compensated for and statistical analysis of the full data was performed. The narrowband small scale fading (SSF) data was extracted and the large scale fading (LSF) data calculated.

### 5.2.3 MIMOSA Database

The result of the MIMOSA measurements is a large database of various environments: open rural, suburban, urban, forest, commercial and highway. Within each environment, each measurement is further classified to describe the environment in detail. For example urban environments may be highly dense areas with high buildings and dense traffic or areas with either narrow or wide streets, and thus classified as urban1 or urban2.

The data is separated and stored in two formats: LSF-TS data and SSF-TS data. The LSF-TS data consists of timeseries data containing information about the large scale fading parameters and therefore describes the slow fading effects of the channel. The SSF-TS data contains the timeseries with the detailed small-scale fast fading effects of the channel. The SSF-TS is sampled at a very high frequency to include the details of these fast-fading effects, i.e. 4232 Hz.

The structure of the database is such that the data is classified by environment, environment sub-type and antenna combination used.

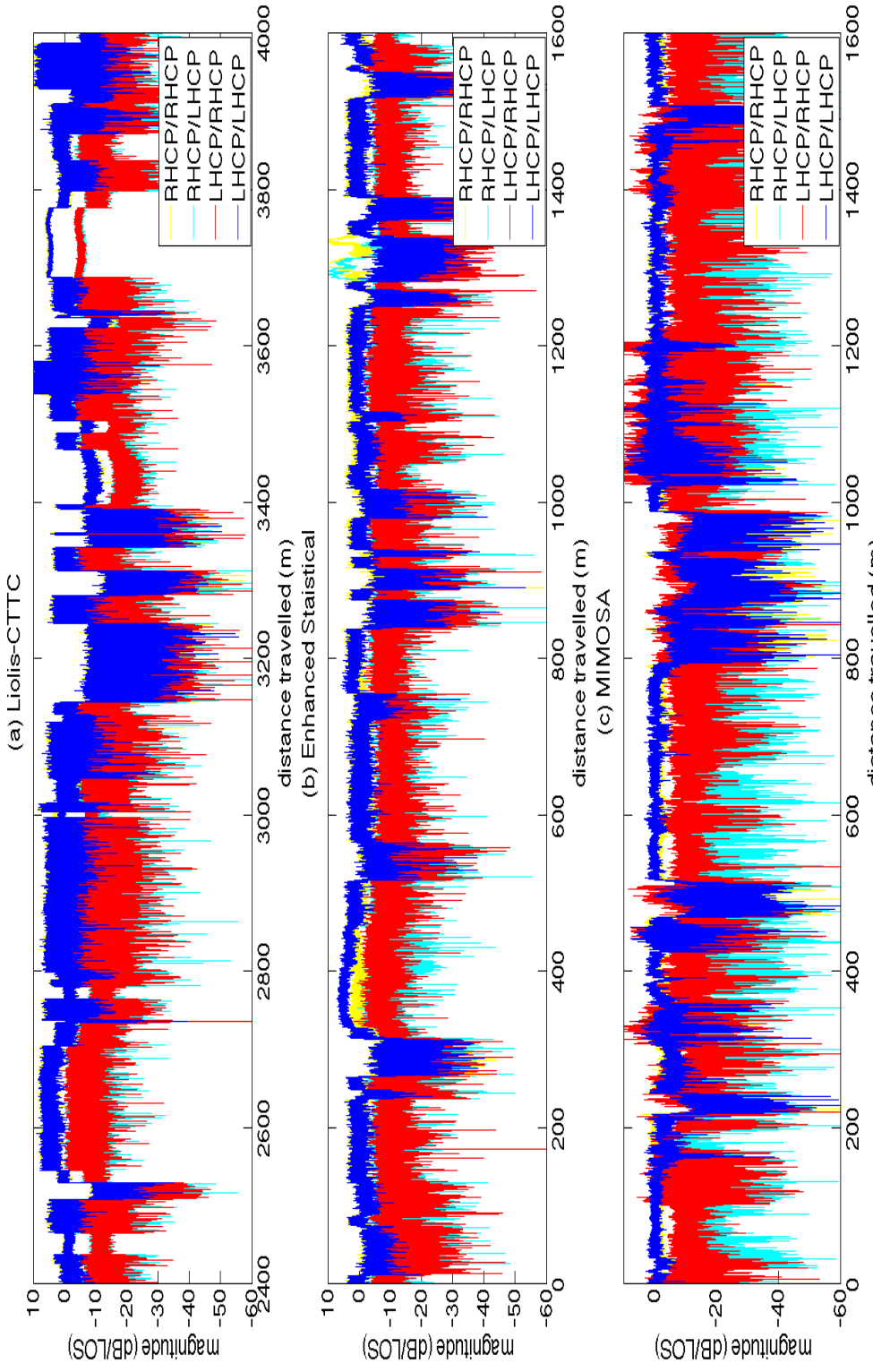


FIGURE 5.1: Timeseries for a mobile travelling within the urban user environment at 50 km/h generated with the Liolis-CTTC model (top), the Enhanced Statistical Model with Jakes Spectrum Doppler (middle) and the MIMOSA data(bottom). The XPD in the Enhanced Statistical model is set to 10dB. The signal level is normalised with respect to the LOS power level in dB.

## 5.3 Analysis of the Urban Environment

### 5.3.1 Timeseries

Figure 5.1 shows the timeseries for the Enhanced Statistical model, the Liolis-CTTC model and the MIMOSA measurement data for a mobile travelling at 50 km/h through an urban environment. Both the Liolis-CTTC timeseries and the Enhanced Statistical model are simulated with an antenna cross-polarisation discrimination (XPD) of 10 dB to match the conditions of that presented in the MIMOSA measurement.

The MIMOSA measurement data shows a greater variation in the magnitude of the received signal than in the received signal in the timeseries produced by either statistical model. This is particularly evident in the cross-polarisation subchannels. For the statistical models the level of variation in the cross-polarisation channels (RHCP/LHCP, LHCP/RHCP) mirrors the level of variation in the co-polarisation channels (RHCP/RHCP, LHCP/LHCP). If there is a particularly good state with a low level of co-polarised signal magnitude variation within the state, then the corresponding cross-polarisation signal demonstrates a similarly low level of signal magnitude variation. If there is a bad state with a high level of variation of the signal magnitude in the co-polarisation subchannels then there is also a high level of variation in the signal magnitude in the corresponding cross-polarisation subchannels.

In the MIMOSA measurement data, the level of variation in the cross-polarisation subchannels is greater than that in the co-polarisation subchannels in every state. In addition, although there isn't a very clear difference between the two co-polarisation subchannels, there is a clear difference between the two cross-polarisation subchannels.

The state transitions in the timeseries of the Enhanced Statistical model gives a better resemblance to the state transitions in the MIMOSA measurement data, as seen in Figure 5.2. The MIMOSA timeseries and the Enhanced Statistical model timeseries show smooth state transitions, Figure 5.3. One observable feature in the MIMOSA data timeseries is the amount of variation that occurs in the cross-polarisation signal, i.e. subchannels LHCP/RHCP and RHCP/LHCP. This is particularly evident

in Figure 5.2 between 280 and 300 m. This level of variation is not demonstrated in the Enhanced LMS model, the signal variation is more uniform within states. Both timeseries in Figure 5.2 begin with similar good states with the co-polarisation subchannel LHCP/LHCP having a signal magnitude of approximately 0 dB. In the MIMOSA timeseries the cross-polarisation LHCP/RHCP signal magnitude for this state is approximately -10 dB, however the lowest value of the LHCP/RHCP signal is approximately -40 dB. In the Enhanced model timeseries the cross-polarisation subchannel LHCP/RHCP signal magnitude is also approximately -10 dB and the lowest value of the signal magnitude in this state is approximately -20 dB.

As in the previous chapter, the unit used for the signal level in the timeseries plots throughout this chapter is dB/LOS. This unit is to reflect the signal level plotted is normalised with respect to the LOS power level (in dB).

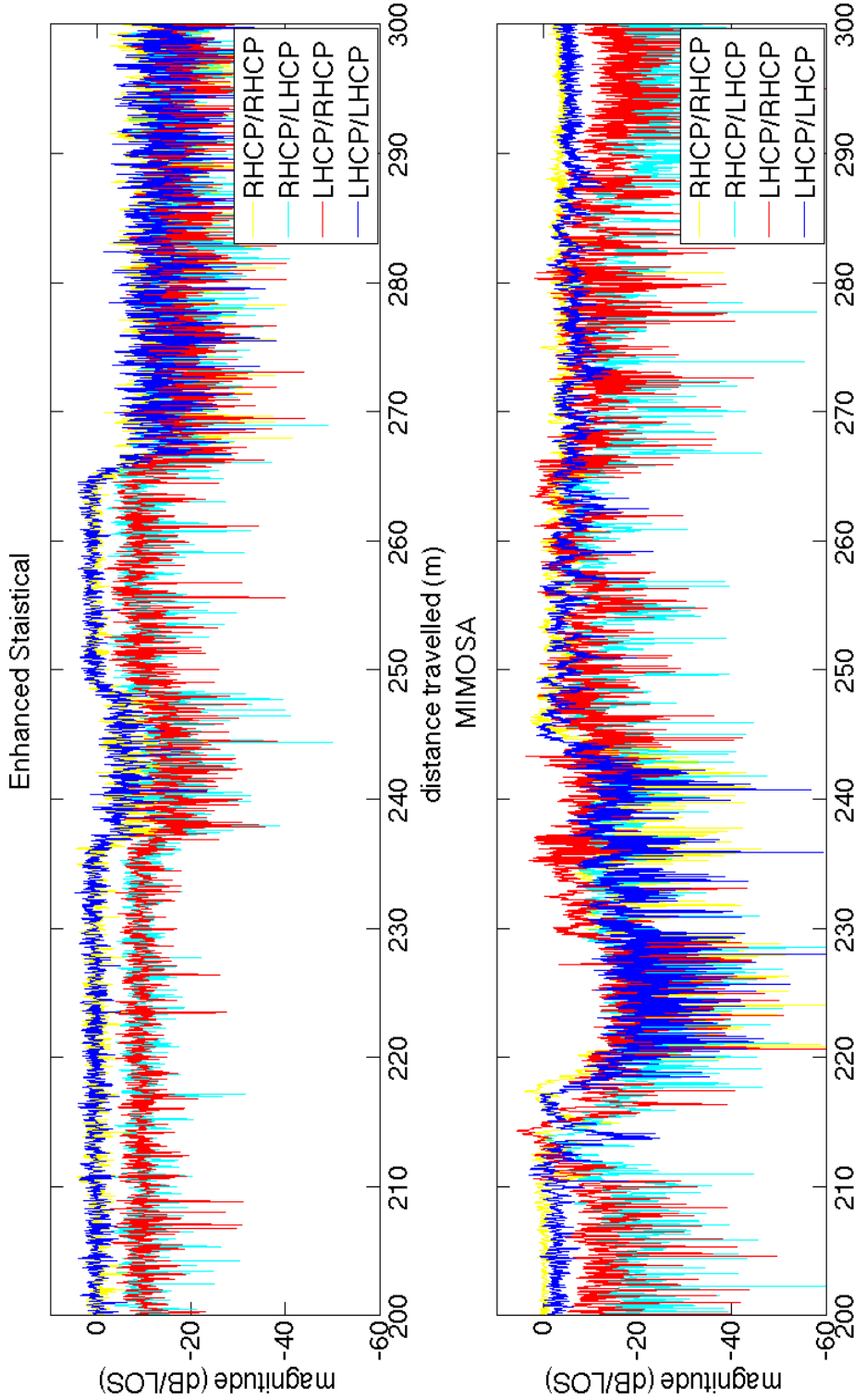


FIGURE 5.2: Close up of the timeseries from Figure 5.1 for a mobile travelling within the urban user environment at 50 km/h with the Enhanced Statistical Model (top) and the MIMOSA data(bottom). These timeseries show the improvement in the state transition process in the Enhanced model and the closer resemblance to real state transitions in the MIMOSA data.

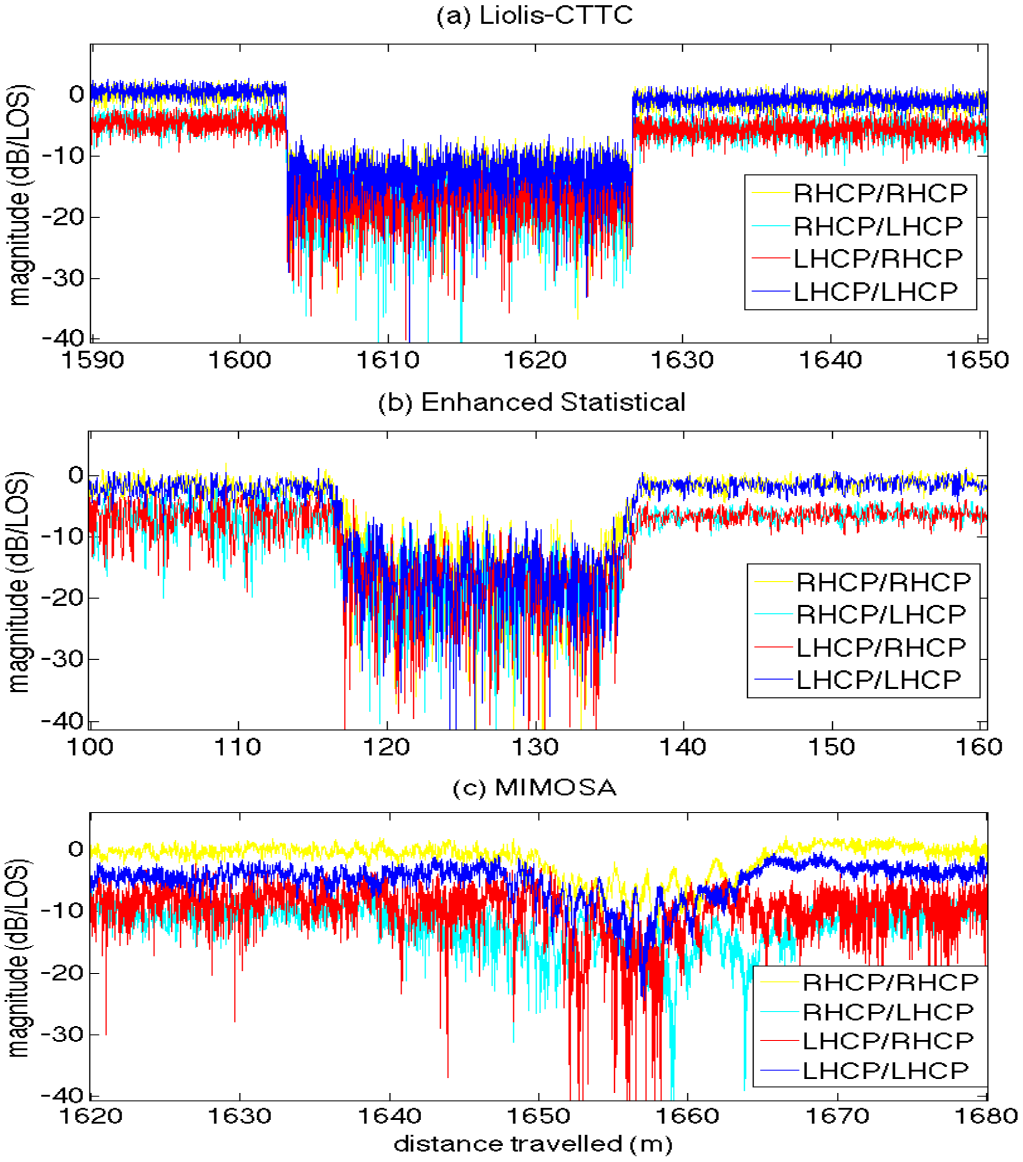


FIGURE 5.3: Comparison of the state transitions in (a) the Liolis-CTTC model, (b) the Enhanced Statistical Model and (c) MIMOSA measurement data all showing a state transition sequence from good to bad to good.

### 5.3.2 2nd order Statistics

#### 5.3.2.1 CDF

Figure 5.4 shows the cumulative distribution function (CDF) of the normalised received signal for the urban user environment for the Liolis-CTTC model, the Enhanced Statistical LMS model with Jakes Doppler Spectrum and the MIMOSA measurement all for a mobile receiver travelling at 50 km/h. The two models are simulated for a journey of 100 km, the particular journey on which the MIMOSA measurement data was 6,664 m.

To make the plot easier to analyse, only one of each of the two co-polarisation and cross-polarisation subchannels are plotted for the timeseries from the two models as there is a high similarity between the two co-polarisation subchannels and the two cross-polarisation subchannels. However, all four subchannels of the MIMOSA data are plotted as there is a difference between the two co-polarisation subchannels and the two cross-polarisation subchannels. It is worth noting the variation between the MIMOSA data plots when considering the two polarisation subchannels of the same type. It seems evident that there is more variation between the two MIMOSA cross-polarisation subchannels, RHCP/LHCP and LHCP/RHCP, than between the two co-polarisation subchannels, RHCP/RHCP and LHCP/LHCP.

The CDF graphs are plotted using a logarithmic scale on each axis to highlight the similarities and differences between the models and the data.

The joint distribution which arises due to the lognormal distribution of the direct signal and the Rician distribution of the multipath is clearly seen in the CDF plot. At high signal levels the received signal is dominated by good states thus the signal level may have a significant LOS component or a shadowed direct signal component with a strong Rice factor. At low signal levels the received signal level is dominated by the multipath component that has a Rayleigh distribution as the direct signal is completely blocked.

If we consider the co-polarised (RHCP/RHCP & LHCP/LHCP) subchannels plotted in Figure 5.4 both the data and the models suggest a lognormal signal distribution at signal levels close to and above 0 dB which then changes significantly in shape into a Rayleigh distribution at lower signal levels with a signal power decrease of 10 dB per decade of probability. The co-polarised RHCP/RHCP subchannel of the Enhanced Statistical model shows very close agreement to the MIMOSA co-polarised RHCP/RHCP & LHCP/LHCP subchannels. The CDF of these co-polarised subchannels indicates that the Doppler shaping of the multipath components in the Enhanced Statistical model produces a more realistic distribution more similar to the real MIMOSA data than the Liolis-CTTC model, thus aiding validation of the Enhanced Statistical model.

The cross-polarised subchannels plotted from each of the models (RHCP/LHCP) both show close agreement to the RHCP/LHCP cross-polarised MIMOSA subchannel. The models also both show a bump in their RHCP/LHCP cross-polarised subchannel indicating a joint distribution as the rice factor decreases. For the Liolis-CTTC model this occurs over a signal level range of $\sim$-10 dB to $\sim$-30 dB and for the Enhanced Statistical model this occurs over a signal level range of $\sim$-10 dB to $\sim$-20 dB. This feature is not observed in either of the MIMOSA cross-polarised subchannels. The MIMOSA cross-polarised subchannels show a smooth Rayleigh distribution, although the RHCP/LHCP subchannel has less signal power than the LHCP/RHCP subchannel.

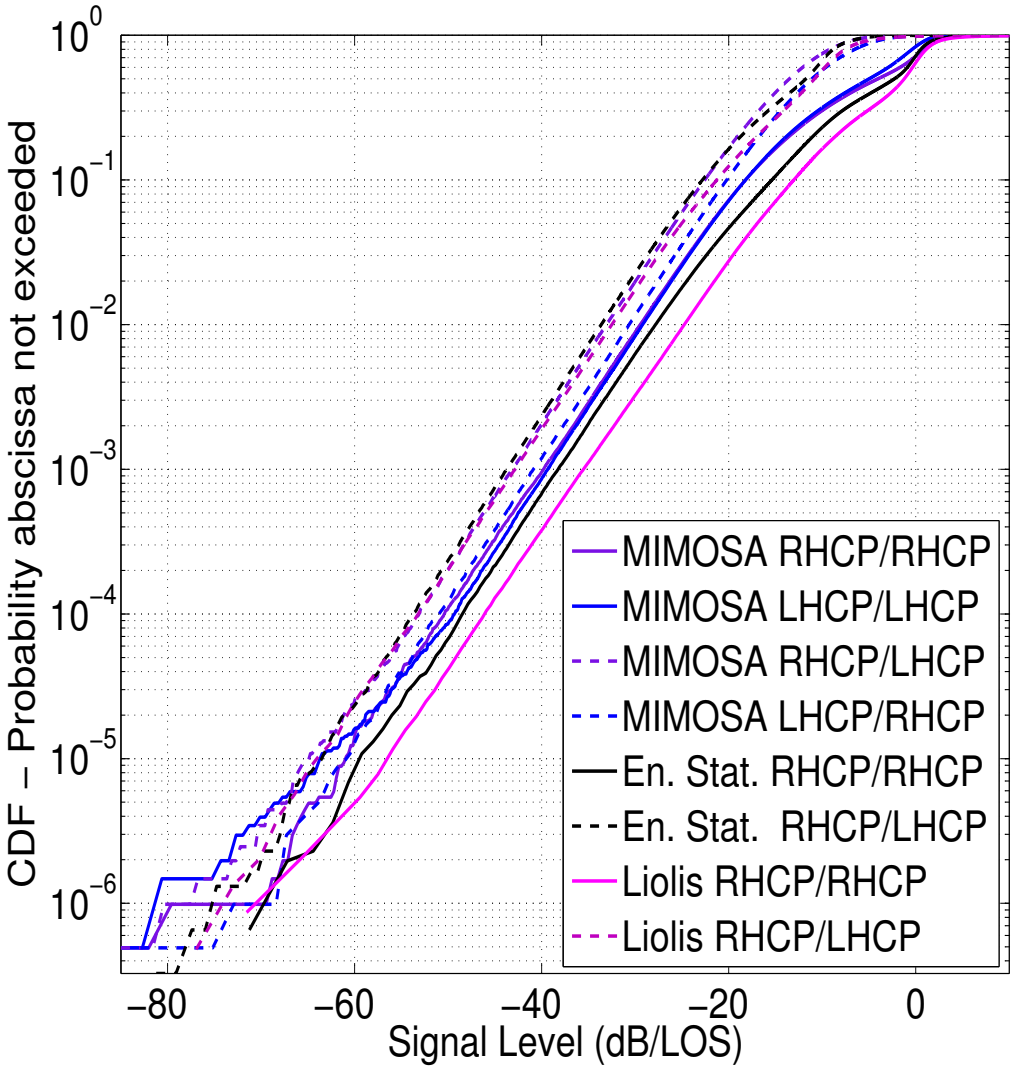


FIGURE 5.4: Comparison of the Cumulative Distribution Function for the Enhanced Statistical model with Jakes Doppler Shaping, the Liolis-CTTC model and the MIMOSA data for the urban user environment.

### 5.3.3 Average Fade Duration

Figure 5.5 shows the average fade duration (AFD) of the normalised received signal for an urban user environment for the original Liolis-CTTC model, the Enhanced Statistical dual polarised LMS model and the MIMOSA measurement data, all three timeseries sampled with a sampling frequency equivalent to that of the MIMOSA timeseries, i.e. 4232Hz.

As with the CDF plot in the previous section, only one of each of the cross- and co-polarisation subchannels are plotted for the analysis of the timeseries of the two models due to the high similarity between them however, all four of the MIMOSA data subchannels are plotted due to the variation between them.

The Liolis-CCTC model shows shorter fade durations compared to the Enhanced Statistical model and the MIMOSA data in both the co-polarised and cross-polarised subchannels. The MIMOSA data shows the longest fade durations of the three plots. Figure 5.5 shows that at a signal level of 0 dB the MIMOSA co-polarisation plots have an average fade duration of 2.5 wavelengths ($\lambda$'s) for RHCP/RHCP and 2.8 wavelengths for LHCP/LHCP, the Enhanced Statistical model has an average fade duration of 0.6 wavelengths for RHCP/RHCP and the Liolis-CTTC model has an average fade duration of 0.1 wavelengths for RHCP/RHCP. At a signal level of -10 dB the AFD in wavelength for the MIMOSA data, Enhanced model and Liolis-CTTC model are 0.7 $\lambda$'s (LCHP/RHCP) & 1.1 $\lambda$'s (RHCP/LHCP), 0.2 $\lambda$'s, 0.08 $\lambda$'s respectively.

For the cross-polarisation subchannels, the Enhanced Statistical models' AFD plot gives average fade duration of similar magnitude to that of the MIMOSA data.

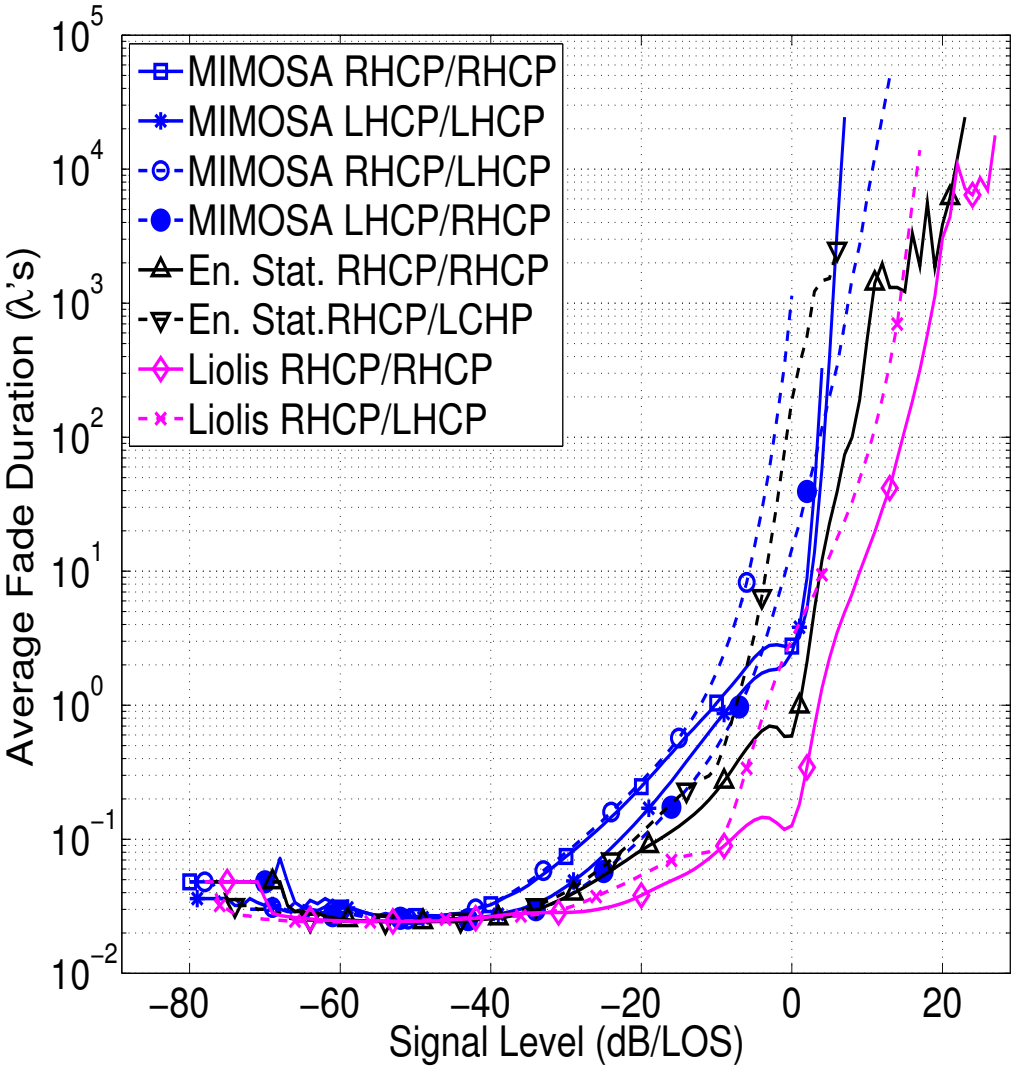


FIGURE 5.5: Comparison of the Average Fade Duration in wavelengths for the Enhanced Statistical model with Jakes Doppler Shaping, the Liolis-CTTC model and the MIMOSA data for the urban user environment, all three timeseries sampled with a sampling frequency equivalent to that of the MIMOSA timeseries, i.e. 4232Hz.

### 5.3.4 Level Crossing Rate

Figure 5.6 shows the Level Crossing Rate (LCR) in crossings per wavelength for the Enhanced Statistical model, the Liolis-CTTC model and the MIMOSA data, all three timeseries sampled with a sampling frequency equivalent to that of the MIMOSA data, i.e. 4232 Hz.

The MIMOSA data shows a significant change in the shape of the LCR curve of the good and bad states for one of the co-polarisation plots (RHCP/RHCP) but not in the other three plots (LHCP/LHCP, RHCP/LHCP, LHCP/RHCP). The Liolis-CTTC plot shows the lowest amount of crossings per wavelength, with a greater variation from the Enhanced model and the MIMOSA data at higher signal levels higher than -10 dB. This shows that the Enhanced Statistical model's level crossing rates are a better representation of the measurement data. For lower signal levels, lower than -30 dB, the two models give a good agreement to the measurement data for the cross-polarisation subchannels.

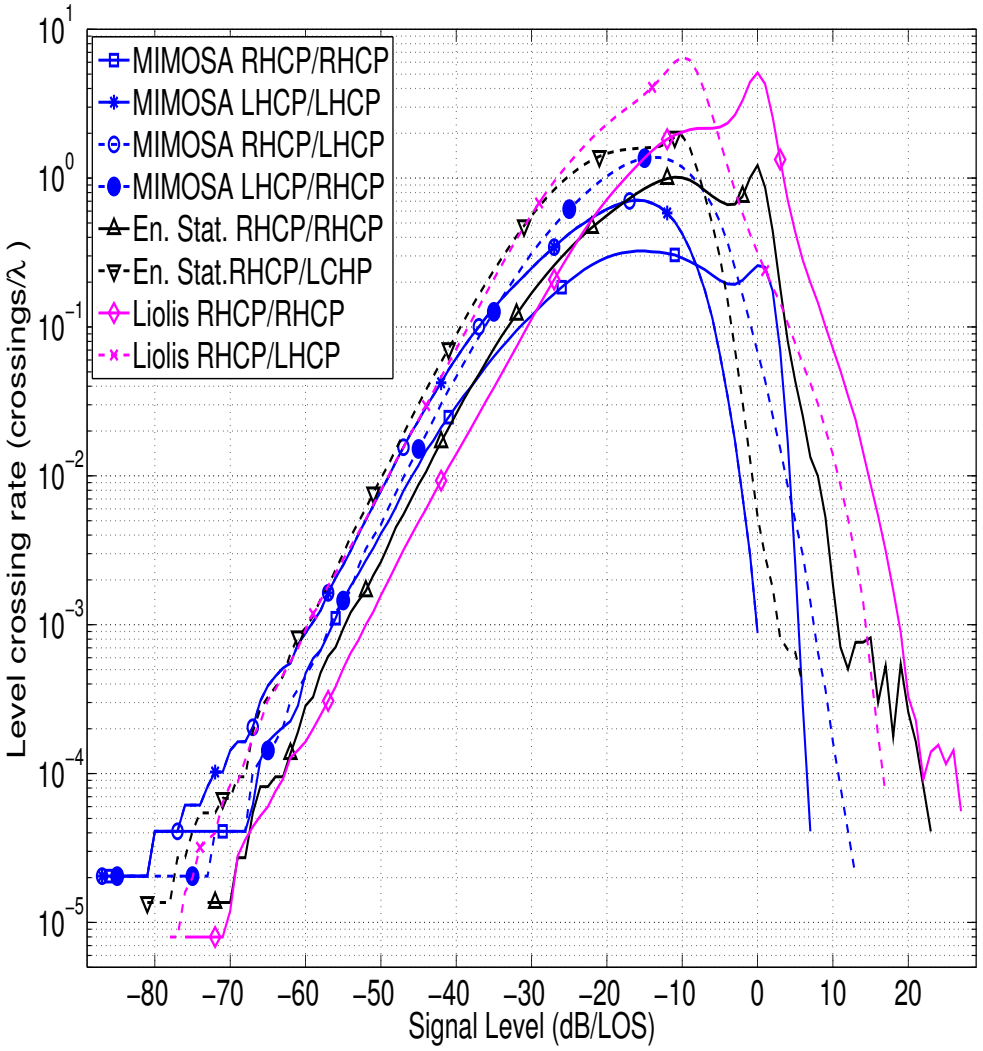


FIGURE 5.6: Comparison of the Level Crossing Rate in crossings per wavelength for the Enhanced Statistical model with Jakes Doppler Shaping, the Liolis-CTTC model and the MIMOSA data for the urban user environment, all three timeseries sampled with a sampling frequency equivalent to that of the MIMOSA data, i.e. 4232Hz.

### 5.3.5 Eigenvalue Analysis

Figure 5.7 plots the CDFs of the eigenvalues obtained from eigen decomposition of bad states in an urban user environment with antenna XPD of 10 dB for the MMOSA measurement data, the Liolis-CTTC model timeseries and the Enhanced Statistical model timeseries. The separation of the two eigenvalue distribution curves $\lambda_1$ and $\lambda_2$ in the Liolis-CTTC plot show that this model gives a better gain from polarisation multiplexing than is achieved in the measurement data from MIMOSA. The Enhanced Statistical model gives a greater separation between the two eigenvalue distribution curves $\lambda_1$ and $\lambda_2$ , therefore, demonstrating more accurately the achievable gains through polarisation multiplexing.

Figure 5.8 plots the CDFs of the eigenvalues obtained from eigen decomposition of good states in an urban user environment with antenna XPD of 10 dB for the MMOSA measurement data, the Liolis-CTTC model timeseries and the Enhanced Statistical model timeseries. The plot shows good agreement between the two models and the measurement data with all three showing rich polarisation multiplexing within the good states. Both the Liolis-CTTC model and the Enhanced Statistical model give a good approximation of the polarisation multiplexing achievable in the real measurement of the dual polarised LMS channel.

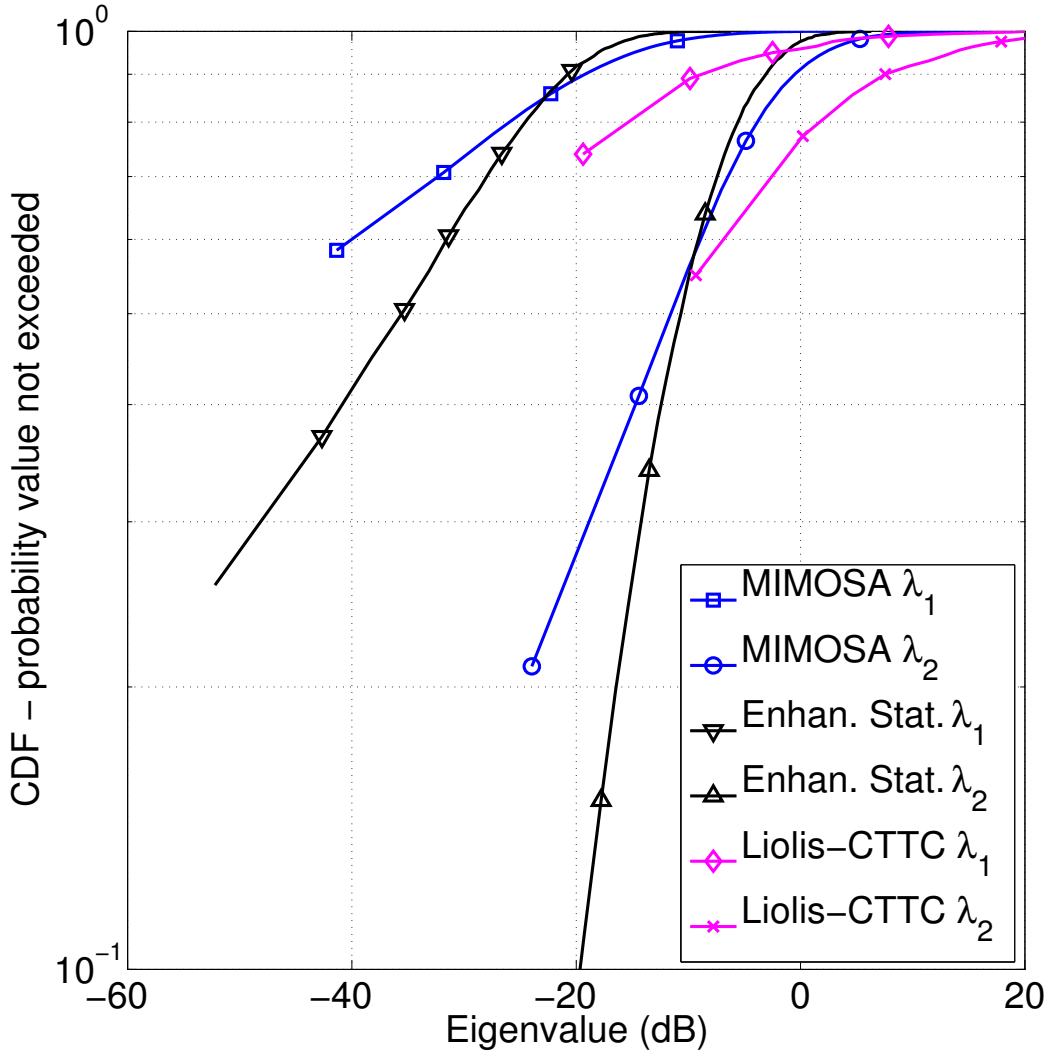


FIGURE 5.7: Eigenvalue analysis: comparison of the eigenvalues obtained during bad states for the Enhanced Statistical model with Jakes Doppler Shaping, the Liolis-CTTC model and the MIMOSA data for the urban user environment.

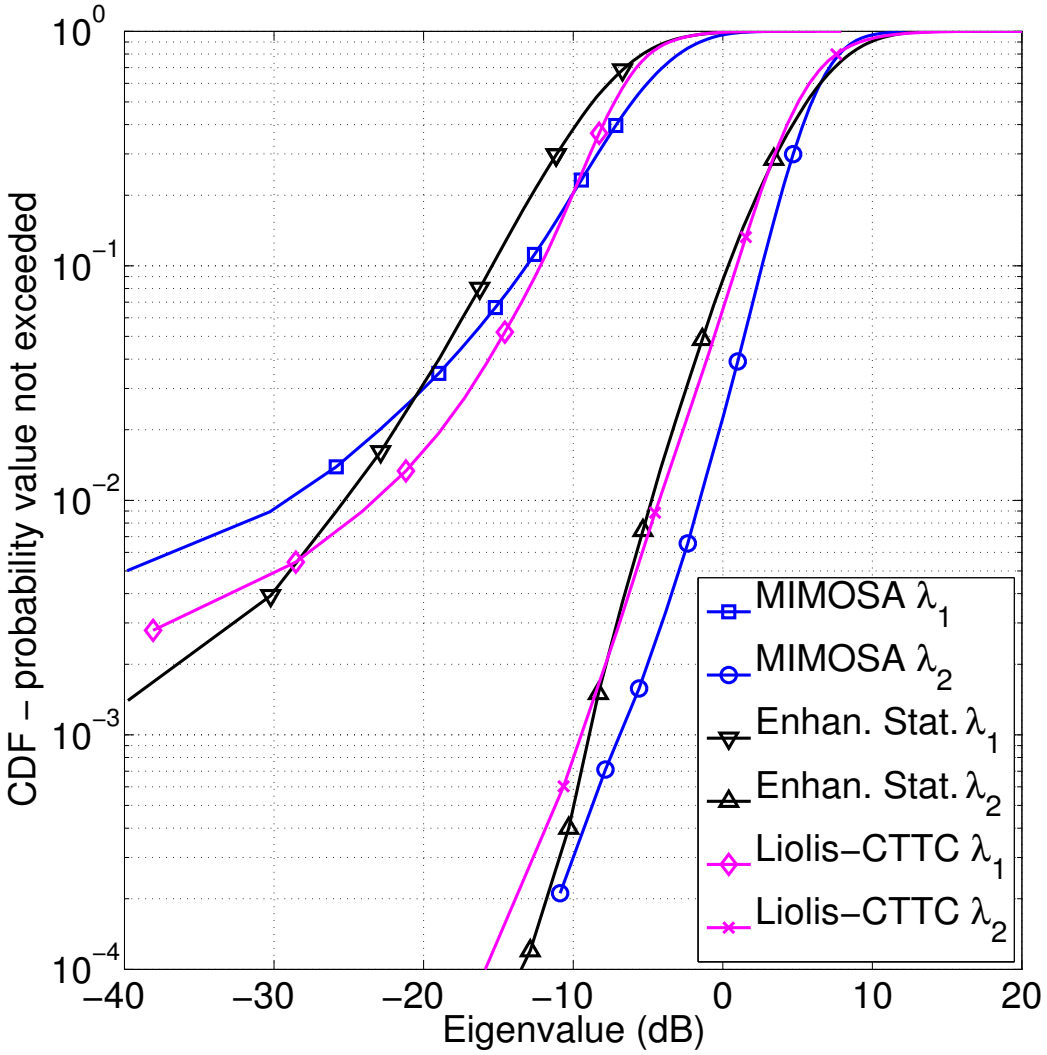


FIGURE 5.8: EigenAnalysis: comparison of the eigenvalues obtained during good states for the Enhanced Statistical model with Jakes Doppler Shaping, the Liolis-CTTC model and the MIMOSA data for the urban user environment.

## 5.4 Spectrum Analysis

Figure 5.9 shows the spectrum of the Enhanced Statistical model simulated using both the Jakes spectrum and a flat spectrum within the frequency range -100 Hz to 100 Hz, the Liolis-CTTC model and the MIMOSA data for an urban user environment for a mobile travelling at 50 km/h. Comparison of the spectra of the two statistical models show that the inclusion of Doppler effects in the Enhanced Statistical model offers a more realistic description of the spectral properties of the channel.

The Jakes Spectrum gives a good approximation of the MIMOSA spectrum as the general shapes of the spectra are similar. If we consider the spectrum of the MIMOSA channel, it appears to more closely resemble a uniform spectrum. It may be possible to further increase the similarity between the frequency response of the Enhanced Statistical Model and the MIMOSA channel measurements by creating and applying a more complex Doppler shape after careful analysis of the frequency response during particular states in the real data from the MIMOSA campaign.

Further work could include careful analysis of the MIMOSA data to identify the Doppler shapes associated with good and bad states and particular events along the recorded journey in order to better inform the modelling process of the Enhanced Statistical model.

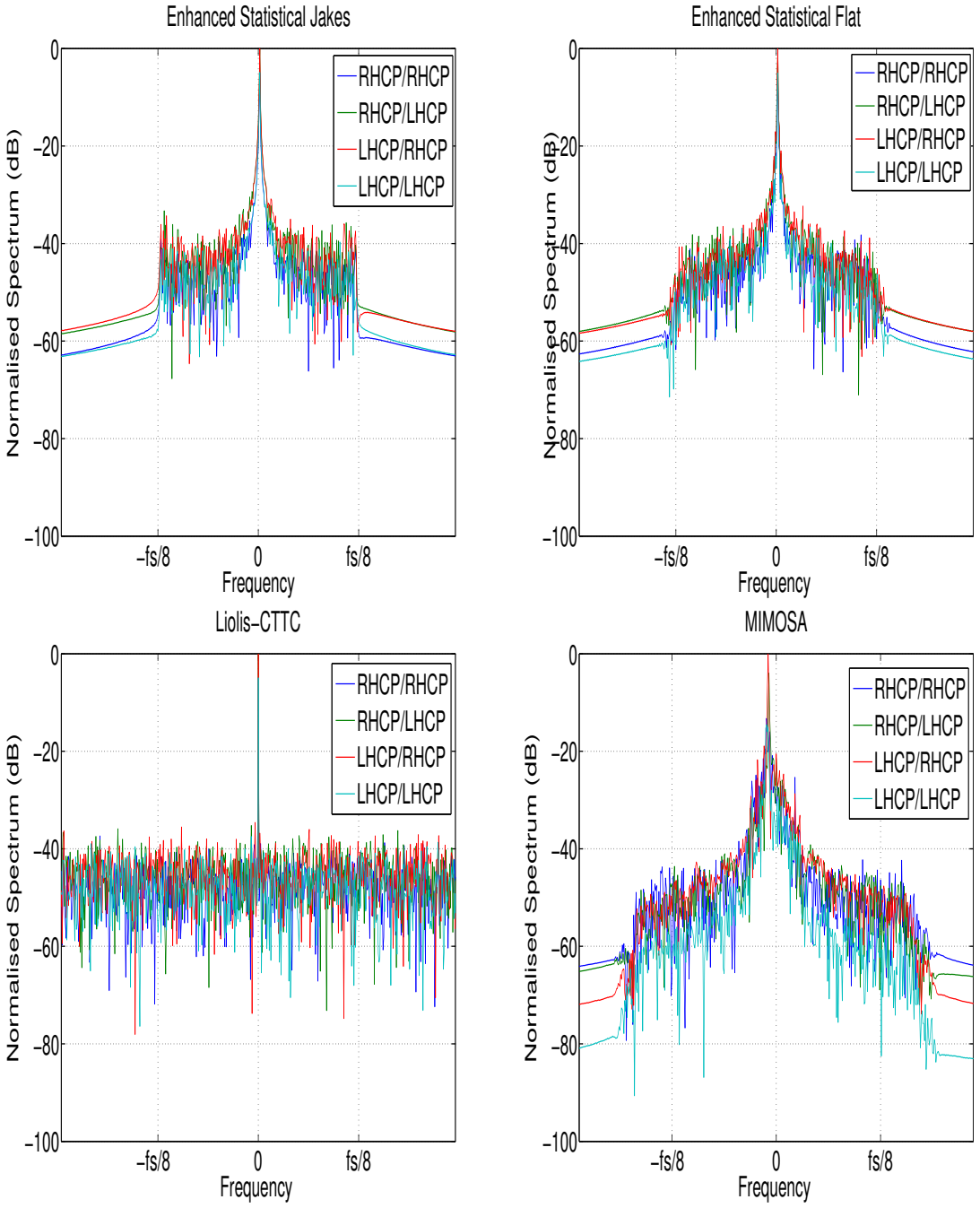


FIGURE 5.9: Four plots showing the frequency response in the urban user environment of the Enhanced Statistical Model with Jakes Doppler spreading (top left), the Enhanced Statistical with Flat Doppler spreading (top right). Also included for comparison are the frequency response of the Liolis-CTTC model (bottom left) and the MIMOSA data (bottom right). The four MIMO subchannels are plotted, i.e the two co-polarisation subchannels RHCP/RHCP & LHCP/LHCP and the two cross-polarisation subchannels RHCP/LHCP & LHCP/RHCP. The Doppler frequency is plotted as a function of the sampling frequency ($f_s$) which has different inherent values for the channel model simulators and real-life measurement data.

## 5.5 Analysis of the Suburban Environment

### 5.5.1 Timeseries

Figure 5.10 shows the timeseries for a mobile travelling within the suburban user environment at 50 km/h generated with the Enhanced Statistical Model and the MIMOSA data with antenna XPD of 10 dB.

The timeseries for the suburban user environment shows that in comparison to the timeseries for urban environment plotted in Figure 5.1, the Enhanced Statistical model's received signal spend more time at higher signal magnitudes. Also the timeseries in general does not go to as low signal magnitudes in either good or bad states, this is to be expected as the suburban user environment is not as challenging as the urban environment for the propagating mobile satellite signal. In comparison to the MIMOSA data timeseries, the Enhanced models's timeseries also show that in general it has higher signal magnitudes throughout the plotted journey and has less variation in both the co-polarisation subchannels and the cross-polarisation subchannels.

The smooth state transitions are observable, particularly with the state change that occurs in the Enhanced Statistical models timeseries just after a travelled distance of 600 m that is comparable in slope to the state change in the MIMOSA data timeseries just after a travelled distance of 1600 m.

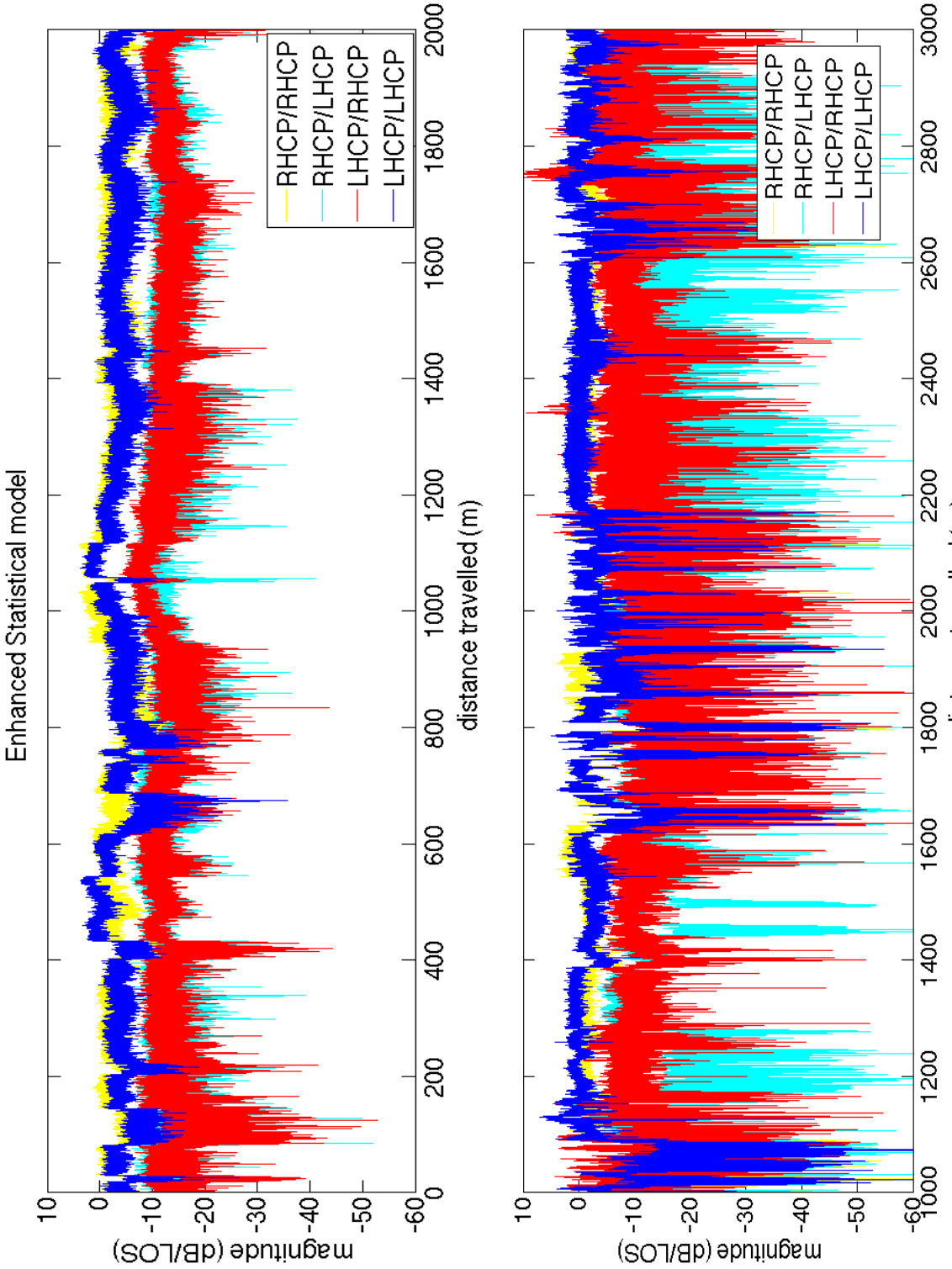


FIGURE 5.10: Timeseries for a mobile travelling within the suburban user environment at 50 km/h generated with the the Enhanced Statistical Model with Jakes Spectrum Doppler (top) and the MIMOSA data (bottom). The XPD in the Enhanced Statistical model is set to 10dB. The signal level is normalised with respect to the LOS power level in dB.

### 5.5.2 CDF

Figure 5.11 shows the CDF of the normalised received signal for the suburban user environment for the Enhanced Statistical LMS model with Jakes Doppler Spectrum and the MIMOSA measurement all for a mobile travelling at 50 km/h. The model was used to create a simulated for a journey of 100 km, the particular journey on which the MIMOSA measurement data was recorded was ∼7.1 km in the highly dense urban environment.

The four subchannels of the MIMOSA suburban data are plotted in Figure 5.11, although in comparison to the MIMOSA urban data CDF plot, there isn't as much variation between the subchannels as was observed in Figure 5.4 plot. The co-polarised MIMOSA subchannels (RHCP/RHCP & LHCP/LHCP) in the CDF plot have an almost identical distributions. The cross-polarised MIMOSA subchannels (RHCP/LHCP & LHCP/RHCP) show very similar distributions with slightly different multipath power at the very low signal levels. The MIMOSA data CDF plot shows a clear joint distribution as also observed in the urban environment, with a clear Rayleigh distribution in all subchannels at low signal levels. This feature isn't observed in the Enhanced Statistical model's CDF plot, there is a smooth distribution as the signal distribution changes from high signal level 'good' states to low signal level 'bad' states. The low signal levels in the Enhanced Statistical model also show a Rayleigh distribution at low signal levels, however the signal power is greater than that observed in the MIMOSA data CDF plot.

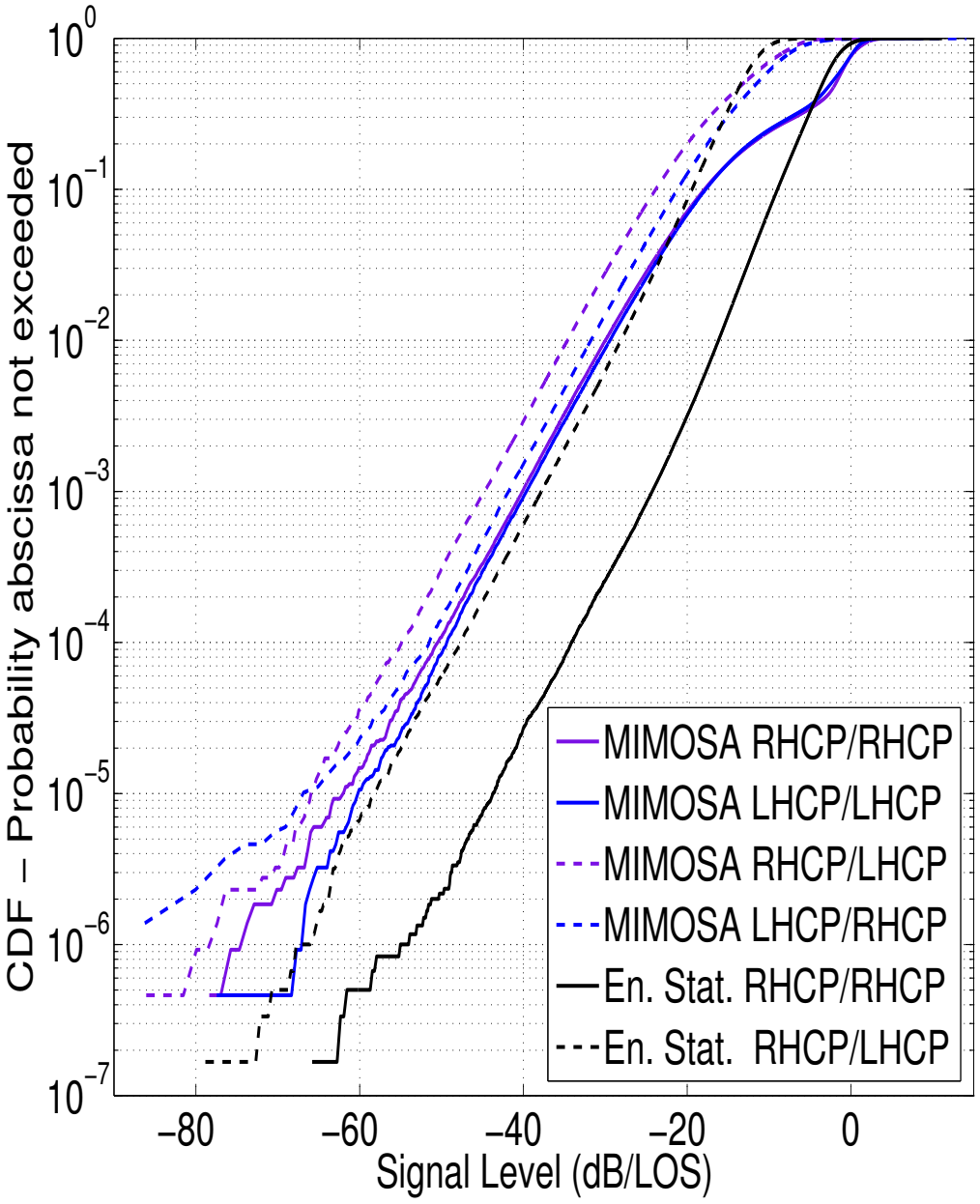


FIGURE 5.11: Comparison of the Cumulative Distribution Function for the Enhanced Statistical model with Jakes Doppler Shaping and the MIMOSA data for the suburban user environment.

### 5.5.3 AFD and LCR

Figure 5.12 shows the average fade duration in wavelengths of the normalised received signal for a suburban user environment for the Enhanced Statistical dual polarised LMS model and the MIMOSA measurement data, sampled at a frequency of 815 Hz and 4232 Hz respectively. Figure 5.13 shows the level crossing rate per wavelength of the normalised received signal for a suburban user environment for the Enhanced Statistical dual polarised LMS model and the MIMOSA measurement data, sampled at a frequency of 815 Hz and 4232 Hz respectively. These plots reflect the observations made from the comparison between the timeseries of the model and the data. The AFD plot shows that for signal magnitudes of approximately -5 dB to -20 dB, the Enhanced Statistical model's co-polarisation RHCP/RHCP subchannel has shorter average fade durations than the MIMOSA data. The LCR plot shows for the Enhanced Statistical model has fewer level crossings per wavelength, especially for the co-polarisation subchannel at signal magnitudes less than -10 dB and cross-polarisation subchannel at signal magnitudes of less than -20 dB.

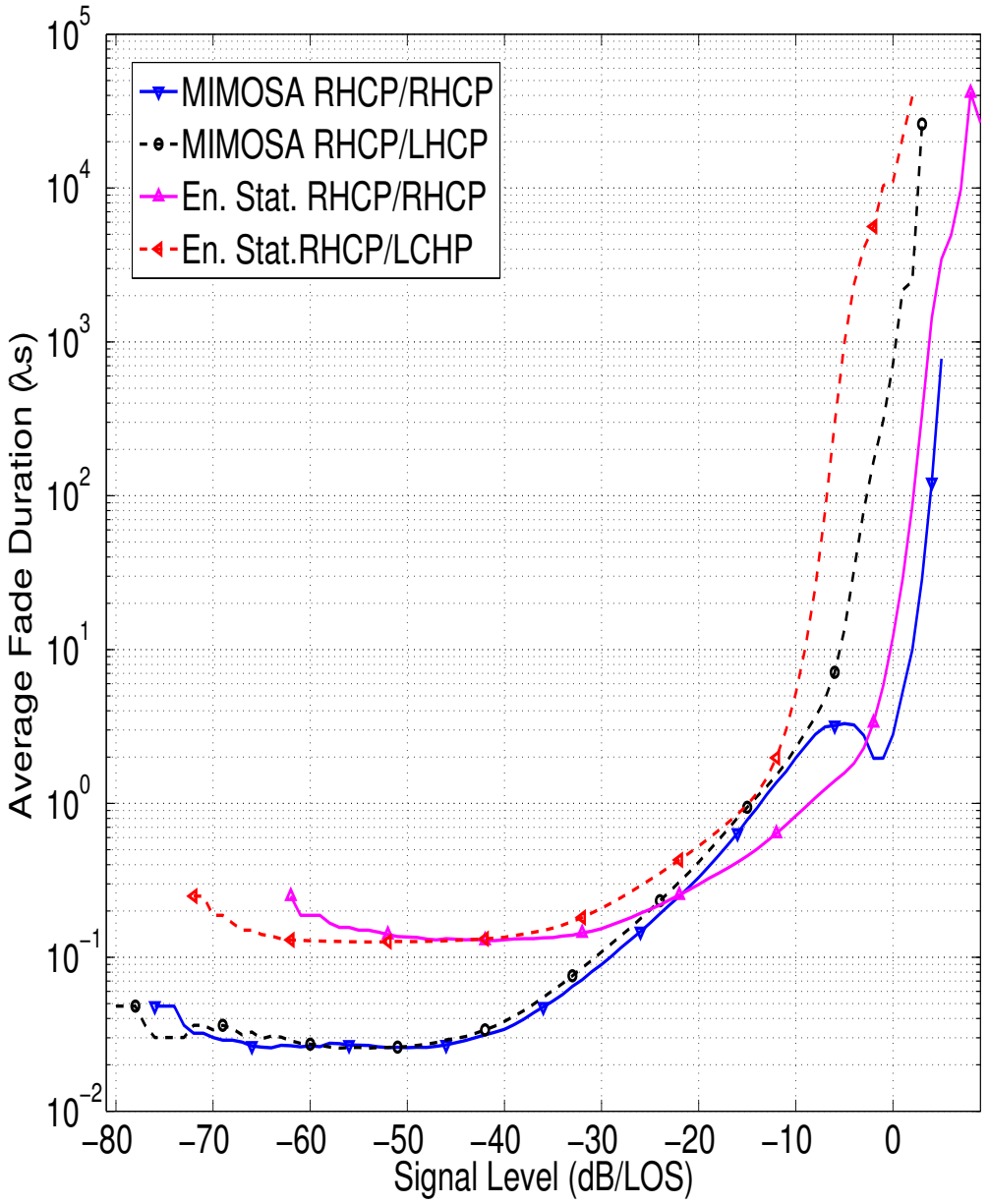


FIGURE 5.12: Comparison of the Average Fade Duration in wavelengths for the suburban user environment for a mobile travelling at 50 km/h for Enhanced Statistical model with Jakes Doppler Shaping sampled at a frequency of 815 Hz and the MIMOSA data sampled at a frequency of 4232 Hz.

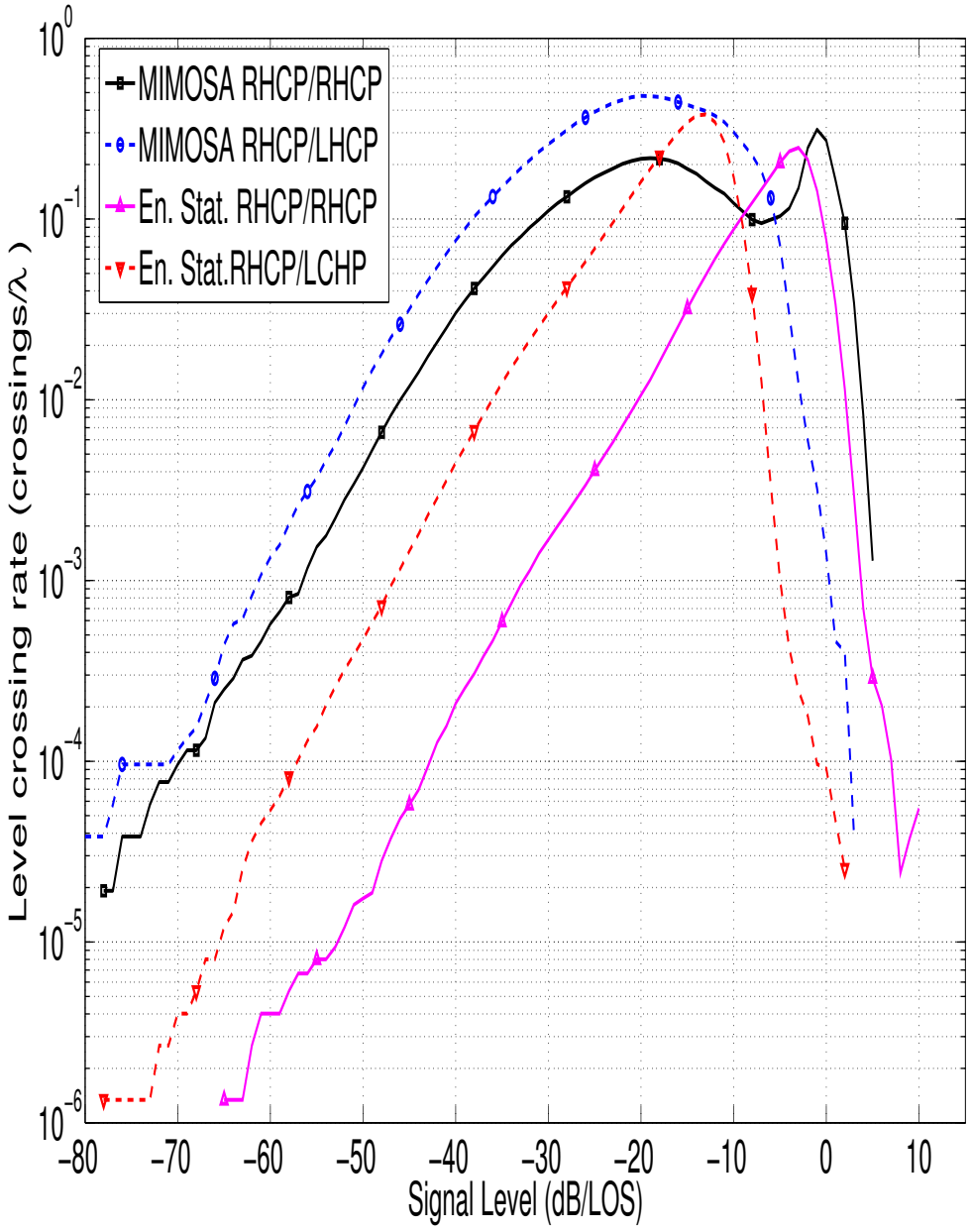


FIGURE 5.13: Comparison of the Level Crossing Rate per wavelength for the sub-urban user environment for a mobile travelling at 50 km/h for Enhanced Statistical model with Jakes Doppler Shaping sampled at a frequency of 815 Hz and the MIMOSA data sampled at a frequency of 4232 Hz.

### 5.5.4 Spectrum

Figure 5.14 shows the spectrum of the Enhanced Statistical LMS model and the MIMOSA data for a mobile unit travelling at 50 km/h in a suburban user environment. The Enhanced model for the suburban environment uses the Jakes spectrum for modelling the Doppler effects in the small-scale fading component. The power profile of the spectrum and the frequency range of the spectrum are very similar to that observed in the MIMOSA spectrum. The shape of the spectrum is a U-shape as defined by the Jakes spectrum and it had a peak at 0 dB due to the Doppler shift of the large-scale fading component defined by the velocity of the mobile and the angle of arrival of the direct signal, which was set to 90°. The expected U-shape of the spectrum is clear at -100 Hz although at 100 Hz the spectrum appears more flat than U-shaped. The shape of the MIMOSA spectrum mirrors this with a U-shape apparent at -100 Hz and a more flat appear at -100 Hz. The peak in power due to the Doppler shift of the large-scale fading component occurs at around -20 Hz, indicating a different angle of arrival of the direct signal than that of the model.

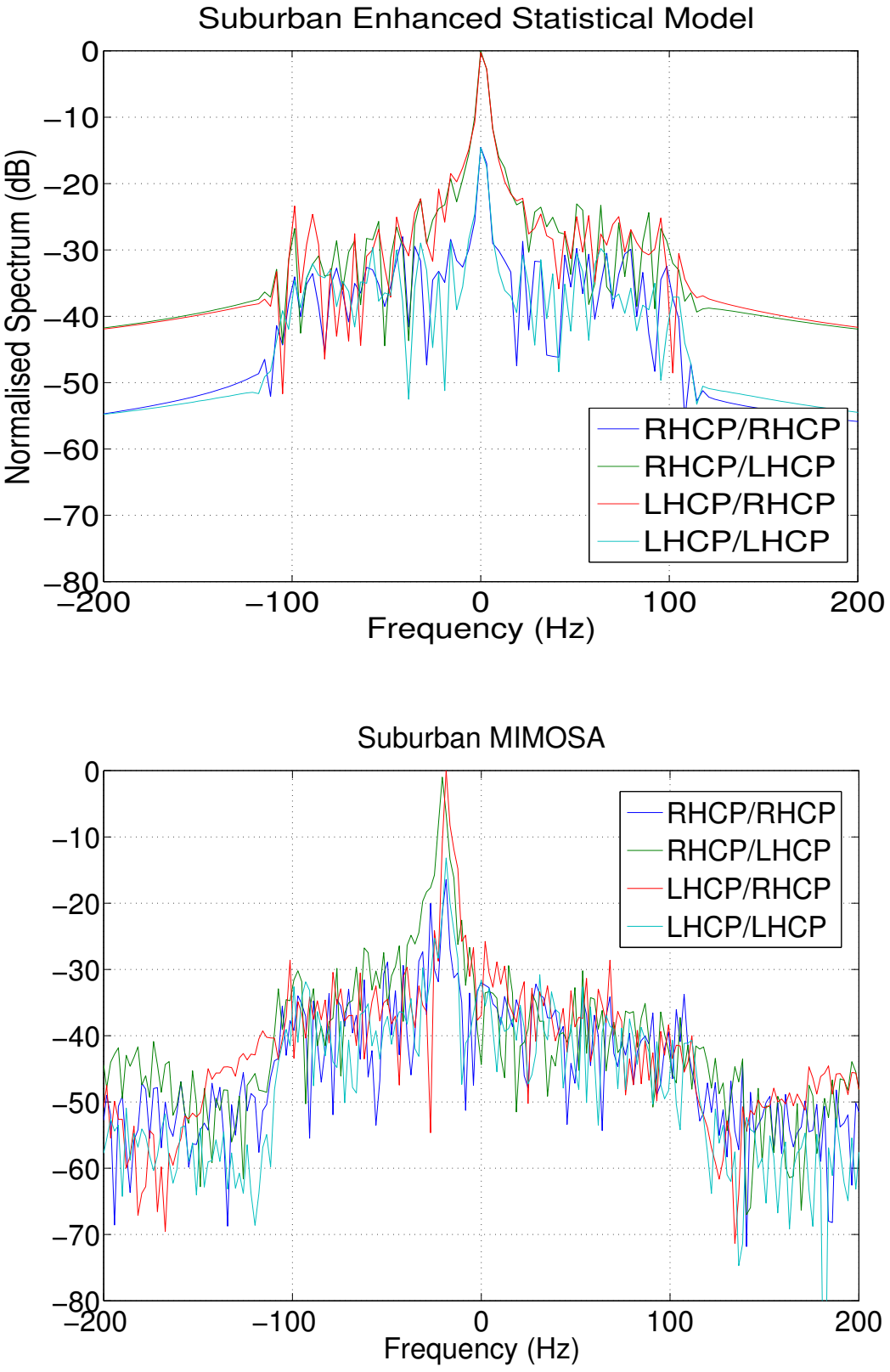


FIGURE 5.14: Comparison of the spectra obtained for the timeseries of the Enhanced Statistical model with Jakes Doppler shaping (top) and the MIMOSA measurement data (bottom) for the suburban user environment.

## 5.6 Analysis of the Open Rural Environment

### 5.6.1 Timeseries

Figure 5.15 shows the timeseries for a mobile travelling within the open user environment at 50 km/h generated with the Enhanced Statistical Model and the MIMOSA data with antenna XPD of 10 dB. This user environment shows the most noticeable differences between the model and the data. The Enhanced model shows little variation in the signal magnitude with the succession of good and bad states having very similar signal magnitudes. The signal magnitude of the co-polarisation subchannels rarely falls below -5 dB in the plotted simulated journey of 7 km and the signal magnitude of the cross-polarisation subchannels rarely falling below -15 dB. The co-polarisation subchannels in the MIMOSA data timeseries also tends to have an average value above -5dB but in some bad states there are short periods of time during which the signal level falls to values down to -50 dB. The cross-polarisation subchannel in the MIMOSA data timeseries shows a greater level of signal magnitude variation in the cross-polarisation subchannels than the Enhanced model timeseries demonstrates, as has been the case with the MIMOSA timeseries for all user environments.

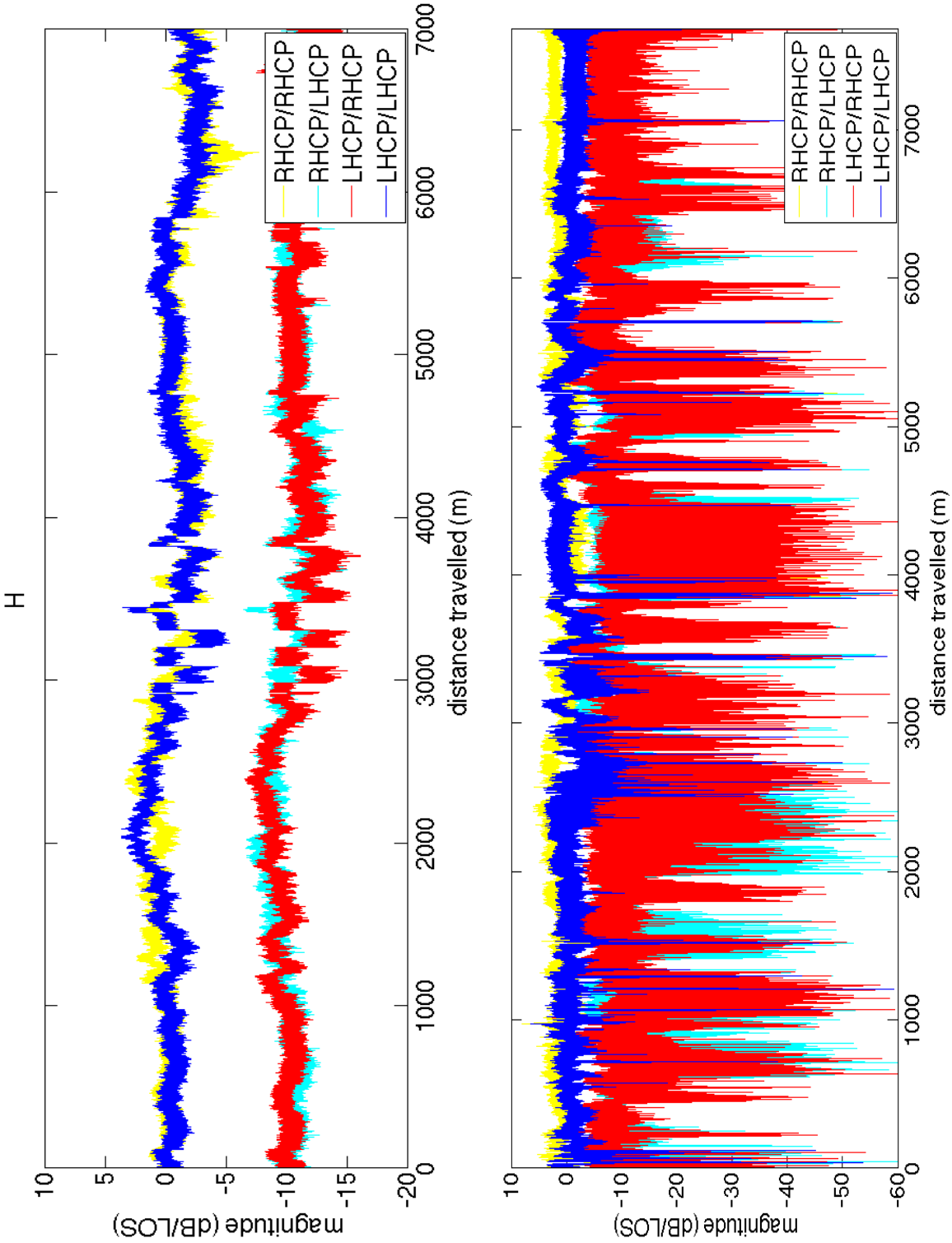


FIGURE 5.15: Timeseries for a mobile travelling within the open user environment at 50 km/h generated with the the Enhanced Statistical Model with Jakes Spectrum Doppler (top) and the MIMOSA data (bottom). The XPD in the Enhanced Statistical model is set to 10dB. The signal level is normalised with respect to the LOS power level in dB.

### 5.6.2 CDF

Figure 5.16 plots the CDF graph for the open rural user environment for the Enhanced Statistical model and the MIMOSA data. The four subchannels of the MIMOSA data are plotted, although in comparison to the urban and the suburban data there isn't as much variation between the subchannels as was observed in Figures 5.4 & 5.11, this is not surprising considering the signal propagating in an open rural environment encounters less scatterers and less interactions with objects which attenuate the signal and thus create greater variations between the different subchannels in the signal.

If we consider the co-polarised subchannels in the MIMOSA data (RHCP/ RHCP & LCHP/LHCP) and the Enhanced Statistical model (RHCP/ RHCP), at high signal levels $\sim$0 dB show a similar distribution reflecting high Rice factors as the received signal will undoubtedly incorporate significant LOS components and light shadowing components of the direct signal. At lower signal levels, i.e. $\sim$-10 dB, the model and the MIMOSA data distributions diverge significantly with the Enhanced Statistical model's CDF displaying a Rician distribution and the MIMOSA data CDF displaying a Rayleigh distribution. This indicates that the modelling of the Loo Parameters within the open rural environment in the Enhanced Statistical model are resulting in too high a Rice factor in comparison to the scenario reflected in the real-life data. The cross-polarised subchannels in the MIMOSA data (RHCP/LHCP & LCHP/RHCP) show a Rayleigh distribution whereas the Enhanced Statistical model's cross-polarised subchannel (RHCP/LHCP) shows a Rician distribution. To resolve this issue and make the model more accurate, further work that could be achieved outside the scope of this thesis would be to carefully analyse individual states within the MIMOSA data for open rural environments and extract information about the signal mean and standard deviation and multipath power in order to inform a more realistic Loo parameters generation process.

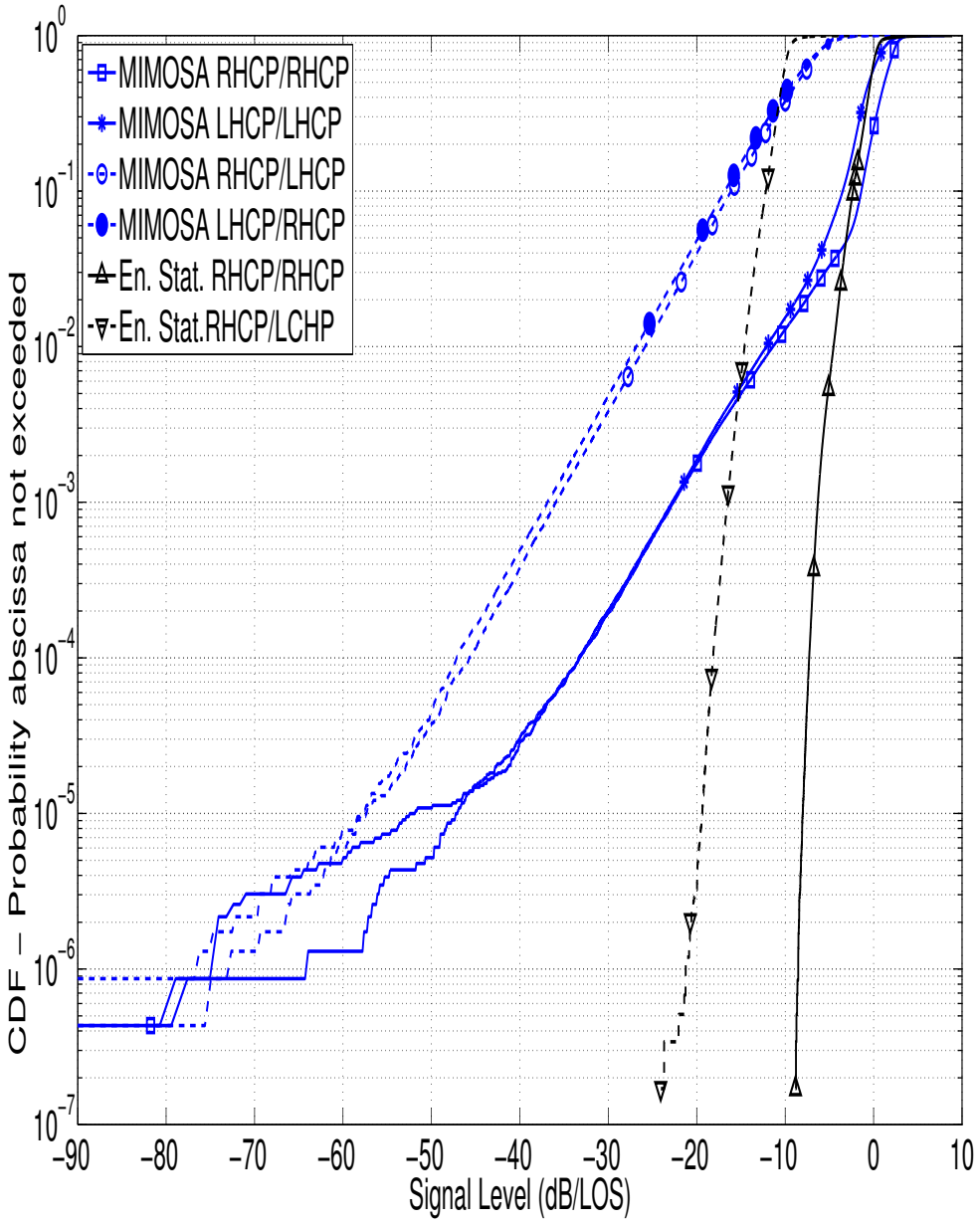


FIGURE 5.16: Comparison of the Cumulative Distribution Function for the open rural user environment for the Enhanced Statistical model with Jakes Doppler Shaping and the MIMOSA data.

### 5.6.3 ACF and LCR

Figure 5.17 and 5.18 show the Average Fade Duration in wavelengths and the Level Crossing Rate per wavelength respectively for the open user environment for a mobile travelling at 50 km/h for Enhanced Statistical model and the MIMOSA data. Figure 5.17 shows good agreement between the Enhanced model and the MIMOSA data for the average fade duration for the cross-polarisation subchannels above signal magnitudes of ∼10 dB and co-polarisation subchannels above signal magnitudes of ∼ dB. The Enhanced model doesn't extend to signal magnitudes below this for the open user environment.

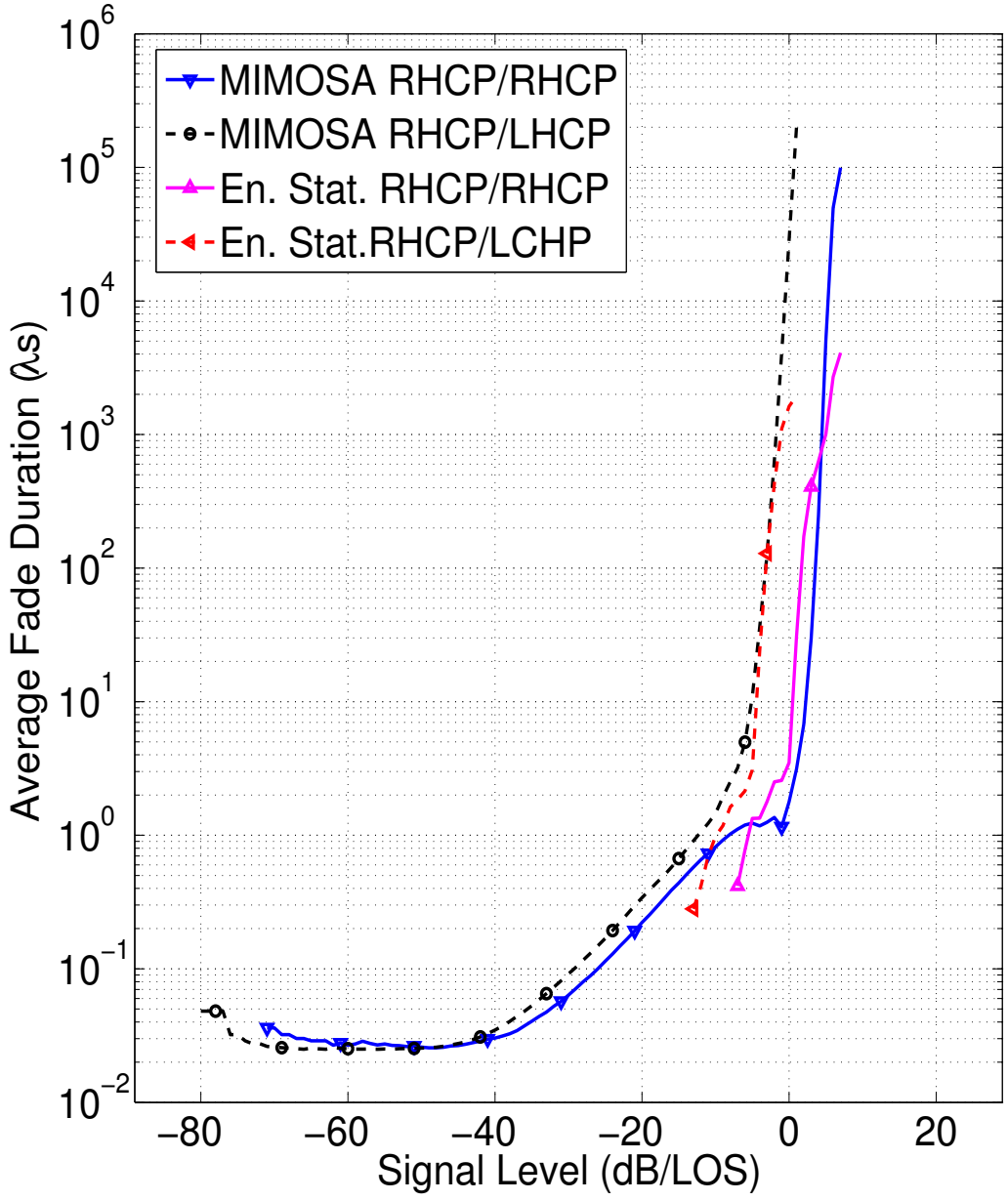


FIGURE 5.17: Comparison of the Average Fade Duration in wavelengths for the open user environment for a mobile travelling at 50 km/h for Enhanced Statistical model with Jakes Doppler Shaping sampled at a frequency of 815 Hz and the MIMOSA data sampled at a frequency of 4232 Hz.

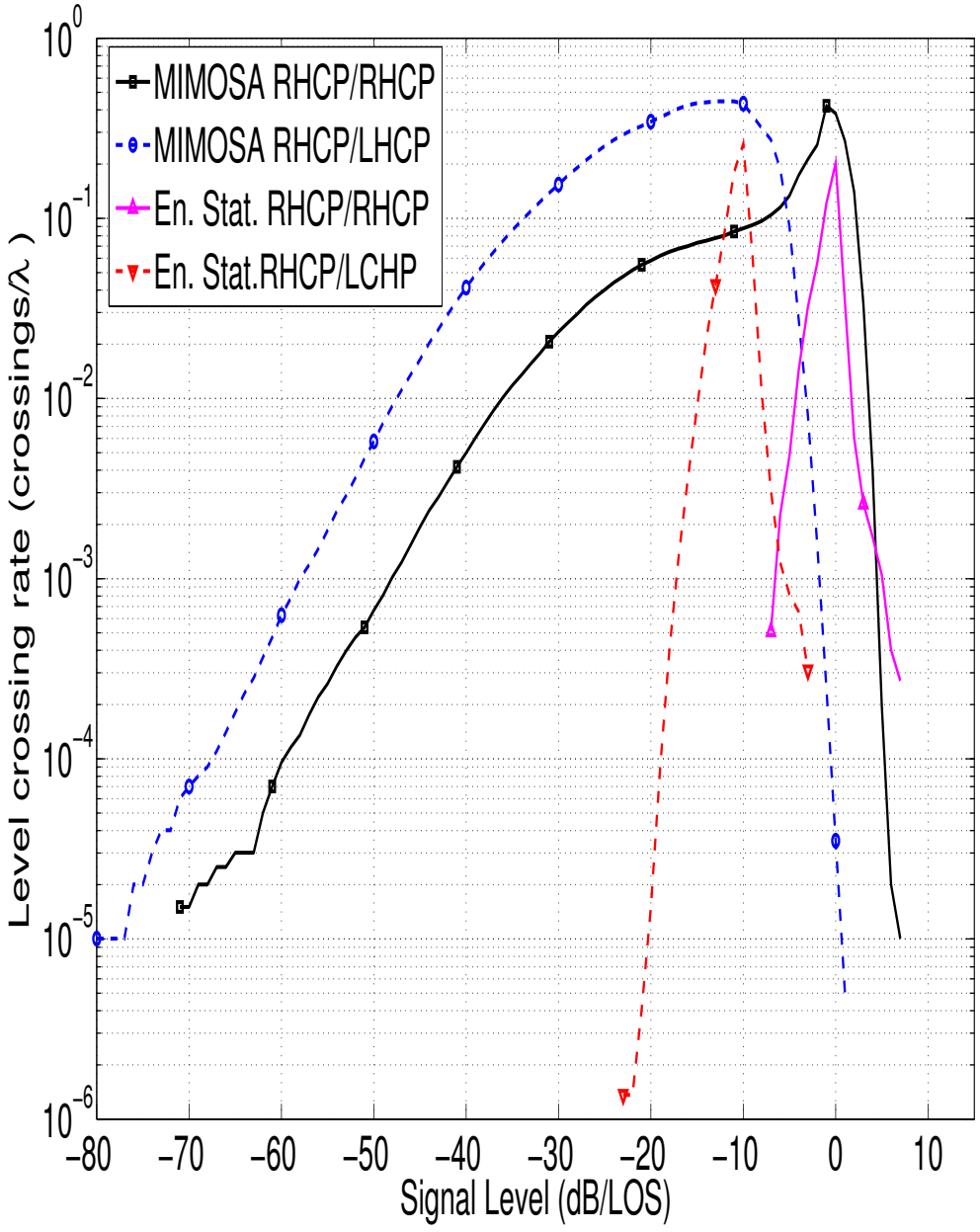


FIGURE 5.18: Comparison of the Level Crossing Rate per wavelength for the open user environment for a mobile travelling at 50 km/h for Enhanced Statistical model with Jakes Doppler Shaping sampled at a frequency of 815 Hz and the MIMOSA data sampled at a frequency of 4232 Hz.

### 5.6.4 Spectrum

Figure 5.19 shows the spectrum of the Enhanced Statistical model and the MIMOSA data for a mobile unit travelling at 50 km/h in an open user environment.

The Enhanced model for the open environment uses the Jakes spectrum for modelling the Doppler effects in the small-scale fading component, although the shape of the spectrum is quite flat at the maximum and minimum Doppler frequencies of -100 and 100 Hz. The MIMOSA spectrum Is similar in shape to that of the Enhanced Statistical model, a peak at -10 Hz indicates an angle of arrival of the direct signal just greater than 90˚and the general shape of the spectrum appear flat with rounded edges at the maximum and minimum Doppler frequencies. The spectrum's maximum Doppler frequency is lower than expected at approximately 90 Hz indicating the spectrum might be better modelled using an Asymmetric Jakes spectrum.

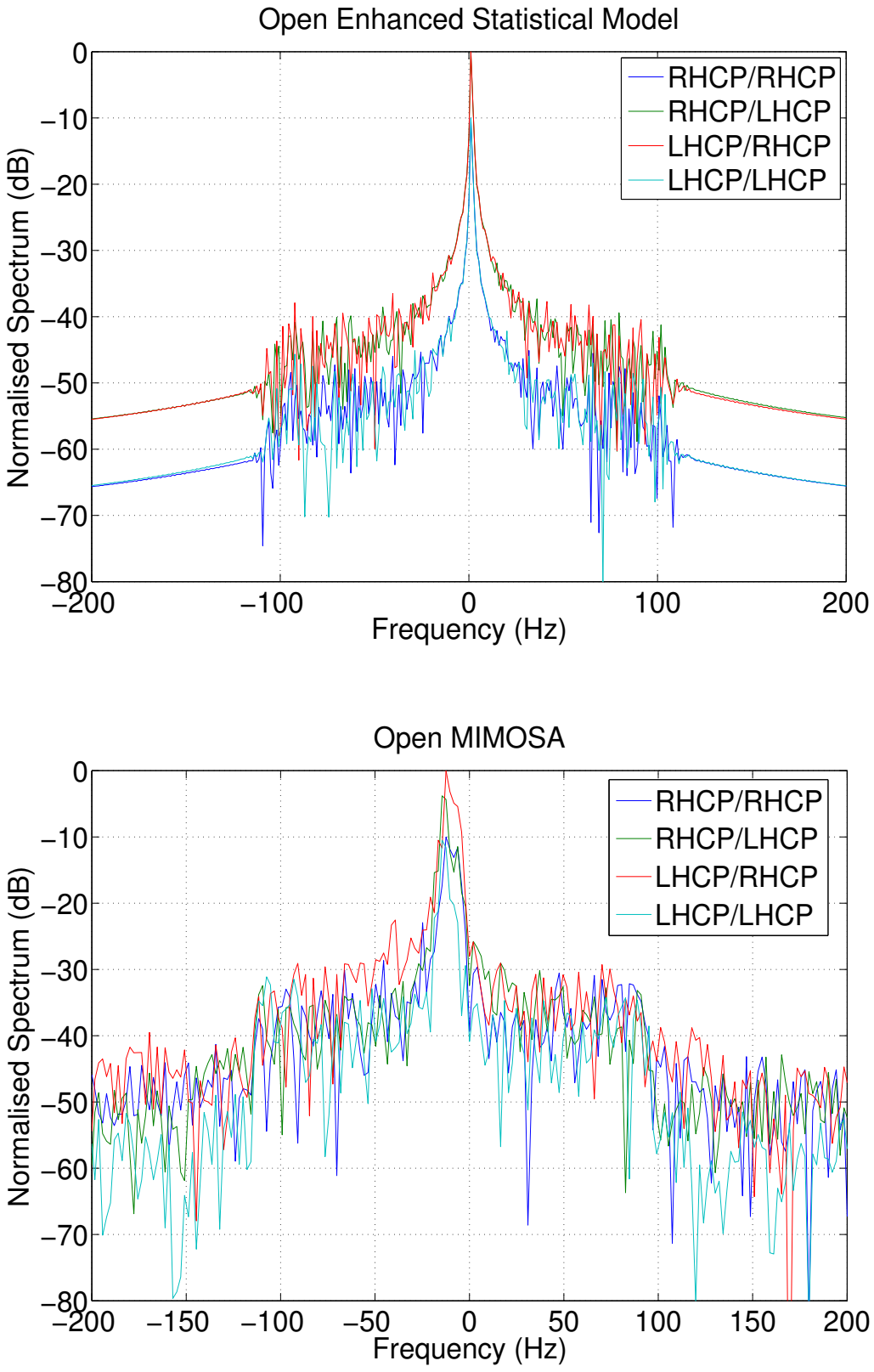


FIGURE 5.19: Comparison of the spectra obtained for the timeseries of the Enhanced Statistical model with Jakes Doppler shaping (top) and the MIMOSA measurement data (bottom) for the open user environment.

## 5.7 Summary

The enhancements made to the statistical model prove to have improved upon the Liolis-CTTC model and this is evident in a number of features in the timeseries output of the models in comparison with the MIMOSA measurement data. The timeseries of the enhanced model better resembles the measurement data, the signal magnitude within the good and bad states has a wider range of values and the variation of the signal magnitude is greater within states. The smooth state transition process is more realistic and mirrors the state transitions in the measurement data. The CDF, AFD and LCR show a better agreement between the enhanced model and the measurement data. The eigenvalue distribution of the enhanced model and the measurement data show a better agreement for the bad states providing better insight into the polarisation multiplexing gain associated with the channel. The spectrum of the enhanced model shows a great improvement over the baseline Liolis-CTTC model and the MIMOSA measurement data show similarities to the Jakes and Uniform spectra for the urban user environment.

The suburban environment and the open environment show less similarity to the MIMOSA measurement data, more variation needs to be introduced to these user environments to resemble the amount of variation of the measurement data, particularly in the cross-polarisation subchannels. These user environments do not have the same range of signal magnitudes as the measurement data.

# Chapter 6

# Conclusions and Further Work

## 6.1 Review of Research Objectives

The aim of the research for this thesis was to build upon the current state-of-the-art research into multiple-input multiple-output (MIMO) implementation in the land mobile satellite channel and create a statistical model for simulating transmissions in this channel. The importance of creating an accurate channel model is that it can then be used for further analysis of the to potential gains achievable through the implementation of polarisation multiplexing in the mobile satellite context. The impact of dual polarisation in the land mobile satellite can be assessed through simulation and other aspects of the communications system can be designed and tested.

Land mobile satellite (LMS) channel models for S-band frequencies were reviewed and it was identified that a gap existed in which dual polarised channel models were underdeveloped, in addition channel measurements of the dual polarised LMS channel did not yet exist. It is worth noting that since starting this research, channel measurements from the MIMO Channel for Mobile Satellite Systems (MIMOSA) measurement campaign have become available and thus informed development of more sophisticated models such as the Quasi Deterministic Radio channel Generator (QuaDRiGa).

The primary aim of this research was to produce a statistical model for the dual polarised (DP) MIMO LMS channel that built on previously published statistical models whichconsolidated validated single-input single-output (SISO) LMS channel model aspects with MIMO aspects achieved through polarisation. The main objective of the new channel model was to include improvements and enhancements to baseline statistical models to create a more accurate timeseries better resembling transmissions obtained in real-life scenarios. This objective was achieved and a realistic and easy-to-use channel model and simulation tool was created. The enhancements incorporated to create the Enhanced Statistical DP MIMO LMS channel model included improvements to the modelling process to increase the reliability of the model output and the addition of modelling procedures to simulate physical effects on the signal create a more realistic model output.

## 6.2 Review of Methodology

Literature on the research of LMS channel models revealed the lack of a detailed channel model for dual polarised MIMO. In order to create a more detailed model, validated statistical approaches of modelling wireless communication channels, dual polarised MIMO channels and SISO LMS channels were considered and aspects were applied to the dual polarised MIMO LMS channel.

The Liolis-CTTC model was used as a baseline model and enhancements were applied to achieve the Enhanced Statistical dual polarised LMS model. This output of this new model was analysed through the generation of a timeseries of a simulated signal transmitted from a satellite and received by a land-based mobile user in various environments. Statistical analysis of the model output was also conducted through the analysis of the cumulative distribution function (CDF), the average fade duration (AFD), the level crossing rate (LCR), eigenvalue analysis and frequency spectrum analysis. The model output was compared to the output of the Liolis-CTTC model as an initial test and also compared to the more complex and detailed Quasi Deterministic Radio channel Generator (QuaDRiGa) model output. The results of this

comparison with these two leading models confirmed the validity of the model. In addition to comparison with other models of the dual polarised MIMO LMS channel, the output of the new model was compared with data from real channel measurements from the MIMO Channel for Mobile Satellite Systems (MIMOSA) campaign. This output of the model in the urban environment showed a better agreement with the data in comparison to the original baseline statistical model. The main aspects of the validation process were the successful modelling of the Doppler shifts in the multipath component of the received signal and the improved statistical probability distribution of the received signal envelope observed in the CDF plots.

## 6.3 Achievements and Limitations

To create the 2x2 channel matrix for the dual polarised MIMO LMS channel the direct signal component and the multipath signal component are generated separated and added together. A step-by-step guide to this process is given in Chapter 3. The new model included enhancements in the process of generating the separate signal components and also in the method of creating the changes in signal power level that occur due to the effects of the user environment.

Modelling of the direct signal component is improved by a number of enhancements. Firstly, the method of implementing the temporal correlation in the direct signal component is addressed; the direct signal was generated with a sample rate equivalent to one sample per metre, filtered with a single coefficient IIR filter and interpolated to match the sample rate of the multipath component. This new method was found to eliminate the observable high frequency components introduced to the direct signal by low-pass filtering alone based on a sampling period of 0.0012 s and the new method also produces a correlated direct signal series with the required exponential autocorrelation function (ACF).

Secondly, the method of implementing the spatial correlation in the four subchannels of the 2x2 channel matrix in the direct signal component and the multipath signal component is implemented through the Weichselberger method. In this method a

covariance matrix is created based on the eigen-decomposition of the covariance matrices of the receiver and the transmitter. This is an improvement over the Kronecker method of obtaining the covariance matrix for the channel by calculating the Kronecker product of the covariance matrices of the receiver and the transmitter as the Weichselberger does not assume the channel is separable.

The modelling of the states that define the quality of the signal power and reception was modified to incorporate a semi-Markov chain model. This process determines the duration of individual states from lognormal distributions. The process of transitions between different state types was adapted to include a state transition slope in which the signal magnitude is gradually changed from the mean signal magnitude of one state to the mean signal magnitude of the next state. The signal magnitude for each sample is determined by imposing a Loo parameter triplet onto each sample in a randomly generated series, the Loo parameter triplet doesn't change within a state and describes the direct signal mean and standard deviation and multipath power. The slope between states was achieved by determining the value of the slope from a mean slope of 5 dB, calculating the number of samples required to achieve the desired slope and generating samples of successively changing Loo parameter triplets to insert into the Loo parameter triplet series.

The main contribution of this work was in achieving an accurate method for the modelling of the Doppler spreading in the multipath components of the signal. To accurately represent the effects of the movement of the mobile receiver unit, Doppler frequency shifts in the direct signal and the multipath signal were included in the channel model. A Doppler shift was applied to the direct signal component based on the velocity of the mobile, the angle of arrival of the signal and the satellite elevation angle and also to the multipath component. To model each of the theoretical multipath components experiencing a Doppler shift, a complex spectrum is designed and applied to the multipath component through autoregressive IIR filtering. A number of Doppler spectra where investigated including the Jakes Doppler spectrum which closely resembled the spectrum observed in the MIMOSA data.

A method of generating the timeseries output of the channel at a rate equivalent to the transmission rate in a typical S-band satellite communication system without increasing the simulation time by an unacceptable amount or distorting the characteristics of the timeseries was developed. This involved a multirate filtering technique comprised of a combination of polyphase and linear interpolation to interpolate the data to the require sample rate. This method provides an improved preservation of the second order statistics of the timeseries than obtained through linear interpolation alone and analysis showed the technique obtained good preservation of the implemented Doppler spectrum.

The limitations of the model and the adopted methodology include the lack of ability in the new statistical model to simulate specific environmental features or scenarios to analyse the effects of a particular event on the propagating signal. This is a drawback or limitation of the statistical modelling process that can only be overcome by considering a different type of model. However, alternative forms of channel model such as deterministic or ray-tracing algorithm models have other drawbacks associated with them such as high complexity and high computational load. The statistical model is useful for determining the general and long-term characteristics of the channel.

The model also relies on parameters and made available in literature from experimental data from various measurement campaigns of the SISO LMS channel. Thus this can lead to a lack of flexibility if parameters for a particular scenario have not been published. As is described in the next section on future areas of research leading from this project, it would be interesting to derive statistical parameters from the MIMOSA data to use as inputs to the channel model, this would result in a highly specialised dual polarised MIMO LMS channel model.

## 6.4 Further Work

The thesis has achieved the original aim of developing a statistical model for simulating the dual polarised MIMO LMS channel capable of producing realistic timeseries for the analysis of the channel. Although it is clear than this model works best for the

urban user environment; when the output is compared to real measurement data from the suburban and open user environments, the modelling of the statistical distribution of the dynamic range of the signal does not quite match that observed in the real data. It is observed in the CDF plots that the k-factor controlling the Rician distribution of the multipath signals are higher in the model than in the data for the suburban and open rural environments. The model produces Loo parameters that define the Rician distribution of the multipath components whereas the real data CDF plot suggests a Rayleigh distribution for the multipath components. It is reasonable that the real life data shows a greater amount of attenuation as it is subject to a much more complex system and thus is influenced by a wide range of factors and obstacles whereas the simulation is a more simple system, completely isolated and free from interference from other systems. It would be worthwhile to investigate in detail the properties of the received signal in the MIMOSA data to find the signal power magnitude & standard deviation and to also extract the multipath power. The analysis of the signal would be conducted for each individual state and thus provide information regarding the statistical distribution of the received signal. When the distribution of the direct signal magnitude, the direct signal standard deviation and multipath power were obtained, parameters could be derived for generating these distributions and thus Loo parameter triplets could be created based on the MIMOSA data specific to the dual polarised LMS channel.

Another aspect for future development is to improve the modelling of the state transition process to include a more realistic method of determining the slope of the signal magnitude during a transition. If we consider a scenario in which a user moves alongside a building that blocks the signal resulting in a bad state and a state transition occurs as the user moves causing the building to no longer blocks the signal resulting in a good state; the physics of diffraction affects the signal when it is incident on the edge of the building during the transition period. The closer the user is to the building the steeper the slope in signal magnitude will be during the state transition. Detailed knowledge of the physics of knife-edge diffraction and careful analysis of the state transitions in the MIMOSA data in various environments would help inform an improved state transition modelling process.

The enhancements made in this model, particularly the modelling of the Doppler effects and the Doppler shaping of the multipath signal components could be applied to other models of the dual polarised MIMO LMS channel, for example the King model [3].

# Appendix A

# Tables of Important Parameters

TABLE A.1: Parameters assumed for the simulation of the 2x2 dual polarised MIMO-LMS channel. [1]

| Parameter | Open Rural | Suburban | Urban |
|---|---|---|---|
| frequency | 2.2GHz | 2.2GHz | 2.2GHz |
| polarisation | RHCP/LHCP | RHCP/LHCP | RHCP/LHCP |
| mobile UT speed | 50km/h | 50km/h | 50km/h |
| satellite elevation | $40^o$ | $40^o$ | $40^o$ |
| $\text{XPD}_{env}$ | 15dB | 6dB | 5dB |
| $\text{XPD}_{ant}$ | 15dB | 15dB | 15dB |
| $\tilde{\rho_{tx}}$ | 0.4 | 0.5 | 0.5 |
| $\tilde{\rho_{rx}}$ | 0.5 | 0.5 | 0.5 |
| $\bar{\text{C}}$ (4x4 matrix) | 1.00 0.86 0.85 0.90<br>0.86 1.00 0.91 0.87<br>0.85 0.91 1.00 0.88<br>0.90 0.87 0.88 1.00 | 1.00 0.76 0.76 0.83<br>0.76 1.00 0.83 0.75<br>0.76 0.83 1.00 0.78<br>0.83 0.075 0.78 1.00 | 1.00 0.86 0.86 0.92<br>0.86 1.00 0.89 0.85<br>0.86 0.89 1.00 0.93<br>0.92 0.85 0.93 1.00 |

% Appendix B

TABLE A.2: Parameters for the probability transition matrix for the Markov chain and the mean and standard deviation of state duration for the semi-Markov chain in Nepers [2]. Good states are denoted with a 1, bad states are denoted with a 2.

| Markov state model | Open Rural | Suburban | Urban |
|---|---|---|---|
| $P_{40^o}=$ $\begin{matrix} p_{11}\ p_{12} \\ p_{12}\ p_{22} \end{matrix}$ | 0.9293 0.0707<br>0.0221 0.9779 | 0.9066 0.0934<br>0.124 0.876 | 0.9155 0.0845<br>0.0811 0.9189 |
| $P_{60^o}=$ $\begin{matrix} p_{11}\ p_{12} \\ p_{12}\ p_{22} \end{matrix}$ | 0.8968 0.1032<br>0.0351 0.9649 | 0.887 0.113<br>0.121 0.876 | 0.9043 00957<br>0.2 0.8 |
| $P_{80^o}=$ $\begin{matrix} p_{11}\ p_{12} \\ p_{12}\ p_{22} \end{matrix}$ | 0.8585 0.1415<br>0.0586 0.9414 | 0.7149 0.2851<br>0.2065 0.7935 | 0.9268 0.0732<br>0.2667 0.7333 |
| Semi-Markov state model | Open Rural | Suburban | Urban |
| lognormal pdf - $40^0$ | $\mu_1 = 27.2413\,\sigma_1 = 12.2861$<br>$\mu_2 = 37.4747\,\sigma_2 = 14.3632$ | $\mu_1 = 27.6756\,\sigma_1 = 10.5979$<br>$\mu_2 = 25.9979\ \sigma_2 = 9.7671$ | $\mu_1 = 26.5354\,\sigma_1 = 10.3825$<br>$\mu_2 = 30.9363\ \sigma_2 = 8.9651$ |
| lognormal pdf - $60^0$ | $\mu_1 = 26.2824\,\sigma_1 = 11.1701$<br>$\mu_2 = 28.341\,\sigma_2 = 14.2473$ | $\mu_1 = 28.0033\,\sigma_1 = 9.0263$<br>$\mu_2 = 25.4416\,\sigma_2 = 9.7479$ | $\mu_1 = 26.505\ \sigma_1 = 9.0036$<br>$\mu_2 = 25.3297\,\sigma_2 = 6.9144$ |
| lognormal pdf - $80^0$ | $\mu_1 = 26.1196\ \ \sigma_1 = 9.437$<br>$\mu_2 = 31.0366\,\sigma_2 = 11.1846$ | $\mu_1 = 21.7268\,\sigma_1 = 6.2475$<br>$\mu_2 = 23.033\ \sigma_2 = 7.2238$ | $\mu_1 = 29.7295\,\sigma_1 = 11.9671$<br>$\mu_2 = 22.1986\ \sigma_2 = 6.8103$ |

TABLE A.3: Statistical parameters for the generation of the Loo parameter triplet for three user environments. 1 represents a good state and 2 represents a bad state. [2]

| | | | $M_A$ | | $\Sigma_A$ | | | | | | MP | |
|---|---|---|---|---|---|---|---|---|---|---|---|---|
| Environment | $\theta$ | State | $\mu_1$ | $\sigma_1$ | $a_1$ | $a_2$ | $a_3$ | $b_1$ | $b_2$ | $b_3$ | $\mu_3$ | $\sigma_3$ |
| Open | 40 | 1 | 0.2237 | 0.2111 | 0.3246 | 0.1419 | 0.1262 | 0.1038 | -0.1173 | 0.0391 | -27.0377 | 2.2871 |
| | | 2 | -0.9379 | 1.0087 | -0.1131 | -0.845 | -0.1786 | -0.007 | -0.1288 | -0.0342 | -27.7143 | 3.0742 |
| | 60 | 1 | 0.1789 | 0.1913 | 1.4914 | -0.4858 | 0.1876 | -0.234 | 0.0934 | 0.0247 | -30.375 | 1.3601 |
| | | 2 | -0.3288 | 0.5366 | 1.4185 | 2.1654 | 0.818 | 0.2624 | 0.4413 | 0.1711 | -29.875 | 2.6802 |
| | 80 | 1 | 0.1867 | 0.1155 | -1.8497 | 1.0743 | 0.1344 | -2.1108 | 0.95 | -0.0149 | -27.8667 | 2.7131 |
| | | 2 | -0.3362 | 0.2001 | 0.1597 | -0.1319 | 0.2341 | -0.4706 | -0.3925 | -0.0057 | -27.3103 | 2.3007 |
| Sub | 40 | 1 | -2.3553 | 0.9962 | -0.0522 | 0.0569 | 1.7999 | -0.0046 | -0.0865 | 0.0401 | -23.3438 | 5.5742 |
| | | 2 | -6.3961 | 2.5466 | 0.0076 | -0.03422 | -0.3842 | 0.0335 | 0.729 | 4.006 | -24.6129 | 5.7889 |
| | 60 | 1 | -0.837 | 0.7241 | 0.0432 | 0.3944 | 1.2329 | 0.0132 | 0.0526 | 0.2896 | -19.9706 | 5.3228 |
| | | 2 | -3.9767 | 1.6285 | -0.0518 | -1.0835 | -1.6244 | -0.0594 | -0.5254 | -0.3656 | -19.5714 | 4.6671 |
| | 80 | 1 | 0.0141 | 0.6167 | -0.0246 | -0.0745 | 1.2703 | -0.07 | -0.2257 | 0.4183 | -13.8571 | 2.3237 |
| | | 2 | -2.4336 | 0.9094 | -0.1106 | -1.0836 | -1.6244 | -0.0594 | -0.5254 | -0.3656 | -19.5714 | 4.6671 |
| Urban | 40 | 1 | 0.0586 | 0.6404 | 0.2837 | 0.0905 | 0.4704 | -0.0638 | 0.0044 | 0.0473 | -15.7778 | 4.4096 |
| | | 2 | -9.7143 | 7.2610 | -0.0024 | -0.02411 | 0.5636 | 0.018 | 0.196 | 0.7561 | -16.8571 | 8.9336 |
| | 60 | 1 | -0.7979 | 0.5787 | 0.3606 | 0.9572 | 1.2722 | -0.4472 | -0.6539 | 0.0404 - | 14.75 | 5.6036 |
| | | 2 | -5.7548 | 4.5841 | -0.0803 | -1.7413 | -5.811 | 0.0052 | 0.1889 | 1.58 | -11.8182 | 5.0362 |
| | 80 | 1 | -0.132 | 0.3835 | 0.165 | 0.104 | 0.4799 | -0.02407 | -0.1212 | 0.053 | -15.6 | 4.7656 |
| | | 2 | -3.8113 | 4.1457 | -0.0672 | -0.7424 | 0.1643 | 0.025 | 0.4532 | 1.9276 | -12.2222 | 5.7397 |

TABLE A.4: 1/e autocorrelation distances obtained by [3] from experimental data

| Polarisation sub-channel | Open Rural (m) | Suburban (m) | Urban (m) |
|---|---|---|---|
| Co-polarised | 23 | 120 | 128 |
| Cross-polarised | 29 | 128 | 129 |

# Appendix B

# QuaDRiGa parameters

Below is an example of the parameters files contained within the QuaDRiGa software package. The parameters below are for the MIMOSA scenario for a satellite elevation range of 35 - 45° for both LOS and NLOS conditions.

% ==========

Config File for scenario "MIMOSA_35-45_NLOS"

Characterisation of the MIMO Channel for Mobile SAtellite Systems (Acronym: MIMOSA)

Satellite Elevation Range 35-45 deg, Non-Line of Sight

% ==========

%Channel model parameters

%See: MIMOSA TN6.1 Data Analysis Report RUSK, Appendix B

% ==========

%These parameters were extracted from a terrestrial measurement from a high building in downtown Berlin, Germany. It is till open, how well they describe a real satellite scenario. The amount of measurement data for those parameters was also quite small, limiting the statistics.

%Large Scale Parameter Statistics DS_mu = -7.1 % Delay Spread (DS) / [log10([s])] mu
DS_ sigma = 0.3 % Delay Spread (DS) / [log10([s])] sig3

%The K-Factor from TN6.1 is very unrealistic. The extraction was probably done with a different method. In order to make the results more realistic, we use the K-Factor from "BERLIN UMa NLOS". KF_mu = -6.3 % K-factor (KF) / [dB] mu
KF_sigma = 3.7 % K-factor (KF) / [dB] sig

AS_A_mu = 1.8 % Azimuth Angle of Arrival Spread (ASA) / [log10([degrees])] mu
AS_A_sigma = 0.2 % Azimuth Angle of Arrival Spread (ASA) / [log10([degrees])] sig
ES_A_mu = 1.3 % Elevation Angle of Arrival Spread (ESA) / [log10([degrees])] mu
ES_A_sigma = 0.2 % Elevation Angle of Arrival Spread (ESA) / [log10([degrees])] sig
SF_sigma = 4.3 % Shadow fading (SF) / [dB] sig
xpr_mu = 7.5 % XPR / [dB] mu
xpr_sigma = 2.6 % XPR / [dB] sig

% Correlation Distances
DS_lambda = 12 % DS correlation distance / [m]
KF_lambda = 3 % KF correlation distance / [m]
AS_A_lambda = 11.5 % ASA correlation distance / [m]
ES_A_lambda = 1.5 % ESA correlation distance / [m]
SF_lambda = 23 % SF correlation distance / [m]

% Cross correlations
ds_kf = -0.52 % DS vs KF
asA_ds = 0.54 % ASA vs DS
esA_ds = -0.01 % ESA vs DS
ds_sf = 0.61 % DS vs SF

asA_kf = -0.21 % ASA vs KF

esA_kf = -0.03 % ESA vs KF

sf_kf = -0.51 % SF vs KF

esA_asA = 0.05 % ESA vs ASA

asA_sf = 0.04 % ASA vs SF

esA_sf = -0.09 % ESA vs SF

% ==========

% Transmitter parameters These are mostly irrelevant due to the large distance between satellite and Earth.]]

% ==========

% The azimuth of departure spread is estimated by utilizing the GEO orbit distance (35,786 km) and % assuming a maximum area from which scattering can occur of 1 km. Additionally, one has to account % for the earth radius of 6,371 km. The average elevation angle is assumed to be 40 deg. % % Formula:

% AS_D_mu = log10( atan( 1/( 35786 + 50/90*6371 )))

% AS_D_sigma = log10( atan( 1.25/( 35786 + 50/90*6371 ))) + AS_D_mu

% PerClusterAS_D = atan( 0.025/( 35786 + 50/90*6371 ))

% % The elevation of departure is further scaled by the tilt of the earth surface.

% % Formula:

% ES_D_mu = log10( 40/90 * atan( 1/( 35786 + 50/90*6371 )))

% ES_D_sigma = log10( 40/90 * atan( 1.25/( 35786 + 50/90*6371 ))) + AS_D_mu

% PerClusterES_D = atan( 40/90 * 0.025/( 35786 + 50/90*6371 ))

AS_D_mu = -4.59 % Azimuth Angle of Departure Spread (ASA) / [log10([degrees])] mu

AS_D_sigma = 0.1 % Azimuth Angle of Departure Spread (ASD) / [log10([degrees])] sig

AS_D_lambda = 1000 % ASD correlation distance / [m] - almost constant

PerClusterAS_D = 0.00000064 % Cluster ASD / [deg] - 25 m diameter as seen from

GEO

ES_D_mu = -4.95 % Elevation Angle of Departure Spread (ESD) / [log10([degrees])]
mu
ES_D_sigma = 0.1 % Elevation Angle of Departure Spread (ESD) / [log10([degrees])]
sig
ES_D_lambda = 1000 % ESD correlation distance / [m] - almost constant
PerClusterES_D = 0.00000028 % Cluster ESD / [deg] - 25 m diameter as seen from
GEO

% Cross correlations % We assume all parameters at the satellite to be independent from the receiver due to the large % distance.

asD_ds = 0 % ASD vs DS
asD_sf = 0 % ASD vs SF
asD_asA = 0 % ASD vs ASA
asD_kf = 0 % ASD vs KF
esD_sf = 0 % ESD vs SF
esD_kf = 0 % ESD vs KF
esD_ds = 0 % ESD vs DS
esD_asD = 0 % ESD vs ASD
esD_asA = 0 % ESD vs ASA
esD_esA = 0 % ESD vs ESA
esA_asD = 0 % ESA vs ASD

% ==========
% Additional Parameters
% These are not covered by MIMOSA but have to be provided by other sources.
% We used the parameters from "WINNER_UMa_C2_NLOS" here.

% ==========

NumClusters = 20 % Number of clusters LOS scatter radius = 0.1 % Distance to the LOS scatterers [m] LNS ksi = 3 % Per cluster shadowing std / [dB] r_DS = 2.3 % Delay scaling parameter rTau

PerClusterAS_A = 15 % Cluster ASA / [deg] PerClusterES_A = 7 % Cluster ESA / [deg]

% ==========
% Path Loss Model % It is assumed that there is a constant path-loss offset. % ==========

% This still has to be verified.

PL_model = constant PL_A = 110
% ==========

% Config File for scenario "MIMOSA_35-45_LOS" % Characterisation of the MIMO Channel for Mobile SAtellite Systems (Acronym: MIMOSA) % Satellite Elevation Range 35-45 deg, Line of Sight %

% ==========

% Channel model parameters % See: MIMOSA TN6.1 Data Analysis Report RUSK, Appendix B

% ==========

% % These parameters were extracted from a terrestrial measurement from a high building in downtown % Berlin, Germany. It is till open, how well they describe a real satellite scenario. % The amount of measurement data for those parameters was also quite small, limiting the statistics.

% Large Scale Parameter Statistics

DS_mu = -7.3 % Delay Spread (DS) / [log10([s])] mu DS_sigma = 0.3 % Delay Spread (DS) / [log10([s])] sig3

KF_mu = 12.2 % K-factor (KF) / [dB] mu KF_sigma = 6.2 % K-factor (KF) / [dB] sig

AS_A_mu = 1.6 % Azimuth Angle of Arrival Spread (ASA) / [log10([degrees])] mu AS_A_sigma = 0.2 % Azimuth Angle of Arrival Spread (ASA) / [log10([degrees])] sig ES_A_mu = 1.6 % Elevation Angle of Arrival Spread (ESA) / [log10([degrees])] mu ES_A_sigma = 0.1 % Elevation Angle of Arrival Spread (ESA) / [log10([degrees])] sig SF_sigma = 2.5 % Shadow fading (SF) / [dB] sig xpr_mu = 8 % XPR / [dB] mu xpr_sigma = 2.4 % XPR / [dB] sig

% Correlation Distances

DS_lambda = 52.5 % DS correlation distance / [m] KF_lambda = 55 % KF correlation distance / [m] AS_A_lambda = 56 % ASA correlation distance / [m] ES_A_lambda = 3 % ESA correlation distance / [m] SF_lambda = 56 % SF correlation distance / [m]

% Cross correlations

ds_kf = -0.6 % DS vs KF asA_ds = 0.54 % ASA vs DS esA_ds = -0.03 % ESA vs DS ds_sf = 0.41 % DS vs SF asA_kf = -0.51 % ASA vs KF esA_kf = 0.06 % ESA vs KF sf_kf = -0.53 % SF vs KF esA_asA = -0.2 % ESA vs ASA asA_sf = 0.67 % ASA vs SF esA_sf = -0.04 % ESA vs SF

% ==========
% Transmitter parameters % These are mostly irrelevant due to the large distance between satellite and Earth.
% ==========

% The azimuth of departure spread is estimated by utilizing the GEO orbit distance (35,786 km) and % assuming a maximum area from which scattering can occur of 1 km. Additionally, one has to account % for the earth radius of 6,371 km. The average elevation angle is assumed to be 40 deg. % % Formula: % AS_D_mu = log10( atan( 1/( 35786 + 50/90*6371 ))) % AS_D_sigma = log10( atan( 1.25/( 35786 + 50/90*6371 ))) + AS_D_mu % PerClusterAS_D = atan( 0.025/( 35786 + 50/90*6371 )) % % The elevation of departure is further scaled by the tilt of the earth surface. % % Formula: % ES_D_mu = log10( 40/90 * atan( 1/( 35786 + 50/90*6371 ))) % ES_D_sigma = log10( 40/90 * atan( 1.25/( 35786 + 50/90*6371 ))) + AS_D_mu % PerClusterES_D = atan( 40/90 * 0.025/( 35786 + 50/90*6371 ))

AS_D_mu = -4.59 % Azimuth Angle of Departure Spread (ASA) / [log10([degrees])] mu AS_D_sigma = 0.1 % Azimuth Angle of Departure Spread (ASD) / [log10([degrees])] sig AS_D_lambda = 1000 % ASD correlation distance / [m] - almost constant PerClusterAS_D = 0.00000064 % Cluster ASD / [deg] - 25 m diameter as seen from GEO

ES_D_mu = -4.95 % Elevation Angle of Departure Spread (ESD) / [log10([degrees])] mu ES_D_sigma = 0.1 % Elevation Angle of Departure Spread (ESD) / [log10([degrees])] sig ES_D_lambda = 1000 % ESD correlation distance / [m] - almost constant PerClusterES_D = 0.00000028 % Cluster ESD / [deg] - 25 m diameter as seen from GEO

% Cross correlations % We assume all parameters at the satellite to be independent from the receiver due to the large % distance.

asD_ds = 0 % ASD vs DS asD_sf = 0 % ASD vs SF asD_asA = 0 % ASD vs ASA asD_kf = 0 % ASD vs KF esD_sf = 0 % ESD vs SF esD_kf = 0 % ESD vs KF esD_ds = 0 % ESD vs DS esD_asD = 0 % ESD vs ASD esD_asA = 0 % ESD vs ASA esD_esA = 0 % ESD vs ESA esA_asD = 0 % ESA vs ASD

% ==========

% Additional Parameters % These are not covered by MIMOSA but have to be provided by other sources.

% We used the parameters from "WINNER_UMa_C2_LOS" here.

% ==========

NumClusters = 8 % Number of clusters LOS_scatter_radius = 0.1 % Distance to the LOS scatterers [m] LNS_ksi = 3 % Per cluster shadowing std / [dB] r_DS = 2.5 % Delay scaling parameter rTau

PerClusterAS_A = 12 % Cluster ASA / [deg] PerClusterES_A = 7 % Cluster ESA / [deg]

% ==========

% Path Loss Model

% It is assumed that there is a constant path-loss offset.

% ==========

% This still has to be verified.

PL_model = constant

PL_A = 95

% ==========

# Bibliography


[1] K. P. Liolis, J. Gomez-Vilardebo, E. Casini, and A. Perez-Neira, "Statistical modeling of dual-polarized MIMO land mobile satellite channels," *IEEE Trans. Commun.*, vol. 58, pp. 3077–3083, Nov. 2010.

[2] R. Prieto-Cerdeira, F. Pérez-Fontán, P. Burzigotti, and et al., "Versatile two-state land mobile satellite channel model with first application to DVB-SH analysis," *Int. J. Satell. Commun. Network*, vol. DOI: 10.1002/sat.964, Jun. 2010.

[3] P. King, *Modeling and Measurement of the land mobile satellite MIMO radio propagation channel*. PhD thesis, Sch. Elect. and Phys. Sci., Uni. of Surrey, UK, Apr. 2007.

[4] F. Pérez-Fontán, M. Vázquez-Castro, C. Cabado, J. García, and E. Kubista, "Statistical modeling of the LMS channel," *IEEE Trans. on Veh. Technol.*, vol. 50, pp. 1549 – 1567, Nov. 2001.

[5] M. Thomas Jost, G. Carrié, F. Pérez-Fontán, W. Wang, and U.-C. Fiebig, "A deterministic satellite-to-indoor entry loss model," *IEEE TRANSACTIONS ON ANTENNAS AND PROPAGATION*, vol. 61, pp. 2223–2230, Apr. 2013.

[6] C. Oestges and al., "Physical statistical modelling of the land mobile satellite channel based on ray tracing," *IEE Proc. on Microwaves, Antennas and Propagation*, vol. 146, pp. 45–49, 1999.

[7] F. Burkhardt, S. Jaeckel, E. Eberlein, and R. Prieto-Cerdeira, "QuaDRiGa: a MIMO channel model for land mobile satellite," in *The 8th European Conference*

*on Antennas and Propagation (EuCAP 2014)*, (The Hague, The Netherlands), Apr. 2014.

[8] F.Ní Mhearáin, M. Sellathurai, and F. Pérez-Fontán, "An enhanced statistical model for the dual polarised mimo land mobile satellite channel," in *The 8th European Conference on Antennas and Propagation*, (The Hague, The Netherlands), Apr. 2014.

[9] P. Kyösti at al., *IST-4-027756 WINNER II D1.1.2 v.1.1: WINNER II channel models*, Sept. 2007. Available: https://www.ist-winner.org/WINNER2-Deliverables/D1.1.2v1.1.pdf.

[10] P. R. King, T. W. C. Brown, A. Kyrgiazos, and B. G. Evans, "Empirical-stochastic LMS-MIMO channel model implementation and validation," *IEEE Trans. Antennas Propag.*, vol. 60, pp. 606– 614, Feb. 2012.

[11] X. Zhang and Z. Wang, "Characteristics of narrow band dual-polarized MIMO over satellite channel model," in *Proc. 5th Int. Conf. Computing, Commun. and Networking Technologies*, (Hefei, China), Jul. 2014.

[12] V. Nikolaidis and A. G. K. N. Moraitis, "Dual-polarized narrowband MIMO LMS channel measurements in urban environments," *IEEE Trans. Antennas Propag.*, vol. 65, pp. 763 – 774, Feb. 2017.

[13] P. Petropoulou, E. T. Michailidis, A. D. Panagopoulos, and A. G. Kanatas, "Radio propagation channel measurements for the multi-antenna satellite communications systems: a survey," *IEEE Ant. Prop. Magazine*, vol. 56, no. 6, pp. 102–122, 2014.

[14] F. Pérez-Fontán, M. Vázquez-Castro, S. Buonomo, J. Poiraes-Baptista, and B. Arbesser-Rastburg, "S-band LMS propagation channel behaviour for different environments, degrees of shadowing and elevation angles," *IEEE Trans. on Broadcasting*, vol. 40, pp. 40–76, Mar. 1998.

[15] T. Qi and Y. Wang, "Capacity analysis of a land mobile satellite system using dual-polarized antennas for diversity," in *Proc. IEEE Veh. Tech.*, (Boston, MA, USA), Sep. 2015.

[16] P.-D. Arapoglou, P. Burzigotti, A. B. Alamanac, and R. D. Gaudenzi, "Capacity potential of mobile satellite broadcasting systems employing dual polarization per beam," in *2010 5th Advanced Satellite Multimedia Systems Conference and the 11th Signal Processing for Space Communications Workshop*, 2010.

[17] D. Arndt, A. Ihlow, A. Heuberger, and E. Eberlein, "Extended two-state narrowband lms propagation model for s-band," in *IEEE Int. Symp. Broadband Multimedia Systems and Broadcasting (BMSB)*, (Seoul, South Korea), Jun. 2012.

[18] P. R. King and S. Stavrou, "Low elevation wideband land mobile satellite MIMO channel characteristics," *IEEE Trans. Wireless Commun.*, vol. 6, pp. 2712–2720, Jul. 2007.

[19] M. Sellathurai, P. Guinand, and J. Lodge, "Space-time coding in mobile satellite communications using dual-polarized channels," *IEEE Trans. Veh. Technol.*, vol. 55, pp. 189 – 199, Jan. 2006.

[20] ESA Communications, *BR-305 The ESA ARTES Programme: From satcom products to services*, 2012. ISBN 978-92-9221-054-0.

[21] E. Eberlein, F. Burkhardt, G. Sommerkorn, S. Jaeckel, and R. Prieto-Cerdeira, "MIMOSA - analysis of the MIMO channel for LMS systems," in *ESA Workshop on Radiowave Propagation*, (Noordwijk, The Netherlands), Nov.-Dec. 2011.

[22] T. Heyn, E. Eberlein, D. Arndt, B. Matuz, F. L. Blasco, R. Prieto-Cerdeira, and J. Rivera-Castro, "Mobile satellite channel with angle diversity: the MiLADY project," in *2010 4th European Conference on Antennas and Propagation (EuCAP)*, (Barcelona, Spain), Apr 2010.

[23] N. Anastasiadou, G. Gardikis, A. Nikiforiadis, and S. Pangalos, "Adaptive coding and modulation-enabled triple play over DVB-S2 (Digital Video Broadcasting-satellite- second generation): a techno-economic study," *Int. J. Satell. Commun. Network.*, March 2012. DOI: 10.1002/sat.1000.

[24] P. Smyth, ed., *Mobile and Wireless Communications: Key Technologies and Future Applications*, ch. The use of Satellites for Mulitmedia connections, M.Finch, pp. 165 – 185. London, UK: The Institute of Electrical Engineers, 2008.

[25] ETSI, *Digital video broadcasting (DVB); framing structure, channel coding and modulation for satellite transmission to handheld (DVB-SH)*, EN 302 583 v1.0.0. ed., 2007.

[26] ETSI, *TM-H NGH study mission report TM 4026r1*, 2008. EN 302 583 V1.0.0.

[27] F. Pérez-Fontán and P. P. Mariño Espiñeira, *Modeling the Wireless Propagation Channel : a simulation approach with MATLAB*, ch. The land mobile satellite channel, pp. 213 – 228. Chicester, UK: John Wiley & Sons Ltd, 2008.

[28] S. Ohmori, *Mobile Satellite Communications*. Artech House, 1997.

[29] P.-D. Arapoglou, P. Burzigotti, M. Bertinelli, A. Bolea-Alamañac, and R. de Gaudenzi, "Practical MIMO aspects in dual polarization per beam mobile satellite broadcasting," *Int. J. Satelll. Commun. Network*, Jan. 2012. DOI: 10.1002/sat.1008.

[30] F. Pérez-Fontán, A. Mayo, D. Marote, R. Prieto-Cerdeira, P. Mariño, F. Machado, and N. Riera, "Review of generative models for the narrowband land mobile satellite propagation channel," *Int. J. Commun. Syst. Network*, 2008. DOI: 10.1002/sat.914.

[31] C. Loo, "A statistical model for a land mobile satellite link," *IEEE Trans. Veh. Technol.*, vol. 34, pp. 122 – 127, Aug. 1985.

[32] H. Suzuki, "A statistical model for urban radio propagation," *IEEE Trans. Commun.*, vol. 25, pp. 673 – 680, Jul. 1977.

[33] T. Brown, E. DeCarvalho, and P. Kyritsi, *Practical guide to the MIMO radio channel with MATLAB examples*, ch. MIMO Channel Models, pp. 145–191. Chichester, West Sussex, U.K.: Wiley, 2012.

[34] M. Jankiraman, "The MIMO Wireless Channel," in *Space-time Codes and MIMO Systems*, pp. 15 – 45, Boston, MA: Artech House, 2004.

[35] A. I. Pérez-Neira, J. S. C. Ibars, A. del Coso, J. Gómez-Vilarebó, M. Caus, and K. Liolis, "A MIMO channel modeling and transmission techniques for multi-satellite and hybrid satellite terrestrial mobile networks," *Physical Commun.*, vol. 4, pp. 127 – 139, Jun. 2011.

[36] A. Paulraj, D. Gore, R. Nabar, and H. Bölckei, "An overview of MIMO communications - A key to gigabit wireless," *Proc. IEEE*, vol. 92, pp. 198–218, Feb. 2004.

[37] P.-D. Arapoglou, M. Zamkostian, and P. Cottis, "Dual polarization MIMO in LMS broadcasting systems: Possible benefits and challenges," *Int. J. Satelll. Commun. Network*, 2010. DOI: 10.1002/sat.986.

[38] P.-D. Arapoglou, P. Burzigotti, M. Bertinelli, A. Bolea-Alamañac, and R. de Gaudenzi, "To MIMO or not to MIMO in mobile satellite broadcasting systems," *IEEE Trans. Wireless Commun.*, vol. 10, pp. 2807–2811, Sept. 2011.

[39] C. Oestges, V. Erceg, and A. J. Paulraj, "Propagation modeling of mimo multipolarized fixed wireless channels," *IEEE Trans. on Veh. Technol.*, vol. 53, pp. 644–654, May 2004.

[40] J. J. A. Lempiainen and J. K. Laiho-Steffens, "The performance of polarization diversity schemes at a base station in small/micro cells at 1800 MHz," *IEEE Trans. Veh. Technol.*, vol. 47, pp. 1087 – 1092, Aug. 1998.

[41] C. Oestges, M. Guillaud, and M. Debbah, "Multi-polarized mimo communications: channel model, mutual information and array optimization," in *IEEE Wireless Comms & Networking Conf. (WCNC)*, (Hong Kong, China), Mar. 2007.

[42] G. Carrie, F. Pérez-Fontán, F. Lacoste, and J. Lemorton, "A generative MIMO channel model encompassing single satellite and satellite diversity cases," in *The ESA Workshop on Radiowave Propagation 2011*, (Noordwijk, The Netherlands), Nov - Dec 2011.

[43] A. G. Kanatas and A. D. Panagopoulos, *Radio Wave Propagation and Channel Modeling for EarthSpace Systems*. CRC Press, 2016.

[44] W. Weichselberger, *Spatial Structure of Multiple Antenna Radio Channels*. PhD thesis, Fac. Elect. Eng. and Inform. Technol., T.U. Wien, Germany, Dec. 2003.

[45] J. P. Kermoal, L. Schumacher, K. I. Pedersen, P. E. Mogensen, and F. Frederiksen, "A stochastic MIMO radio channel model with experimental validation," *IEEE J. Sel. Areas Commun.*, vol. 20, pp. 1211–1226, Aug. 2002.

[46] K. E. Baddour and N. C. Beaulieu, "Autoregressive modeling for fading channel simulation," *IEEE Trans. Wireless Commun.*, vol. 4, pp. 1650–1662, Jul. 2005.

[47] C.-D. Iskander, "A matlab®-based object-orientated approach to multipath fading channel simulation," *Hi-Tek Multisystems*, Feb. 2008.

[48] K. Liolis, I. Andrikopoulos, and P. Cottis, "On statistical modeling and performance evaluation of SIMO land mobile satellite channels," in *4th Advanced Satellite Mobile Systems Conference*, (Bologna, Italy), Aug. 2008.

[49] M. Rieche, D. Arndt, A. Ihlow, and G. D. Galdo, "State modeling of the land mobile satellite channel by an image-based approach," in *2013 7th European Conference on Antennas and Propagation (EuCAP)*, (Gothenburg, Sweden), Apr 2013.

[50] M. Ait-Ighil, F. Pérez-Fontán, J. Lemorton, F. Lacoste, G. Artaud, C. Bourga, and M. Bousquet, "Simplified model for building scattering in urban environment for GNSS propagation channels," in *The ESA Workshop on Radiowave Propagation 2011*, (Noordwijk, The Netherlands), Nov - Dec 2011.

[51] S. Jaeckel, L. Raschkowski, K. Börner, L. Thiele, F. Burkhardt, and E. Eberlein, "Quasi deterministic radio channel generator user manual and documentation," tech. rep., Fraunhofer Heinrich Hertz Institute, 2013. Tech. Rep. v1.0.5-171.

[52] R. C. Jones, "A new calculus for the treatment of optical systems, description and discussion of the calculus," *Journal of the Optical Society of America*, vol. 31, pp. 488–493, Jul. 1941.

[53] D. Arndt, T. Heyn, A. Heuberger, R. Prieto-Cerdeira, and E. Eberlein, "State modeling of the land mobile satellite channel with angle diversity," in *6th European Conference on Antennas and Propagation (EUCAP)*, 3140 - 3144 2012.